INFORMATION TO USERS

This manuscript has been reproduced from the microfilm master. UMI films the text directly from the original or copy submitted. Thus, some thesis and dissertation copies are in typewriter face, while others may be from any type of computer printer.

The quality of this reproduction is dependent upon the quality of the copy submitted. Broken or indistinct print, colored or poor quality illustrations and photographs, print bleedthrough, substandard margins, and improper alignment can adversely affect reproduction.

In the unlikely event that the author did not send UMI a complete manuscript and there are missing pages, these will be noted. Also, if unauthorized copyright material had to be removed, a note will indicate the deletion.

Oversize materials (e.g., maps, drawings, charts) are reproduced by sectioning the original, beginning at the upper left-hand corner and continuing from left to right in equal sections with small overlaps.

Photographs included in the original manuscript have been reproduced xerographically in this copy. Higher quality 6" x 9" black and white photographic prints are available for any photographs or illustrations appearing in this copy for an additional charge. Contact UMI directly to order.

UMI®

University of Alberta

Colloidal Interactions in
Water-in-Diluted-Bitumen Emulsions

by

Shawn David Taylor   Ⓒ

A thesis submitted to the Faculty of Graduate Studies and Research
in partial fulfillment of the requirements for the degree of
Doctor of Philosophy in Chemical Engineering.

Department of Chemical and Materials Engineering

Edmonton, Alberta
Spring 2002

Canada

Library Release Form

Name of Author: Shawn David Taylor

Title of Thesis: Colloidal Interactions in Water-in-Diluted-Bitumen Emulsions

Degree: Doctor of Philosophy

Year this Degree Granted: 2002

Permission is hereby granted to the University of Alberta Library to reproduce single copies of this thesis and to lend or sell copies for private, scholarly or scientific research purposes only.

The author reserves all other publication and other rights in association with the copyright in this thesis, and except as herein before provided, neither the thesis nor any substantial portion thereof may be printed or otherwise reproduced in any material form whatever without the author's prior written permission.
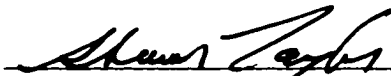
Shawn David Taylor
444 Huntington Hill
Edmonton, Alberta
T6H 5W6

January 10, 2002

University of Alberta

Faculty of Graduate Studies and Research

The undersigned certify that they have read, and recommend to the Faculty of Graduate Studies and Research for acceptance, a thesis entitled *Colloidal Interactions in Water-in-Diluted-Bitumen Emulsions* in partial fulfillment of the requirements for the degree Doctor of Philosophy in Chemical Engineering.

Dr. Jacob H. Masliyah (co-supervisor)

Dr. Jan Czarnecki (co-supervisor)
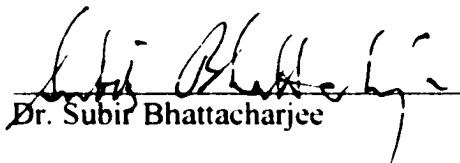
Dr. Subir Bhattacharjee

Dr. Janet A. Elliott
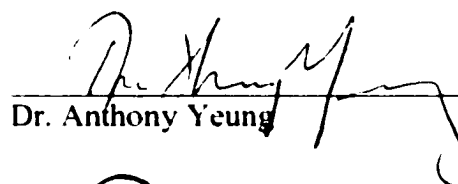
Dr. Anthony Yeung

Dr. Zhenghe Xu
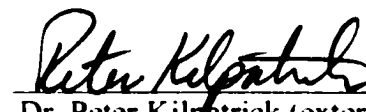
Dr. Peter Kilpatrick (external examiner)

Date: Dec. 7th, 2001

Abstract

The large scale development of heavy oil and oil sand reserves poses several technical challenges including the elimination of undesirable water-in-oil emulsions. In the oil sands industry, water-in-bitumen emulsions are formed during the water extraction process used to separate bitumen from oil sands. Asphaltenes are commonly identified as the bitumen fraction responsible for emulsion stability. However, very little is known about how the asphaltenes stabilize the emulsions. There is a need for quantitative information about the structure of the bitumen/water interface and the surface forces that exist between emulsified water droplets.

The stability of water-in-bitumen emulsions depends, among other things, on the thin film of oil formed between two approaching water droplets. In this study, the Thin Liquid Film-Pressure Balance Technique is used to create microscopic water/solvent-diluted-bitumen/water films. The films provide a physical model to study the interaction between two water droplets immersed in a continuous phase of diluted bitumen. Several properties of the film were measured as a function of solvent:bitumen ratio, including film thickness, drainage rate, and film lifetimes. Information about the surface forces and film structure was also obtained from measured disjoining pressure-thickness isotherms. Results indicate that the film was probably stabilized by steric repulsion generated by surface active material from the asphaltene fraction of bitumen. It was estimated that the surfactant material had a length of about 4 nm. There was also evidence that a change in the solvent:bitumen ratio may have caused a change in the surfactant structure within the film. Hence, a relationship probably exists between the surfactant structure within a film and the bulk phase behaviour.

To study this relation, comparisons were made between the bulk phase behaviour and thin foam film behaviour of a model sodium naphthenates-water system. There appeared to be a clear link between the formation of bulk lamellar liquid crystal and the formation of a liquid crystal-like layered structure within the film. A lamellar structure was also observed in the films drawn from an isotropic solution, although it was not clear if the structuring was due to layers of spherical micelles or liquid crystal-like layers of sodium naphthenates.

Acknowledgements

Table of Contents

List of Tables

List of Figures

Nomenclature

a	fitting parameter
b	fitting parameter
c	fitting parameter
C_e	electrolyte concentration
C_1	integration constant
C_2	integration constant
D	separation distance
f	volume fraction
$\bar{f}$	average volume fraction
f_1	volume fraction of component 1
f_2	volume fraction of component 2
f_A	volume fraction of asphaltenes
f_B	volume fraction of bitumen
f_i	volume fraction of component i
f_M	volume fraction of maltenes
F	Faraday's constant; force (Appendix D)
g	acceleration due to gravity
h	film thickness
h_{CR}	critical thickness
h_{in}	thickness of film core
h_o	initial thickness
h_{out}	thickness of the surfactant layers in the film
h_{trip}	film thickness estimated from triple layer model
I	intensity of reflected light
I_{max}	intensity of reflected light at last maximum
I_{min}	intensity of reflected light at last minimum
k	Boltzmann constant
k_1	Fresnel coefficient
k_2	Fresnel coefficient

K	Hamaker constant; reflectance (Appendix B)
K_{max}	maximum reflectance
m	number of data points
n	refractive index
n_1	refractive index of component 1
n_2	refractive index of component 2
n_A	refractive index of asphaltenes
n_B	refractive index of bitumen
n_f	refractive index of film
n_{hep}	refractive index of heptane
n_i	refractive index of component I
n_{in}	refractive index of film core
n_M	refractive index of maltenes
n_{out}	refractive index of surfactant layer in the film
n_s	refractive index of fluid surrounding the film
n_{tol}	refractive index of toluene
$\hat{n}_j$	RI predicted from Eq. [5.3] at f_j
N	relation for n_f and n_s; Eq. [2.1]
N_s	specific refraction
P	pressure
P_1	pressure outside of film
P_2	pressure in plateau border region
$P_{applied}$	applied pressure inside measuring cell
P_{atm}	atmospheric pressure
P_c	capillary pressure
P_{cell}	absolute pressure inside measuring cell
P_{max}	maximum pressure
P_{ref}	reference pressure
r	film radius; radial direction (Appendix D)
R	hole radius; disc radius (Appendix D)
R_g	gas constant

R_{max}	maximum pore radius
Re	Reynolds number
s	radial distance from the center of the hole
t	time
T	absolute temperature (Chapter 1); Student-t statistic (Chapter 5)
u	disc velocity
V_r	velocity in r-direction
V_z	velocity in z-direction
V_θ	velocity in θ-direction
z	valence; z-direction (Appendix D)
z_o	height of oil phase
z_w	height of water phase

Greek Letters

α	confidence level
δ	thickness of polymer brush
Δ	ratio of measured to maximum reflectance
ε	dielectric constant
ϕ	potential; angle of refraction (Appendix B)
γ	interfacial tension
φ	wetting contact angle
κ	Debye length
η	bulk viscosity
λ	wavelength
π	pi (constant)
Π	disjoining pressure
Π_{dyn}	disjoining pressure measured by dynamic method
Π_{EL}	electrostatic contribution to disjoining pressure
Π_{SC}	structural contribution to disjoining pressure
Π_{ST}	steric contribution to disjoining pressure

Π_{VW} London-van der Waals contribution to disjoining pressure

ρ bulk density

ρ_1 bulk density of component 1

ρ_2 bulk density of component2

ρ_i bulk density of component i

ρ_o bulk density of oil phase

ρ_w bulk density of water phase

θ film contact angle; angle of incidence (Appendix B)

τ film lifetime

v rate of film drainage

Subscripts

1   component 1

2   component 2

A   asphaltene

atm   atmospheric

B   bitumen

c   capillary

CR   critical

dyn   dynamic method

e   electrolyte

EL   electrostatic

f   film

hep   heptane

i   component I

in   film core

M   maltenes

max   maximum

min   minimum

o   initial

out	surfactant layer of film
O	oil phase
ref	reference
s	surrounding fluid
S	solvent
SC	structural
ST	steric
tol	toluene
trip	triple layer model
VW	London-van der Waals
W	water phase

Chapter 1

Introduction to Thin Liquid Films and Water-in-Bitumen Emulsions

1.1 Introduction

Conventional crude oil sources in North America have been declining for some years. As a result, the North American economy has begun to rely more heavily on alternative or technically challenging sources of crude oil such as crude oil extracted from enhanced oil recovery wells and synthetic crude oils obtained from bitumous oil sands. One of the largest alternative crude oil sources is the oil sand deposit found in the northern portion of Alberta, Canada. Oil sands are deposits of silica sand and fine clays that contain an average of 9 to 13 %wt bitumen and up to about 2 %wt water (Shaw et al., 1996; Czarnecki, 2001). The bitumen recovered from the oil sands is converted into a light synthetic crude oil and sold to refineries for final upgrading to consumable products. Over 20% of the crude oil production in Canada is currently derived from the oil sand deposits and it is expected that production of synthetic crude from oil sands will account for about 50% of Canada's total crude oil production by year 2010 (Czarnecki, 2001).

To make alternative crude oil sources more economically attractive, research efforts have been focused on solving some of the technical problems associated with oil production. A major problem that has existed since the inception of the oil industry is the formation of undesirable water-in-crude-oil emulsions. The emulsions may be formed by the emulsification of table water, by the entrainment of water droplets during the steam cleaning of crude oil in refiners, and the emulsification of water as waves lap into crude oil spills (McLean et al., 1998; Yarranton et al., 2000a). In addition to environmental concerns, the formation of emulsions often results in significant losses of crude oil and contributes to increased treatment and transportation costs.

In the oil sands industry, water-in-bitumen emulsions are an unavoidable outcome of the bitumen extraction process. A schematic of a typical extraction process is shown in Figure 1.1. For deposits close to the surface, the oil sands are mined using conventional

truck and shovel surfacing mining techniques. The mined ore is crushed, mixed with water and pumped to the extraction plant via a hydrotransport pipeline. In the pipeline, the ore undergoes a digestion process where lumps are broken down into smaller sizes and the bitumen is liberated from the sand grains. During this process, some air becomes entrained in the slurry in the form of small air bubbles. At the extraction plant, the slurry is sent to the primary separation vessel (PSV) where the bitumen is floated to the top of the unit and 'cleaned' sand is removed from the bottom as tailings. The bitumen froth contains about 60 % bitumen, 30 % water and 10 % solids. To remove the solids and water, the froth is first diluted with solvent, normally a locally produced naphtha. Dilution reduces the density and viscosity of the bitumen allowing the water and solids to be easily separated from the bitumen. The water and solids are removed in the froth treatment process where the diluted froth is sent through a series of low gravity separation vessels (e.g. inclined plate settlers) as well as scroll and disk centrifuges. The treated froth passes through a diluent recovery unit where the solvent is reclaimed. The bitumen is finally sent to the upgrading process where it is converted into synthetic crude oil.

In the extraction process described above, the diluted bitumen leaving the froth treatment plant still contains about 1 to 2% of the process water in the form of micron sized droplets. This water-in-diluted-bitumen is extremely stable. The droplets of water also contain chloride salts. Due to conditions in the upgrading process, it is possible for the chloride salts to be converted into ammonium chloride. The presence of ammonium chloride poses a serious risk of causing severe corrosion of plant equipment. This is a problem that has potential implications for both plant safety and production costs. One of the first steps in solving this problem is to learn how the water-in-diluted-bitumen emulsion is stabilized. The stability of a water-in-bitumen emulsion depends, to a large extent, on the thin film of oil that is formed between two approaching water droplets. If the thin oil film is unstable, it will rupture and the water droplets will coalesce into larger and larger droplets. Thus, an unstable film suggests that the emulsion will be unstable over time. On the other hand, a stable thin film will not rupture and the water droplets will be prevented from coalescing. This means that stable thin films will lead to stable emulsions.

Due mainly to the technical difficulties associated with studying thin films, most of the work to date on water-in-bitumen emulsions has focused on standard emulsion stability tests and chemical analysis. For example, a significant amount of research has been dedicated to determining the conditions under which stable water-in-bitumen (or water-in-crude-oil) emulsions form (e.g. Johansen, et al., 1988/89; McLean and Kilpatrick, 1997a; Yan et al., 1999). Researchers have also tried to identify which molecular compounds within the bitumen are surface active and responsible for emulsion stability. Bitumen, like crude oil, is a complex mixture of thousands of different hydrocarbon molecules. Isolating and identifying the individual surface active molecules is a nearly impossible task. Thus, previous researchers began by looking at large fractions of bitumen. The heptane insoluble fraction of bitumen, commonly known as asphaltenes, has been identified as the main fraction responsible for the stability of water-in-bitumen emulsions (Yarranton, 1997; McLean et al., 1998). Based on these past investigations, a few models have been developed to explain the stability of water-in-bitumen emulsions. These models have attempted to link the solubility (or phase) behaviour of asphaltenes in the diluted bitumen to the structure of the surface active material at the water/oil interfaces and, in turn, how the structure determines the type and magnitude of the surface forces (e.g. McLean and Kilpatrick, 1997b). Unfortunately, the literature contains very little quantitative information about the surfactant structure at the water/oil interface or the type and magnitude of the surface forces between emulsion water droplets.

The goal of this thesis is to begin a quantitative investigation of the surface forces within the water-in-diluted-bitumen emulsions. This information will be obtained by using thin liquid films to model the colloidal interactions within the emulsion. As a result of this work, some inferences will be made about the surfactant structure within the thin film. To avoid the complexities of a varying diluted bitumen source, a single model system was chosen on the basis of its uniform composition and its similarity to the original diluted bitumen. A system of simulated industrial water, toluene, and bitumen was chosen as the primary model for this investigation. This model system will be used as the basis for comparison to other systems that will be used to study the effects of solvent type and bitumen fractionation on emulsion stability.

1.1.1 Objectives

The main purpose of this thesis was to identify the type and relative magnitude of the surface forces that exist between water droplets within a water-in-toluene-diluted-bitumen emulsion. To measure these surface forces, the first objective was to develop a new modification of the Thin Liquid Film-Pressure Balance Technique (TLF-PBT). The technique had to be modified to mimic the interactions between two water droplets separated by a thin film of diluted bitumen. Once the modified TLF-PBT was operational, the second objective was to investigate the basic behaviour of a water/toluene-diluted-bitumen/water film including film lifetime, film drainage rate, drainage patterns, and equilibrium film thickness. The third objective was to measure the surface forces in water/toluene-diluted-bitumen/water films with the results expressed in terms of disjoining pressure-thickness isotherms. Part of the TLF-PBT investigation required knowledge of the refractive index of the diluted bitumen at various concentrations. This requirement lead to the fourth objective of using experimental data to develop a mixing model for the refractive index of diluted bitumen solutions.

There was also a desire in this thesis to begin to link the phase behaviour of the water-toluene-bitumen system to the behaviour observed in thin films. As mentioned earlier, the solubility (or phase) behaviour of asphaltenes may be related to emulsion stability. This also means that the bulk phase behaviour of asphaltenes may be related to the behaviour of the thin films. The bulk phase behaviour in a system of water-toluene-bitumen is quite complex and it is difficult to link the bulk phase behaviour to the behaviour of the thin films. For this reason, a simple model system was used for the initial investigation into the possible link between phase behaviour and the behaviour of the thin film. For this study, a mixture of sodium naphthenates and water was chosen as the model system. The objective was to link the bulk phase behaviour of the sodium naphthenates-water mixtures to the behaviour of the thin films formed from these mixtures.

The five objectives of this thesis are summarize below:

1. Develop a new modification of the TLF-PBT that allows for the investigation of toluene-diluted-bitumen films formed in an aqueous environment.

2. Determine the basic behaviour of a water/toluene-diluted-bitumen/water film, including observations of equilibrium film thickness, drainage rate, drainage pattern, and film lifetime.

3. Identify the type and magnitude of the surface forces in a water/toluene-diluted-bitumen/water film from measurements of the disjoining pressure-thickness isotherms.

4. Determine if there is a link between the phase behaviour of a sodium naphthenates-water system and the behaviour of the foam films formed from the same sodium naphthenates-water system.

5. Measure the refractive index of various diluted bitumen solutions and use the data to develop a mixing model for the refractive index of diluted bitumen solutions.

1.1.2 Thesis Outline

Chapter 1 provides a general introduction to thin liquid films and the properties of bitumen. Sections 1.2 and 1.3 provide a review of the basic principles of thin liquid films as well as introducing some of the parameters used to describe thin film behaviour. Particular attention will be given to disjoining pressure-thickness isotherms that describe the surface forces within thin liquid films. Section 1.4 provides a review of the basic physical and chemical properties of bitumen and its components as well as a brief discussion on the current understanding of water-in-bitumen emulsion stability and the effects of aging. Chapter 1 is intended to provide background information and context for the chapters that follow.

The body of the thesis is presented in Chapters 2 through 5. The chapters are organized in paper format where the figures appear at the end of each chapter instead of being interspersed throughout the text. Objectives 1 and 2 are addressed in Chapter 2. The experimental portion of Chapter 2 provides a detailed description of the new modifications to the TLF-PBT. The results include a description of the drainage behaviour for water/toluene-diluted-bitumen/water films and water/heptane-diluted-bitumen/water films. The results also contain a quantitative measure of the effect of

toluene:bitumen and heptane:bitumen weight ratios on the drainage rate and film thickness.

The third objective is considered in Chapter 3. This chapter describes how the modified TLF-PBT apparatus was used to measure disjoining pressure-thickness isotherms of water/toluene-diluted-bitumen/water films. Measurements were obtained for five different toluene:bitumen weight ratios ranging from (1:1) to (10:1). These results are then compared to isotherms generated for water/toluene-diluted-asphaltene/water films. The asphaltene concentrations were comparable to the asphaltene concentrations found within the toluene-bitumen mixtures. Two different methods were used to prepare the 'solids-free' asphaltenes and a comparison was done to determine if the asphaltene preparation procedure affected the measured isotherms.

Chapter 4 deals with the fourth objective of trying to link the phase behaviour of a model sodium naphthenates-water system with the behaviour of thin films formed from the same sodium naphthenates-water mixtures. The results begin with a description of the bulk phase behaviour of mixtures between 5 and 50 %wt sodium naphthenates. This is followed by a description of the stratification phenomena observed in the thin films formed from these mixtures. Quantitative information about the film structure was obtained from film thickness measurements.

The last objective is covered in Chapter 5. The chapter presents a simple mixing model which relates the volume fraction of bitumen to the refractive index of the diluted bitumen solution. The model requires an estimate of the refractive index of 'pure' bitumen. Since this value cannot be measure directly, the refractive index of several different solvent-bitumen solutions was measured using a bench-top refractometer. The data was then extrapolated to find the refractive index of bitumen. The same technique was also used to estimate the refractive index of asphaltenes and maltenes (i.e. deasphalted bitumen). The final model was then used to detect the onset of asphaltene precipitation in heptane-bitumen solutions.

All of the findings from Chapter 2 to 5 are summarized in Chapter 6. The final chapter also discusses the contribution of this thesis to the general knowledge of thin films and emulsions. The chapter ends with recommendations for future work.

1.2 Thin Liquid Films

The study of thin liquid films has long been considered to be a valuable approach for both experimental and theoretical studies on colloidal interactions. Studies have been conducted on both asymmetric and symmetric films. Figure 1.2(a) shows an example of an asymmetric film where a solid phase is separated from air by a thin film of water. This is commonly referred to as a gas/liquid/solid film. Such a film may be used to model the interactions between an air bubble and a solid particle in a flotation process. Symmetric films are generally used to model colloidal interactions within foams and emulsions. In the case of a water-in-toluene-diluted-bitumen emulsion, thin liquid films may be used to model the colloidal interactions between water droplets within a medium of toluene-diluted-bitumen. The symmetric film example in Figure 1.2(b) shows that such an emulsion can be modeled as two volumes of water separated by a thin film of oil. This type of film is commonly referred to as a water/oil/water film. It is important to note that symmetry requires the properties of the water on either side of the oil film to be identical.

1.2.1 Thin Liquid Film - Pressure Balance Technique

To better understand how a thin film can be used to model colloidal interactions within an emulsion, consider two water droplets of equal diameter surrounded by toluene-diluted-bitumen (Figure 1.3). At large distances (i.e. greater than a few hundred nanometers), there are no colloidal interactions between the droplets. As the droplets begin to approach one another, the oil is forced to drain from between the droplets. When the two droplets come within a few hundred nanometers of one another, the interfaces of the droplets flatten and a flat disk of oil will form between the two droplets. The thin liquid film of interest consists of the two interfaces and the small volume between the two interfaces.

Due to the changing curvature of the oil-water interface, a capillary pressure (i.e. a pressure difference) arises between the film and the surrounding oil. This capillary pressure forces the oil to drain from the film. As the film becomes thinner, the two droplets begin to interact through surface forces, such as electrostatic, London-van der Waals, and steric forces. The overall effect of these forces is known as disjoining pressure. If there is a strong repulsive force between the droplets, then the disjoining

pressure will balance the capillary pressure and the film will remain stable. This means the film will stop thinning and the two water droplets will be prevented from coalescing. Conversely, if there is only a weak repulsive force or an attractive force between the droplets, then the capillary pressure will be larger than the disjoining pressure. As a result, the film will continue to thin until it ruptures and the two droplets coalesce. It is quite clear from the above description that thin water/oil/water films have a significant influence on the stability of water-in-oil emulsions. Therefore, a great deal of information about emulsion stability can be obtained by studying thin liquid films.

There are several experimental techniques available that are capable of creating thin liquid films, although most of these techniques are designed to study specific systems. The most appropriate technique for this study was the Thin Liquid Film-Pressure Balance Technique (TLF-PBT) introduced by Scheludko and Exerowa (Scheludko, 1967; Exerowa and Kruglyakov, 1998). In this technique, a microscopic, horizontal thin film is formed inside a specially designed glass measuring cell (Figure 1.4). The measuring cell consists of a small film holder attached to the end of a long glass capillary. Both the glass capillary and film holder are sealed inside the measuring cell. The film holder is generally made from either a small glass capillary or a thin, rectangular shaped plate of porous glass into which a small, vertical hole has been drilled. The radius of the glass capillary film holder is typically between 0.5 and 1.0 mm. Also, the inside surface of the holder is usually etched with fine vertical lines to improve its wetting characteristics. The porous plate holder is normally 2 to 3 mm thick and the radius of the drilled hole is typically between 150 and 500 μm. Several other variants of these two basic designs may also be found in the literature (e.g. Exerowa and Kruglyakov, 1998). The microscopic thin films are formed inside the hole of the film holders. These holders may be used to form thin films of 10 to 250 μm in radius. The bottom of the measuring cell is normally made from an optical flat that allows the film to be viewed from below with a reflected light microscope.

The design of TLF-PBT apparatus allows for the direct measure of various thin film parameters such as, film thickness, contact angle, and capillary pressure. These values may be used to calculate the thermodynamic and kinetic properties of the films, including the surface potential, film tension, and disjoining pressure-thickness isotherms.

For brevity, the sections that follow will introduce only those parameters or properties discussed in the body of the thesis. A complete review of thin film parameters and properties may be found in Ivanov (1988) and Exerowa and Kruglyakov (1998).

1.2.2 Terminology

In this section, a number of terms are introduced that are commonly encountered in the thin liquid film literature. Figure 1.5 is a schematic of a thin water/oil/water film formed in the cylindrically shaped hole of a porous plate film holder. Contained within the *hole* of radius, R, is the *thin film* and a large amount of bulk liquid. The film is located in the geometric center of the hole and is usually circular in shape with a radius, r, and thickness, h. The bulk liquid that surrounds the thin film is also known as the *plateau border region*. To be able to form a thin film, the liquid in the plateau border must preferentially wet the walls of the film holder. It is normally assumed that the oil/water interfaces of the plateau border touch the film holder near the top and bottom of the hole at a *wetting contact angle*, φ. Due to the difficulty in measuring this angle, it is normally assumed that $\varphi = 0$. The oil/water interfaces of the plateau border region also touch the thin film at a so-called *film contact angle*, θ. This angle is usually quite small and may be measured experimentally using either the topographic technique or film expansion technique (Exerowa and Kruglyakov, 1998).

In most sketches or models of thin liquid films, the *film interfaces* are assumed to be plane-parallel to one another. This is generally true for films of small radius (r < 50 μm) and films that are approaching or have reached their final, stable state (i.e. *equilibrium thickness*). However, this assumption does not hold true during the initial formation of larger diameter films. A small amount of oil will often become trapped in the film resulting in a bulge in the middle of the film (see Figure 1.6). This bulge is commonly referred to as a *dimple*.

Once a film has reached an equilibrium thickness, it may be classified as one of several types, including (Kruglyakov, 1988):

1. A *common thin film*, which is also known as a *grey film*.
2. A *black film*.
3. A *stratified film*.

A schematic of each of these film types is shown in Figure 1.7.

Grey films are generally formed from aqueous solutions with low electrolyte concentrations. The long range electrostatic forces that dominant these types of films often lead to relatively thick films (h < 30nm) that appear grey in reflected light. Black films refer to films in which short range repulsive forces are dominant. These films tend to be relatively thin (h < 30 nm) and often appear black in reflected light. When the black films are formed from an aqueous solution, the films may be further classified as either *common black films* or *Newton black films*. A common black film consists of two film interfaces separated by a very thin core of liquid. Newton black films are generally thinner than common black films and consist of only the two film interfaces (i.e. a *surfactant bilayer*). Stratified films generally refer to films in which layered surfactant structures are formed. A lamellar liquid crystal structure and layers of spherical micelles between the two interfaces are two examples of possible stratified films. These films are formed from solutions containing high surfactant concentrations, although stratified films have also been formed from mixtures containing a high volume fraction of monodisperse nanospheres (Nikolov and Wasan, 1992).

1.2.3 Film Thickness

The film thickness is one of the most important parameters used to describe thin liquid films. It may be measured using either optically or conductometrically based methods. In a conductometric measurement, the film thickness is determined from changes in film conductivity. Since data from this method becomes inaccurate when measuring the thickness of black films, the use of conductometrically based methods are generally limited to relatively thick films (h > 30 nm). In optical techniques, the film thickness is related to the ratio of reflected light intensity to incident light intensity. A model for the film structure is required to convert the light intensity into a film thickness. The choice of model determines, to a large extent, the accuracy of the optical technique (Kruglyakov, 1988).

The technique used in this study is an optically based technique known as microinterferometry. In this technique, a monochromatic beam of light is directed onto the film (Figure 1.8). A portion of the incident light is reflected from each film interface.

Since the second reflected beam of light has traveled further than the first reflected beam, there will be a phase difference between the two beams of reflected light. The phase difference results in interference between the reflected light beams. A photo-multiplier or high-sensitivity photo-diode is used to detect the reflected light intensity and convert it into a voltage signal. Using a recorder, a voltage-time (or photocurrent-time) curve may be produced from the thinning film. The interference between the reflected light beams appears as a periodic fluctuation in the recorded voltage/time curve. The maximum and minimum voltages correspond to the maximum and minimum reflected light intensities, I_{max} and I_{min} respectively.

As mentioned, a model of the film structure is required to convert the recorded intensity to a film thickness. In the commonly used single layer model, the film is treated as a thin slab of liquid where the refractive index of the liquid is assumed to be constant. From this model, the following equation for the thickness can be derived:

$$h = \left(\frac{\lambda}{2\pi n_f}\right)\left[k\pi \pm \arcsin\left(\frac{\Delta}{1+\left[4N/(1-N)^2\right]\left[1-\Delta\right]}\right)^{1/2}\right] \qquad [1.1]$$

where

$$\Delta = \frac{I - I_{min}}{I_{max} - I_{min}} \qquad [1.2]$$

and

$$N = \frac{(n_f - n_s)^2}{(n_f + n_s)^2} \qquad [1.3]$$

Here, h is known as the *equivalent film thickness*, λ is the wavelength of the incident light, I is the recorded light intensity with I_{max} and I_{min} corresponding to last maximum and minimum interference values, and n_f and n_s are the refractive indices of the film and surrounding fluid, respectively. The order of interference, k, depends on the film thickness. For film thicknesses between zero and $\lambda/4$, k = 0. For thicknesses between $3\lambda/4$ and $\lambda/4$, k = 1. In general, k = 0, 1, 2.... for film thicknesses less than $(2n-1)\lambda/4$ where n = 1, 2, 3.... A complete derivation of Eq. [1.1] can be found in Appendix A.

Film thickness also has a thermodynamic definition. In a surface region, the intensive thermodynamic properties gradually change when moving from one phase to another. For a thin film, the two surface regions overlap. The overlap affects the properties of the two surfaces. Thus, a typical feature of thin films is that the intensive thermodynamic properties of the film depend on film thickness. The thermodynamic thickness may be defined using the surface excess convention originally proposed by Rusanov (Ivanov, 1988). In the surface excess convention, the film is defined as two dividing surfaces separated by a volume portion. The dividing surfaces are similar to a Gibbs dividing surface in that the surface properties are defined as excess properties relative to a reference phase. By convention, the reference phase for the dividing surfaces is the fluid that surrounds the film (e.g. the water phase that surrounds the diluted bitumen film). The reference phase for the volume portion is the bulk liquid of the plateau border region (e.g. diluted bitumen). The thermodynamic film thickness is simply the distance between the dividing surfaces.

1.2.4 Capillary Pressure

A capillary pressure is generated in the plateau border region by the curved oil/water interfaces. Both the upper and lower interfaces are generally assumed to have the same spherical curvature. Hence, the radius of curvature of the oil/water interface will be equal to the hole radius, R. In this case, the capillary pressure, P_C, may be calculated from the following equation (Exerowa and Kruglyakov, 1998):

$$P_c = 2\gamma \frac{R \cos \varphi - r \sin \theta}{R^2 - r^2} \qquad [1.4]$$

where γ is the interfacial tension, r is the film radius, φ is the wetting contact angle, and θ is the film contact angle (see Figure 1.5). To obtain a precise estimate of the capillary pressure, all of the terms must be known. Except for the wetting contact angle, all of the terms can be measured experimentally. The derivation of Eq. [1.4] can be found in Appendix B.

In general, both contact angles are assumed to be sufficiently small such that $\cos \varphi \approx 1$ and $\sin \theta \approx 0$. Eq. [1.4] can then be simplified as:

$$P_C = 2\gamma \frac{R}{R^2 - r^2}$$

[1.5]

It is important to note that Eq. [1.4] indicates that the capillary pressure depends on both the size of the hole in the film holder and the size of the film. Larger hole sizes will lead to lower capillary pressures while larger film sizes will result in higher capillary pressures.

Under certain conditions, it is possible for the capillary pressure to be on the order of about 10 Pa. Utilizing Eqs. [1.4] or [1.5] in this low pressure range may lead to inaccurate estimates of the capillary pressure. It is possible to directly measure low capillary pressures for air/water/air films. The measurement involves using a cathetometer to observe the height of the liquid rise in the glass capillary. The liquid height is directly related to the capillary pressure in the plateau border region of the air/water/air film. The measurements must be performed using a glass capillary holder. It is extremely important that the glass capillary is made from the same glass as the film holder and that both the film holder and the glass capillary have the same inner diameter.

1.2.5 Drainage Rate and Film Lifetime

Film lifetime is commonly used to describe the kinetic behaviour of thin liquid films. It is the time from the initial film formation to film rupture. By this definition, stable films will have an infinite lifetime. In the case of films that rupture before reaching an equilibrium thickness, the film lifetime may be estimated from the relation (Exerowa and Kruglyakov, 1998):

$$\tau = \int_{h_0}^{h_{cr}} \frac{dh}{v}$$

[1.6]

where h_o is the initial film thickness, h_{CR} is the critical thickness at which the film ruptures and v is the change in film thickness over time (commonly referred to as the rate of film drainage).

A prediction of the film lifetime requires a model for the rate of film drainage. In the simplest case, the film may be treated as a pair of plane-parallel discs. As the two discs approach each other, the liquid in between will drain to the edge (i.e. plateau border) in an axially symmetric fashion. Using lubrication theory, the following expression for the rate of drainage may be derived (Scheludko, 1967):

$$v \equiv -\frac{dh}{dt} = \frac{2h^3 \Delta P}{3\eta r^2} \qquad [1.7]$$

where h is the film thickness, t is time, η is the bulk viscosity, and ΔP is the pressure drop between the film and the plateau border region. The pressure drop is normally assumed to be equal to the difference between the capillary pressure and disjoining pressure, $\Delta P = P_C - \Pi$. Eq. [1.7] is known as the Reynolds relation, although it is also commonly referred to as the Stefan-Reynolds equation when describing the drainage rate of thin films.

A number of assumptions are required to derive the Stefan-Reynolds equation. These include:

1. The film interfaces must be parallel;

2. The film interfaces must be tangentially immobile (i.e. the velocity at each interface is zero);

3. The bulk viscosity is independent of the film thickness;

4. There is no diffusion of oil into the surrounding water phase;

5. The capillary pressure remains constant during film drainage.

These assumptions impose severe restrictions on the use of the Stefan-Reynolds equation. For example, accelerated drainage rates have been observed in aqueous foam films containing weak surfactants, such as low molecular weight fatty alcohols (Manev et al., 1976). The drainage of liquid from such a film creates a Maragoni effect where the adsorbed surfactant molecules begin to flow along the film interfaces. The resulting

tangential velocity leads to a faster rate of drainage. In this case, the Stefan-Reynolds equation could not be used to describe the drainage rate since the second assumption would not be satisfied.

In general, the Stefan-Reynolds equation is limited to relatively small film sizes (e.g. film radius of less than 100 μm). For larger films, dimples often appear in the middle of the film indicating that the interfaces are no longer parallel. While symmetric drainage is possible in larger films, it is common to observe more complex, asymmetric film drainage. The symmetry of the dimple is often broken by the spontaneous formation of one or more thick bands of liquid known as *channels* (Figure 1.9). An attempt has been made to model the appearance of channels (Joye et al., 1994). The model is based on the concept that the thickness of the film boundary fluctuates over time. Under certain conditions, the fluctuations grow large enough to allow for the formation of channels. Once formed, the channels allow liquid to drain quickly from the middle of the film to the plateau border. A plane-parallel film often remains after the liquid has drained from the dimple and the channels have disappeared. At this point, symmetric drainage of the liquid from the film may continue. The overall effect is a rate of drainage that is much faster than the rate predicted by the Stefan-Reynolds equation.

Finally, it is important to note that unstable films will not always rupture during film drainage. It is possible for films to reach an equilibrium thickness and then rupture at a later time. In this case, the film lifetime will depend on both the rate of drainage and the kinetics of the rupture process. Exerowa and Kruglyakov (1998) provide an overview on the kinetics of film rupture.

1.3 Disjoining Pressure -Thickness Isotherms

In thin liquid films, the experimental and theoretical calculations of surface forces are described by isotherms of disjoining pressure versus thickness, $\Pi(h)$. In general, $\Pi(h)$ is defined as the excess pressure that arises from the molecular interactions between the film interfaces. The disjoining pressure is a function of film thickness and it acts normal to the film interfaces. By convention, repulsive forces are positive and attractive forces are negative (Bergeron and Radke, 1992). A direct measure of the disjoining pressure may be obtained from the TLF-PBT technique. As mentioned, a film reaches an

equilibrium thickness when the disjoining pressure balances the capillary pressure. A disjoining pressure-thickness isotherm may be generated by monitoring how the equilibrium film thickness changes with small incremental increases in applied capillary pressure.

The measured $\Pi(h)$ isotherm represents the net disjoining pressure acting within the film. Several individual surface forces may contribute to the net disjoining pressure, including electrostatic interactions, London-van der Waals interactions, steric interactions, and various other interactions due to the structure of the film. Assuming that the individual surface forces are independent of each other, the net disjoining pressure is simply the sum of the individual disjoining pressures:

$$\Pi = \Pi_{EL} + \Pi_{VW} + \Pi_{ST} + \Pi_{SC} \qquad [1.8]$$

where Π_{EL}, Π_{VW}, Π_{ST}, and Π_{SC} are the disjoining pressure contributions due to electrostatic, London-van der Waals, steric, and film structure related interactions, respectively. Other surface forces may also contribute to the net disjoining pressure. Israelachvili (1992) provides a complete review of various surface forces.

1.3.1 Electrostatic Interactions

A repulsive electrostatic force arises from the long-range interaction between two charged surfaces. A surface charge may be acquired from adsorbed ions or from adsorbed surfactant molecules. For aqueous films, charge neutrality is maintained by a diffuse layer of counter-ions that are attracted to the charged surfaces (Figure 1.10). The diffuse layer partially screens the interaction between the charged surfaces. Therefore, it is important to consider the distribution of the counter-ions in the diffuse layer when modeling the electrostatic interactions.

For a thin film, the contribution of the electrostatic interactions can be estimated from the following equation (Scheludko, 1967, Exerowa and Kruglyakov, 1998):

$$\Pi_{EL} = 2C_e R_g T \left(\cosh \frac{zF\phi_{h/2}}{R_g T} - 1 \right)$$ [1.9]

where C_e is the electrolyte concentration, R_g is the gas constant, T is the absolute temperature, z is the valence of the electrolyte, F is the Faraday constant, and $\phi_{h/2}$ is the potential at the center of the film. $\phi_{h/2}$ is related to the potential at the film interface, ϕ_o, through the following relation:

$$\kappa h = \sqrt{2} \int_{y_{h/2}}^{y_0} (\cosh y - \cosh y_{h/2})^{-1/2} \, dy$$ [1.10]

where

$$y = \frac{zF\phi}{R_g T}$$ [1.11]

and

$$\kappa = \sqrt{\frac{8\pi z^2 F^2 C_e}{\varepsilon_r \varepsilon_o R_g T}}$$ [1.12]

Here, κ is the inverse Debye length, ε_r is the relative dielectric constant, and ε_o is the electrical permittivity in a vacuum. In the expression for y, the subscripts O and h/2 mean that the term has been evaluated for the potential at the film interface and the center of the film, respectively. A complete discussion of electrostatic forces in thin liquid films may be found in Ivanov (1998).

In the case of water-in-oil emulsions, the relative dielectric constant of the diluted bitumen film is quite small (i.e. on the order of 4 to 5) and the counter-ion concentration is expected to be quite low (i.e. on the order of 10^{-6} M). Under these conditions, conventional DLVO theory suggests that the screened electrostatic force within the water/oil/water film will be negligible (Becher, 1987; Claesson et al., 2001). However, the low counter-ion concentration in the oil only suggests that there is no diffuse layer near the film interfaces of the water/oil/water film. It is still possible that a repulsive electrostatic force may still act between the film interfaces across the diluted bitumen

media. Recent attempts have been made to describe electrostatic repulsion in a non-polar media (Zholkovskij et al., 2001a; Zholkovskij et al., 2001b).

1.3.2 London-van der Waals Interactions

In an emulsion, an attractive London-van der Waals force arises from the interaction of two droplets of the same phase immersed in a continuous second phase. The London-van der Waals interactions are considered to be an accumulation of three different interactions: (1) dipole-dipole interactions, (2) dipole-induced dipole interactions, and (3) dispersion or induced dipole-induced dipole interactions. The dispersion interactions are due to the spontaneous fluctuations of the electron cloud in one molecule causing corresponding fluctuations of the electron cloud in a neighboring molecule (Masliyah, 1994). The sum of these fluctuations for all pair interactions leads to an attractive force between the two droplets.

There are two basic approaches to estimating the London-van der Waals force, the microscopic approach proposed by Hamaker and the macroscopic approach of Lifshitz. The first step in the microscopic approach is to estimate the interaction between two molecules. The total interaction between the two droplets across a continuous media is then obtained by summing the pair interactions. In the macroscopic approach, the London-van der Waals interaction is derived by considering the interaction of fluctuating electromagnetic fields between the two droplets as a whole.

In the microscopic approach, the contribution from the London-van der Waals interactions in thin films is usually calculated from the following simple relation (Exerowa and Kruglyakov, 1998):

$$\Pi_{vw} = -\frac{K}{h^3}$$ [1.13]

where K is the Hamaker constant. For a water/toluene-diluted-bitumen/water film, the Hamaker constant is on the order of 4×10^{-21} J (Nir and Vassilieff, 1988; Lyklema, 1991). Nir and Vassilieff (1988) provide a complete review of London-van der Waals interactions within thin films.

1.3.3 Steric Interactions

A steric force arises from the short range interactions between two interfaces containing adsorbed polymeric surfactants or nonionic surfactants. Steric forces also occur with adsorbed ionic surfactants when there is a sufficient electrolyte concentration to suppress the electrostatic force (Tadros, 1988). For example, a dense layer of polymeric surfactant may surround the water droplets of a water-in-oil emulsion. As two droplets approach one another, the layers of polymeric surfactant begin to overlap forcing the chains of the polymer surfactant into entropically unfavorable configurations. The result is a repulsive steric force. Steric interactions depend on several factors including the size of the surfactant, the orientation of the surfactant on the interface, whether the surfactant is physically or chemically adsorbed at the interface, and the nature of the continuous phase (Ivanov, 1988; Hiemenz and Rajagopalan, 1997). For this reason, it is difficult to develop a general expression that describes the steric interactions within a thin film.

An expression has been adapted from de Gennes (1987) for the simple case of polymer brushes adsorbed on two, plane parallel interfaces. Consider a thin film in which the film interfaces contain polymeric surfactants (Figure 1.11). The polymer chains are physically adsorbed onto the film interfaces such that the individual chains are separated by an average distance. D. The densely packed polymer surfactant forms a 'brush' that extends out into the solvent a distance, δ. As two film interfaces draw close together, the brushes begin to interact resulting in a positive disjoining pressure (i.e. repulsive force). The steric contribution to the disjoining pressure, Π_{ST}, is estimated from the following relation (Exerowa and Kruglyakov, 1998):

$$\Pi_{ST} = \frac{kT}{D^3}\left[\left(\frac{h}{\delta}\right)^{-\frac{9}{4}} - \left(\frac{h}{\delta}\right)^{\frac{3}{4}}\right]$$

[1.14]

where k is the Boltzmann constant and T is the absolute temperature. It is important to note that Eq. [1.14] is limited to film thicknesses less than twice the brush thickness

(i.e. h $\leq$ 2δ). The polymer brush model assumes that the steric contribution to disjoining pressure is zero when h > 2δ.

Eq. [1.13] follows a classical approach of separating the steric interactions into two different contributions. The first term in the brackets represents the contribution due to the osmotic pressure that arises from the increase in polymer concentration. The second term in the brackets is the entropic contribution or the elastic restoring force that arises from the coiling of the polymer chains (Exerowa and Kruglyakov, 1998). Tadros (1988) provides a review of more modern approaches to modeling steric interactions in thin liquid films.

1.3.4 Interactions Due to Film Structure

A 'structural' contribution to the disjoining pressure may arise from the formation of organized layers between the two film interfaces. For example, spherical micelles will form in an aqueous solution of sodium dodecyl sulfate (SDS) at concentrations above the critical micelle concentration. In the bulk solution, spherical micelles will be distributed randomly throughout the solution. In the confined volume of a thin film, the spherical micelles may form a lamellae structure between the two film interfaces. These types of films are commonly referred to as stratified films. Examples of stratified films include films containing layers of spherical SDS micelles (Manev et al., 1984; Nikolov and Wasan, 1989; Bergeron and Radke, 1992), layers of caseinate submicelles (Husband and Wilde, 1998), layers of silica nanospheres (Nikolov and Wasan, 1992), and layers of liquid crystal (Frieberg et al., 1974; Manev et al., 1977; Perez et al., 1988).

The drainage of stratified films occurs in a series of discrete decreases in film thickness, a process known as stepwise thinning. A schematic of the stepwise thinning process is shown in Figure 1.12. Here, the removal of a single layer of material (either micelles or liquid crystal) begins within a small region of the film. This region grows as more material is drained from the film. Eventually, an entire layer of the lamellae structure drains from the film resulting in a step decrease in film thickness. The size of each stepwise decrease in film thickness roughly corresponds to the thickness of a single layer. In the case of spherical micelles, the thickness of a single layer is equal to the effective diameter of the micelles where the effective diameter is the micelle diameter

plus twice the inverse Debye length (Nikolov and Wasan, 1989). For a liquid crystal structure, the thickness of the step decrease roughly corresponds to twice the length of the surfactant molecule (Perez et al., 1988). This process repeats until either film rupture or a stable film is obtained.

The structural contribution to disjoining pressure is related to the long range (Nikolov et al., 1989) or short range interactions (Perez et al., 1988) between the layers of the lamellae structure. As the film thins, the magnitude of the surface forces between the layers increases. The result is an oscillatory disjoining pressure-thickness isotherm similar to the one shown in Figure 1.13. The distance between each peak in the oscillatory force corresponds to the size of a single layer. An expression for the structural disjoining pressure, Π_{SC}, has been developed by Nikolov et al. (1989) for a film containing a layered structure of spherical micelles. The model assumes long range electrostatic repulsion between the layers of spherical micelles.

1.4 Bitumen and Water-in-Bitumen Emulsions

1.4.1 Defining Bitumen

Bitumen is a hydrocarbon mixture that exists in a solid or semi-solid state in natural deposits. Like most crude oils sources, bitumen contains thousands of different hydrocarbon compounds. Due to the complexity of these mixtures, it is impractical to classify the different crude oil sources based on their chemical composition. Instead, crude oils are normally classified by one or more of their physical properties. For example, UNITAR utilizes density and viscosity to define the different grades of crude oil (Table 1.1). The properties are generally reported at a standard temperature of 15.6°C.

TABLE 1.1: UNITAR definition of oils and bitumens (Gray, 1994).
Properties are reported at a standard temperature of 15.6°C.

Type	Viscosity (mPa.s)	Density (g/cm^3)	API Gravity
Conventional Oil	< 10^2	< 0.934	> 20
Heavy Oil	10^2 - 10^5	0.934 - 1.0	20 - 10
Bitumen	> 10^5	> 1.0	< 10

It is also common to report the density in terms of API gravity. API gravity is an expanded density scale that is defined, as follows (Gray, 1994):

$$°API = \frac{145}{\text{specific gravity at } 15.6°C} - 131.5$$ [1.15]

By this definition, water has an API gravity of 10. The molar ratio of hydrogen to carbon (H/C ratio) is another property known to vary between different types of fuels and crude oils. The H/C ratio is a good indicator of the heating value and combustion properties of a fuel. Table 1.2 provides a partial list of the H/C ratios for different fuels and crude oils.

Bitumens and crude oils may be separated into several classes or fractions on the basis of solubility and adsorption characteristics. The most commonly used solubility classes are solids, asphaltenes, and maltenes. Solids are considered to be any material that is insoluble in an aromatic solvent, like toluene. This includes fine clays, sands, and insoluble organic material. Asphaltenes are generally considered to be the fraction of bitumen that is soluble in aromatic solvents but insoluble in aliphatic solvents, such as heptane or pentane. Maltenes include all of the material that remains soluble in the aliphatic solvents. The maltenes may be further separated by column chromatography into resins (I and II), aromatics and saturates. The entire separation protocol is commonly known as SARA (Saturates, Aromatic, Resins, Asphaltenes) (Bulmer and Starr, 1979).

TABLE 1.2: H/C ratios for various fuels and crude oils (Gray, 1994).

Type	H/C Ratio
Methane	4.0
Gasoline, Diesel	1.9
Light Crude	1.8
Bitumen	1.4 - 1.6
Coal	0.5 - 0.8

Note that the separation between the various bitumen fractions is somewhat arbitrary. For example, the amount of asphaltenes that may be extracted from bitumen will depend strongly on the choice of solvents and the exact procedure used to perform the separation (Mitchell and Speight, 1973). Such an arbitrary separation will also affect the properties of each bitumen fraction.

1.4.2 Properties of Bitumen

This thesis is concerned primarily with bitumen taken from the Athabasca region of Alberta. The following review of the properties of Alberta bitumen is primarily drawn from Strausz (1989) and Gray (1994). The physical and chemical properties of bitumen and its fractions vary between samples taken from different sites. Significant variation has also been observed in the properties of samples taken from different locations within a single site (Prowse, 1983). For this reason, "typical" values or a range of values for the bitumen properties are normally quoted in the literature (Prowse, 1983). The typical values for the chemical and physical properties of Alberta bitumen are summarized in Tables 1.3 and 1.4. The typical fractional composition of Alberta bitumen is reported in Table 1.5. An elemental analysis of the SARA fractions obtained from an Athabasca bitumen is provided in Table 1.6.

TABLE 1.3: Elemental composition of Alberta bitumen (Strausz, 1989).

Element	Composition (wt%)
Carbon	81 – 84
Hydrogen	10 – 11
Nitrogen	0.3 – 0.6
Oxygen	0.8 – 1.6
Sulfur	4.6 – 5.6
Ash	0.5 – 1.0
Nickel	60 – 100 mg/kg
Vanadium	160 – 300 mg/kg

TABLE 1.4: Physical properties of Alberta bitumen (Strausz, 1989).

Property	Range of Values
H/C Ratio	1.46 – 1.50
Molar Mass	490 – 620 g/mol
Density (at 15°C)	0.97 – 1.02 g/cm^3
Viscosity (at 15°C)	10^4 - 10^6 mPa.s
Heat of Combustion	41.0 – 42.6 kJ/g

As mentioned, bitumen may be fractionated into saturates, aromatics, resins, and asphaltenes. The bulk of the saturate fraction is composed of a variety of alkyl cycloalkanes of one to five rings and a small amount of six ring compounds. The dicyclic compounds are generally the most abundant. The aromatic fraction consists of monoaromatic compounds as well as dinuclear and trinuclear aromatic compounds. A small amount of sulfur is present in the aromatic fraction in the form of benzothiophenes and alicyclic sulfides. A small amount of nitrogen is also present in the form of alkylated benzoquinolines and carbazoles. The resins consist primarily of heterocycles and a small

TABLE 1.5: Fractional composition of Alberta
bitumens (Strausz, 1989).

Bitumen Fraction	Composition (wt%)
Asphaltenes	13 – 22
Resins	29 – 49
Aromatics	18 – 32
Saturates	15 – 21

TABLE 1.6: Elemental analysis of SARA fractions from a typical Athabasca bitumen
(Prowse, 1983).

Bitumen Fraction	wt%	wt% C	wt% H	wt% N	wt% O	wt% S	H/C ratio
Whole Bitumen	-	83.31	10.59	0.41	0.88	4.78	1.53
Saturates	24.6	86.75	13.52	0.03	0.35	0.00	1.87
Aromatics	26.2	84.22	10.19	0.00	0.44	6.96	1.45
Resins I	27.6	81.16	9.70	0.77	2.60	6.17	1.43
Resins II	4.9	76.00	9.53	0.82	7.98	4.31	1.50
Asphaltenes	14.6	77.63	7.83	1.20	2.02	8.31	1.21

amount of carboxylic acids. The compounds in the resin fraction are similar to the heteroatom species found in the aromatic fraction. For this reason, the transition between the aromatic and resin fractions is not clear. In general, the resin fraction has a higher concentration of aromatic carbon, a higher concentration of heteroatoms, and a lower H/C ratio compared to the compounds found in the aromatic fraction. The distinction between resins and asphaltenes is even less clear. On average, the compounds that make up the asphaltene fraction have a higher molar mass, higher heteroatom concentration, and lower H/C ratio than the resin compounds (Strausz, 1989, Yarranton, 1997).

TABLE 1.7: Reported values of asphaltene molar mass (Yen and Chilingarian, 1994, Yarranton, 1997, 2000b, Mullins and Groenzin, 2000).

Experimental Method	Molar Mass (g/mol)
Cryoscopic	600 – 6000
Dynamic Light Scattering	20,000 – 100,000
Ebullioscopic	2500 – 4000
Equal Vapor Pressure	2000 - 3000
Fluorescence Depolarization	500 – 1000
Gel Permeation Chromatography	20,000 – 60,000
Monomolecular Film	80,000 – 140,000
Osmotic Pressure	20,000 – 80,000
Ultracentrifuge	20,000 – 300,000
Vapor Pressure Osmometry	1000 – 5000
Viscosity Determination	1000 – 4000
X-ray Diffraction	40,000

A large amount of research has focused on determining the chemical nature and size of the asphaltene molecules. Chemical analysis suggests that a 'typical' asphaltene molecule consists of several fused ring structures linked by flexible hydrocarbon chains (Strausz et al., 1992). A hypothetical example of an asphaltene molecule is shown in Figure 1.14. More recent findings indicate that the 'typical' asphaltene molecule may consist of only one or two fused ring structures with only one or two heteroatoms associated with each molecule (Groenzin and Mullins, 2000; Groenzin and Mullins, 2001). A hypothetical example of this smaller asphaltene molecule is shown Figure 1.15.

A variety of experimental techniques have been used to estimate the size or molar mass of asphaltenes. Table 1.7 lists just some of the wide range of values that have been reported. The large variation in molar mass is due mainly to the ability of asphaltene molecules to self associate. Asphaltenes are capable of forming micelles or colloidal particles at relatively low asphaltene concentrations. The most recent findings indicate

that a single asphaltene molecule has an average molar mass of 500 to 2000 g/mol (Yarranton, 2000b; Groenzin and Mullins, 2000; Groenzin and Mullins, 2001).

Athabasca bitumen is also known to contain about 2% low molecular weight natural surfactants, the largest fraction being naphthenic acids (Strausz, 1988). Naphthenic acids are a mixture of mono- and poly-cycloalkane carboxylic acids with aliphatic side chains of various lengths (Herman et al., 1993). Figure 1.16 shows some of the typical structures of naphthenic acids. The naphthenic acids may be extracted from bitumen by treating the bitumen with an alkaline solution. In the extraction process, naphthenic acids are converted into water-soluble sodium naphthenates. The molar mass of these surfactant ranges from 166 to 450 g/mol (Schramm et al., 2001).

1.4.3 Water-in-Bitumen Emulsions

As mentioned, extremely stable water-in-diluted-bitumen emulsions are formed during the bitumen extraction process. The water droplets are 2 to 5 μm in diameter and remain well-dispersed in the naphtha diluted bitumen. There is a very limited amount of fundamental information about the stability of water-in-diluted-bitumen emulsions, although a significant amount of information has been published on the stability of water-in-crude-oil emulsions. While not directly applicable, information from crude oil emulsions may be used to develop a hypothesis about the stability of bitumen emulsions. One of the keys to understanding water-in-bitumen emulsion stability is determining the surface active material that lies at the bitumen/water interface.

Both bitumen and crude oil contain a number of surface active compounds including waxes, resins, asphaltenes, low molecular weight surfactants (e.g. naphthenic acids), and fine solids partially coated with organic material (Sheu and Mullins, 1995; Yan et al., 1999; Yarranton, 1997; Kotlyar et al., 1998; Mouraille et al., 1998; Horváth-Szabó et al., 2001). In crude oils, most studies suggest that asphaltenes are primarily responsible for emulsion stability. McLean and Kilpatrick (1997a; 1997b) have proposed that the emulsion stability may be related to the solubility state of asphaltenes in the bulk crude oil. Their hypothesis suggests that the maximum emulsion stability occurs just before the onset of asphaltene precipitation when the asphaltenes are partially soluble in the crude oil and are highly surface active. This ideal solubility state may occur at low

resin to asphaltene ratios or in a crude oil diluted with a mixture of aromatic and aliphatic solvents. The hypothesis also suggests that the stability of the emulsion may be reduced by changing the solubility state of the asphaltenes. For example, the asphaltenes become highly soluble in the crude oil with the addition of large amounts of resinous or aromatic material. Under this condition, the asphaltenes are weakly surface active and hence, unable to provide a sufficient barrier to droplet coalescence. Alternatively, the emulsion stability may be reduced by using an aliphatic solvent to precipitate the asphaltenes. Without asphaltenes, there is very little surface active material to prevent the droplets from coalescing. Asphaltenes are also known to play a major role in the stability of water-in-diluted-bitumen emulsions (Yarranton, 1997). An experimental study by Xu et al. (1999) showed that emulsion stability may be reduced by removing only 2% of the material in bitumen. Since asphaltenes account for 13 to 22% of bitumen, this suggests that only a fraction of the asphaltenes may be responsible for emulsion stability. Kilpatrick (2001) and McLean et al. (1998) provide thorough reviews of the role of asphaltenes in emulsion stability.

Knowledge of the interaction forces between the water droplets is also important in understanding the stability of water-in-diluted-bitumen emulsions. It is generally assumed that the electrostatic forces are negligible in a water-in-bitumen emulsion and that the droplets must be stabilized by a steric force. While this appears to be a reasonable assumption, there is virtually no experimental evidence to support it. There are only a few studies on the interactions between colloidal particles within an oil media. A microcolloider has been used to measure the surface forces between two water droplets in a very dilute bitumen solution. It was concluded that the droplets were prevented from coalescing by a repulsive steric force created by an adsorption layer of non-uniform thickness (Wu et al., 1999). Another study used solid polar surfaces (e.g. mica) separated by a thin film of model oil to mimic the interactions between droplets of a water-in-oil emulsion (Claesson et al., 2001). Here, regions of both strong and weak repulsion were observed. It was assumed that both repulsive forces were due to steric origins. Christenson and Israelachvili (1987), using a surface force apparatus, measured a 'polymer-like' resistance and a 'hard wall' steric repulsion at 3.5 nm between two clay surfaces separated by a thin film of crude oil.

1.4.4 Affect of Aging on Bitumen and Emulsion Stability

In developing our understanding of water-in-bitumen emulsion stability, it is important to recognize the difference between industrial reality and the model emulsions created within a lab setting. A potentially important difference is related to the sampling and storage of a 'representative' sample of bitumen. It is well known that the properties of a crude oil and the stability of water-in-crude-oil emulsions may vary over time due to aging effects that occur during storage. There are several effects of aging including the loss of light ends due to evaporation, aggregation or precipitation of asphaltenes, and the oxidation of the different fractions of crude oil (Ronnisgsen et al., 1995). Such effects can lead to significant changes in the properties of bitumen including density, viscosity, interfacial tension, and solubility.

Sjoblom and coworkers have performed a series of studies that attempted to quantify the effect of aging on the properties of North Sea crude oil and on the stability of water-in-crude-oil emulsions. In these studies, several crude oils were aged in air at 50°C for upwards of 2 months. During this time, slight increases in the density and viscosity were observed which could be attributed to the evaporation of volatile components from the crude oil (Ronnisgsen et al., 1995). Other parameters, such as surface tension and acid number, were surprisingly unaffected by aging (Sjoblom et al., 1995). FT-IR spectrums of the crude oil indicated that the resinous and asphaltene fractions acquired oxygen in the form of carbonyl groups during the oxidation process (Sjoblom et al., 1995). No significant oxidation of the lighter saturate and aromatic fractions was observed. It was suggested that the oxidation of the resin and asphaltene fractions led to the generation of more interfacially active material and/or material that displayed higher interfacial activity. This notion is supported by interfacial tension measurements between crude oil and artificial formation water. It was found that the interfacial tension of all the crude oils tested decreased from 28-30 mN/m on the first day to as low as 15-16 mN/m after about 2 months of aging (Sjoblom et al., 1995). However, the authors also advised that a lower interfacial tension only favours the formation of small water droplets; it does not ensure more stable emulsions.

The effect of aging on emulsion stability was also found to depend on the specific source of North Sea crude oil. Sjoblom and coworkers studied emulsions made from

three different crude oils and from the interfacially active fractions (asphaltenes) of those three crude oils. In each case, the oil phase was aged in air at $50^\circ C$ for upwards of 2 months before being used to make a fresh emulsion. In general, the fresh water-in-crude-oil emulsions became more stable as the oil phase aged with a maximum stability eventually being achieved. Further aging of 2 of the 3 crude oils tested resulted in a *decrease* in the emulsion stability. The amount of increase or decrease in emulsion stability and the age at which the maximum stability occurred depended on the crude oil source (Sjoblom et al., 1995; Ronnisgsen et al., 1995). In the case of water-in-diluted-asphaltene emulsions, it is possible to see both an increase to a maximum in the emulsion stability with aging and a continuous decrease in emulsion stability throughout the entire time of aging (Ese et al., 1997).

Athabasca bitumen (the source of bitumen used throughout this particular study) is also known to age or oxidize over time. A series of studies by Moshopedis and Speight (1971; 1978) have identified a number of factors that enhance the rate of oxidation. For example, the presence of catalytic amounts of metal salts or the addition of an oxidizing agent (e.g. nitric acid) led to much faster rates of oxidation. A comparison of the elemental analysis on the bitumen before and after oxidation indicated that much of the oxygen uptake occurred in the resinous and asphaltene fractions of the bitumen. No significant oxygen uptake occurred in the lighter saturate and aromatic fractions of the bitumen (Moschopedis and Speight, 1973). Using infra-red spectroscopy, Moschopedis and Speight (1971) found that most of the oxygen was incorporated into the asphaltene molecules as carboxyl and phenolic hydroxyl groups. Oxidation also leads to a significant decrease in the resin content and a corresponding increase in the asphaltene or pentane-insoluble portion of bitumen (Moschopedis and Speight, 1973; 1975; 1977). Some degradation of the aromatic clusters was also observed, although this reaction required longer oxidation times and appeared to be much less significant than the oxidation reactions (Moschopedis and Speight, 1977).

The presence of a diluent and temperature, two factors that are of great importance to this thesis, have also been shown to influence the rate of oxidation (or aging). Moschopedis and Speight (1977) noted that "...bitumen oxidation with oxygen in the presence of a diluent causes marked increases in asphaltene content with a noticeable

reduction in asphaltene solubility". In particular, it was noted that the asphaltene content increased with both time and higher temperatures.

For this thesis, it is clear that aging (i.e. oxidation) could have an effect on the properties of the water/solvent-diluted-bitumen/water films. However, it is not clear how or to what extent that the aging will affect the measured surface forces. The emulsion studies on the North Sea crude oil suggest that aging could affect the stability of the thin films and the estimated magnitude of the surface forces. For this reason, several precautions were taken to reduce the affects of aging during the preparation and storage of the bitumen and asphaltenes. During the preparation of bitumen fractions, care was taken to ensure that the oil phase was never exposed to temperatures higher than 40°C for long periods of time. All samples of bitumen and its fractions were stored in a cool dark place in sealed glass containers. Diluents were not added to the samples until the day of testing and diluted samples were never used for more than one day. Some diluted samples were aged in a sealed container up to one week before being tested, although no significant changes in the film properties were observed.

It was expected that these precautions limited that amount of oxidation and hence, were adequate to ensure that aging did not lead to any significant variation in the measured thin film properties. However, the original bitumen sample had remained on a freezer shelf in a sealed metal container for more than twelve years before being used for this study. This raises the possibility of differences between the tested bitumen samples and fresh bitumen at the mine site. Future aging studies are required to determine the affect of long term bitumen storage on thin film behaviour.

1.5 References

Becher, P., *in* "Interfacial Phenomena in Apolar Media" edited by Eicke, H.F. and Parfitt, G.D., p.275-281. Marcel Dekker, New York, 1987.

Bergeron, V. and Radke, C.J., *Langmuir* **8** (1992) 3020-3026.

Bulmer, J.T. and Starr, J. (Eds.), "Syncrude Analytical Methods for Oil Sand and Bitumen Processing", Alberta Oil Sands Technology and Research Authority (AOSTRA), Edmonton, 1979.

Christenson, H.K. and Israelachvili, J.N., *J. Colloid Interface Sci.* **119** (1987) 194-202.

Claesson, P.M., Blomberg, E., and Poptoshev, E., *in* "Encylopedic Handbook of Emulsion Technology" edited by Sjöblom, J., p.305. Marcel Dekker, New York, 2001.

CONRAD, "Naphthenic Acids Background Information Discussion Report", CONRAD Environmental Aquatics Technical Advisory Group, Edmonton, June 1998.

Czarnecki, J., *in* "Encyclopedic Handbook of Emulsion Technology", edited by Sjöblom, J., p.497, Marcel Dekker, New York, 2001.

de Gennes, P.G., *Adv. Coll. Interface Sci.* **27** (1987) 189.

Ese, M.-H., Sjöblom, J., Førdedal, H., Urdahl, O., and Rønningsen, H.P., *Colloid Surf. A* **123-124** (1997) 225-232.

Exerowa, D. and Kruglyakov, P.M., "Foam and Foam Films", Elsevier, New York, 1998.

Friberg, S., Linden, St.,E., and Saito, H., *Nature* **251** (1974) 494-495.

Gray, M.R., "Upgrading Petroleum Residues and Heavy Oils", Marcel Dekker, New York, 1994.

Groenzin, H. and Mullins, O.C., *Energy & Fuels* **14** (2000) 677-684.

Groenzin, H. and Mullins, O.C., *Petrol Sci Technol* **19** (2001) 21-230.

Herman, D.C., Fedorak, P.M., MacKinnon, M.D., and Costerton, J.W., *in* "Hydrocarbon Bioremediation", edited by Hichee, R.E., Alleman, B.C., Hoeppel, R.E. and Miller, R.N., pp.274-277, Lewis Publishers, Boca Raton, 1993.

Hiemenz, P.C. and Rajagopalan, R., "Principles of Colloid and Surface Chemistry", 3rd Ed., Marcel Dekker, New York, 1997.

Horvath-Szabó, G., Czarnecki, J. and Masliyah, J., *J. Colloid Interface Sci.* **236** (2001) 233-241.

Husband, F.A. and Wilde, P.J., *J. Colloid Interface Sci.* **205** (1998) 316-322.

Israelachvili, J., "Intermolecular and Surface Forces", 2nd Ed., Academic Press, San Diego, 1991.

Ivanov, I.B. (Ed.), "Thin Liquid Films" Marcel Dekker, New York, 1988.

Johansen, E.J., Skjärvö, I.M., Lund, T., Sjöblom, J., Söderlund, H., and Boström, G., *Colloid Surf. A* **34** (1988/89) 353-370.

Joye, J.L., Hirasaki, G. and Miller, C., *Langmuir* **10** (1994) 3174.

Kilpatrick, P.K., *in* "Encyclopedic Handbook of Emulsion Technology", edited by Sjöblom, J., p.707, Marcel Dekker, New York, 2001.

Kotlyar, L.S., Sparks, D.B., Woods, J.R., Raymond, S., LePage Y. and Shelfantook, W., *Petroleum Science and Technology*, **16** (1998) 1.

Kruglyakov, P.M., *in* "Thin Liquid Films", edited by Ivanov, I.B., p.767, Marcel Dekker, New York, 1988.

Lyklema, J., "Fundamentals of Interface and Colloid Science", Vol.1, Academic Press, New York, 1991.

Manev, E., Proust, J.E. and Ter-Minassian-Saraga, L., *Colloid & Polymer Sci.* **255** (1977) 1133-1135.

Manev, E.D., Sazdanova, S.V. and Wasan, D.T., *Dispersion Sci.Technol.* **5** (1984) 111-117.

Manev, E., Vassilieff, C. and Ivanov, I.B., *Colloid Polym Sci* **254** (1976) 99.

McLean, J.D. and Kilpatrick, P.K., *J. Colloid Interface Sci.* **196** (1997a) 23-34.

McLean, J.D. and Kilpatrick, P.K., *J. Colloid Interface Sci.* **189** (1997b) 242-252.

McLean, J.D., Spiecker, P.M., Sullivan, A.P., and Kilpatrick, P.K., *in* "Structures and Dynamics of Asphaltenes", edited by Mullins, O.C. and Sheu, E.Y., p.377, Plenum Press, New York, 1998.

Mitchell, D.L. and Speight, J.G., *FUEL* **52** (1973) 149-152.

Moschopedis, S.E. and Speight, J.G., *FUEL* **50** (1971) 34-40.

Moschopedis, S.E. and Speight, J.G., *FUEL* **52** (1973) 83.

Moschopedis, S.E. and Speight, J.G., *FUEL* **54** (1975) 210-212.

Moschopedis, S.E. and Speight, J.G., *J. Materials Sci.* **12** (1977) 990-998.

Moschopedis, S.E., and Speight, J.G., *FUEL* **57** (1978) 235-240.

Mouraille, O., Skodvin, T., Sjöblom, J. and Peytany, J.L., *J. Dispersion Sci. Techn.*, **19** (1998) 339.

Nikolov, A.D. and Wasan, D.T., *J. Colloid Interface Sci.* **133** (1989) 1-12.

Nikolov, A.D. and Wasan D.T., *Langmuir* **8** (1992) 2985-2994.

Nir, S. and Vassilieff, C.S., *in* "Thin Liquid Films", edited by Ivanov, I.B., p.207, Marcel Dekker, New York, 1988.

Perez, E., Proust, J.E., and Ter-Minassian-Saraga, L., *in* "Thin Liquid Films", edited by Ivanov, I.B., p.891, Marcel Dekker, New York, 1988.

Prowse, D.R. (Ed.), "Some Physical Properties of Bitumen and Oil Sand", AOSTRA/ARC Industry Access Report, Alberta Research Council, Edmonton, 1983.

Rønningsen, H.P., Sjöblom, J., and Mingyuan, L., *Colloids Surf. A* **97** (1995) 119-128.

Schramm, L.L., Stasiuk, E.N. and MacKinnon, M., *in* "Surfactants, Fundamentals and Applications in the Petroleum Industry", edited by Schramm, L.L., 2001, in press.

Shaw, R.C., Schramm, L.L., and Czarnecki, J., *in* "Suspensions: Fundamentals and Applications in the Petroleum Industry", edited by Schramm, L.L., p.639, American Chemical Society, Washington, 1996.

Scheludko, A., *Adv. Coll. Interface Sci.* **1** (1967) 391.

Sheu, E.H. and Mullins, O.C. (Eds.), "Asphaltenes: Fundamentals and Applications", Plenum Press, New York, 1995.

Sjöblom, J., Mingyuan, L., Christy, A.A., Rønningsen, H.P., *Colloids Surf. A* **96** (1995) 261-272.

Strausz, O.P., *in* "44th UNITAR/UNDP International Conference on Heavy Crude and Tar Sands", Vol.2, p.607, 1988.

Strausz, O.P., *in* "AOSTRA Technical Handbook on Oil Sands, Bitumens and Heavy Oils", edited by Hepler, L.G. and His, C., AOSTRA Technical Publication Series #6, Edmonton, 1989.

Strausz, O.P., Mojelsky, T.W., and Lown E.M., *FUEL* 71 (1992) 1355-1363.

Tadros, Th.F., *in* "Thin Liquid Films", edited by Ivanov, I.B., p.331, Marcel Dekker, New York, 1988.

Wu. X., van de Ven, T.G.M., and Czarnecki, J., *Colloid Surf. A* 149 (1999) 577-583.

Xu, Y., Dabros, T., Hamza, H., and Shelfantook, B., *Petrol Sci Technol* 17 (1999) 1051-1070.

Yan, Z., Elliott, J.A.W., and Masliyah, J.H., *J. Colliod Interface Sci.* 230 (1999) 329-337.

Yarranton, H.Y., Ph.D. Thesis, University of Alberta, Edmonton, 1997.

Yarranton, H.W., Alboudwarej, H., and Jakher, R., *Ind. Eng. Chem. Res.* 39 (2000a) 2916-2964.

Yarranton, H.Y., Hussein, H. and Masliyah, J.H., *J. Colloid Interface Sci.* 228 (2000b) 52-63.

Yen, T.F. and Chilingarian, G.V. (Eds.), "Asphaltenes and Asphalts, 1", Elsevier Science, Amsterdam, 1994.

Zholkovskij, E., Czarnecki, J. and Masliyah, J., *J. Colloid Interface Sci.* 234 (2001a) 293-315.

Zholkovskij, E., Mishchuk, N., Dukhin, S., Masliyah, J. and Czarnecki, J., *J. Colloid Interface Sci.* (2001b) Submitted.
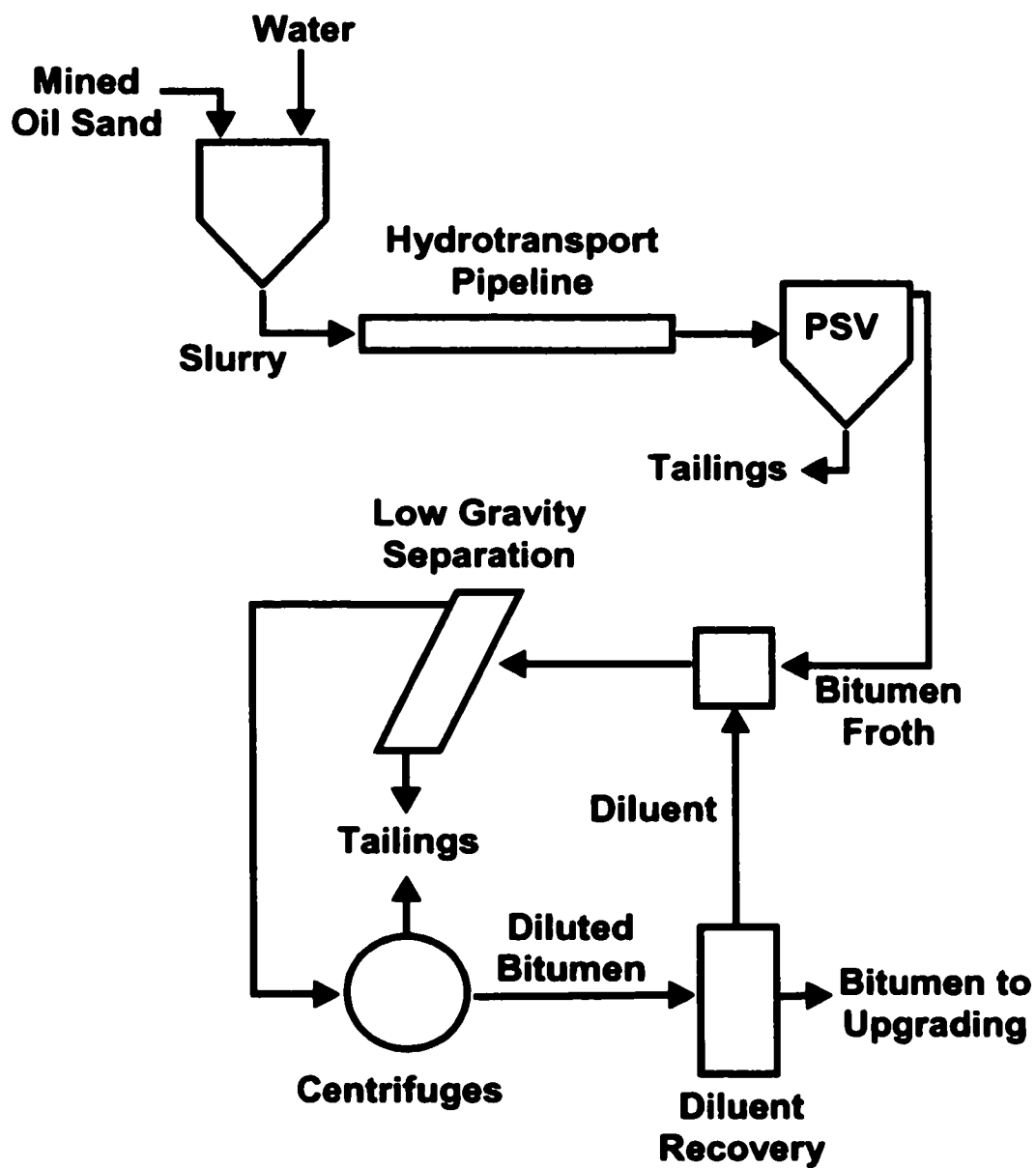
FIGURE 1.1: Schematic of typical bitumen extraction process.

air
———————
water
————————
solid

water
———————
oil
————————
water

(a)   (b)
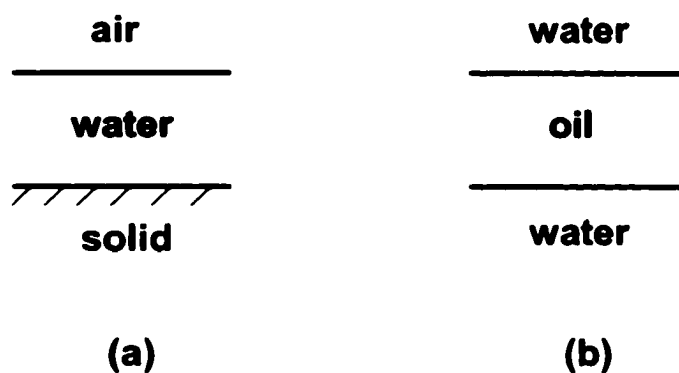
FIGURE 1.2: Examples of (a) an asymmetic film and (b) a symmetric thin film.

Coalescence

Unstable
Film

Stable
Film

Droplets
Approach

Thin Film
Formation

No
Coalescence
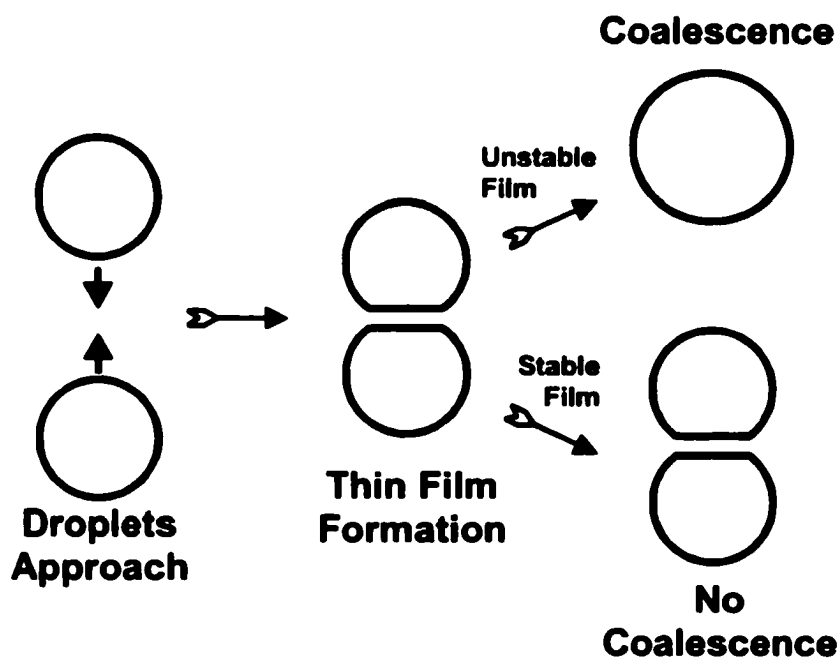
FIGURE 1.3: Schematic showing the dependence of water-in-bitumen emulsion stability on the stability of the thin film of oil formed between water droplets.
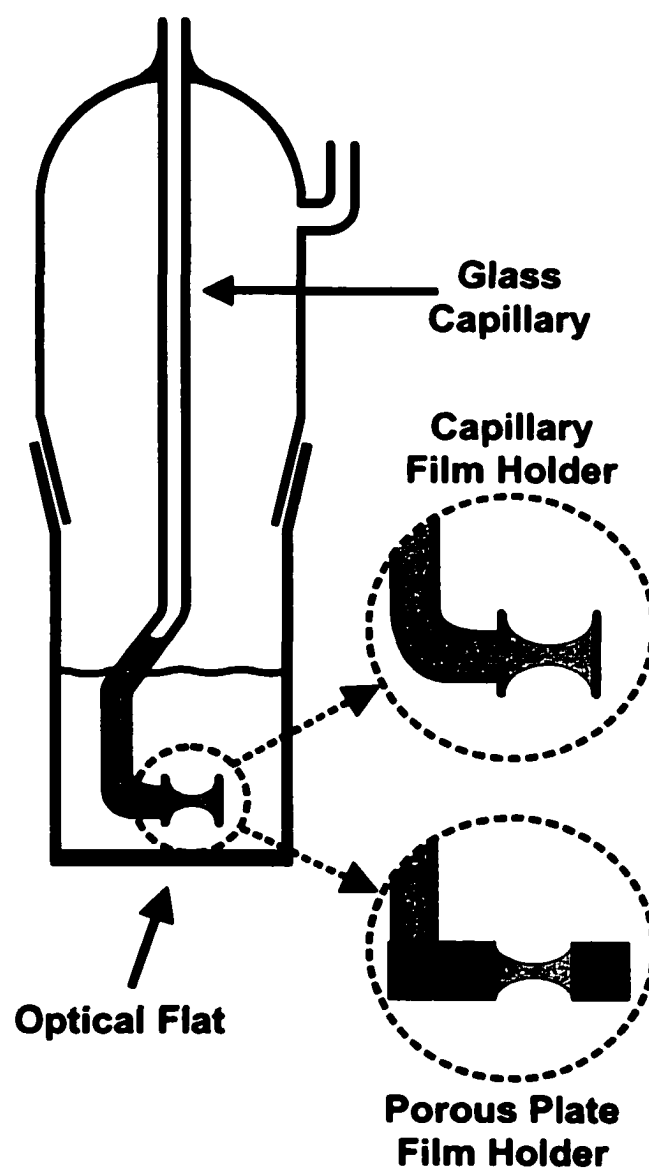
FIGURE 1.4: Schematic of glass measuring cell used in the Thin Liquid Film – Pressure Balance Technique showing the two basic types of film holders.
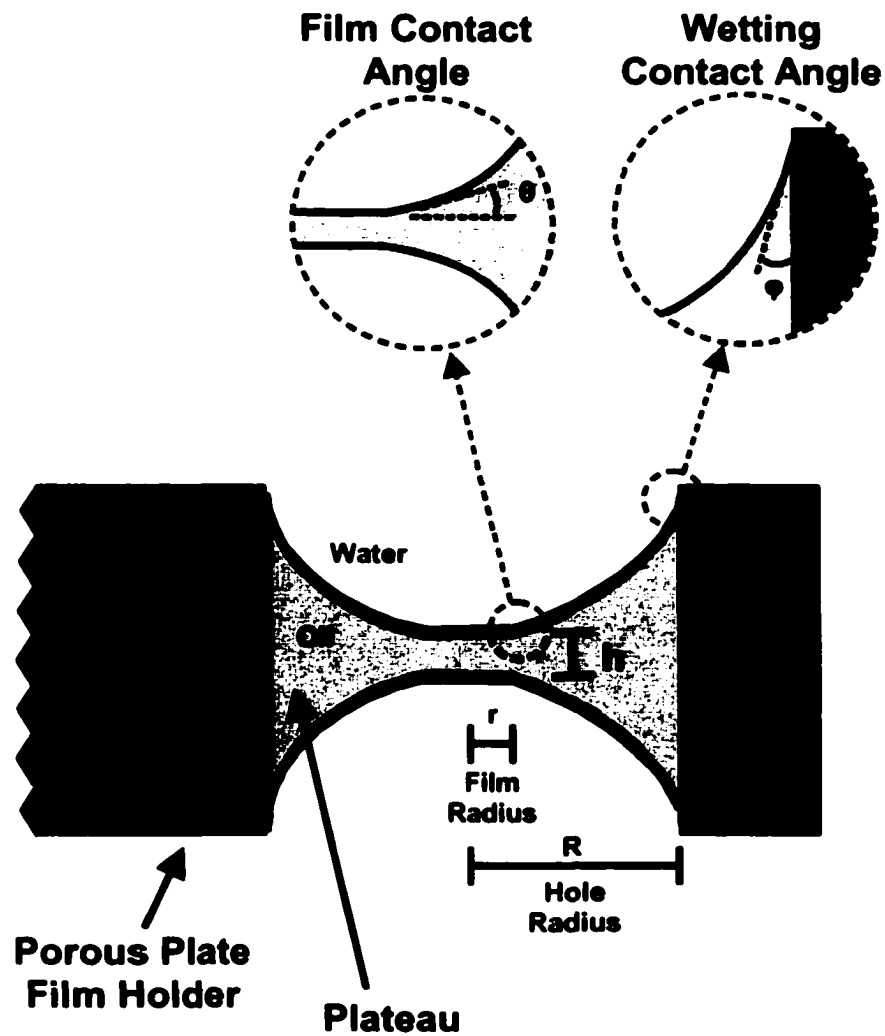
FIGURE 1.5: Terminology used to describe thin liquid films. The schematic is an example of a water/oil/water film formed using a porous plate film holder.
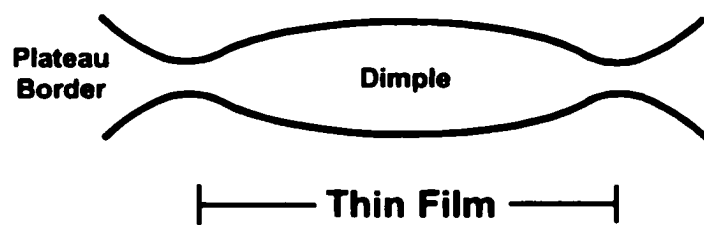
FIGURE 1.6: Schematic of thin film that contains a dimple.
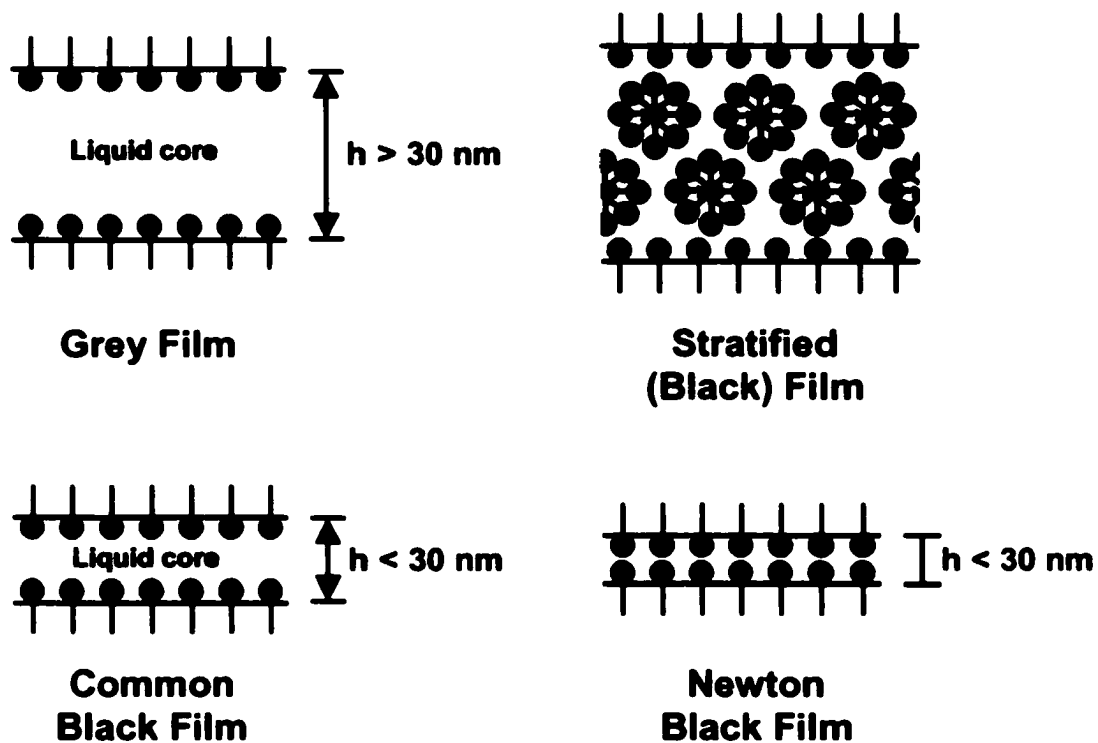
FIGURE 1.7: Schematic of the different types of films.
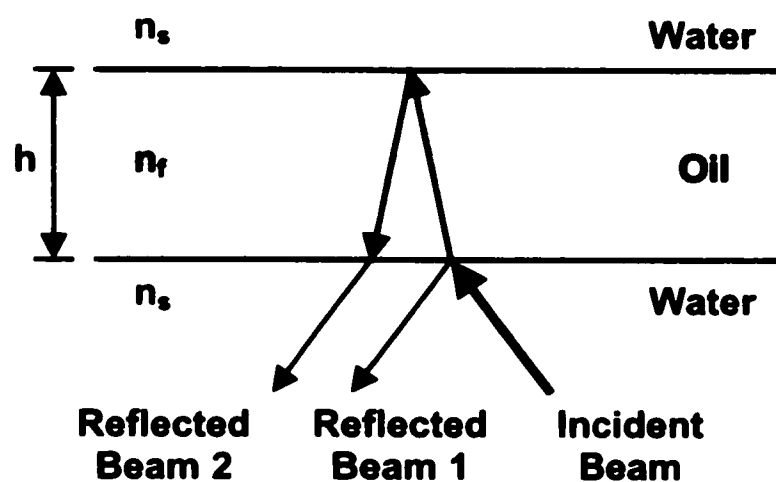
FIGURE 1.8: Single layer model of light reflection from a thin liquid film.
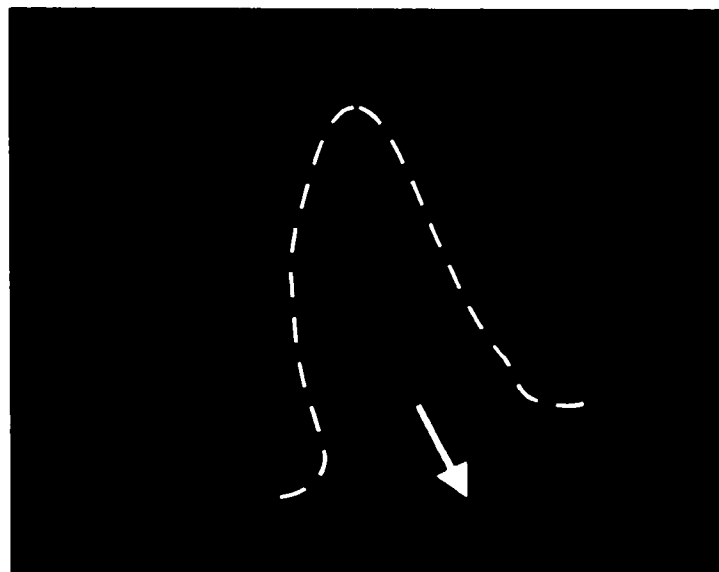
FIGURE 1.9: Image of asymmetric drainage in a water/toluene-diluted-bitumen/water film. The channel is outlined by the dashed white line and the direction of flow is indicated by the white arrow.
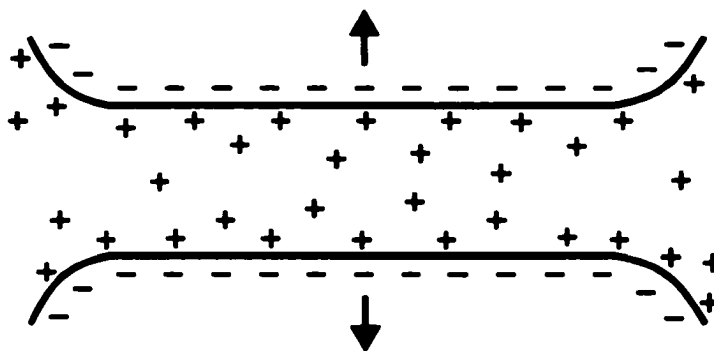
FIGURE 1.10: Electrostatic repulsion in an aqueous film.
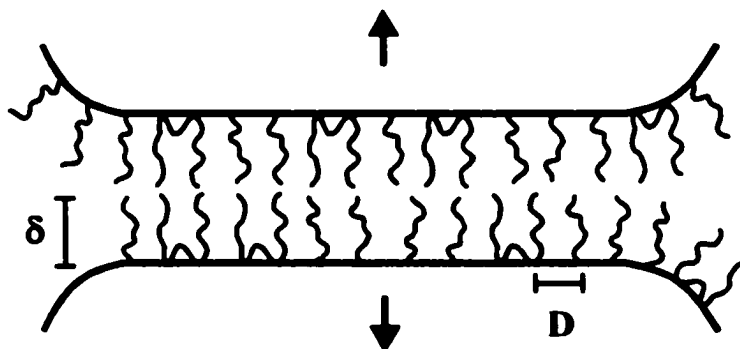
FIGURE 1.11: Steric repulsion created by a polymer brush.
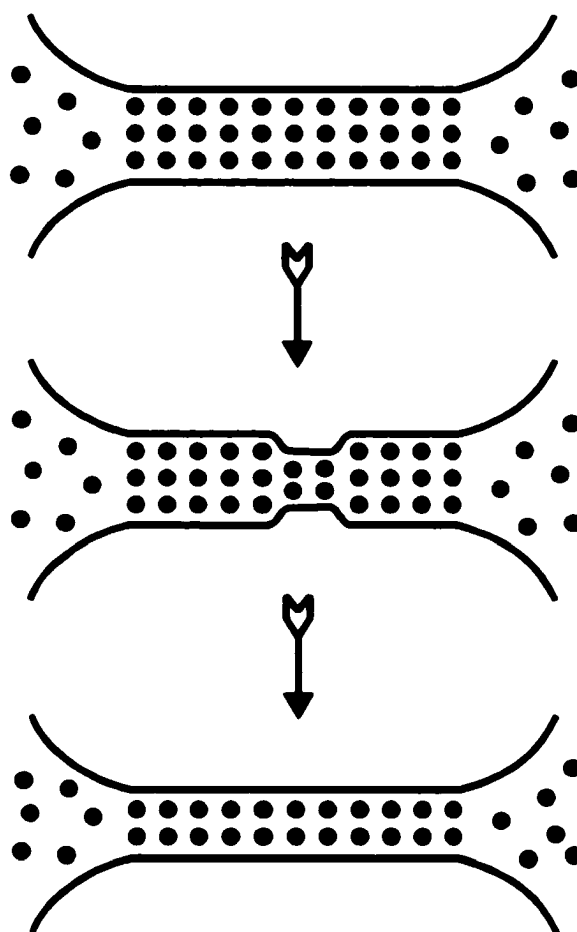
FIGURE 1.12: Schematic of the stepwise thinning process within a stratified film. The black circles may represent spherical micelles or silica nanospheres.
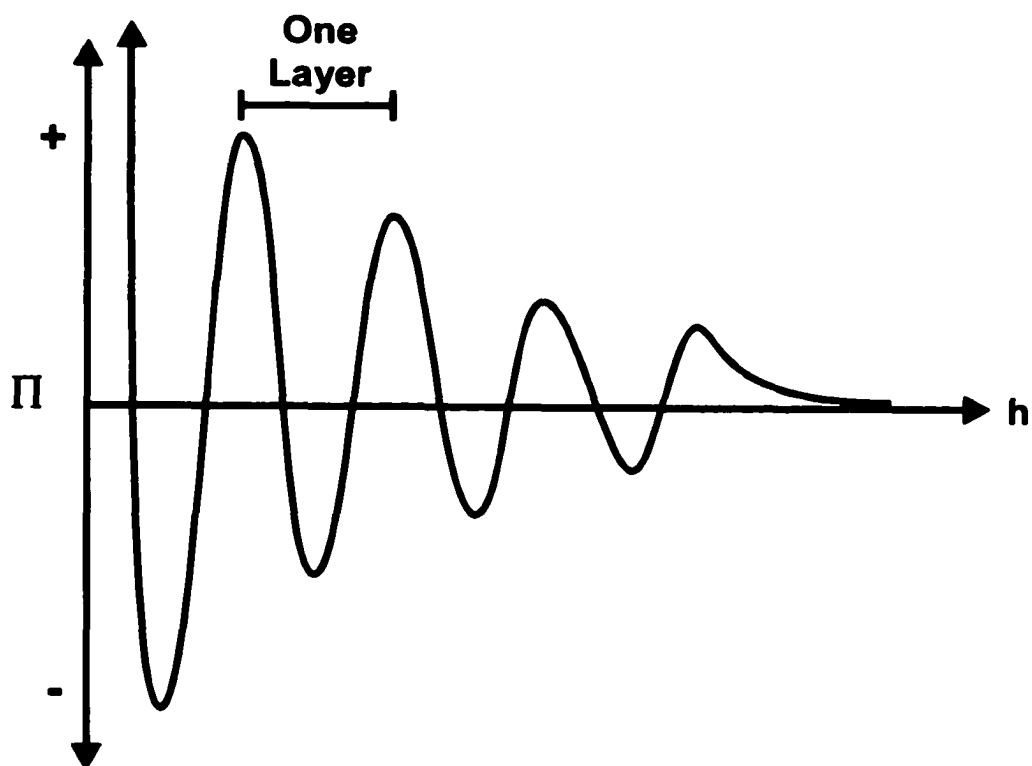
FIGURE 1.13: Schematic of the oscillatory disjoining pressure-thickness isotherm created by a lamellar structure within the film.
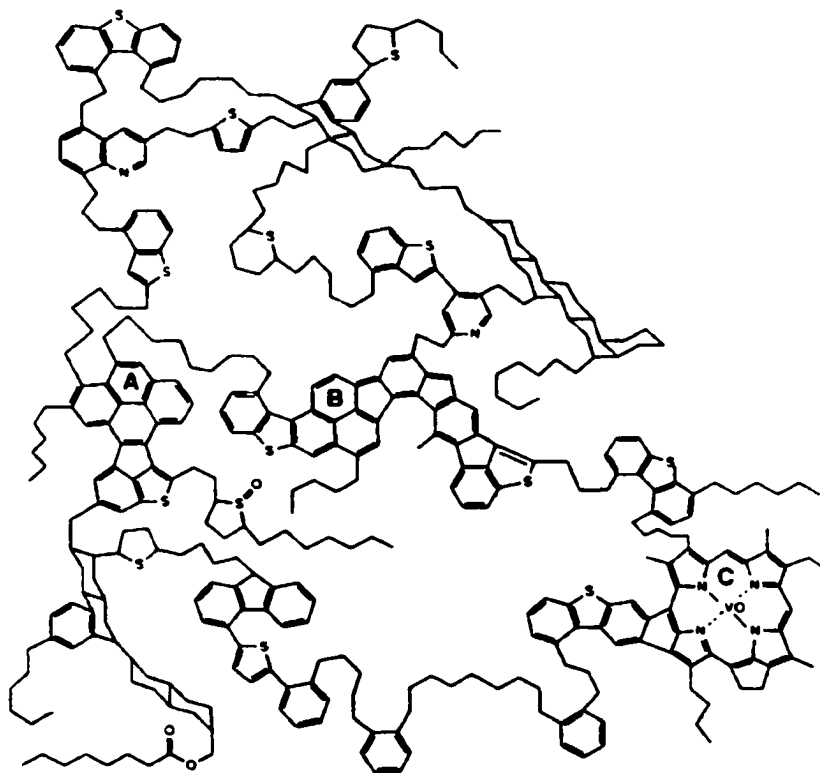
FIGURE 1.14: Hypothetical asphaltene molecule. A, B, and C represent large aromatic clusters. (Reproduced from Strausz et al. (1992)).
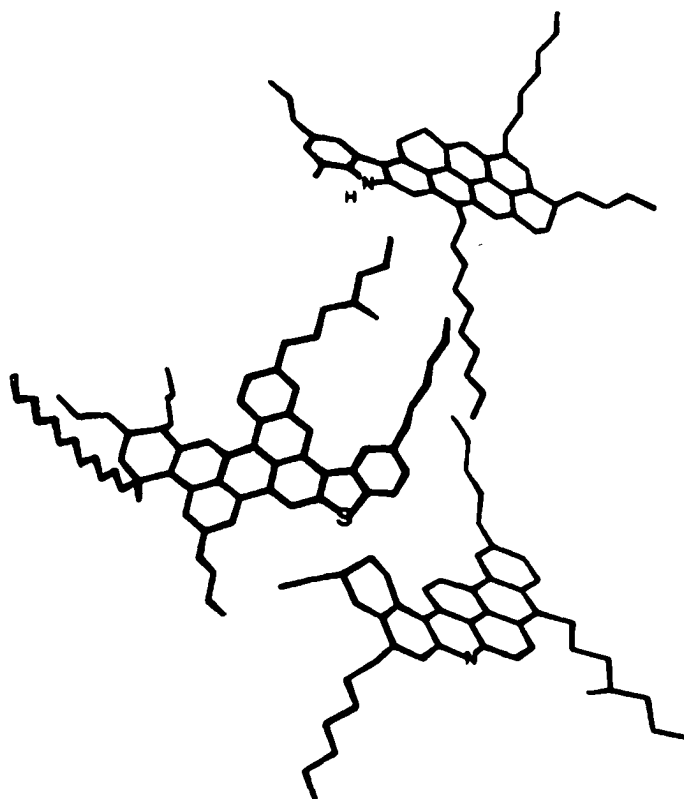
FIGURE 1.15: Hypothetical smaller apshaltene molecule. (Reproduced from Groenzin and Mullins (2000)).
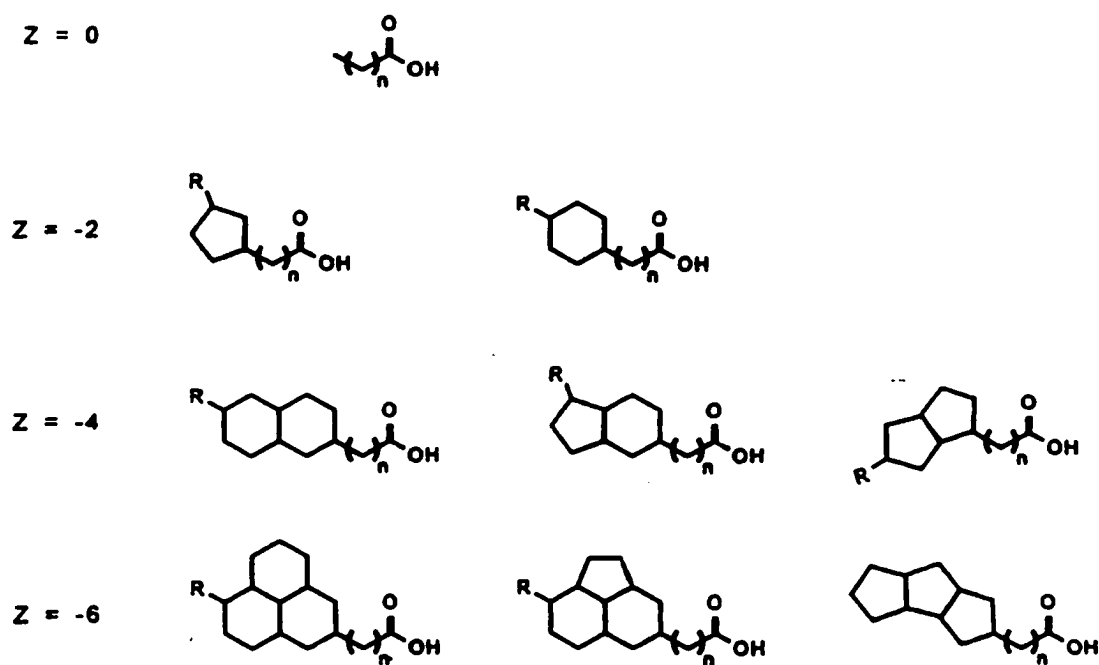
FIGURE 1.16: Typical structures of naphthenic acids. Z represents the number of hydrogen atoms lost with the formation of cyclic structures. (Reproduced from CONRAD (1998))

Chapter 2

Drainage Behaviour and Equivalent Thickness of Water-in-Diluted-Bitumen Emulsion Films[†]

2.1 Introduction

Up until last decade, oil-in-water emulsions have received significantly more attention in the literature than water-in-oil emulsions (Becher, 1987). Only recently has there been a focus on water-in-oil emulsions, particularly those occurring in the oil industry (Johansen et al., 1988; Ese et al., 1997; McLean and Kilpatrick, 1997a, 1997b; Mouraille et al., 1998; Opawale and Burgess, 1998). Very stable water-in-oil emulsions are a particular problem in the oil sands industry where water is used to extract bitumen from individual sand grains. However, in the process of bitumen upgrading to synthetic crude oil the salts contained within the emulsified water may cause severe corrosion problems (Kotlyar et al., 1998)

A number of studies (Johansen et al., 1988; Ese et al., 1997; McLean and Kilpatrick, 1997a, 1997b; Yan et al., 1999; Kotlyar et al., 1998; Mouraille et al., 1998; Opawale and Burgess, 1998) have been dedicated to elucidating the role of the various crude oil or bitumen components that are known to effect the stability of water-in-oil emulsions. Bitumen is a complex mixture of hydrocarbons that can be divided into several material classes. The classes include saturates, aromatics, resins, and asphaltenes. Asphaltenes are generally defined as the bitumen fraction that is soluble in an aromatic hydrocarbon, but insoluble in an aliphatic solvent. In the case of heptane, large asphaltene molecules begin to precipitate at a heptane:bitumen volume ratio of around 1.4:1 to 1.7:1 (Clarke and Pruden, 1998) with complete asphaltene precipitation occurring at volume ratios above 40:1. The asphaltene molecules are polyaromatic hydrocarbons that consist primarily of aromatic clusters and aliphatic chains along with a variety of functional

---

groups (Mitchell and Speight, 1973; Strausz et al., 1992). Resins consist of similar chemical species except the molecules, on average, have a lower molar mass, fewer functional groups, and a higher H/C ratio. Unlike asphaltenes, the resin molecules are soluble in both aromatic and aliphatic solvents. It is well-known that asphaltenes play a significant role in the stability of the water-in-bitumen emulsions (Johansen et al., 1988; Ese et al., 1997; McLean and Kilpatrick, 1997a, 1997b; Mouraille et al., 1998). Resins are considered to be surface active (Sheu and Mullins, 1995; McLean and Kilpatrick, 1997a, 1997b) and, to a limited extent, are capable of stabilizing an emulsion. McLean and Kilpatrick (1997a) have shown that the combination of resin and asphaltene at a ratio of around 1:3 (resin:asphaltene by weight) provides the most stable emulsions. The bitumen extracted from oil sands also contains very fine solids comprised of mainly clay particles coated with strongly bound toluene insoluble organic material. These solids are also suspected of playing a role in water-in-oil emulsion stability (Yan et al., 1997; Kotlyar et al., 1998).

An overview of the literature on water-in-bitumen emulsions reveals that the role of the thin liquid film formed between two approaching water droplets has remained relatively neglected. In fact, there are only a handful of studies in the literature on non-aqueous emulsion or foam films. Bergeron et al. (1997) showed that foam films of dodecane could be stabilized by steric forces generated by a fluorocarbon surfactant. Stericly stabilized systems have also been reported by other authors for both non-aqueous foam and emulsion films (Taylor and Haydon, 1966; Friberg et al., 1984; Friberg and Solans, 1986; Becher, 1987). To the author's knowledge there has been only one previous attempt to study water-bitumen-water films, made by Nikolov et al. (1997), which indicated that bitumen films diluted with heptane ruptured within a minute while films diluted with toluene were stable.

The goal of this chapter is to gain some insight into the mechanisms that stabilize water-in-bitumen emulsions through a systematic exploration of the properties of water/solvent-diluted-bitumen/water films using the Thin Liquid Film Pressure Balance Technique. Furthermore, we aim at determining the effect of the asphaltene, resin, and solid fractions on the film properties (drainage rate and equilibrium thickness) and

stability as well as how the film behavior is affected by a change from an aromatic to an aliphatic diluent.

2.2 Experimental Description

A thin liquid film is formed between two approaching water droplets, indicated by the rectangle in Figure 2.1(a). Since it is not practical to study a thin film within an emulsion, we use the Thin Liquid Film-Pressure Balance Technique (TLF-PBT) to recreate a single microscopic thin film inside a specially designed measuring cell (Exerowa and Scheludko, 1971). The drawing of the cell is shown in Figure 2.1(b). The principle of the technique involves balancing the imposed capillary pressure with the film disjoining pressure. A biconcave drop of oil is formed in the hole of a porous plate holder. The holder is immersed in water and some of the oil is withdrawn. A capillary pressure then arises at the edge of the film due to the curvature of the oil-water interface and the resulting pressure gradient forces liquid to drain from the film. As the liquid drains, the interfaces that bound the film begin to interact through van der Waals, electrostatic, steric, or other such surface forces. The overall effect of these forces is known as disjoining pressure. If the capillary pressure is balanced by the disjoining pressure, the film remains stable. However, the film is unstable and ruptures if the capillary pressure is larger than the maximum disjoining pressure. The stability of the thin film directly determines the stability of the emulsion.

The TLF-PBT uses reflected light to obtain an image of the film. A typical image is shown in Figure 2.1(c). From the pattern of light in the image and the changes in the light intensity over time, we are able to measure various parameters of the film (e.g. film thickness, film lifetime, and contact angle). These parameters allow us to determine the surface forces and surface structure that produce a stable film. To date, most of the research involving the TLF-PBT has focused mainly on aqueous foam and emulsion films. The result has been a well-developed theoretical background to interpret the vast amount of experimental data gathered during the years, enabling a better understanding of the mechanisms of stabilization of foam and oil/water/oil emulsion systems (Ivanov, 1995; Exerowa and Kruglyakov, 1998).

For this study, a number of modifications were made to the porous plate technique (Exerowa and Scheludko, 1971; Exerowa and Kruglyakov, 1998) to account for the special requirements of a water/solvent-diluted-bitumen/water film. First, the hole radius was drilled to 1 mm or less to prevent the less dense solvent-diluted-bitumen from floating out of the hole and up to the air/water surface. Second, special preparation methods were developed to ensure the porous plate holder functioned properly. Before use, new film holders were soaked for a minimum of 24 hr in a solution of equal parts bitumen and toluene to improve the wetting characteristics of the glass porous plate. Without this step, it was not possible to form the necessary biconcave drop in the hole of the plate. Finally, prior to every measurement the film holder was cleaned with ethanol and toluene. The bottom part of the cell was washed with glass cleaner followed by a thorough rinsing with copious amounts of deionized-ultra filtrated (DIUF) water. The entire cell was then placed in an oven at $175^{\circ}C$ for a minimum of 2 hr. Strict adherence to this cleaning procedure was required to ensure reproducible results.[+]

2.2.1 Apparatus

A schematic of the TLF-PBT set-up is shown in Figure 2.2. The porous plate measuring cell was placed in a thermostating device that was capable of regulating the temperature to within $\pm 0.1^{\circ}C$. The device rested on a X-Y transverse stage mounted on top of an Axiovert 100 reflected light microscope (Carl Zeiss Canada Ltd.). An optical flat welded to the bottom of the glass cell allowed the film to be observed from below. The film was viewed on a monitor (PVM-14N2A, Sony Corporation) via a CCD video camera (VK-C370, Hitachi) and images of the film were recorded using a VCR (M-752C, Toshiba) or 35 mm camera. The microscope itself rested on top of an anti-vibration table (Model 63-531, Technical Manufacturing Corporation). The capillary pressure was controlled by adjusting the height of the solution inside the capillary tube using a manually operated micrometer syringe (Gilmont Instruments). The syringe was mounted inside the thermostating device to reduce any possible temperature fluctuations. The

---

[+] A complete description of the cell preparation and calibration procedures can be found in Appendix C.

chamber temperature was monitored using a thermocouple linked to the same acquisition board.

2.2.2 Film Thickness Measurement

The film thickness was determined by the microinterferometric method of Scheludko and Exerowa (Scheludko, 1957; Scheludko, 1967; Exerowa and Scheludko, 1971; Exerowa and Kruglyakov, 1998). Heat-filtered light from a 100 W mercury arc lamp was directed through a monochromatic filter (λ = 546 nm). The incident light was directed through a pin-hole or iris diaphragm creating a ~10 μm spot focused onto the centre of the film. The reflected light passed through a second pin-hole diaphragm located just prior to the photodiode. Both diaphragms were required to eliminate any unnecessary light scatter from the porous plate or film meniscus. The intensity of reflected light was measured with a highly sensitive low-light, low-noise Si-photodiode (Hamamatsu Corporation) and recorded using a strip chart.

The equivalent thickness, h, was calculated using the equation developed by Scheludko and Platikanov (1961):

$$h = \left(\frac{\lambda}{2\pi n_f}\right) \arcsin\left(\frac{\Delta}{1 + \left[4N\ (1-N)^2\right]\left[1-\Delta\right]}\right)^{1/2} \qquad [2.1]$$

where $\Delta = (I - I_{min})/(I_{max} - I_{min})$ and $N = (n_f - n_s)^2/(n_f + n_s)^2$. I is the intensity of light reflected from the film with I_{min} and I_{max} correspond to the last minimum and maximum interference values. The refractive indices of the diluted bitumen film and the surrounding water are denoted by n_f and n_s, respectively. There were no attempts to calculate the actual film thickness since knowledge of the optical properties and the structure of the surface active materials at the oil-water interface were not known.

TABLE 2.1: Values of refractive index for liquids used in thin film experiments. All values at 20°C (Lide, 1990).

Material	Refractive Index
Toluene	1.4961
Heptane	1.3876
DIUF Water	1.332
Industrial Water	1.334

In calculating the equivalent thickness, Eq. [2.1] assumes that the film was optically homogeneous with n_f equal to the refractive index of the bulk bitumen solution. Unfortunately, values of refractive index for diluted bitumen could not be obtained by conventional methods (ASTM, 1992) due to the very dark (nearly black) color of the solution. The refractive index could only be measured for very dilute bitumen solutions (Buckley et al., 1998). Therefore, to be able to calculate a thickness, it was necessary to assume that the refractive index of the diluted bitumen solutions, n_f, was equal to the value of the pure diluent. A list the refractive indices of the diluting solvents and surrounding water are given in Table 2.1.

2.2.3 Capillary Pressure

For flat films that have reached an equilibrium thickness, the disjoining pressure, Π, is balanced by the applied capillary pressure, P_C. An expression for the capillary pressure may be obtained by performing a pressure balance over the entire cell:

$$\Pi = P_C = P_{atm} + \rho_w g z_w - \rho_o g z_o - P_{ref}$$

[2.2]

where g is the acceleration due to gravity, z_w is the height of the water above the film, z_o is the height of the oil in the capillary, P_{atm} is atmospheric pressure within the cell and ρ_w and ρ_o are the densities of the water and oil phases, respectively. Both pressures are

defined in Figure 2.3 along with z_w and z_o, which are the column heights of the water and oil, respectively.

The reference pressure, P_{ref}, inside the cell can be assumed to be equal to atmospheric pressure plus an applied pressure, $P_{ref} = P_{atm} + P_{applied}$. Substituting this relation into Eq. [2.2] provides a working relation for the disjoining pressure:

$$\Pi = P_C = \rho_w g z_w - \rho_o g z_o - P_{applied}$$ [2.3]

Although tedious, all of the parameters on the right side of Eq. [2.3] are measurable. For simplicity, the capillary pressure was estimated using the well-known relation for the capillary pressure of a plane-parallel film (Exerowa et al., 1964):

$$P_C = 2\gamma \frac{R}{R^2 - r^2}$$ [2.4]

where γ is the interfacial tension, r is the film radius and R is the hole radius.

All experiments were conducted with a hole radius of R = 750 μm. The film radius was kept constant at r = 100 μm by adjusting the capillary pressure with the micrometer syringe. Using the measured interfacial tensions given in Figure 2.4, the calculated capillary pressure ranged from 38 to 48 Pa for toluene diluted bitumen films and from 34 to 42 Pa for the heptane diluted bitumen films.

2.2.4 Materials[+]

Coker feed Athabasca bitumen was supplied by Syncrude Canada, Ltd. Coker feed bitumen had already been treated to remove coarse sand and water and was ready for upgrading. Deasphalted bitumen (i.e. bitumen with asphaltenes and solids fractions removed) was obtained by diluting bitumen with heptane to a volume ratio of 40:1 (heptane:bitumen). The mixture was stirred for 4 h and left to settle overnight. The supernatant liquid was filtered to remove the precipitate and then placed in an oven at

---

[+] A complete description of the procedures used for materials preparation can be found in Appendix D.

40°C to evaporate the solvent. When the change in mass was less than 0.1 % over a 24 h period, the deasphalted bitumen was removed from the oven. The asphaltene fraction was recovered by dissolving the dried precipitate with toluene and then centrifuging the solution at 9400g for about 5 min to remove the fine solids associated with the precipitated asphaltenes. The supernatant was decanted and placed into an oven at 40°C until the asphaltenes were completely dry (Yarranton, 1997). The resin fractions (I & II) of bitumen were obtained using the SARA method (Bulmer and Starr, 1979) although only the resins-I fraction was used in the thin film measurements.

Solids-free bitumen was prepared by first diluting bitumen with toluene to a volume ratio of 100:1 (toluene:bitumen). The mixture was shaken for 1 h before being placed in a centrifuge for 45 min at 19,200g. The supernatant was then filtered through a 0.22 μm filter (Millipore Corporation, Cat. No. GSWP 047 00) and placed in an oven at 40°C to evaporate the solvent. The solids-free bitumen was removed from the oven when the change in mass over a 24 h period was less than 0.1 %. This procedure removed all solid material larger that 0.1 μm.

The thin film measurements utilized mixtures of diluted bitumen that were prepared with HPLC-grade toluene or HPLC-grade n-heptane (Fisher Scientific). The mixtures were prepared by mixing a predetermined weight ratio of solvent:bitumen. The samples were then shaken for 1 to 2 h to ensure that all the bitumen material was dissolved. Since diluted bitumen is suspected of altering its chemical composition over time when exposed to air (Moschopedis and Speight, 1977), samples were used immediately after preparation to avoid any possible aging effects. Three separate samples were made at each weight ratio for sample repeatability.

All films were immersed in a simulated industrial water (pH ~ 8.2). The simulated industrial water was practically identical in ionic strength and pH to the average values observed in Syncrude's recycled plant water. The simulated industrial water was prepared be adding 0.014 M sodium chloride, 0.012 M sodium bicarbonate, and 0.004 M sodium sulfate to deionized ultra filtrated (DIUF) water (Fisher Scientific). Additional thin film studies were conducted with DIUF water to determine whether the added salts affected the film behavior.

2.2.5 Procedures

Prior to each measurement, the holder was soaked in the diluted bitumen sample for 10 min to ensure the sample completely penetrated the entire porous plate. A small amount of sample was also drawn up into the capillary tube. Approximately 10 mL of industrial water was added to the bottom portion of the cell and the holder was then immersed in the water as the cell was assembled. The cell was placed inside the thermostating device and the temperature allowed to equilibrate to $23.0 \pm 0.1^{\circ}C$. A biconcave drop of diluted bitumen was formed in the holder and the pressure slowly increased until a thin film appeared. In addition to visual observations, equilibrium film thickness and film lifetime were measured. A series of films were made over several hours to obtain repeat data and to note any significant changes in film behavior with time.

2.2.6 Interfacial Tension

Interfacial tensions of diluted bitumen over simulated industrial water were measured with a Fisher deNouy ring tensiometer accurate to ± 0.5 mN/m. The results are displayed in Figure 2.4. For each measurement, the platinum ring was placed in the water and the surface tension of water checked. The diluted bitumen was then added drop by drop to the water surface and the two-phase system left to equilibrate for two hours before pulling the ring through the interface. Before each measurement, the ring was cleaned with toluene and placed in a flame to burn off any surface contaminants. All measurements were corrected for the solvent density using an equation based on the Harkins and Jordan tables (Harkins and Jordan, 1930; Yarranton, 1997).

2.2.7 Viscosity

The viscosity of toluene diluted bitumen was measured using a double gap bob viscometer (Rheomat 115, Contraves). Solutions for viscosity measurement were prepared using the preparation procedure outlined above for thin film samples. All solutions were made and tested on the same day to avoid aging consequences.

2.3 Results and Discussion

2.3.1 Film Drainage: Toluene Diluted Bitumen Films

Figure 2.5 displays a series of images of the typical drainage pattern for a toluene diluted bitumen film, from the initial formation of the film to the equilibrium grey film. A single centre dimple appeared upon initial film formation (Figure 2.5(a)) and after about 30 s, the liquid in the dimple would drain off through channels (Figure 2.5(b)) until a uniform white/yellow film was reached. The film would then continue to slowly drain as a nearly plane-parallel film. As equilibrium was approached, it was common for a slightly thinner, dark grey region to appear in the centre of the film that would subsequently disappear once an equilibrium film was obtained (Figure 2.5(c)). The final, stable film was a uniform grey color with the shade of grey growing darker with increasing diluent ratio (i.e. light grey for 1:1 toluene:bitumen films compared to a very dark grey for films of dilution 20:1 or greater). At higher diluent ratios (10:1 to 20:1), several 'blurry' white dimples of trapped liquid approximately 3 to 5 μm in diameter often appeared in the dark grey films similar to those observed by Bergeron (1997) in hydrocarbon foam films. The only exception to the described drainage pattern occurred at toluene:bitumen ratios of 40:1 or higher. In this case a black film was formed via unevenly shaped black spots and small 'blurry' white spots again appeared on the equilibrium film. A slight decrease in the film thickness to an equilibrium value was also observed after the black film had been formed. All of the toluene diluted bitumen films remained stable for over an hour although films of toluene ratio 40:1 tended to occasionally rupture after only about five minutes.

The rate of film drainage depended strongly on the toluene:bitumen ratio with the most concentrated solution (i.e. 1:1) taking nearly an hour to drain to its final thickness while more dilute solutions (i.e. 5:1 or greater) required only 5 min or less to reach equilibrium. The most dominant factor in determining the drainage rate appeared to be the bulk viscosity of the bitumen solution. To check the effect of viscosity, the drainage time, t, was calculated using the Stefan-Reynolds relation adapted to thinning circular microscopic films (Scheludko, 1967, Exerowa and Scheludko, 1971):[+]

[+] A complete derivation of the Stefan-Reynolds equation can be found in Appendix E

TABLE 2.2: Viscosity of toluene diluted bitumen at 23°C.

Toluene:Bitumen (wt:wt)	Viscosity (mPa s)
1:1	9.16
3:1	2.02
5:1	1.42
10:1	1.01*
20:1	1.01*

(*Viscosity of pure toluene)

$$-\frac{dh}{dt} = \frac{2}{3}\frac{h^3 \Delta P}{\eta r^2}$$

[2.5]

At large film thicknesses, the disjoining pressure is negligible and the driving force, ΔP, is simply equal to the capillary pressure. Integration of Eq. [2.5] leads to an expression for the drainage time, t:

$$t = \frac{3}{8}\frac{\eta R r^2}{\gamma}\left(h^{-2} - h_o^{-2}\right)$$

[2.6]

where h_o and h are the initial and final film thickness, respectively. The hole radius, $R = 750$ μm, and the film radius, $r = 100$ μm, remain constant throughout the experiment. The data for viscosity, η, is given in Table 2.2 and the oil-water interfacial tension, γ, is given in Figure 2.4.

The values of the drainage time calculated from Eq. [2.6] for a film of thickness $h_o = 91$ nm (i.e. thickness at I_{max}) to a thickness of $h = 30$ nm are shown on Figure 2.6 (solid diamonds - ◆). It was assumed that the disjoining pressure was negligible over this range of thickness. There is good agreement between the experimentally measured drainage times (open triangles - △) and the calculated values confirming that viscosity was a dominant factor in determining the drainage rate of the toluene-diluted bitumen films.

2.3.2 Film Drainage: Heptane Diluted Bitumen Films

With no asphaltene precipitation (i.e. at 1:1 heptane:bitumen where no asphaltene precipitation occurs), the behavior of the heptane diluted bitumen films were very similar to the toluene diluted bitumen films described above. The film was formed with a single centre dimple, followed by channel drainage to a uniform white/yellow film that would continue to drain to an equilibrium grey film via plane-parallel drainage. When asphaltene precipitation began to occur at heptane:bitumen ratios of 1.7:1 or higher (Clarke and Pruden, 1998), black spots would appear within 5 to 10 s after film formation (Figure 2.7(a) and 2.7(b)). The black spots quickly coalesced into a uniform black film with several small white spots of about 1 to 3 μm in diameter (Figure 2.7(c)). A slight decrease in film thickness was observed once the black film had been formed.

In the dilution range of 2:1 to 7.5:1 heptane:bitumen, the white spots appeared to be a random scatter of individual spots similar to the white spots (dimples) observed by other researchers (Joye et al., 1992; Bergeron et al., 1997; Horiuchi et al., 1998). The ability to drain these white spots from the film by reducing the film diameter indicated that the spots were simply small amounts of liquid trapped within the film. For dilutions between 10:1 and 20:1, several small white spots formed a fine network of mainly 5- and 6-sided shapes with the bright white spots occupying the corners and light grey 'struts' joining the corners (Figure 2.8). The network only became clear a few seconds after the black film had been formed. The cause for the repeatable geometric pattern observed in the network was unclear although it was probably related to the presence of tiny precipitated asphaltene particles and/or soluble asphaltene-resin aggregates.

About half an hour after loading the cell, small aggregates of asphaltene precipitate began to appear near the oil/water interface. The aggregates were approximately 5 to 10 μm in diameter close to the mean particle size of 7.0 ± 4.0 μm reported by Li and Wan (1995). Over time (>2 hr), the number of asphaltene aggregates would continue to increase until any newly formed film would become completely clogged preventing it from draining.

The stability of the heptane-bitumen emulsion films depended strongly on the diluent ratio. At a ratio of 1:1, the film remained stable for at least an hour while films of

2:1 to 3:1 dilution remained stable for at least 20 min. The stability of the film then dramatically decreased with increasing diluent ratio causing the film lifetime to fall to less than 25 s for ratios of 20:1 or more (Figure 2.9).

2.3.3 Film Thickness: Bitumen

Measurements of equivalent thickness were performed for films at a constant radius, r = 100µm. The effect of the diluent:bitumen ratio on the film thickness is shown in Figure 2.10 for toluene-diluted bitumen emulsion films. At toluene:bitumen ratios from 1:1 to 3:1, the thickness values scattered within a wide range. These films required long periods of time to reach equilibrium and the film diameter would start to fluctuate resulting in a large variation in the measured film thickness. At dilution ratios of 20:1 or greater, the thickness reached a value of about 15 nm, which did not change with further dilution (i.e. a plateau was reached). The diluted bitumen films at these dilution ratios probably acquired a bilayer structure while films of lower dilutions ($\leq 3:1$) probably have a multilayer structure, although this assumption cannot be proven without measuring the disjoining pressure isotherms, $\Pi(h)$ (see Chapter 3).

The effect of the diluent:bitumen ratio on thickness for the heptane-diluted bitumen films is presented in Figure 2.11. Below the precipitation point, at a heptane:bitumen ratio of 1:1, the film drained to an equilibrium grey film of about 27 nm thickness. Above the precipitation point, at a heptane/bitumen ratio of 2:1, the black film reached a thickness of about 28 nm. The film thickness then decreased with increasing diluent:bitumen ratio to about 10 nm at a ratio of 20:1. The thickness then remained constant indicating that a bilayer film was probably reached. At lower diluent ratios (<20:1), the greater thickness of heptane-bitumen films may be caused by the presence of unprecipitated asphaltenes.

A comparison of the thickness of both heptane- and toluene-diluted films (Figure 2.12, curves 1 and 2, respectively) indicated a consistently lower thickness for heptane-diluted films. One would expect that the presence of the resins, asphaltenes, and solids fractions determined the thickness and behavior of the emulsion films. The effect

of each fraction can be isolated to determine which fraction(s) dominated the film behavior in each solvent.

2.3.4 Film Thickness: Solids Free Bitumen

The solids fraction of bitumen consists of fine submicron clay particles that have been rendered 'asphaltene-like' due to the adsorption of highly aromatic, polar material onto the particles surfaces (Kotlyar et al., 1998). To determine if this solid fraction played a role in the film behaviour, a 'solids-free' bitumen was prepared where all solid material larger than 0.1 μm was removed from the bitumen. Films of toluene- and heptane-diluted solids-free bitumen showed little or no change in both the drainage patterns and the film thickness (open squares - □- in Figures 2.10 and 2.11) indicating that the fine solids had no effect on the behavior of water/solvent-diluted-bitumen/water films. This finding appears to contradict Yan et al. (1999) who found that fine solids larger than 0.22 μm showed a strong ability to stabilize water-in-bitumen emulsions.

Solid particles were observed at or near the oil-water interface on several occasions in toluene-diluted-bitumen films. The particles were easily pushed away from the film when the films were first formed and never appeared in the film itself. For the solids fraction to play a role in emulsion stability, we expect that the fine clay particles probably build up in the Plateau borders around water droplets and clog the drainage routes through the emulsion. The drainage of the continuous oil phase from between the water droplets would be much slower thus providing the emulsion with additional kinetic stability.

2.3.5 Film Thickness: Simulated Industrial Water Versus DIUF Water

To determine whether the presence of salt in the aqueous phase had an effect on the film behavior, a few experiments were repeated using DIUF water instead of the simulated industrial water. Figures 2.10 and 2.11 (open triangle - Δ) show that the film thickness remained unchanged in the absence of salt. The drainage pattern of both types of films also remained unaffected. Both results indicated that at the given concentration,

the presence of salt in simulated industrial water had no observable affect on the film behavior.

2.3.6 Film Thickness: Resins

The effect of the resins was isolated by studying a number of thin films of diluted deasphalted bitumen (i.e. free of asphaltene and solid fractions) and diluted resins-I. Most of the experiments were conducted using deasphalted bitumen due to the high cost and long time needed to isolate a small amount of resin-I through the SARA method (Bulmer and Starr, 1979). The experiments with deasphalted bitumen diluted in either toluene or heptane showed similar film behavior to the heptane-diluted bitumen films with a black film being formed via black spots. The film thickness was also independent of the solvent type, ranging from 14 nm at a dilution of 1:1 to 12 nm for a 10:1 diluent ratio (open squares - □ - and open diamonds - ◊ - in Figure 2.13). We expect that the thickness would continue to decrease to approximately 10 nm at higher diluent ratios. Unfortunately, we could not obtain thickness measurements at ratios higher than 10:1 due to the short lifetimes of the diluted-deasphalted bitumen films. Experiments with resin-I diluted to 5:1 and 10:1 in toluene displayed similar drainage patterns to the deasphalted bitumen films and a nearly identical film thickness (solid triangles - ▲ - in Figure 2.13).

The similarity in film thickness and behavior of the deasphalted bitumen and resin-I to the heptane-diluted-bitumen in the plateau region of curve 1 (Figure 2.13) indicated that the resin fraction determined the properties of heptane-diluted bitumen films at high diluent ratios (≥20:1). Since the thickness remained constant with further dilution, the film probably had a bilayer structure. The dominance of the resin fraction was not a surprise since all the asphaltenes completely precipitated at dilution ratios of 20:1 or larger. For lower diluent ratios (<20:1) up to the precipitation point of 1.7:1, the heptane-diluted-bitumen solutions still contained a portion of unprecipitated asphaltenes in the form of asphaltene-resin aggregates. These aggregates were probably responsible for the difference in thickness between the heptane-diluted bitumen and the deasphalted bitumen emulsion films.

The relative instability of both heptane-diluted bitumen, deasphalted bitumen, and resin-1 films agree well with emulsion experiments of Yan et al. (1999) where deasphalted bitumen lead to poorly stabilized water-in-bitumen emulsions.

2.3.7 Film Thickness: Asphaltenes

Since asphaltenes have been identified as the most common stabilizer of water-in-bitumen emulsions (Yarranton, 1997), it was expected that the asphaltenes would be responsible for the stability of the toluene-diluted-bitumen films. A single experiment on a film of toluene-diluted-asphaltenes at a weight ratio of 15:1 followed a similar drainage pattern to the toluene-diluted-bitumen films with a uniform grey film being formed. However, the film unexpectedly ruptured after only a few minutes at a thickness of 36 nm. McLean and Kilpatrick (1997a) showed that stable water-in-oil emulsions could be obtained with pure asphaltenes. They also found that the combination of resin and asphaltene at a ratio of 1:3 (resin:asphaltene) resulted in the most stable emulsions. A thin film of resin-1 and asphaltene diluted in toluene (2:1 resin-1:asphaltene by weight) displayed very similar behavior to the toluene-diluted-bitumen films with slow drainage to a stable grey film. The equilibrium thickness of the resin-1:asphaltene film was also very similar to the thickness of the toluene-diluted-bitumen films (solid diamonds - ♦ - in Figure 2.13). These results indicated that the combined interaction of resins and asphaltenes are important to the film stability.

As with the heptane:bitumen films, the toluene:bitumen films of dilution $\geq 20:1$ probably had a bilayer structure with the film being stericly stabilized mainly by asphaltenes. Yudin et al. (1998) have suggested that *pure asphaltenes* in toluene reach critical micelle concentration (CMC) around 3 gL^{-1} where as Yarranton (1997) found that CMC is at least 44 gL^{-1} for *Athabasca bitumen* diluted in toluene. This suggests that asphaltene molecules do not (or weakly) associate with one another at higher diluent ratios, a finding supported by the work of Fenistein et al. (1998). Furthermore, the radius of gyration of asphaltenes in toluene was found to be between 4.0 nm and 6.1 nm (Fenistein et al., 1998; Sirota, 1998), which is slightly less than half the thickness of the grey films. Results from Sitora (1998) and Bardon et al. (1996) suggest the resins are

about half the length of asphaltenes indicating that a lower thickness should have been expected for heptane:bitumen films of high dilutions ($\geq$20:1). Thus, the difference between the size of the asphaltene and resin molecules appears to account for the observed difference in film thickness in the plateau region of the heptane-diluted and toluene-diluted-bitumen films (Figure 2.13, curves 1 and 2).

The cause of the increase in film thickness at lower diluent ratios (<20:1 toluene:bitumen by weight) was not so clear. The film probably has a multilayer structure since asphaltenes and resins are known to form aggregates at lower diluent ratios (Li and Wan, 1995; Sheu and Mullins, 1995; Buckley et al., 1998; Horiucki et al., 1998). However, this assumption can only be proven with measurements of the disjoining pressure-thickness isotherms (see Chapter 3).

2.4 Conclusions

In this chapter, we have shown that the TLF-PBT may be used to study water/solvent-diluted-bitumen/water emulsion films. Images obtained with a reflected light microscope show that heptane-diluted-bitumen films formed a black film via black spot formation. These films often contained a number of small white spots indicating dimples of trapped liquid within the film. Images also revealed that a new geometric pattern or 'network' of spots of unknown origin formed at heptane:bitumen ratios between 10:1 and 15:1.

Other images show that films formed from toluene-diluted-bitumen drained continuously until a stable, uniform grey film was achieved. Those at lower dilutions ($\leq$3:1) probably had a multilayer structure while films formed from more dilute solutions ($\geq$20:1) had a bilayer structure with a film thickness of about 15 nm. However, additional information is needed to confirm that such film structures occur at the lower and higher diluent ratios.

2.5 References

ASTM D1218-92 "Standard Test Method for Refractive Index and Refractive Dispersion of Hydrocarbon Liquids". ASTM (1992) 409.

Bardon. C., Barré. L., Espinat. D., Guille. V., Li. M.H., Lambard. J., Ravey. J.C., Rosenberg, E. and Zemb, T., *Fuel Sci. Technol.* 14 (1996) 203.

Becher, P., *in* "Interfacial Phenomena in Apolar Media", edited by Eicke. H.F. and Parfitt. G.D., Marcel Dekker, 1987.

Bergeron, V., Hanssen, J.E. and Shoghl, F.N., *Colloid Surf. A* 123-124 (1997) 609.

Buckley, J.S., Hirasaki, G.J., Liu, Y., Von Drasek, S., Wang, J-X. and Gill, B.S., *Petroleum Science and Technology* 16 (1998) 251.

Bulmer. J.T. and Starr. J. (Eds). "Syncrude Analytical Methods for Oil Sand and Bitumen Processing". Syncrude Canada Ltd., Edmonton, 1979, Method 5.1.

Clarke, P.F. and Pruden, B.B., *Petroleum Science and Technology*, 16 (1998) 287.

Ese, M.-H., Sjöblom. J., Førdedal. H., Urdahl. O. and Rønningsen. H.P., *Colloids Surface A*, 123-124 (1997) 225.

Exerowa, D., Ivanov, I. and Scheludko, A., *in* "Issledovaniya v oblasti poverkhnostnykh sil". edited by Derjaguin. B.V., Nauka. Moscow, 1964, p.158 (in Russian).

Exerowa, D. and Kruglyakov. P.M., "Foam and Foam Films" Elsevier, New York, 1998.

Exerowa, D. and Scheludko. A., *Compt. Rend. Acad. Bulg. Sci.* 24 (1971) 47.

Fenistein. D., Barré. L., Broseta. D., Espina. D., Livet. A., Roux. J.N. and Scarsella. M., *Langmuir* 14 (1998) 1013.

Friberg, S.E. and Solans, C., *Langmuir* 2 (1986) 121.

Friberg, S.E., Wohn, C.S., Greene, B. and Van Gilder, R., *J. Colloid Interface Sci.* 101 (1984) 593.

Harkins, W.D. and Jordan, H.F., *J. Amer. Chem. Soc.* 52 (1930) 1751.

Horiuchi, Y., Matsumura, H. and Furusawa, K., *J. Colloid Interface Sci.* 207 (1998) 41.

Ivanov, I.B. (Ed). "Thin Liquid Films" Marcel Dekker, New York, 1995.

Johansen. E.J.. Skjärvö. I.M.. Lund. T.. Sjöblom. J.. Söderlund. H. and Boström. G.. *Colloids Surf.* **34** (1988/89) 353.

Joye. J.L.. Miller. C.A. and Hirasaki. G.J., *Langmuir* **8** (1992) 3083.

Kotlyar. L.S., Sparks. D.B.. Woods. J.R.. Raymond. S., LePage Y. and Shelfantook. W., *Petroleum Science and Technology,* **16** (1998) 1.

Li, H. and Wan. W.K.. International Heavy Oil Symposium. Calgary. 19 – 21 June 1995, Society of Petroleum Engineers, Inc., 1995. p.709.

Lide. D.R. (Ed.). "CRC Handbook of Chemistry and Physics" 71st Ed.. CRC Press. Boston. 1990.

McLean. J.D. and Kilpatrick. P.K.. *J. Colloid Interface Sci.* **196** (1997a) 23-34.

McLean. J.D. and Kilpatrick. P.K.. *J. Colloid Interface Sci.* **189** (1997b) 242-252.

Mitchell. D.L. and Speight. J.G.. *FUEL,* **52** (1973) 149.

Moschopedis. S.E. and Speight. J.G.. *J. Materials Sci.* **12** (1977) 990.

Mouraille. O.. Skodvin. T.. Sjöblom. J. and Peytany. J.L.. *J. Dispersion Sci. Techn.,* **19** (1998) 339.

Nikolov. A.. Wasan. D. and Czarnecki, J., Presented at 47th Canadian Chemical Engineering Conference. Edmonton, October 1997.

Opawale. F.O. and Burgess. D.J.. *J. Colloid Interface Sci.,* **197** (1998) 142.

Scheludko. A.. *Kolloid Z.,* **155** (1957) 39.

Scheludko. A.. *Adv. Coll. Interface Sci.* **1** (1967) 391.

Scheludko. A. and Platikanov. D., *Kolloid Z.* **175** (1961) 150.

Sheu. E.H. and Mullins. O.C. (Eds.). "Asphaltenes: Fundamentals and Applications". Plenum Press, New York, 1995.

Sirota. E.B.. *Petroleum Science and Technology* **16** (1998) 415.

Strausz, O.P., Mojelsky. T.W. and Lown, E.M.. *FUEL,* **71** (1992) 1355.

Taylor, J. and Haydon, D.A., *Discuss. Faraday Soc.* **42** (1966) 51.

Yan, Z., Elliott, J.A.W., and Masliyah, J.H., *J. Colliod Interface Sci.* **230** (1999) 329-337.

Yarranton, H.W., Ph.D. Thesis, University of Alberta, Edmonton, 1997.

Yudin, I.K., Nikolaenko, G.L., Gorodetskii, E.E., Markhashov, E.L., Frot, D., Briolant, Y., Agayan, V.A. and Anisimov, M.A., *Petroleum Science and Technology* **16** (1998) 395.
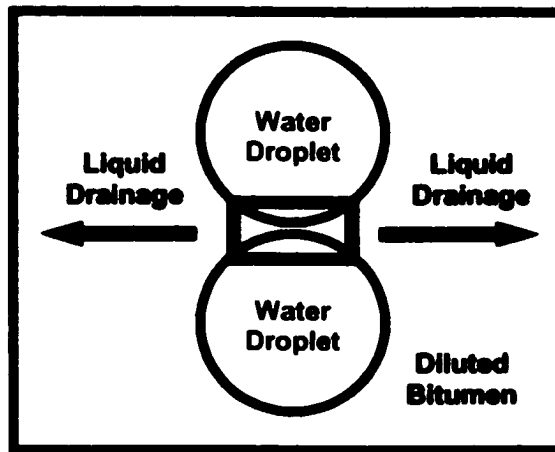
(a)
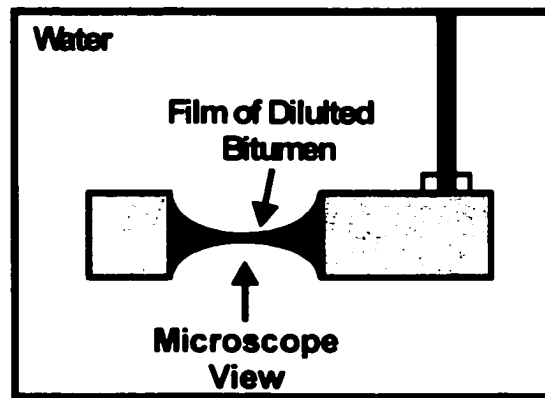
(b)

(c)

FIGURE 2.1: Concept of Thin Liquid Film-Pressure Balance
Technique. The thin film formed between two water droplets (Image a)
is recreated in a specially designed measuring cell (Image b) and may
be viewed using reflected light (Image c).
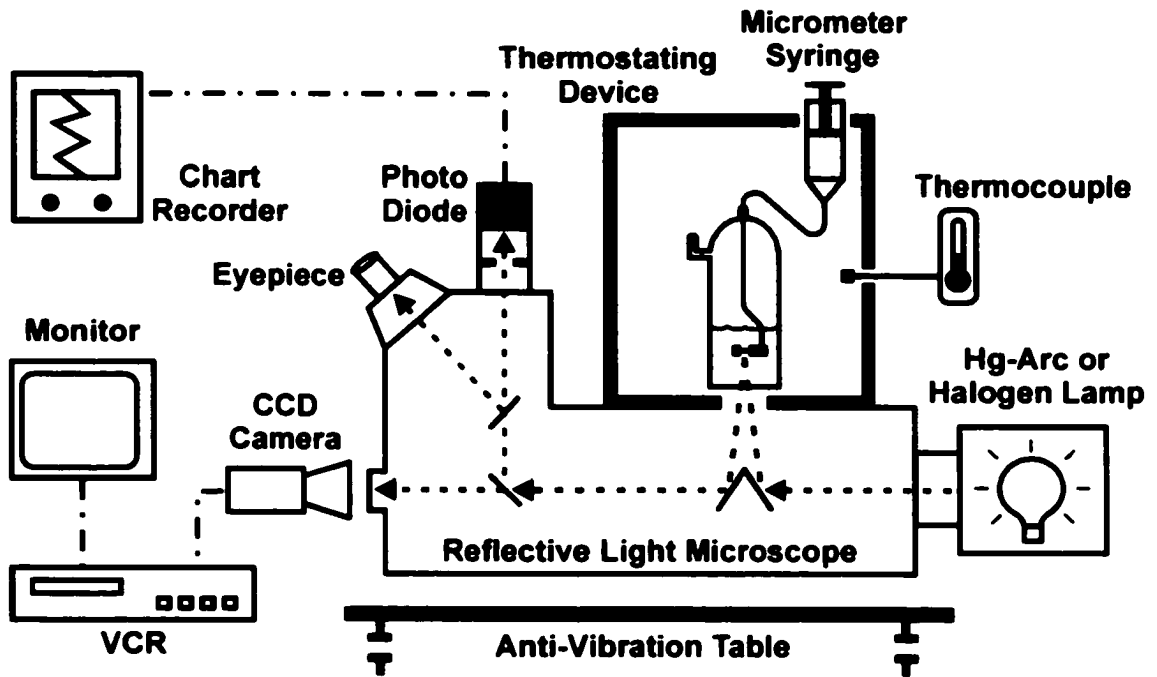
FIGURE 2.2: Schematic of set-up for Thin Liquid Film-Pressure Balance Technique.
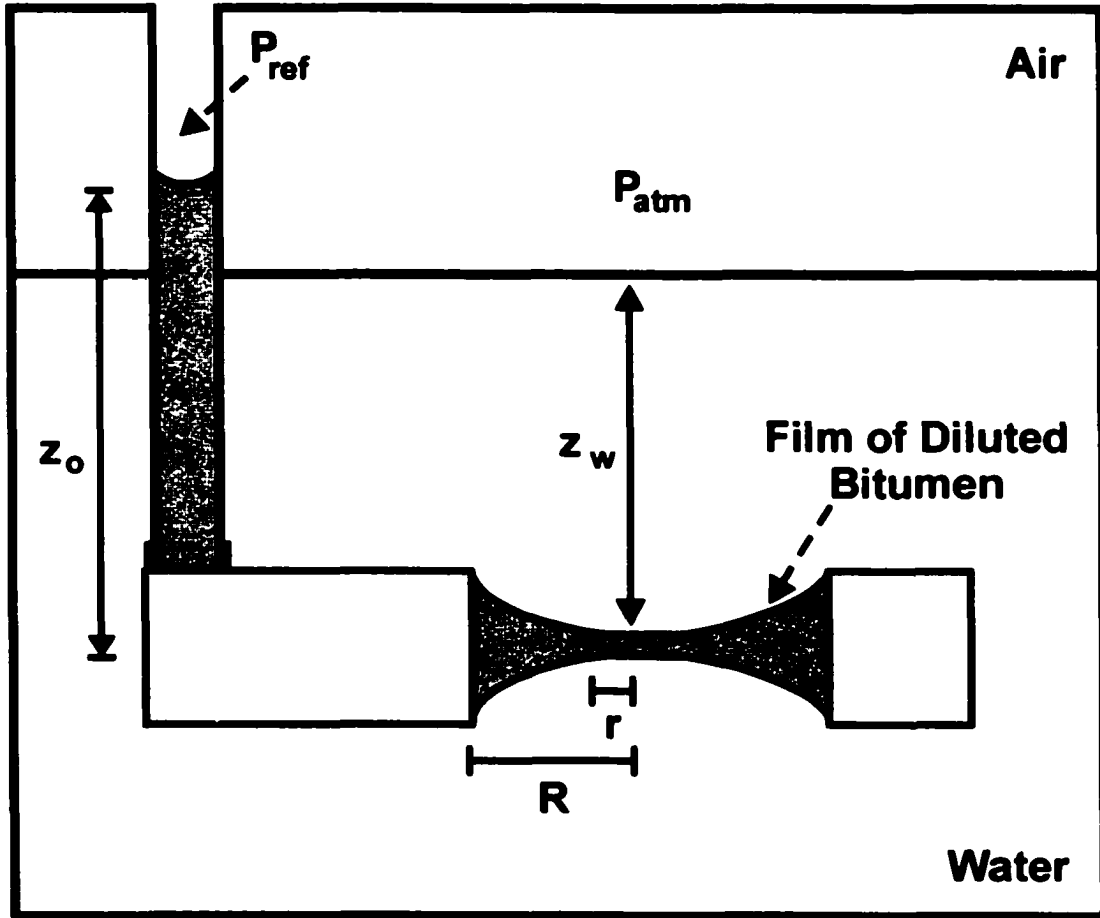
FIGURE 2.3: Schematic of the cell and film holder where the parameters needed to calculate the applied capillary pressure are defined.
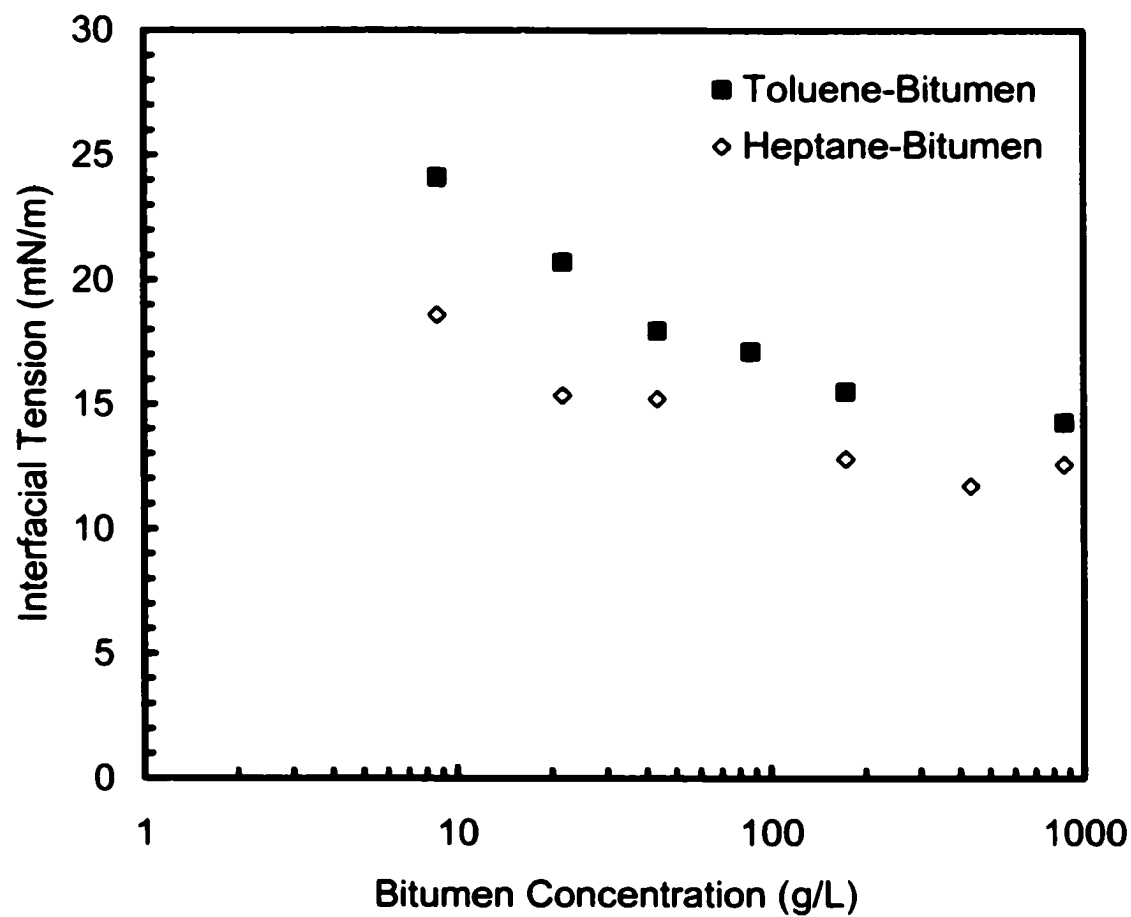
FIGURE 2.4: Interfacial tension between industrial water and diluted bitumen measured with a DuNouy ring apparatus. Each point represents an average of 3 measurements.

(a)

(b)

(c)
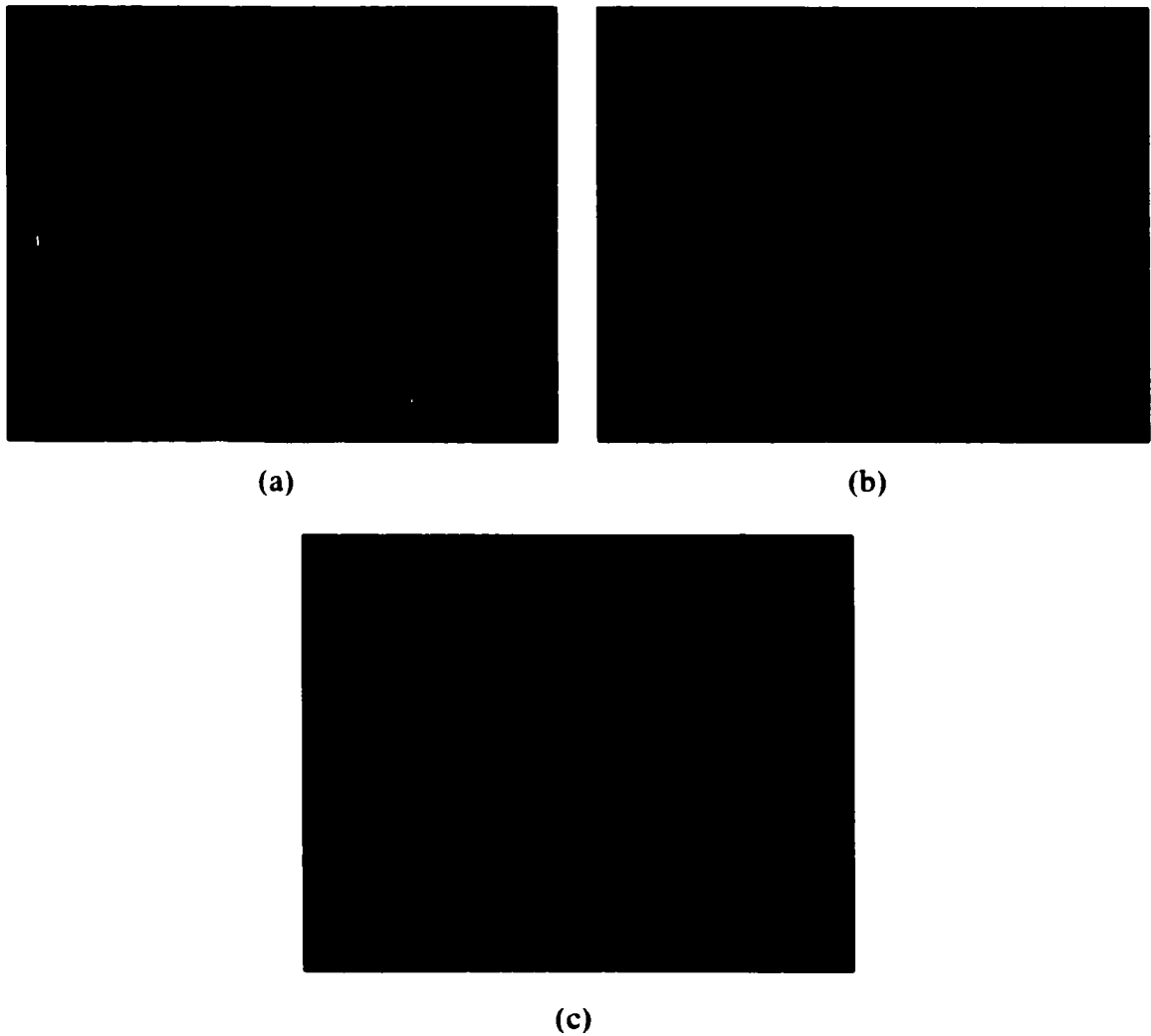
FIGURE 2.5: Images of a typical toluene diluted bitumen film. In this case, the images are for a (3:1) toluene:bitumen film. (a) Initial film formation with appearance of center dimple; (b) Channel drainage; (c) Equilibrium grey film.
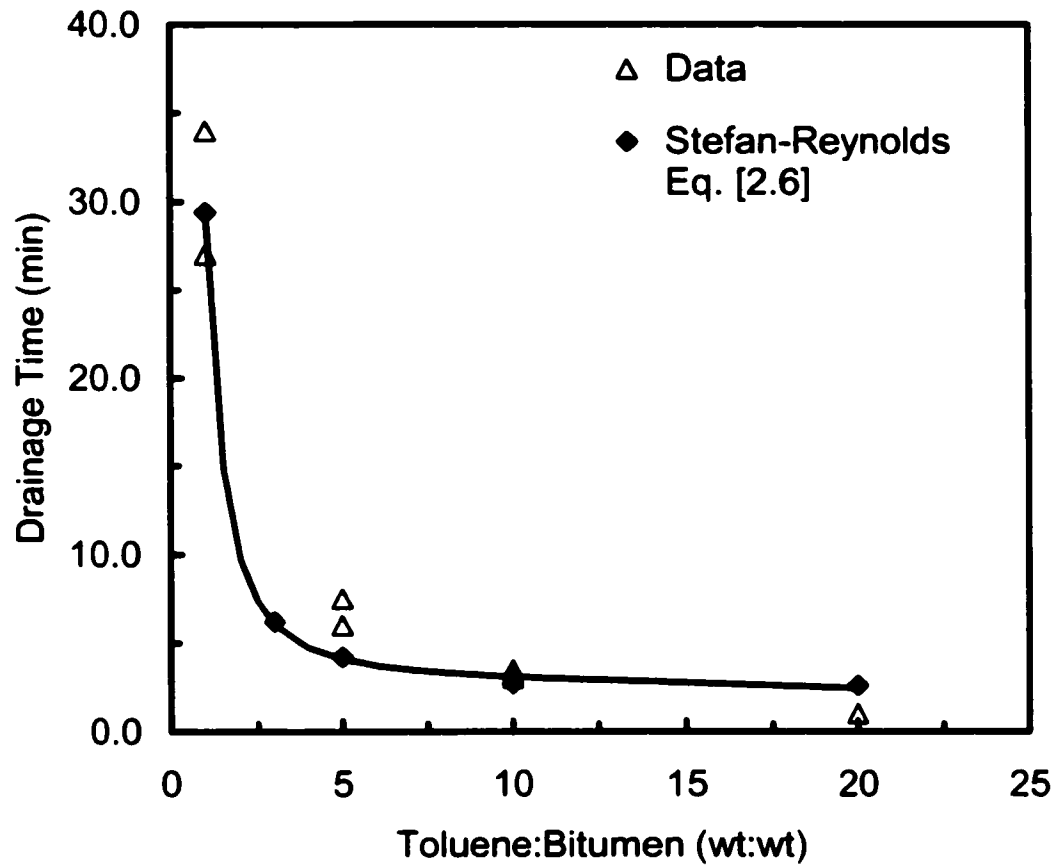
FIGURE 2.6: The dependence of film drainage time on toluene:bitumen ratio. The open triangles represent the measured drain times and the solid diamonds represent the drainage time calculated using the Stefan-Reynolds equation. Drainage time calculated from the Stefan-Reynolds equation using an initial thickness of 91 nm and final thickness of 30 nm. Note that the line is drawn to guide the eye.

(a)   (b)

(c)
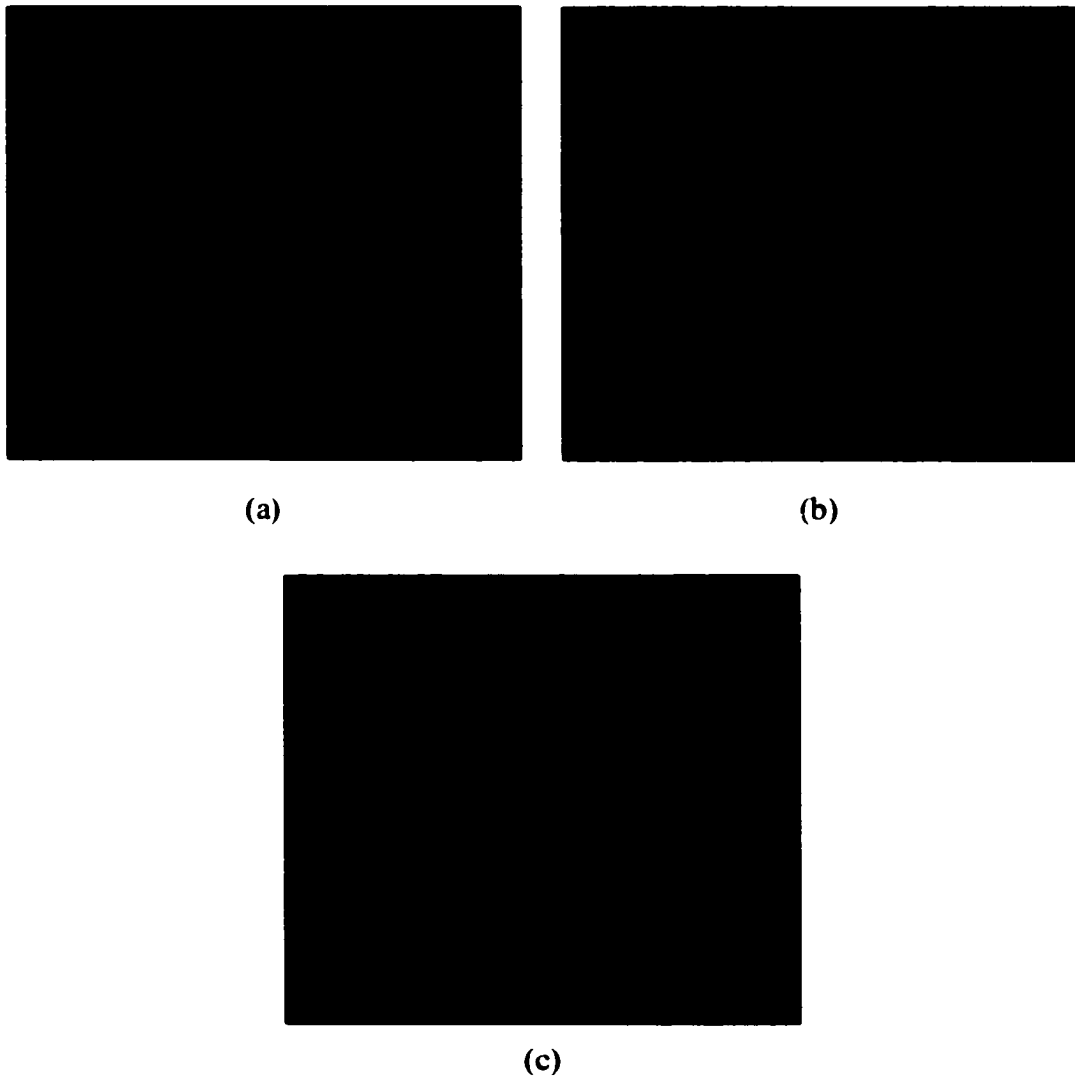
FIGURE 2.7: Images of a typical heptane diluted bitumen film. In this case, the images are from a (5:1) heptane:bitumen film. (a) Initial film formation with appearance of center dimple; (b) Black spot formation; (c) Equilibrium black film.
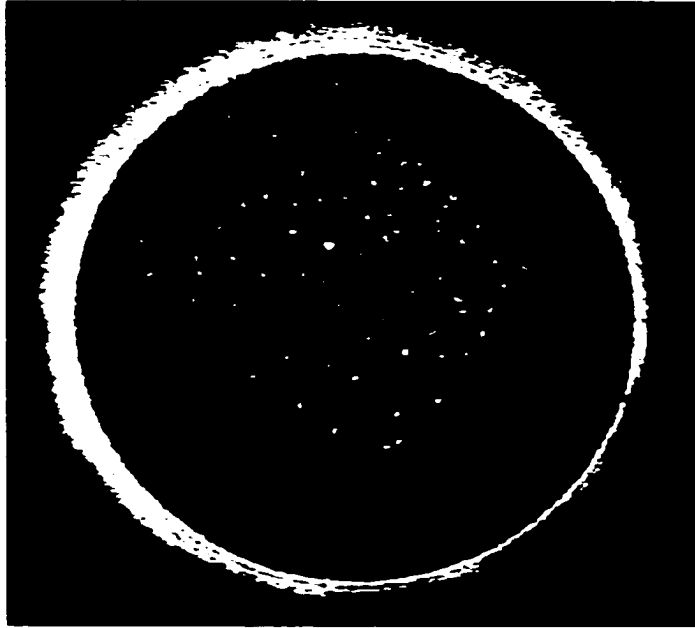
FIGURE 2.8: Image of network formed in heptane diluted bitumen
films of dilution ratio 10:1 or larger.
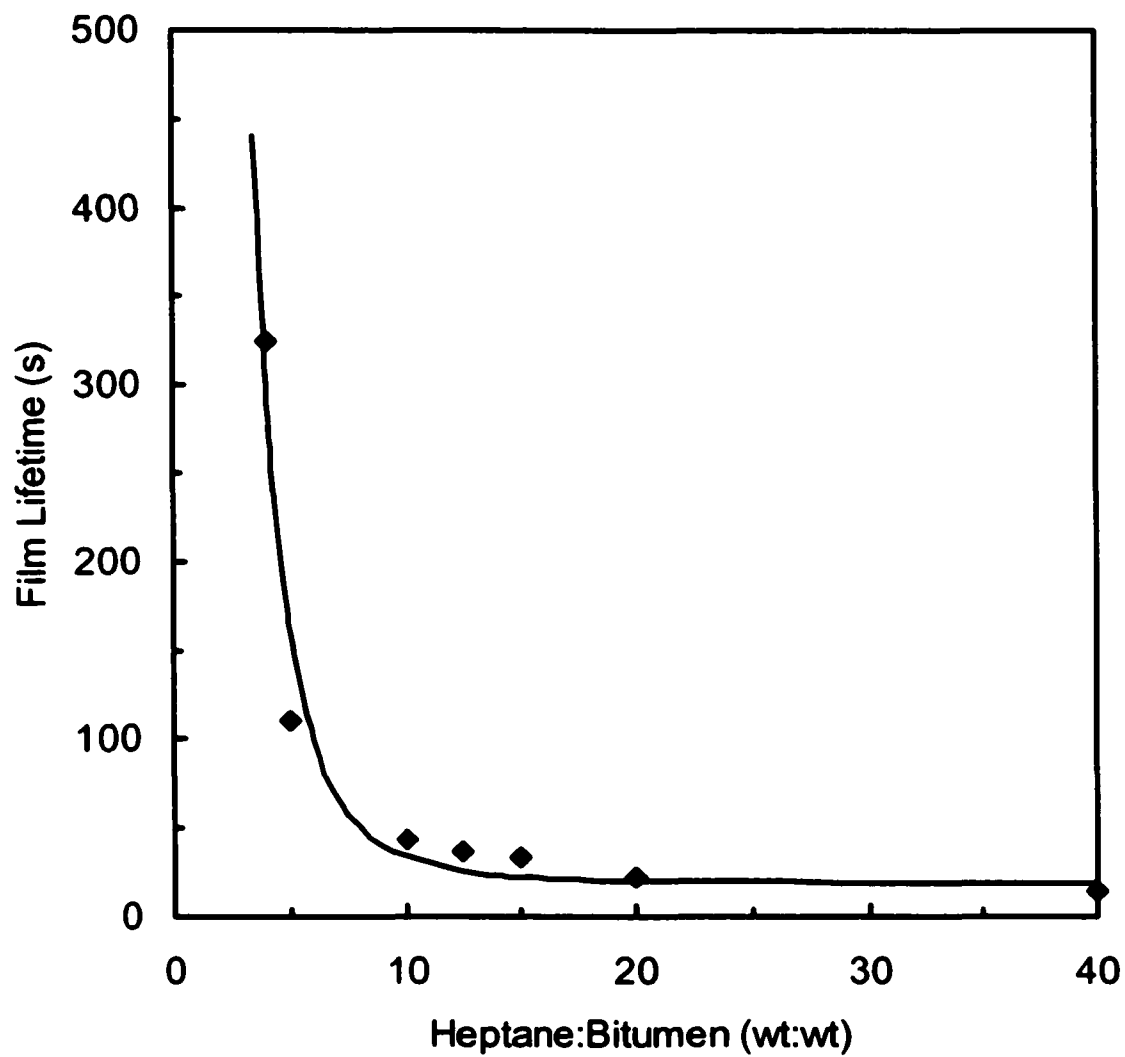
FIGURE 2.9: Dependence of film lifetime on heptane:bitumen ratio. Each point represents an average of at least 10 measurements. Line drawn to guide the eye.
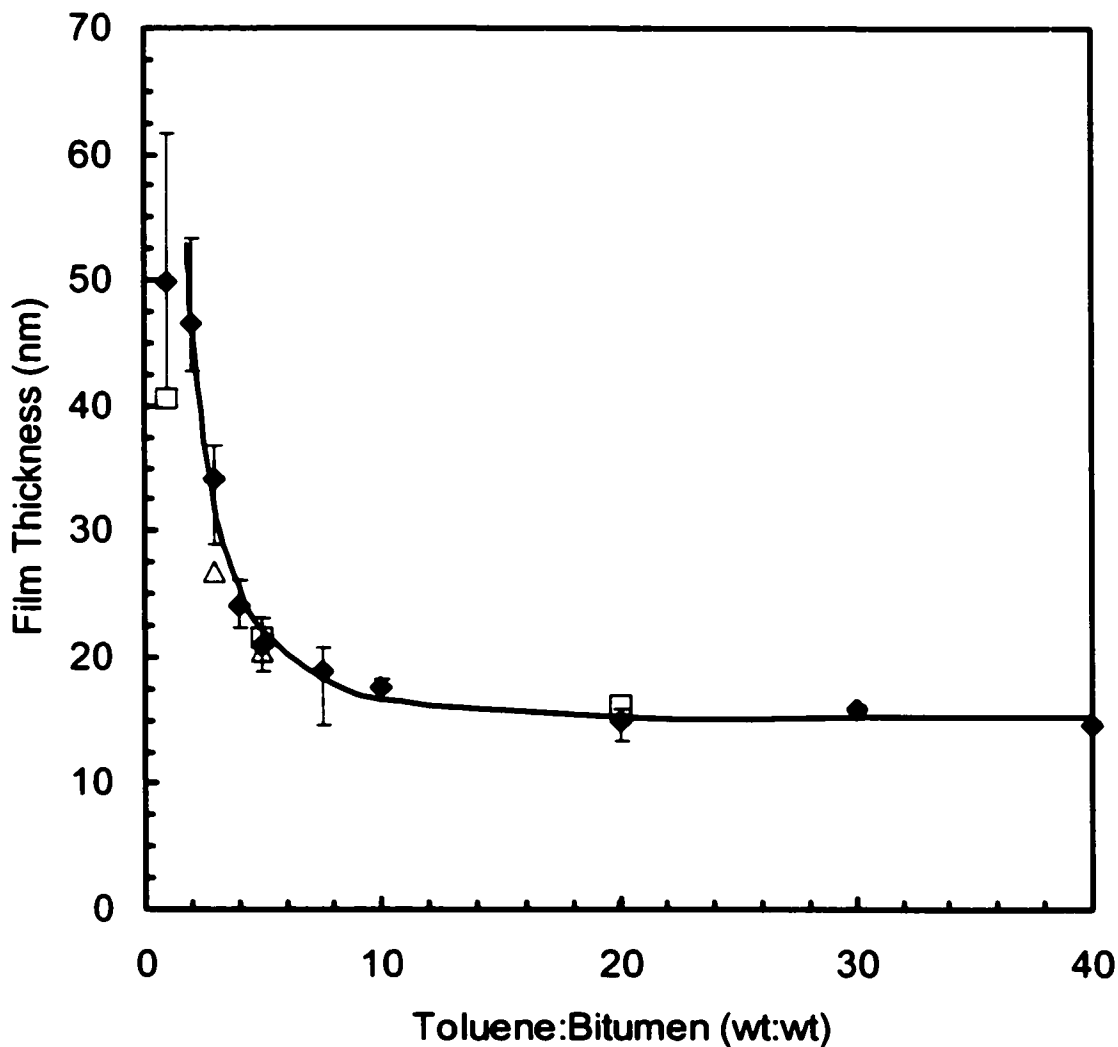
FIGURE 2.10: Dependence of equivalent film thickness on toluene:bitumen ratio. Line drawn to guide the eye. (♦ – simulated-industrial-water/diluted-bitumen/simulated-industrial-water; □ – simulated-industrial-water/diluted-solids-free-bitumen/simulated-industrial-water; △ – DIUF-water/diluted-bitumen/DIUF-water)
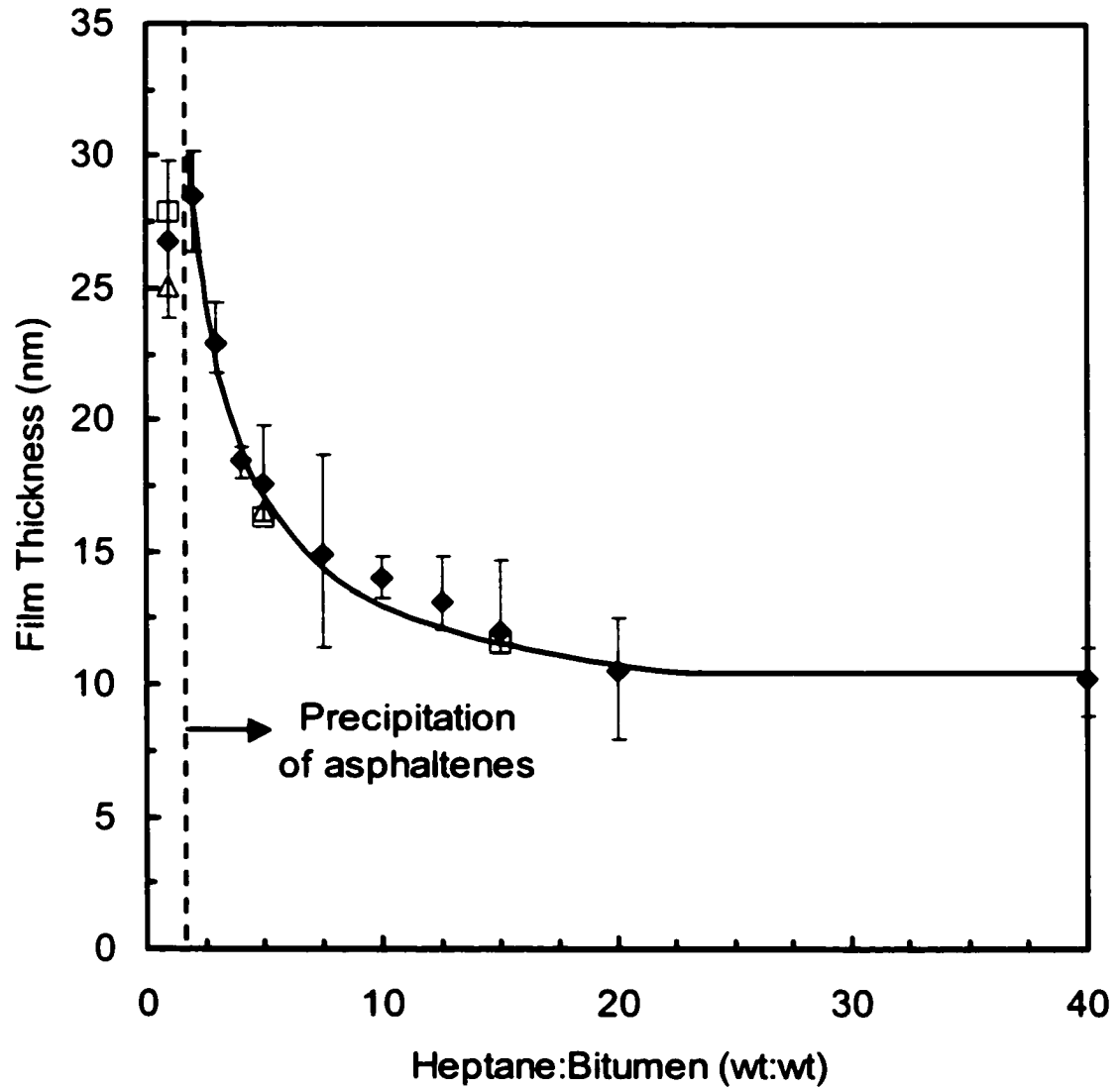
FIGURE 2.11: Dependence of equivalent film thickness on heptane:bitumen ratio. Line drawn to guide the eye. (♦ – industrial-water/diluted-bitumen/industrial-water; □ – industrial-water/diluted-solids-free-bitumen/industrial-water; △ – DIUF-water/diluted-
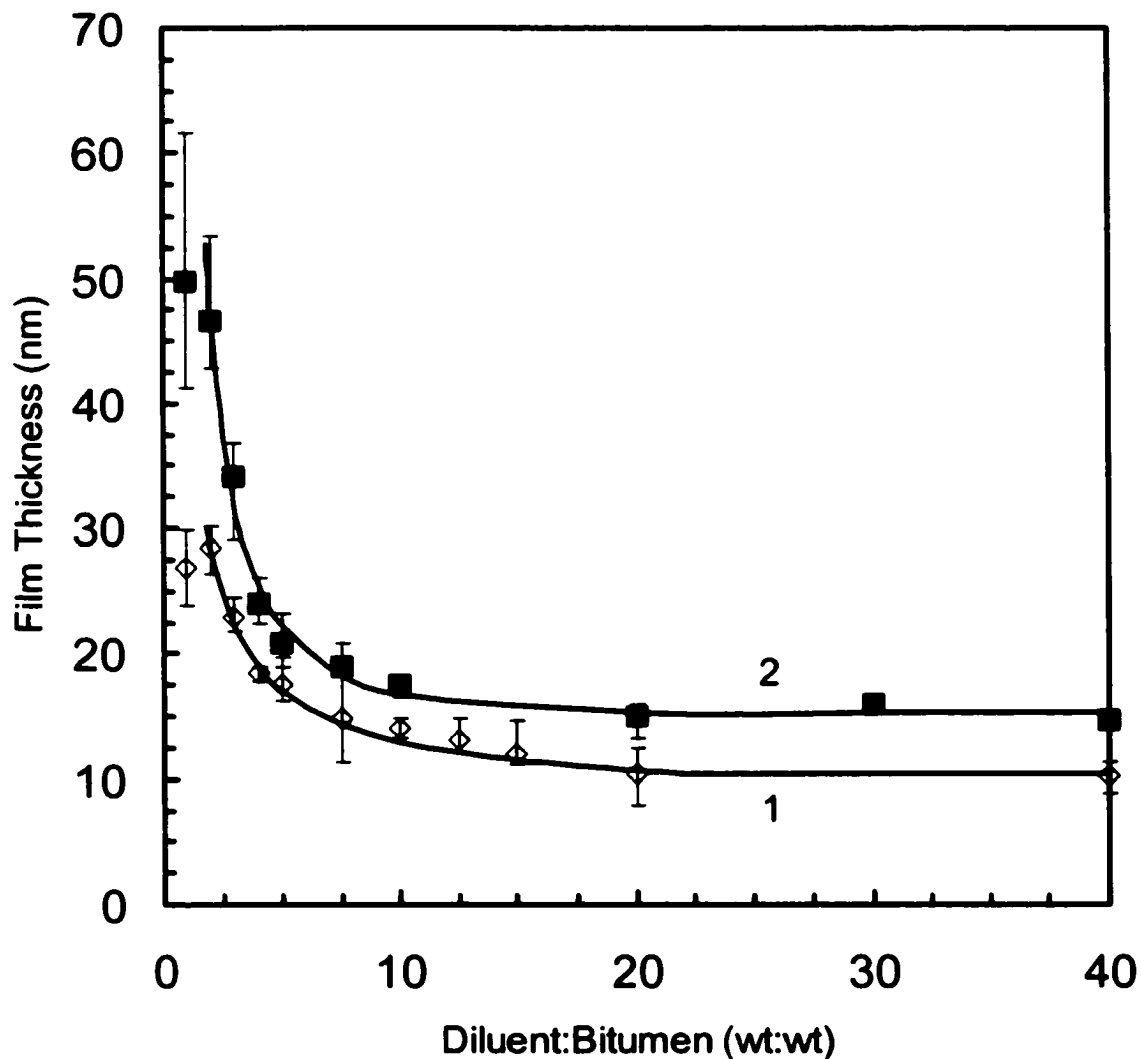
FIGURE 2.12: Comparison of the equivalent film thickness obtained for heptane and toluene diluted bitumen films. Each point represents an average of at least 5 measurements taken from 3 independent solution samples. Lines 1 and 2 were drawn to guide the eye. (◊ – data for industrial-water/heptane-diluted-bitumen/industrial-water; ■ – data for industrial-water/toluene-diluted-bitumen/industrial-water)
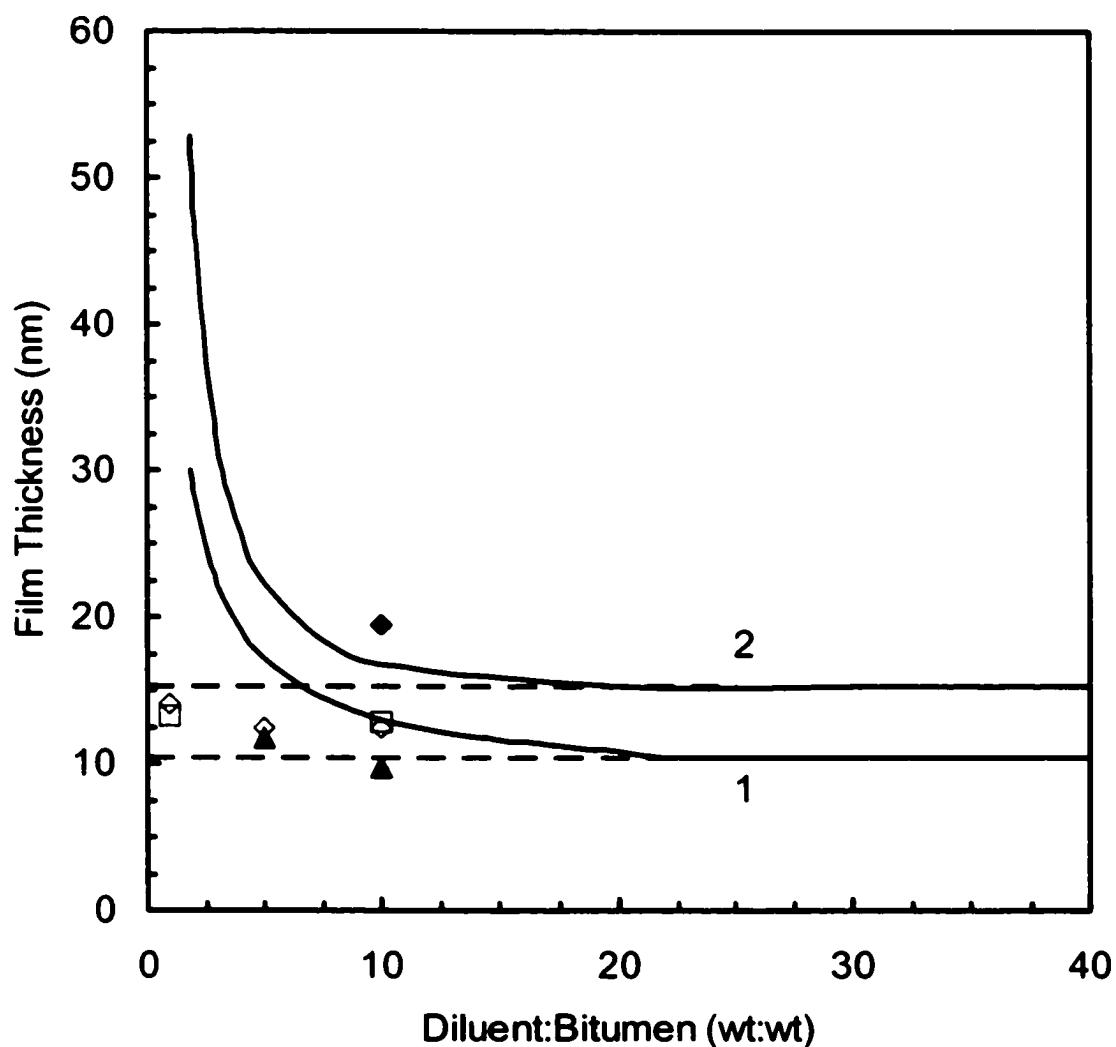
FIGURE 2.13: Comparison of the equivalent thickness of deasphalted bitumen, resin-I only, asphaltene only, and resin-I + asphaltene films to the equivalent thickness of toluene:bitumen and heptane:bitumen films. Lines 1 and 2 are identical to those drawn in Figure 2.12. Both lines were drawn to guide the eye. (□ - industrial-water/toluene-diluted deasphalted-bitumen/industrial-water; ◊ - industrial-water/heptane-diluted-deasphalted-bitumen/industrial-water; ▲ - industrial-water/toluene-diluted-resin-I/industrial-water; ◆ - industrial water/toluene-diluted-resin-I and asphaltenes/industrial-water)

Chapter 3

Disjoining Pressure Isotherms of Water-in-Bitumen Emulsion Films[†]

3.1 Introduction

An understanding of the colloidal forces between water droplets interacting across a crude oil media is of great interest to the oil industry where water-in-crude-oil emulsions are a common occurrence. Typical examples quoted in the literature include droplets of sea water becoming entrained in oil spills, emulsified table water being extracted with crude oil from underground reservoirs, and the emulsification of water during the washing of crude oils to remove contaminates (McLean et al., 1998; Yarranton et al., 2000a). Of particular interest to this study are the water-in-diluted-bitumen emulsions that are formed during the water extraction process used to separate bitumen from oil sands (Czarnecki, 2001).

Bitumen is a complex mixture of hydrocarbons that can be separated into several material classes or fractions. Asphaltenes are generally defined as the fraction of bitumen that is soluble in aromatic solvents like toluene, but insoluble in aliphatic solvents such as pentane or heptane. The asphaltene fraction consists of polyaromatic hydrocarbons with a monomer molar mass on the order of 500-2000 g/mol, (Groenzin and Mullins, 2000; Yarranton et al., 2000b). The asphaltene monomers typically contain heteroatom functional groups, including some acids and bases. (Speight, 1994; Groenzen and Mullins, 2000). Asphaltenes are known to be surface active and most of the literature identifies the asphaltene fraction as the main component in bitumen that is responsible for the stability of water-in-diluted-bitumen emulsions. Results from studies on emulsion dewatering, Langmuir-Blodgett films, interfacial tension, and chemical analysis have lead to some speculation as to the structure of the asphaltene molecules at the water-bitumen (or water-crude oil) interface (Johansen et al., 1988; Sheu and Mullins, 1995; Ese et al., 1997; McLean and Kilpatrick, 1997a, 1997b; Ese et al., 1998; Mouraille et al., 1998;

Singh et al., 1999, Yarranton et al., 2000a; Yang et al., 2001). The more predominant models relate the structure of the asphaltenes at the interface to the solubility of asphaltenes in the bulk oil. Given favorable solubility conditions, asphaltenes in the form of monomers or aggregates will adsorb onto the oil-water interface. A build-up of asphaltenes at the interface will provide steric stabilization between the emulsion water droplets (Yarranton et al., 2000a). A similar model suggests that favorable solubility conditions can produce asphaltene aggregates that will build up on the interface. The aggregates physically interact to form a rigid interface (or 'skin') around a water droplet and thus prevent droplet coalescence (McLean and Kilpatrick, 1997b; McLean et al., 1998; Singh et al., 1999).

Knowledge of the colloidal forces between the water droplets would help to increase our understanding of how water-in-diluted-bitumen emulsions are stabilized. There are a limited number of studies on the interactions between water droplets in an oil media or on the interaction between oil-water interfaces across an oil media. A microcolloider has been used to measure the colloidal forces between two water droplets in a solution of toluene-diluted-bitumen. It was concluded that the droplets were prevented from coalescing by a repulsive steric force. The force was created by an adsorption layer of non-uniform thickness of 7.5 to 40 nm. (Wu et al., 1999). In Chapter 2, it was shown that an adaptation of the Thin Liquid Film-Pressure Balance Technique (TLF-PBT) may be used to study the interaction of bitumen/water interfaces separated by a thin layer of diluted bitumen (Khristov et al., 2000). Results indicated that at capillary pressures less than 40 Pa, water/toluene-diluted-bitumen/water films were stable for extremely long periods of time. For dilutions of 10:1 (wt:wt of toluene:bitumen) or more, the thickness of the film remained constant at about 15 nm. However, films of dilution 3:1 or less showed dramatically higher film thicknesses, typically in the range of 40 to 60 nm. It was suggested that such a dramatic variation in thickness may be related to a change in the structure of the surfactants at the interface, possibly from a bilayer to multilayer structure. Solid polar surfaces (e.g. mica) separated by a thin film of model oil have been used to mimic the type of colloidal forces that would be encountered in a water-in-oil emulsion (Claesson et al., 2001). Christenson and Israelachvili (1987), using

a surface force apparatus, measured a 'polymer-like' resistance and a 'hard wall' repulsion of 3.5 nm between two clay surfaces separated by a thin film of crude oil.

The TLF-PBT technique may be used to determine the type of interaction between water droplets within a water-in-bitumen emulsion. In such an apparatus, the colloidal forces are measured as disjoining pressure isotherms. Disjoining pressure (Π) is defined as the excess pressure arising from the molecular interactions between two interfaces and it is a function of the film thickness (Bergeron and Radke, 1992). A positive disjoining pressure indicates that a net repulsive force exists between the oil-water interfaces while a negative value corresponds to a net attractive force between the oil-water interfaces. In general, measurements of disjoining pressure isotherms have been limited to aqueous foam and emulsion films of the oil-in-water type (Ivanov, 1988; Exerowa and Kruglyakov, 1998). In the present work, the TLF-PBT technique was used to measure the disjoining pressure isotherms within a thin film of water/toluene-diluted-bitumen/water. In order to clarify the role played by asphaltenes in water-in-diluted-bitumen emulsions, disjoining pressure isotherms were also measured for thin films of water/toluene-diluted-asphaltenes/water.

3.2 Experimental Description

The disjoining pressure isotherms, $\Pi(h)$, were measured using a modified version of the Thin Liquid Film-Pressure Balance Technique described in Chapter 2. The modified TLF-PBT apparatus uses a specially designed measuring cell that consists of film holder sealed inside a glass cell (Figure 3.1). The film holder itself is made of a porous glass plate about 2 mm in thickness with an 800 μm diameter vertical hole drilled through the plate and a glass capillary fused to the top of the plate.

The film holder has been treated to convert the porous glass plate from a hydrophilic to more hydrophobic nature. The treatment involves soaking the porous plate holder in a solution of equal parts toluene and bitumen for a minimum of 24 h. Following treatment, the plate was cleaned with copious amounts of toluene and ethanol and then baked in an oven at 175°C for a minimum of 2 h. This procedure was repeated a minimum of two more times to ensure that the entire plate was hydrophobic. Additional

information about the porous plate film holder, including the preparation and cleaning procedures, may be found in Appendix C.

To create a water/oil/water film, a biconcave drop of oil is first formed in the hole that was drilled through the porous plate. Next, the plate is immersed into a small pool of water at the bottom of the measuring cell, as shown in Figure 3.1. The sealed measuring cell contains a large pocket of air above the water phase. By increasing the air pressure in the cell, oil is forced to drain from the biconcave drop and up into the capillary. The top of the capillary is left open to an atmosphere of constant pressure and temperature. When sufficient pressure is applied, a water/oil/water film is formed.

3.2.1 Apparatus

A schematic of the TLF-PBT apparatus is shown in Figure 3.2. The measuring cell was placed inside a thermostating device that maintained the temperature of the cell at $23.0 \pm 0.1^{\circ}C$. The thermostating device rested on a X-Y transverse stage mounted on top of an Axiovert 100 reflected light microscope (Carl Zeiss Canada Ltd.). An optical flat on the bottom of the cell allowed the film to be viewed from below. Images of the film were captured with a CCD camera (VK-C730, Hitachi) and recorded using a VCR (M-752C, Toshiba).

Disjoining pressure measurements were performed by adjusting the air pressure inside the cell. This air pressure was regulated using a gas-tight syringe (Model 1010, Hamilton Company) mounted on an infusion/withdraw syringe pump (Model 210, KD Scientific). The amount of applied pressure was monitored using an inclined tube manometer (Model M-700, Dwyer Instruments, Inc.) or a U-tube manometer (Model M-200-D, Dwyer Instruments, Inc.) depending on the range of pressure being studied. A reference pressure was established by leaving the top of the glass capillary open to the constant temperature and constant pressure atmosphere of the thermostating chamber. Finally, the microscope and syringe pump rested on top of an anti-vibration table (Model 63-531, Technical Manufacturing Corp.).

3.2.2 Disjoining Pressure

For a plane-parallel film that has reached an equilibrium thickness, the disjoining pressure is normally assumed to be equal to the capillary pressure (Exerowa and Kruglyakov, 1998). The capillary pressure, P_C, is simply the difference of the pressure in the water just outside of the film, P_1, and the pressure of the hydrocarbon in the plateau border region, P_2:

$$\Pi \equiv P_C = P_1 - P_2 \tag{3.1}$$

A pressure balance taken over the entire cell provides a relation for $P_1 - P_2$ in terms of measurable parameters (see Figure 3.3):

$$\Pi = P_C = P_{cell} + \rho_w g z_w - \rho_o g z_o - P_{atm} \tag{3.2}$$

where g is the acceleration due to gravity, z_w is the height of the water above the film, z_o is the height of the oil in the capillary, P_{atm} is atmospheric (reference) pressure within the thermostating device and ρ_w and ρ_o are the densities of the water and oil phases, respectively. The pressure inside the cell can be assumed to be equal to atmospheric pressure plus the applied pressure, $P_{cell} = P_{atm} + P_{applied}$. Substituting this relation into Eq. [3.2] gives a working relation for the disjoining pressure:

$$\Pi = P_C = P_{applied} + \rho_w g z_w - \rho_o g z_o \tag{3.3}$$

Although tedious, all of the parameters on the right side of Eq. [3.3] are measurable. To simplify the disjoining pressure measurement, we made use of a well-known relation for the capillary pressure of a plane-parallel film (Exerowa et al., 1964):

$$P_C = 2\gamma \frac{R}{R^2 - r^2} \qquad \text{for} \qquad r \ll R \tag{3.4}$$

where γ is the oil/water interfacial tension, R is the hole radius, and r is the radius of the film.

The first step in measuring the disjoining pressure isotherm involved increasing the applied pressure in the cell until a film of radius r = 100 μm was formed. The film was allowed to drain to an equilibrium film thickness. Since the film radius was significantly smaller than the hole radius (R = 400 μm), the disjoining pressure for the first equilibrium thickness was estimated from Eq. [3.4]. Using increments of about 30 Pa, the applied pressure was slowly increased. The film was allowed to reach its new equilibrium thickness after each increment in applied pressure. With the increased applied pressure, Eq. [3.4] was no longer valid since the film radius quickly approached the radius of the hole. The disjoining pressure for each new equilibrium thickness was then estimated using Eq. [3.3] where the difference in the static pressures (i.e. $\rho_w g z_w$ - $\rho_o g z_o$) was assumed to be constant. This meant that the disjoining pressure for each subsequent equilibrium thickness could be obtained by subtracting the 'constant' static pressure difference from the measured applied pressure. A 'constant' static pressure difference is a reasonable assumption since each term in the static pressure difference was constant once the film radius approached the hole radius. Strictly speaking, the value of z_o was not constant, although it was relatively insensitive to changes in the applied pressure since the total volume hydrocarbon liquid in the film was relatively small compared to the volume of hydrocarbon in the glass capillary. An estimate of the 'constant' static pressure difference was obtained from the first data point by subtracting the initial applied pressure from the disjoining pressure calculated from Eq. [3.4]. The constant static pressure difference was normally on the order of 10 to 100 Pa.

Note that the calculations from Eq. [3.4] employed interfacial tensions of diluted bitumen over water (see Figure 2.4) and diluted asphaltenes over water obtained from previously published data (Yarranton et al., 2000b). Also, the maximum pressure that could be measured was limited by the pore diameter of the porous plate. In general, a smaller pore diameter allows higher pressures to be applied to the film. Due to the 'dirty' nature of working with bitumen, porous plates designed with smaller pores often become

clogged by solids or precipitated material. This imposed a limit of about 700 Pa for the maximum disjoining pressure that could be measured.

3.2.3 Equivalent Film Thickness

The film thickness was obtained using the microinterferometric technique developed by Scheludko and Exerowa (Scheludko, 1957; Scheludko, 1967; Exerowa and Scheludko, 1971; Exerowa and Kruglyakov, 1998). Heat filtered light from a 100 W mercury arc lamp was directed through a monochromatic filter (λ = 546 nm). The light then passed through an iris (or pin-hole) diaphragm creating a ~10 μm diameter beam of light that was focused onto the centre of the film. Light reflected from the film was directed through a second pin-hole diaphragm to eliminate any unnecessary light scatter from the film meniscus or the porous plate. Intensity of the reflected light was measured using a highly sensitive low-light, low-noise Si-photodiode (Hamamatsu Corp.). The voltage signal from the photodiode was recorded using a strip chart.

The recorded light intensity was converted into an equivalent (or optical) film thickness using the equation developed by Scheludko and Platikanov (1961):

$$h = \left(\frac{\lambda}{2\pi n_r}\right) \arcsin\left(\frac{\Delta}{1 + [4N/(1-N)^2][1-\Delta]}\right)^{1/2} \qquad [3.5]$$

where $\Delta = (I - I_{min})/(I_{max} - I_{min})$ and $N = (n_r - n_s)^2/(n_r + n_s)^2$. Here, I is the recorded light intensity with I_{max} and I_{min} corresponding to last maximum and minimum interference values. The refractive index of the surrounding water, n_s, was reported in Chapter 2 and was taken to be 1.334. The refractive index of the film, n_r, would typically be set equal to the refractive index of the bulk solution. Unfortunately, at the time of the disjoining pressure measurements, no refractive index data was available for solutions of toluene and bitumen and such values could not be readily obtained. For this reason, n_r was assumed to be equal to the refractive index of the pure diluting solvent, namely toluene (n = 1.4961). Using data from Chapter 5 for the refractive index of solutions of toluene

and bitumen, the error associated with this assumption has been found to be less than 2.5% of the measured thickness or less than 0.2 nm for an 8 nm thick film.

3.2.4 Materials[†]

Chemicals included HPLC grade toluene, HPLC grade heptane, asphaltenes, and bitumen. The bitumen, supplied by Syncrude Canada Ltd, is a coker feed bitumen that has been treated to remove coarse mineral solids and water. The asphaltenes were prepared using two different methods. Both methods began by dissolving bitumen in heptane at a volume ratio of 40:1 (heptane:bitumen). The mixture was stirred for 4 h and left overnight to allow the asphaltene-solid precipitate to settle. The mixture was then centrifuged and vacuum filtered to recover the precipitate.

In the first method, the precipitate was dissolved in toluene at a volume ratio of 100:1 (toluene:asphaltenes-solids). The mixture was stirred for a minimum of 1 h to ensure that all the asphaltenes were dissolved. The mixture was centrifuged at 9400g for about 45 min. Following centrifugation, the supernatant was vacuum filtered through a 0.22 μm filter and then placed in an oven at 40°C to evaporate the toluene. The recovered 'solids-free' asphaltenes and discarded solids accounted for about 15.5 %wt and 0.9 %wt of the total bitumen, respectively. This first method, referred to as method-I, was expected to remove at least all of the fine solids larger than 0.2 μm.

In the second method, referred to as method-II, 5 g of the asphaltene-solid precipitate was mixed with 225 mL of toluene. The mixture was stirred for a minimum of 1 h to ensure the asphaltenes were completely dissolved. While stirring, 275 mL of heptane was slowly added to the mixture. The final mixture had a heptane:toluene volume ratio of 55:45 and an asphaltene-solids concentration of 10 g/L. The mixture was stirred for an additional hour and then centrifuged at 9400g for about 45 min. Following centrifugation, the supernatant was vacuum filtered through a 0.22 μm filter and then placed into an oven set to 40°C to evaporate the solvent. For this method, the recovered 'solids-free' asphaltenes and discard precipitate account for about 14.9 %wt and 1.5 %wt of the total bitumen, respectively. Note that the amount of asphaltenes recovered from

---

[†] A complete description of the procedures used for materials preparation can be found in Appendix D.

method-II was slightly less than the amount recovered from method-I. This was due to the small amount of high molecular weight asphaltenes that precipitated with the fine solids. It was assumed that this small amount of asphaltene precipitation would remove the ultra-fine solids that could not be removed by centrifugation and filtration (i.e. solids smaller than 0.2 μm). As a matter of convenience, the asphaltenes generated from method-I and method-II will be referred to as asphaltene-I and asphaltene-II, respectively.

A sample of the asphaltenes obtained from method-I (i.e. asphaltene-I) was also treated with a series of heptane-toluene solutions. The purpose of this treatment was to fractionate the asphaltenes into several narrow fractions or cuts based on solubility where the amount of asphaltene precipitate depended on the heptane:toluene ratio. The first step in the treatment involved diluting asphaltene-I with a heptane-toluene solution of (1:1) volume ratio. The mixture was then stirred for 1 h. The first cut of asphaltenes was obtained by centrifuging the mixture at 9400g for 45 min and then decanting the supernatant through a vacuum filter. The recovered precipitate was dried in a 40°C oven. This dried material was designated asphaltene-cut#1. Heptane was added to the recovered supernatant to increase the heptane-toluene volume ratio to (1.5:1). Again, the mixture was stirred for 1 h, centrifuged, and filtered. The dried precipitate recovered from this step was designated asphaltene-cut#2. The same procedure was repeated for heptane-toluene volume ratios of (2:1), (3:1), (4:1), and (5:1). A total of seven asphaltene fractions were obtained with the last fraction, apshaltene-cut#7, containing all of the material that remained soluble in the (5:1) heptane-toluene solution. Note that asphaltene-cut#1 was expected to contain the highest molecular weight material whereas asphaltene-cut#7 was expected to contain the lowest molecular weight asphaltenes.

All samples used in the disjoining pressure measurements were prepared by mixing predetermined amounts of toluene and bitumen (or asphaltenes) for about 1 h. Since bitumen solutions are suspected of changing chemical composition when exposed to air for long periods of time (Moschopedis and Speight, 1977), all samples were used immediately after preparation.

All films were immersed into simulated industrial water. The simulated industrial water was practically identical in ionic strength and pH to the average values observed in

Syncrude's recycled plant water. The simulated industrial water was prepared be adding 0.014 M sodium chloride, 0.012 M sodium bicarbonate, and 0.004 M sodium sulfate to deionized ultra filtrated (DIUF) water (Fisher Scientific). The pH of the water was approximately 8.2.

3.2.5 Molecular Weight

The molecular weight of the asphaltene-I and asphaltene-II samples was measured using a Jupiter Model 833 vapour pressure osmometer (VPO). Details of the VPO measurements can be found elsewhere (Yarranton et al., 2000b).

3.3 Results and Discussion

3.3.1 Isotherms for Water/Toluene-Diluted-Bitumen/Water Films

The disjoining pressure isotherms for water/toluene-diluted-bitumen/water films are displayed in Figures 3.4 and 3.5. Isotherms were measured for five different toluene to bitumen mass ratios: (1:1), (2:1), (3:1), (5:1) and (10:1). At a toluene:bitumen mass ratio of (1:1), the isotherm began in a region of soft repulsion where the film was easily compressed from about 32 nm to less than 10 nm. At a film thickness of 8.5 nm, the film could no longer be compressed with increases in applied pressure. The film remained stable over the entire measurable range of pressure. Also, the same thickness measurements were obtained when the applied pressure was decreased indicating that the disjoining pressure was completely reversible.

The region of hard-wall repulsion is most likely due to steric interactions between the two interfaces of the film however, the origin of the soft repulsion region is not clear. It is possible that the soft repulsive force may be due to weak steric interactions similar to those observed for two mica surfaces separated by a thin film of anhydrous oil containing polyclycerol polyricinoleate (Dedinaite and Campbell, 2000). Alternatively, the shape of the curve in the soft repulsive region suggests a possible weak electrostatic repulsion may be present in the film. In the non-polar toluene-bitumen solutions, the relative dielectric constant is quite small (i.e. on the order of 4 to 5) and the counter-ion concentration is expected to be quite low (i.e. on the order of 10^{-6} M). Under these conditions,

conventional DLVO theory suggests that a colloidal force due to a screened electrostatic double layer within the water/oil/water film is expected to be negligible (Becher, 1987; Claesson et al., 2001). However, it is possible that an electrostatic force may still be present between the interfaces of the film. Recent attempts have been made to describe electrostatic repulsion in a non-polar media (Zholkovskij et al., 2001a; Zholkovskij et al., 2001b).

Dilution to higher toluene:bitumen mass ratios was expected to reduce the concentration of surface active material at the oil-water interfaces and hence, produce a weaker force within the film. However, an increase to a mass ratio of (2:1) produced an isotherm identical to the isotherm for a (1:1) mass ratio. A further increase in dilution to a mass ratio of (5:1) produced a new, separate isotherm. This isotherm began in a region of soft repulsion where the film was easily compressed from 20 nm to about 10 nm. The film ruptured before reaching hard wall repulsion. The film rupture occurred consistently at a disjoining pressure of 220 ± 20 Pa and a critical thickness of about 10 nm. The (10:1) mass ratio produced an isotherm identical to the isotherm for a (5:1) mass ratio.

There are several important implications to the isotherms displayed in Figure 3.4:

1. At low dilution ratios, an 8.5 nm thick bilayer was obtained. The thickness of the bilayer indicated that the surface active material at the oil-water interface had a length dimension of about 4.2 nm when the film was compressed.

2. The stability of the films at mass ratios of (1:1) and (2:1) suggests that water-in-oil emulsions created from low toluene:bitumen mass ratios are likely to be stable over time. Conversely, the appearance of a low rupture pressure for the films of (5:1) and (10:1) mass ratios suggests that emulsions created from higher toluene:bitumen mass ratios are likely to be unstable over time. A similar trend has been observed in dewatering experiments performed on water-in-crude-oil emulsions where increases in the aromatic solvent concentration led to greater amounts of resolved water (McLean and Kilpatrick, 1997a; Mouraille et al., 1998).

3. The disjoining pressure-thickness data were collected from several films that cover a broad range of bitumen concentration and it was expected that a separate isotherm would be produced at each concentration. Instead, only two well-defined isotherms were obtained. It is suspected that this observation may be related to a transition from

one distinct organization of surfactant molecules at the interfaces to another. It is possible that each one of these organizations are similar to a distinct organization of molecules or phase within the bulk system. It is known that a particular molecular organization at an interface can be formed at a concentration much lower than that required for the formation of the corresponding bulk phase. (Pomianowski and Czarnecki, 1974; Pomianowski and Czarnecki, 1987). Therefore, if such a transition between distinct organizations does occur within the film, then it may occur at much lower surfactant concentration than that would be required for the corresponding bulk phase change in the toluene-bitumen-water system.

4. It is well known that water-oil-surfactant systems may form more than two bulk phases (Friberg, 2001). For example, multiple bulk phase behavior does occur in a system of water and sodium naphthenates, natural surfactants found in bitumen (Horváth-Szabó et al., 2001a). It has also been shown that a system of water, toluene and sodium naphthenates may produce as many as five separate bulk phases (Horváth-Szabó et al., 2001b). While these findings certainly do not provide any proof that multiple phase behavior occurs in a system of water, toluene, and bitumen, the findings do suggest that the *possibility* does exist that the two isotherms may correspond to two different bulk phases. Hence, a corresponding change in the molecular arrangement at the interface may be responsible for the change in film stability that is observed in Figure 3.4.

It is important to note at this point that care must be taken to make only qualitative comparisons between the behavior of the thin film and the behavior of an emulsion. For example, comparisons can be made between trends in concentration that are observed in thin films and the trends in concentration that are observed in emulsions. Direct quantitative comparisons require that the film be formed under conditions that are identical to the conditions of the corresponding emulsion. For example, the stability of a film, as measured by its rupture pressure, depends to some extent on the film diameter. The stability typically decreases with increased film diameter. In this study, the film diameter was approximately 800 μm. The water-in-diluted-bitumen emulsions encountered in a typical industrial situation contain water droplets that are only a few

microns in diameter. Clearly, the rupture pressure of these two systems are quite different.

The suggestion of a phase change at the interface implies the existence of a critical mass ratio. Above the critical mass ratio, it is expected that the film stability would be described by the isotherm for the (5:1) and (10:1) mass ratios. Below the critical mass ratio, the film stability would be described by the isotherm for the (1:1) and (2:1) mass ratios. The disjoining pressure-thickness data displayed in Figure 3.5 suggests that a mass ratio of (3:1) is close the critical mass ratio. As a reference, the isotherms from Figure 3.4 are plotted using the open symbols.

The disjoining pressure-thickness data for a (3:1) mass ratio depended on time. If the experiment was started after the water and oil phases were in contact for over 30 min, then the disjoining pressure-thickness data for a film of a (3:1) mass ratio coincided with the isotherm for a mass ratios of (1:1) and (2:1). Again, the same data was obtained for both increasing and decreasing applied pressures (i.e. the isotherm was reversible). Unlike the films of mass ratios (1:1) and (2:1), the film of (3:1) mass ratio ruptured consistently at a thickness of about 10 nm and disjoining pressure of 330 ± 20 Pa. Hard steric repulsion was never observed. If the experiment was started almost immediately after the initial contact between the water and oil phases, the first few disjoining pressure-thickness data points would fall onto the isotherm for mass ratios of (5:1) and (10:1). About 30 min into the measurement, independent of pressure or thickness, the film would then spontaneously increase in thickness so that the disjoining pressure-thickness data would begin to fall onto the isotherm for the (1:1) and (2:1) mass ratios. For example, Figure 3.5 shows that the film increased in thickness from 17.2 nm to 21.4 nm at a constant disjoining pressure of 135 Pa. After the spontaneous increase in thickness, all subsequent disjoining pressure-thickness data coincided with the isotherm for mass ratios of (1:1) and (2:1). The spontaneous increase in thickness was irreversible suggesting that just below the critical mass ratio, time is needed for the phase change or conformational rearrangement to occur. The spontaneous increase in thickness occurred against externally applied pressure (i.e. the film was performing work on its surroundings). The energy for this work is likely to come from the free energy change corresponding to the phase transition discussed above.

3.3.2 Isotherms Obtained Using the Dynamic Method

The pattern of drainage for a water/toluene-diluted-bitumen/water film has been described qualitatively in Chapter 2. In Chapter 2, it was observed that the film drains in a plane-parallel fashion once the film thickness is less than 100 nm. Additional observations indicate that the plane-parallel drainage was limited to films where the applied pressure was below 40 Pa and the film radius was 150 μm or less. The occurrence of plane-parallel drainage suggests that the dynamic method of Scheludko (Scheludko, 1967; Ivanov, 1988) could be used to extend the disjoining pressure isotherms to larger thicknesses in order to determine if any other significant oscillatory or attractive forces exist.

The dynamic method makes use of the Stefan-Reynolds equation (Scheludko, 1967; Ivanov, 1988):

$$\frac{dh}{dt} = -\frac{2h^3}{3\eta r^2}\left(P_C - \Pi_{dyn}(h)\right)$$

[3.6]

where t is time, η is the bulk viscosity of the oil phase, and Π_{dyn} is the disjoining pressure. The subscript 'dyn' is used to emphasize that the disjoining pressure was measured using the dynamic method. The derivation of the Stefan-Reynolds equation requires several important assumptions, including: 1) the two interfaces of the film are plane-parallel, 2) the film drains in an axi-symmetric fashion, and 3) the two interfaces are tangentially immobile. Measurements of the film thickness at three different locations confirm that the film was indeed plane-parallel. The presence of a saturated layer of surfactants adsorbed on an interface would reduce the mobility at the interface to zero (Jeelani and Hartland, 1994; Claesson et al., 2001). The high bitumen concentrations used in this study ensure that there is sufficient interfacially active material to provide complete coverage of the interfaces. Therefore, the interfaces were probably tangentially immobile.

Changes in film thickness over time for mass ratios of (3:1) and (5:1) are shown in Figures 3.6 and 3.7, respectively. Each figure contains a plot of the Stefan-Reynolds equation for the case of $\Pi_{dyn} = 0$ (denoted by the dashed line). The similarity in the plot

to the thickness-time data indicates that the Stefan-Reynolds provides a reasonable description of the drainage rate within the thin film. A three parameter, exponential decay equation was fit to the thickness-time data using least squares regression:

$$h = a + b \exp(-ct)$$ [3.7]

where a, b, and c were the fitting parameters. The fit of Eq. [3.7] to the data is shown as solid lines in Figures 3.6 and 3.7. The calculation of Π_{dyn} from the experimental data requires an estimate of the rate of drainage (dh/dt) at each point in time. The rate of drainage was estimated from the derivative of Eq. [3.7]:

$$\frac{dh}{dt} = -bc\exp(-ct)$$ [3.8]

Substitution of Eq. [3.8] into the Stefan-Reynolds equation provides a working relation for the calculation of Π_{dyn}:

$$bc\exp(-ct) = \frac{2h^3}{3\mu r^2}\left(P_c - \Pi_{dyn}(h)\right)$$ [3.9]

Isotherms of $\Pi_{dyn}(h)$ for water/toluene-diluted-bitumen/water films for mass ratios of (3:1) and (5:1) were calculated from Eq. [3.9] where the values of b and c were obtained from the fitted curves in Figures 3.6 and 3.7. The viscosity was taken from Table 2.2. The capillary pressure, P_c, was calculated using Eq. [3.4] and it was assumed to be constant over time. The film radius was also constant and could be obtained from visual observations of the film.

The disjoining pressure isotherms obtained using the dynamic method are shown in Figure 3.8. The results appear to be consistent with the previously measured isotherms (denoted by the open symbols). The isotherms obtained from the dynamic method indicate that, at larger distances, no significant colloidal forces existed within the film.

For the (5:1) mass ratio, the data becomes slightly negative around 30 nm and it is tempting to suggest that a weak attractive force existed in the film. However, the minimum calculated disjoining pressure was only about –20 Pa. This is smaller than the error associated with the dynamic method.

3.3.3 Isotherms for Water/Toluene-Diluted-Asphaltene/Water Films

As mentioned earlier, asphaltenes have been identified as the fraction of bitumen that is primarily responsible for the stability of water-in-diluted-bitumen (and water-in-crude oil) emulsions. It is therefore beneficial to determine how the disjoining pressure isotherms presented in Figure 3.4 are influenced by surface active material found in the asphaltene fraction. Thin films of water/toluene-diluted-asphaltenes/water were created using heptane precipitated asphaltenes. These asphaltenes contain a small fraction of toluene-insoluble material or 'fine solids'. It has been suggested that these fine solids may aid in the emulsion stability (Kotlyar et al., 1998; Yan et al., 1999) and hence, may influence the thin film stability. Therefore, it was important to remove any fine solid material from the precipitated asphaltenes. Since it is very difficult to obtain a 'clean' separation between the fine solids and asphaltenes, two different methods were used to separate the asphaltenes and fine solids. Method-I was expected to remove all fine solid material larger than 0.2 μm. Method-II was expected to remove all of the fine solid material and a small fraction of the least soluble asphaltenes.

The isotherms for water/toluene-diluted-asphaltene-I/water films are displayed in Figure 3.9. The isotherms were generated for two asphaltene-I concentrations, 60 g/L and 25 g/L. The two concentrations roughly correspond to the asphaltene-I concentration in toluene-bitumen solutions of mass ratios (1:1) and (3:1), respectively. For comparison, the isotherm from Figure 3.4 for a film of toluene:bitumen mass ratio of (1:1) is also shown. From Figure 3.9, it is clear that the isotherms for water/toluene-diluted-asphaltene-I/water films have been shifted to the right as compared to the isotherms for water/toluene-diluted-bitumen/water films. This clearly indicates that the asphaltenes alone produce a stronger steric repulsion. However, the toluene-asphaltene-I film was compressed to the same 8.5 nm bilayer thickness that was observed earlier. This suggests that the surface active material at the bitumen-water interface was composed primarily of

asphaltenes or some component associated with the asphaltene precipitate. It is also interesting to note that the same isotherm was obtained for both the 25 g/L and 60 g/L concentrations, again suggesting the possibility of a phase change at the interface. As will be shown later, a different film behavior is observed at lower asphaltene-I concentrations.

Only the isotherm for the 60 g/L asphaltene-I concentration proved to be completely reversible (i.e. the same disjoining pressure-thickness data was obtained with increasing and decreasing applied pressures). Figure 3.10 shows that, at a 25 g/L asphaltene-I concentration, slightly different disjoining pressure-thickness data was obtained for increasing and decreasing applied pressures.

The isotherm for water/toluene-diluted-asphaltene-II/water film is shown in Figure 3.11. A comparison between Figures 3.9 and 3.11 indicates that the procedure used to obtain asphaltenes had a significant effect on the isotherms. When method-I was used, only one isotherm was obtained for a given asphaltene concentration. When method-II was used, a single asphaltene concentration produced a narrow distribution of possible disjoining pressure isotherms. The distribution of possible isotherms is shown by the dashed lines in Figure 3.11. These isotherms are similar to the previous isotherms in that a hard steric wall was encountered after a region of soft steric repulsion. However, the films of toluene-diluted-asphaltenes-II ruptured at an average pressure of about 590 Pa. Also, the thickness of the bilayer at the hard wall ranged from 7.3 nm down to about 5.1 nm, significantly less than the previously measured thickness of 8.5 nm. Unlike method-I, a small amount of the highest molecular weight asphaltenes was expected to be removed with the ultra-fine solids in method-II. It appears that the removal of the high molecular weight asphaltenes and the ultra fine solids is responsible for the reduction in the hard wall thickness and reduced thin film stability.

The removal of the high molecular weight asphaltenes should result in a change in the average molecular weight of asphaltenes. Vapor pressure osmometry was used to obtain the molecular weight of asphaltene-I and asphaltene-II in toluene at concentrations of both 25 and 60 g/L. At such high concentrations, asphaltenes are known to form aggregates in toluene solutions (Yarranton et al., 2000a). Hence, the results given in Table 3.1 clearly show that aggregates of asphaltene-I have a higher average molecular

TABLE 3.1: Molecular weight of asphaltene-I and asphaltene-II as measured by vapor pressure osmometry.

Concentration (g/L)	Molecular weight of Asphaltene-I (g/mol)	Molecular weight of Asphaltene-II (g/mol)
25	4017	3096
60	4337	3276

weight compared to the aggregates of asphaltene-II. It is not clear if this means that the average *monomer* molecular weight of asphaltene-I is larger than the average *monomer* molecular weight of asphaltene-II or that the aggregates in the toluene-asphaltene-I solutions are simply larger than the aggregates in the toluene-asphaltene-II solutions. However, it is interesting to note that the reduction in the molecular weight correlates with the reduction in the bilayer thickness.

As mentioned, Figure 3.11 showed that a distribution of isotherms was obtained for a single asphaltene-II concentration. This observation could be explained from direct viewing of the film. Unlike the previously described films, the film created from toluene-diluted-asphaltene-II was not uniform in thickness. The film appeared to contain several large areas that differed slightly in shading. Thickness measurements confirmed that each area was plane-parallel and that the equilibrium thickness differed slightly between each area. The boundaries between each area were well defined, although these boundaries often moved causing a slow shift in the shape, size, or location of each area. It was suspected that as each isotherm was measured, the small (10 μm) spot of light used to measure the thickness was focused on only one of these areas within the film. The measured isotherm then applied only to that specific area within the film. Repeated measurements of the isotherm would result in the spot of light being focused onto a different area and a slightly different isotherm would be obtained for that area. After several repeated measurements, the final result was the distribution in disjoining pressure isotherms that appear in Figure 3.11. Hence, the isotherms in Figure 3.11 represent the range of possible behavior that would occur with a film of toluene-diluted-asphaltene-II.

3.3.4 Formation of Rigid Interfaces

The behavior of the water/toluene-diluted-asphaltene/water films changed dramatically for asphaltene concentrations lower than those reported in Figures 3.9 and 3.11. At concentrations lower than 25 g/L for asphaltene-I and 60 g/L for asphaltene-II, the films began to show indications that the oil-water interfaces were becoming rigid. Early indications of rigidity included the appearance of several small dimples throughout the film, loss of circular symmetry, and extremely long drainage times. These effects became more severe over time. After the water and oil phases had been in contact for some time, film drainage would become negligible and the interfaces would appear more like the protective 'skins' that have been observed in other studies (Isaacs and Morrison, 1985, Yeung et al., 1999). An example of the protective skin is shown in Figure 3.12. The images show a water droplet formed at the tip of a micropipette (Figure 3.12(a)). The water droplet is immersed in a mixture of heptol (1:1 heptane:toluene by volume) and bitumen. The protective skin that surrounds the droplet can be clearly observed when attempts are made to reduce the size of the water droplet (Figure 3.12(b)). In the case of thin films, the protective skin normally appears after more than an hour of contact between the water and oil phases. For more dilute asphaltene solutions, the protective skin did appear after only a few minutes of contact between the water and oil phases.

Observations of films from toluene-diluted-asphaltene-cut#1 and toluene-diluted-asphaltene-cut#4 showed behavior similar to that described above. In the case of asphaltene-cut#4, the interfaces appeared quite fluid shortly after the initial contact between the water and oil phases. An image of the film with fluid interfaces is shown in Figure 3.13(a). The film is circular with clearly defined Newton rings around its boundary and a single large centre dimple in the middle. Following channel drainage, this film becomes uniform in thickness. Once a uniform thickness is obtained, the film continues to drain at a rate of drainage that is well described by the Stefan-Reynolds equation (see Chapter 2). After about an hour of contact time, the film began to show signs of rigidity. Figure 3.13(b) is an image of the film considered to have rigid interfaces. The image clearly shows several small dimples scattered randomly throughout the film and that the film is no longer perfectly symmetric. The drainage rate within this film was extremely slow, often requiring more than an hour to detect any significant

decrease in film thickness. Once this type of rigid interface appeared, it was impossible to obtain any meaningful quantitative measurements.

After nearly two hours of contact between the water and hydrocarbon phases, a protective skin was formed. Under these conditions, the behavior of the film became very inconsistent. The film appearance was often similar to the image in Figure 3.13(b) although, there were instances where it was impossible to form a well-defined film. An example of this situation is shown in Figure 3.13(c) where several small films were formed within the larger area of contact between the two interfaces. It was possible to force the film containing the protective skin to rupture. A portion of the ruptured skin often remained in the hole of the porous plate and could be clearly seen with normal incident lighting (Figure 3.13(d)). The described transition from a fluid oil/water interface to a protective skin occurred consistently at low asphaltene-I and asphaltene-II concentrations as well as at concentrations as high as 60 g/L for asphaltene-cut#1 and asphaltene-cut#4. However, a film created from a toluene-asphaltene-cut#7 solution did not show any indication of rigidity in the oil-water interfaces. The interfaces appeared to remain completely fluid even after eight hours of contact between the water and oil phases.

Asphaltene-cut#1 was the first fraction of asphaltene to be precipitated from the heptane-toluene solution during the fractionation procedure. This first fraction was expected to contain the most polar and highest molecular weight asphaltenes (Yarranton, 1997). Subsequent cuts were expected to contain, on average, asphaltenes of lower molecular weight and lower polarity with the last cut from the fractionation procedure (asphaltene-cut#7) containing the lowest molecular weight and least polar asphaltenes. Since asphaltene-cut#7 produced only fluid interfaces, it appears that the middle to higher molecular weight and the more polar fraction of asphaltenes are responsible for the formation of the rigid interfaces or 'protective skin'.

3.4 Conclusions

A modified version of the Thin Liquid Film-Pressure Balance Technique has been used to obtain disjoining pressure-thickness isotherms for films of water/toluene-diluted-bitumen/water and water/toluene-diluted-asphaltene/water. The isotherms from both types of film were similar suggesting that surface active material from the asphaltene fraction of bitumen resides on the oil-water interfaces. Stable films were formed for both low toluene:bitumen mass ratios and high asphaltene concentrations. The stability was likely due to a surfactant bilayer that produced a strong, short range repulsive force. In the case of high toluene:bitumen ratios, only a weak repulsive force was present causing the film to rupture at low disjoining pressures. The transition between stable and unstable film behavior did not occur gradually. Instead, the film stability over a large range of mass ratio was described by only two isotherms. The transition between the two isotherms occurred at a critical mass ratio just above (3:1). This sharp transition suggested that a change may be occurring in the molecular arrangement of the surfactant molecules at the film interfaces.

Isotherms of water/toluene-diluted-asphaltene/water films also suggested that the procedure used to prepare the asphaltenes affects film stability. Comparison between the two procedures indicates that the removal of the highest molecular weight asphaltenes and ultra fine solids reduces both the thickness of the film bilayer and the film stability. At low asphaltene concentrations, disjoining pressure isotherms could not be measured since the oil-water interfaces became rigid.

While we have been successful in measuring the interactions within a water/bitumen/water film, several unanswered questions still remain. For example, more traditional emulsion stability studies have tried to link the solubility state of asphaltenes to emulsion stability. However, our work has been limited to a single aromatic solvent. This raises the question of how a change in solvent strength towards a more aliphatic solvent will affect the film stability. Also, other researchers have initiated studies on the multiple phase behavior that occurs in a system of water, toluene and natural surfactants extracted from crude oil (e.g. sodium naphthenates). Our results suggest a change in the molecular arrangement at the film interfaces when there is a change in the bulk concentration of bitumen. This raises additional questions as to the role of natural

surfactants in the stability of water-in-diluted-bitumen emulsions and how the phase behavior of natural surfactants in bulk liquids may be related to film behavior for both toluene-diluted-bitumen films or films stabilized by sodium naphthenates. Future studies directed toward answering these questions may yield some new insights into the molecular structure at a bitumen-water interface.

3.5 References

Becher, P., in "Interfacial Phenomena in Apolar Media" edited by Eicke, H.F. and Parfitt, G.D., p.275-281. Marcel Dekker, New York, 1987.

Bergeron, V. and Radke, C.J., *Langmuir* **8** (1992) 3020-3026.

Christenson, H.K. and Israelachvili, J.N., *J. Colloid Interface Sci.* **119** (1987) 194-202.

Claesson, P.M., Blomberg, E., and Poptoshev, E., in "Encylopedic Handbook of Emulsion Technology" edited by Sjöblom, J., p.305. Marcel Dekker, New York, 2001.

Czarnecki, J., in "Encyclopedic Handbook of Emulsion Technology", edited by Sjöblom, J., p.497. Marcel Dekker, New York, 2001.

Dedinaite, A. and Campbell, B., *Langmuir* **16** (2000) 2248-2253.

Ese, M.-H., Sjöblom, J., Fordedal, H., Urdahl, O., and Rønningsen, H.P., *Colloid Surf. A* **123-124** (1997) 225.

Ese, M.-H., Yang, X., and Sjöblom, J., *Colloid Polym. Sci.* **276** (1998) 800-809.

Exerowa, D. and Kruglyakov, P.M. "Foam and Foam Films", Elsevier, New York, 1998.

Exerowa, D., Ivanov, I. and Scheludko, A., in "Issledovaniya v oblasti poverkhnostnykh sil" (Derjaguin, B.V., Ed.) p.158. Nauka, Moscow, 1964. *(in Russian)*

Exerowa, D. and Scheludko, A., *Comp. Rend. Acad. Bulg. Sci.* **24** (1971) 47.

Friberg, S.E., in "Encyclopedic Handbook of Emulsion Technology" (J. Sjöblom, Ed.) p.47-48. Marcel Dekker, New York, 2001.

Groenzin, H. and Mullins, O.C., *Energy & Fuels*, **14** (2000) 677-684.

Horváth-Szabó, G., Czarnecki, J. and Masliyah, J., *J. Colloid Interface Sci.* **236** (2001a) 233-241.

Horváth-Szabó, G., Czarnecki, J. and Masliyah, J., *J. Colloid Interface Sci.* (2001b) In press.

Isaacs, E.E. and Morrison, D.N., *AOSTRA J. Res.* **2** (1985) 113-119.

Ivanov, I.B. (Ed.) "Thin Liquid Films" Marcel Dekker, New York, 1988.

Jeelani, S.A.K. and Hartland, S., *J. Colloid Interface Sci.* **164** (1994) 296-308.

Johansen, E.J., Skjärvo, I.M., Lund, T., Sjöblom, J., Söderlund, H., and Boström, *Colloid Surf* **34** (1988) 353.

Khristov, K, Taylor, S.D., Czarnecki, J. and Masliyah, J., *Colloid Surf. A* **174** (2000) 183-196.

Kotlyar, L.S., Sparks, B.D., Woods, J.R., Raymond, S., LePage, Y. and Shelfantook, W., *Petroleum Sci. Technol.* **16** (1998) 1-19.

McLean, J.D. and Kilpatrick, P.K., *J. Colloid Interface Sci.* **189** (1997a) 242-252.

McLean, J.D. and Kilpatrick, P.K., *J. Colloid Interface Sci.* **196** (1997b) 23-34.

McLean, J.D., Spiecker, P.M., Sullivan, A.P., and Kilpatrick, P.K., *in* "Structures and Dynamics of Asphaltenes", edited by Mullins, O.C. and Sheu, E.Y., p.377. Plenum Press, New York, 1998.

Moschopedis, S.E. and Speight, J.G., *J. Materials Sci.* **12** (1977) 990-998.

Mouraille, O. Skodvin, T., Sjöblom, J., and Peytany, J.-L., *J. Dispersion Sci. Technol.* **19** (1998) 339.

Pomianowski, A. and Czarnecki, J., *J. Colloid Interface Sci.* **47** (1974) 315.

Pomianowski, A. and Czarnecki, J., *Fizykochemiczne Problemy Mineralurgii* **19** (1987) 83.

Singh, S., McLean, J.D., and Kilpatrick, P.K., *J. Dispersion Sci. Technol.* **20** (1999) 279-293.

Speight, J.G., *in* "Asphaltenes and Asphalts, 1", edited by Yen, T.F. and Chilingarian, G.V., p.7. Elsevier Science, Amsterdam, 1994.

Sheu, E.H. and Mullins, O.C. (Eds.) "Asphaltenes: Fundamentals and Applications". Plenum Press, New York, 1995.

Scheludko, A., *Kolloid Z.* **155** (1957) 39.

Scheludko, A., *Adv. Colloid Interface Sci.* **1** (1967) 391-464.

Scheludko, A. and Platikanov, D., *Kolloid Z.* **175** (1961) 150.

Wu. X., van de Ven, T.G.M., and Czarnecki, J., *Colloid Surf. A* **149** (1999) 577-583.

Yan, Z., Elliott, J.A.W., and Masliyah, J.H., *J. Colliod Interface Sci*, **230** (1999) 329-337.

Yang, X., Lu, W., Ese, M.-H., and Sjöblom, J., *in* "Encyclopedic Handbook of Emulsion Technology", edited by Sjöblom, J., p.525. Marcel Dekker, New York, 2001.

Yarranton, H.Y., Ph.D Thesis, University of Alberta, Edmonton, 1997.

Yarranton, H.W., Alboudwarej, H., and Jakher, R., *Ind. Eng. Chem. Res.* **39** (2000a) 2916-2964.

Yarranton, H.Y., Hussein, H. and Masliyah, J.H., *J. Colloid Interface Sci.* **228** (2000b) 52-63.

Yeung, A., Dabros, T., Czarnecki, J. and Masliyah, J., *Proc. R. Soc. Lond. A* **455** (1999) 3709-3723.

Zholkovskij, E., Czarnecki, J. and Masliyah, J., *J. Colloid Interface Sci.* **234** (2001a) 293-315.

Zholkovskij, E., Mishchuk, N., Dukhin, S., Masliyah, J. and Czarnecki, J., *J. Colloid Interface Sci.* (2001b) Submitted.
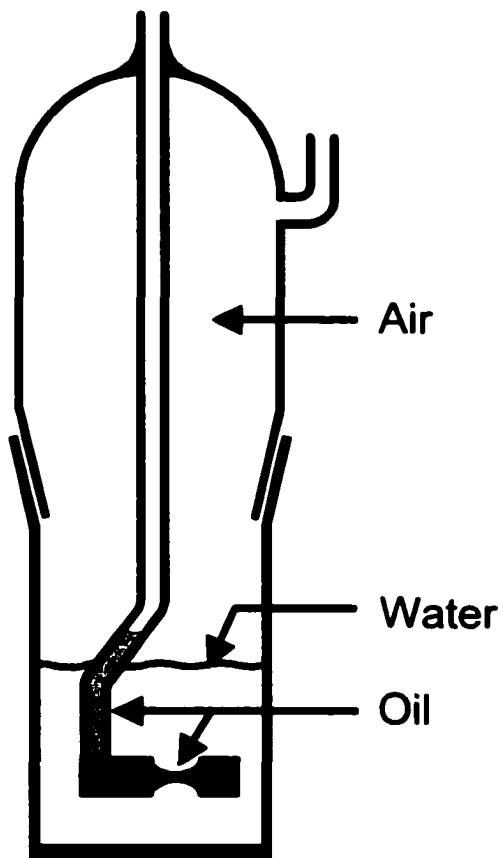
FIGURE 3.1: Porous plate measuring cell used to measure disjoining pressure – thickness isotherms.
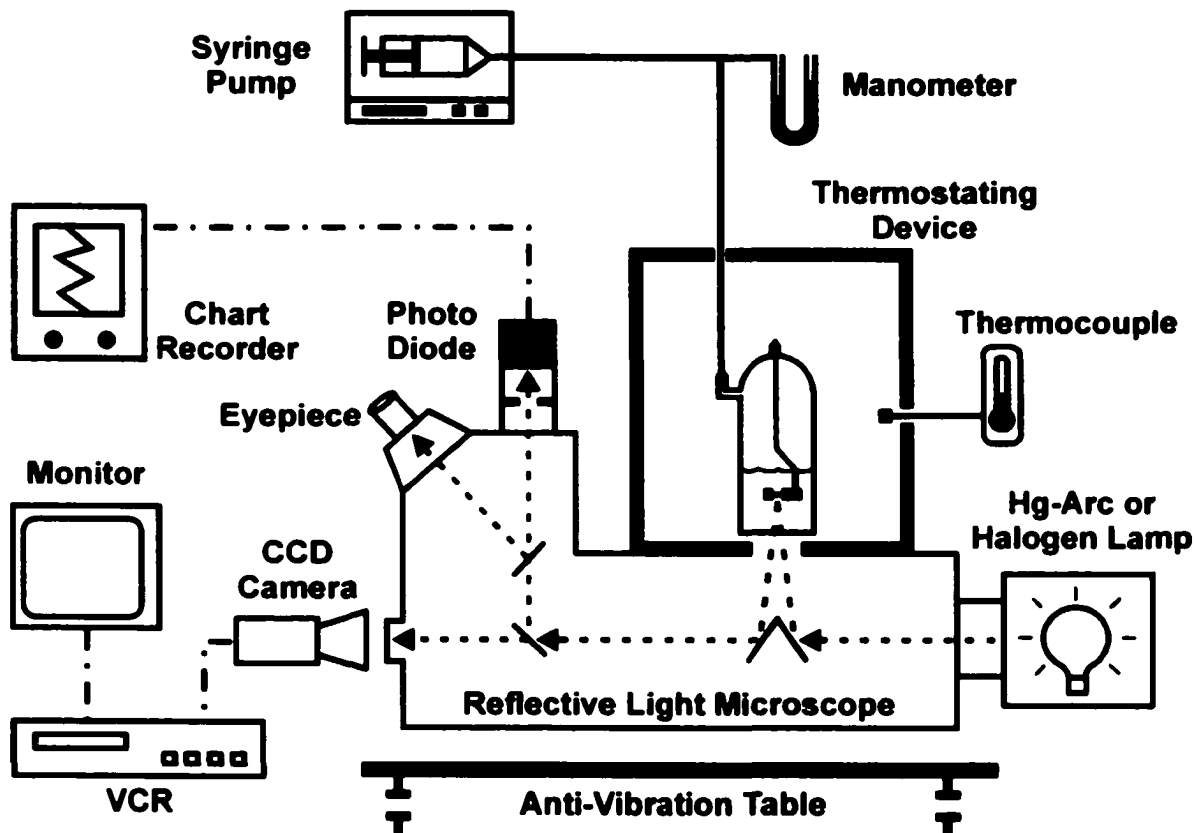
FIGURE 3.2: Schematic of the TLF-PBT apparatus used to measure disjoining pressurem - thickness isotherms.
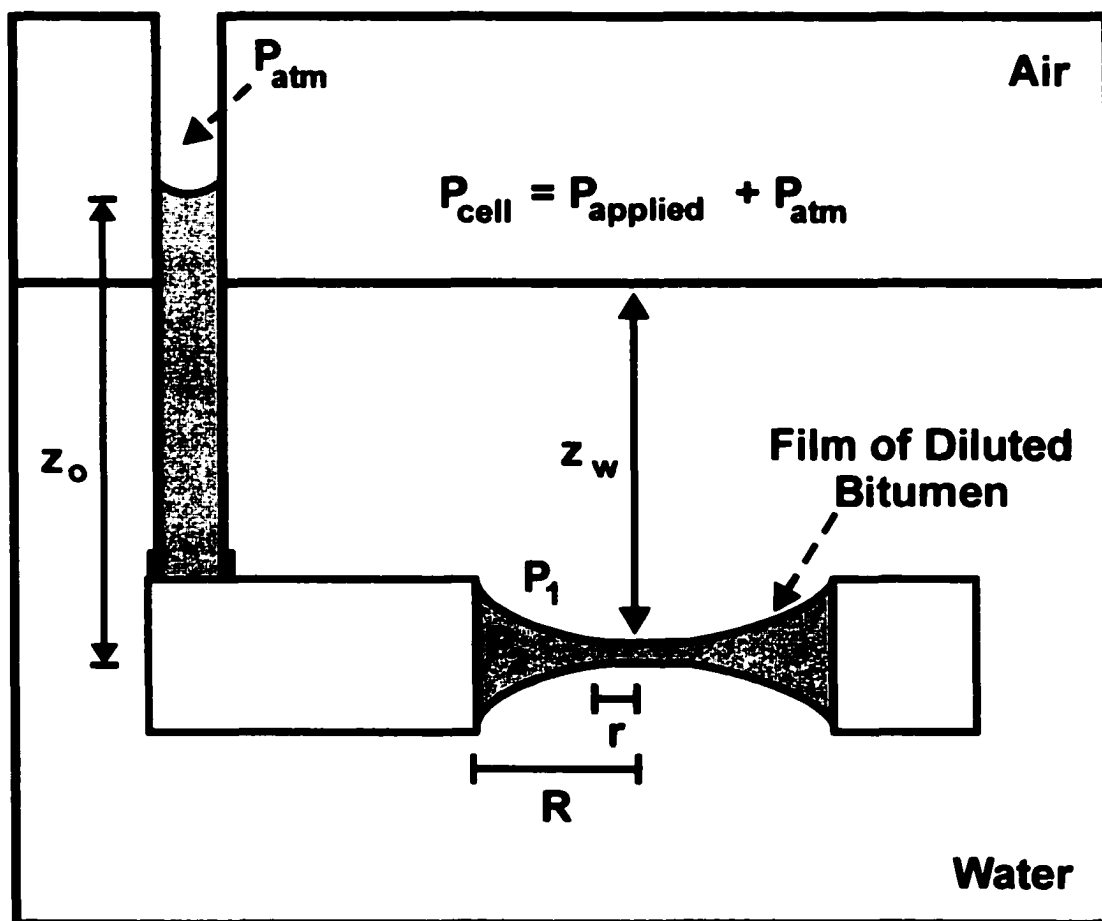
FIGURE 3.3: Schematic view of the porous plate holder.
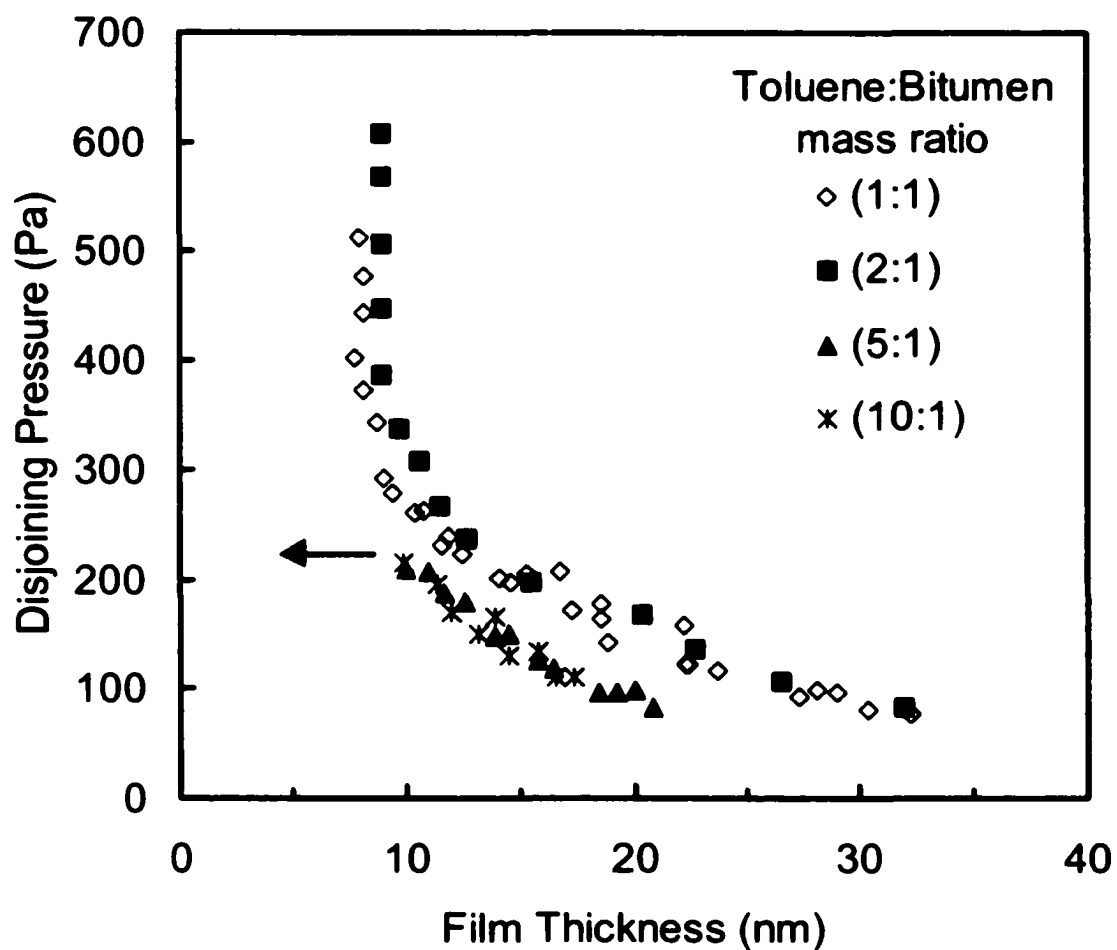
FIGURE 3.4: Disjoining pressure isotherms for films of water/toluene-diluted-bitumen/water at various mass ratios of toluene-bitumen. Arrow indicates the rupture of films at mass ratios of (5:1) and (10:1).
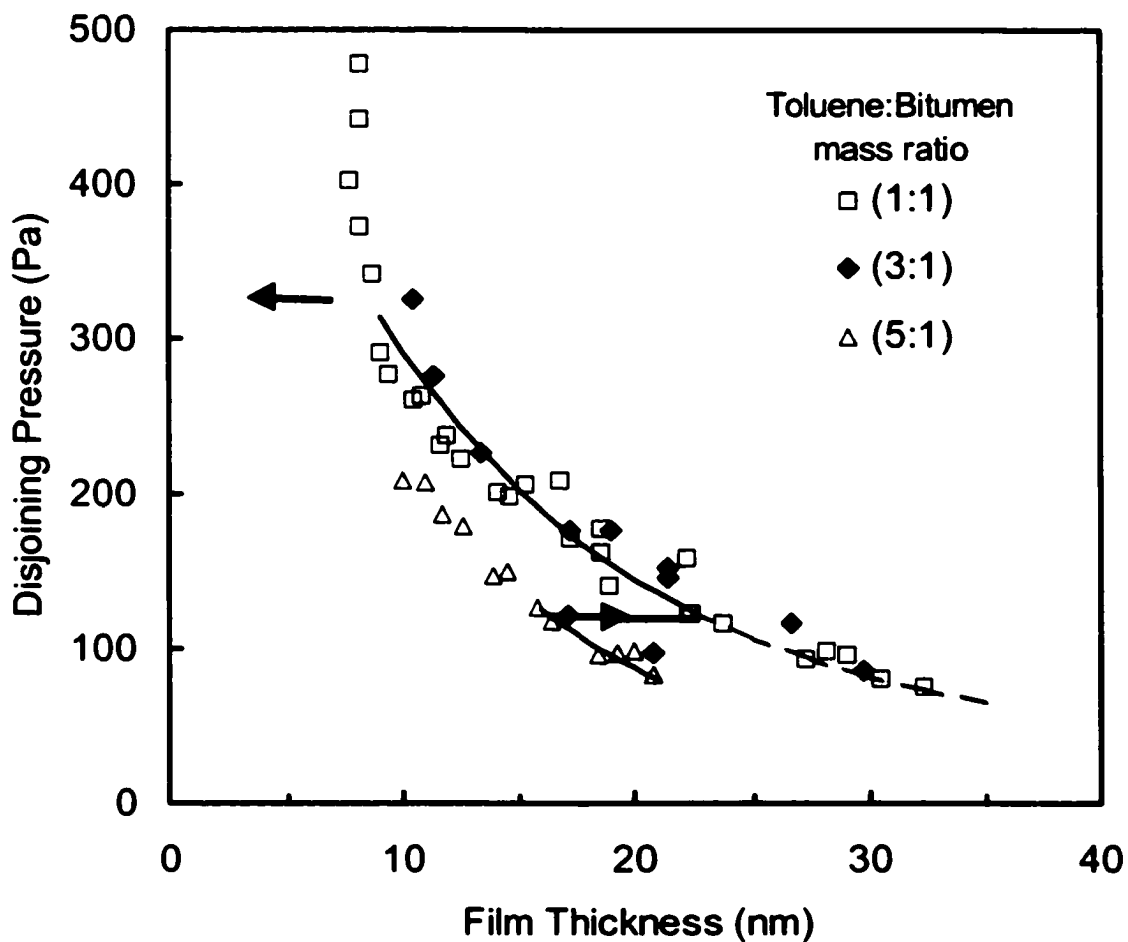
FIGURE 3.5: The disjoining pressure isotherm for a film of water/toluene-diluted-bitumen/water at a mass ratio of (3:1) toluene-bitumen shows a jump from the inner to outer isotherm about 30 minutes into the measurement. Arrows indicate rupture of the films at mass ratios of (3:1) and (5:1).
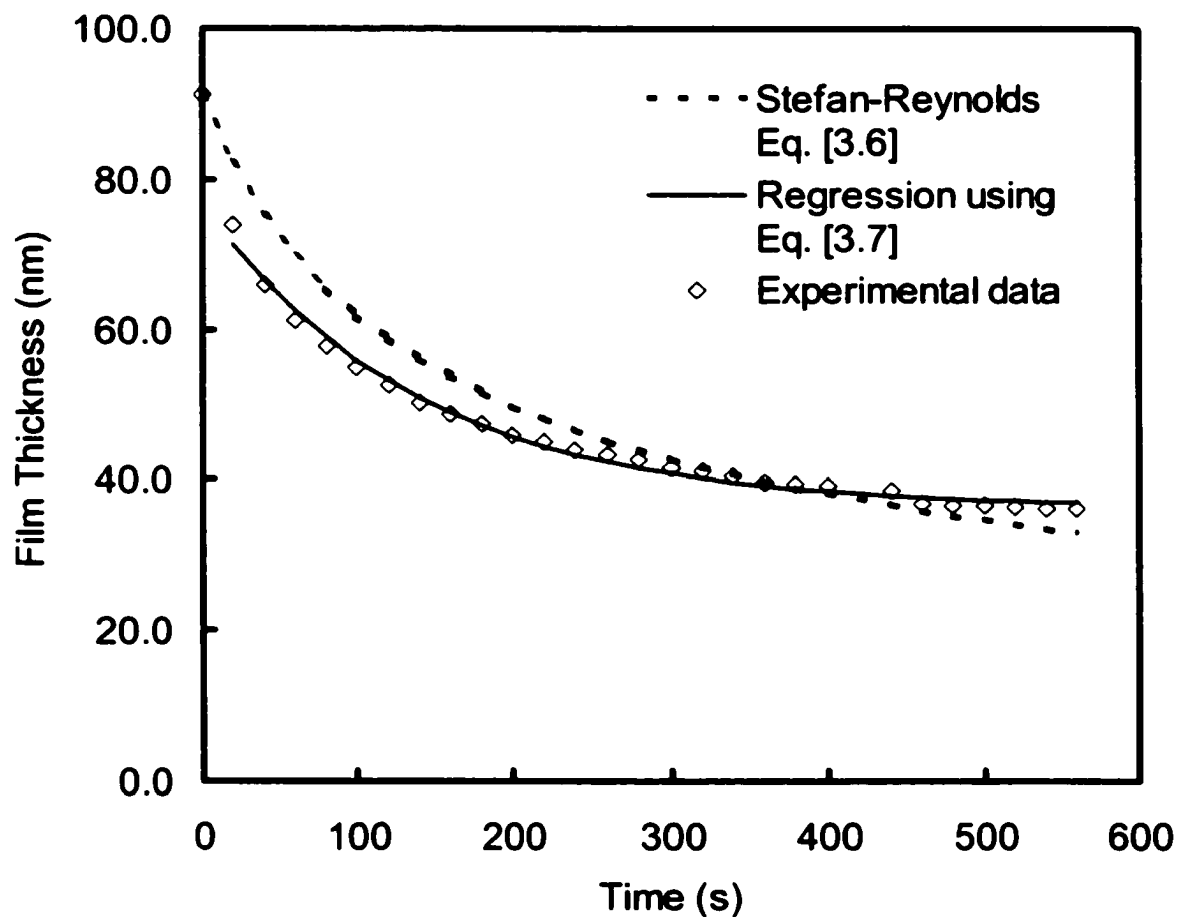
FIGURE 3.6: Thinning of a water/toluene-diluted-bitumen/water film
at a toluene-bitumen mass ratio of (3:1). The Stefan-Reynolds
calculation is obtained from Eq. [3.6] assuming $\Pi_{dyn} = 0$. (a = 36.3 nm,
b = 40.5 nm, c = 0.0073)
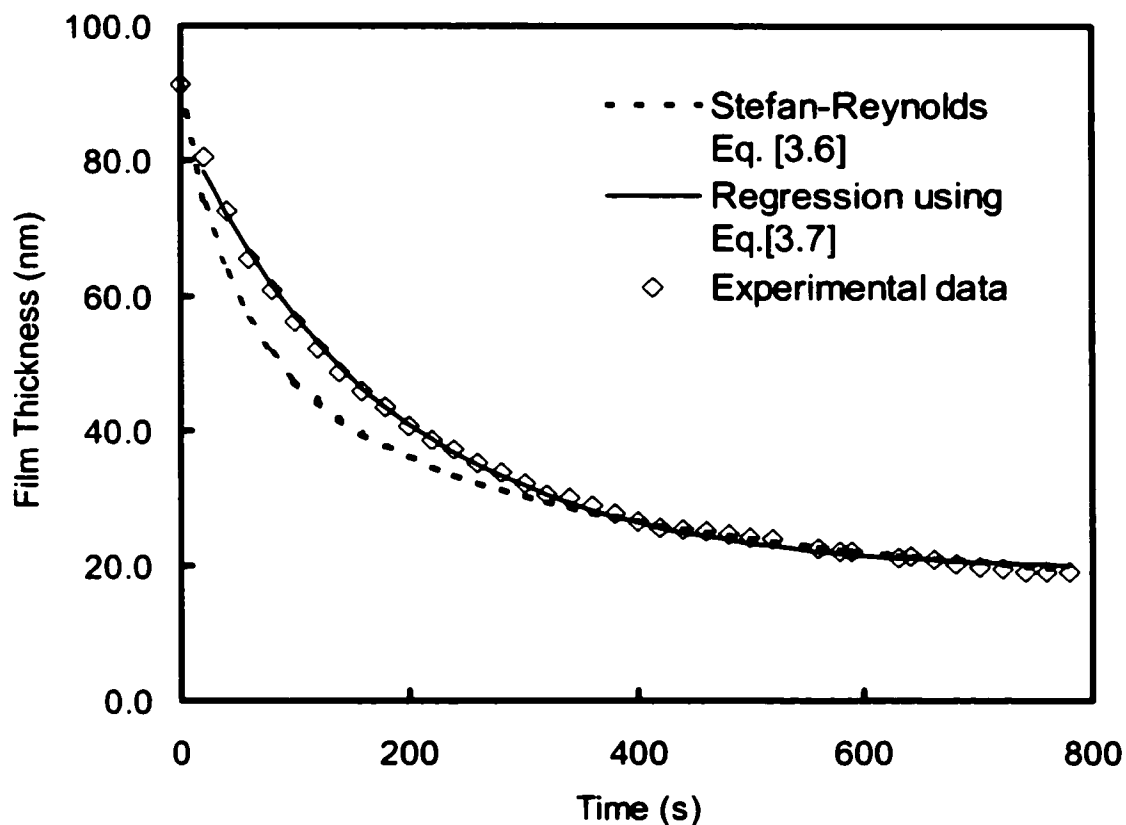
FIGURE 3.7: Thinning of a water/toluene-diluted-bitumen/water film at a toluene-bitumen mass ratio of (5:1). The Stefan-Reynolds calculation is obtained from Eq. [3.6] assuming $\Pi_{dyn} = 0$. (a = 19.1 nm, b = 66.2 nm, c = 0.0055)
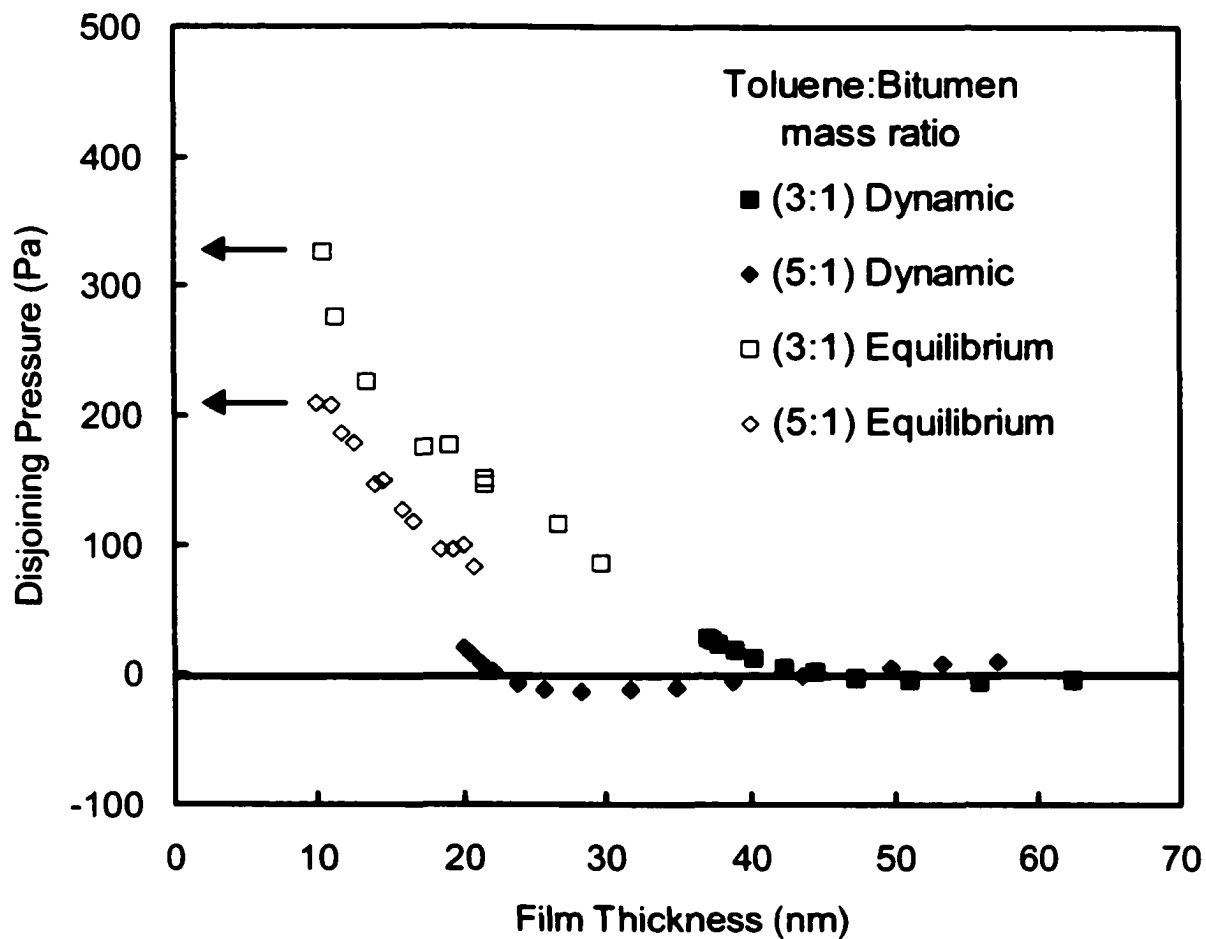
FIGURE 3.8: Dynamic disjoining pressure isotherms calculated from the thinning data in Figures 3.6 and 3.7. Arrows indicate rupture of the films at mass ratios of (3:1) and (5:1).
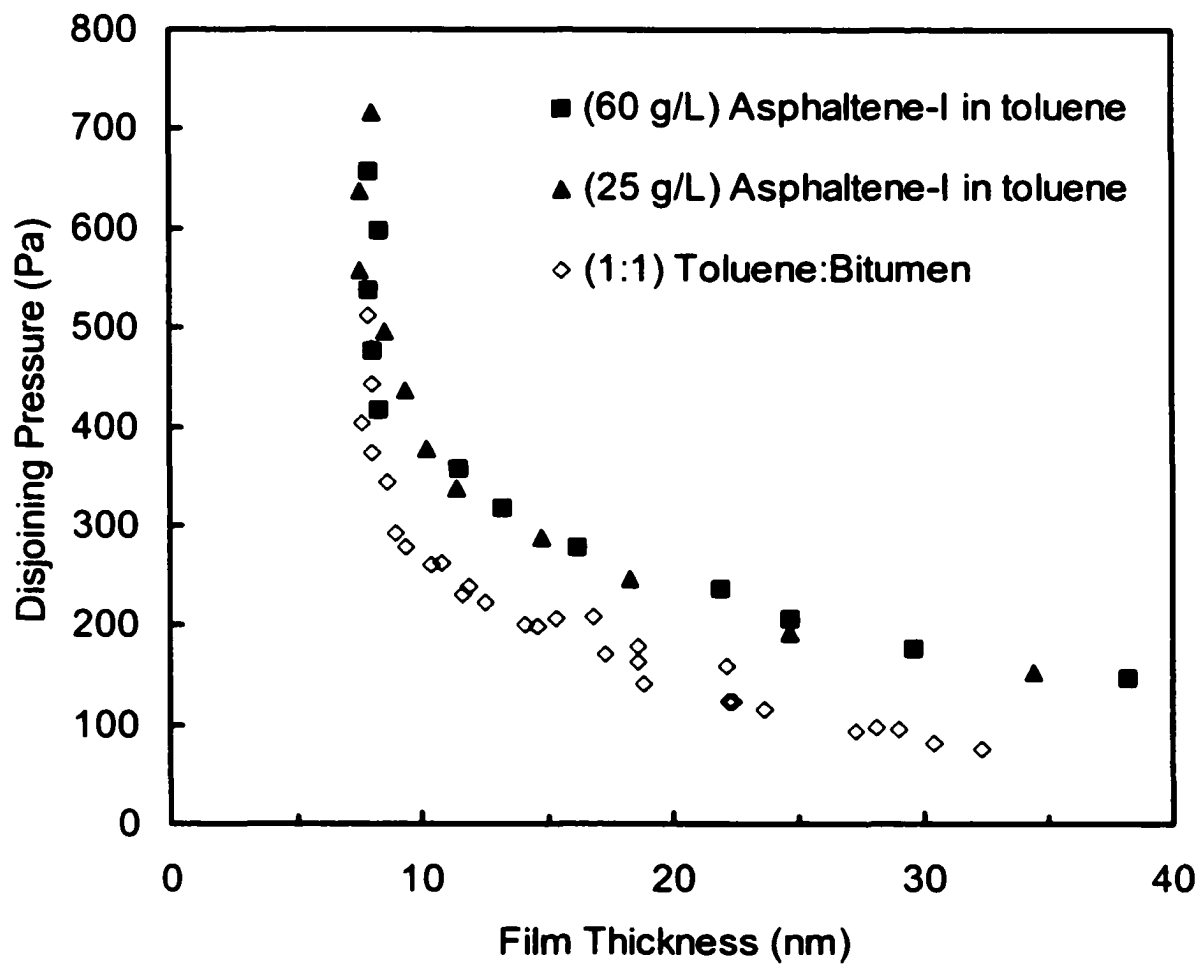
FIGURE 3.9: Disjoining pressure isotherms of water/toluene-diluted-asphaltene-1/water films. Asphaltenes were produced using method-1 to remove fine solids.
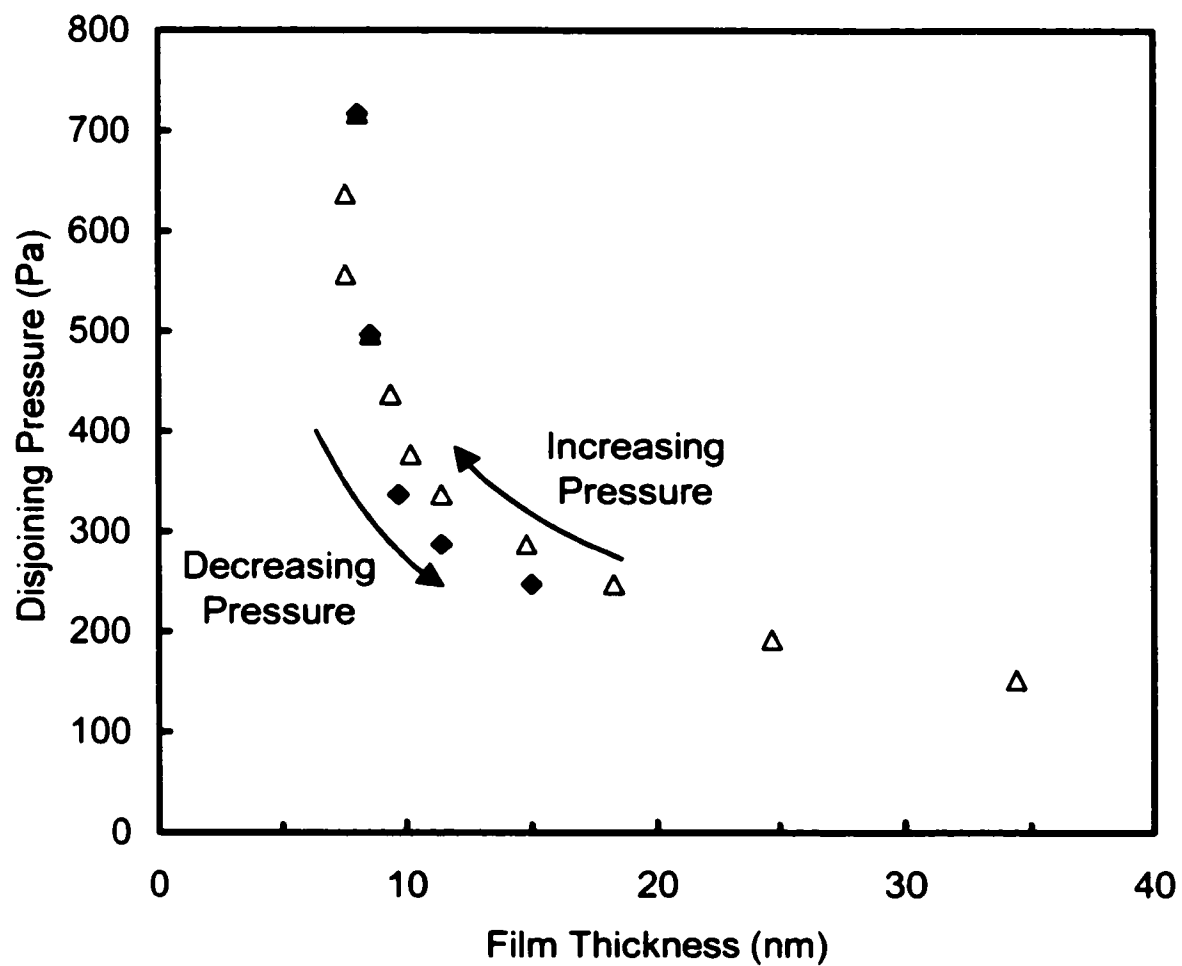
FIGURE 3.10: Non-reversibility in the disjoining pressure isotherm of water/toluene-diluted-asphaltene-l/water films at a concentration of 25 g/L.
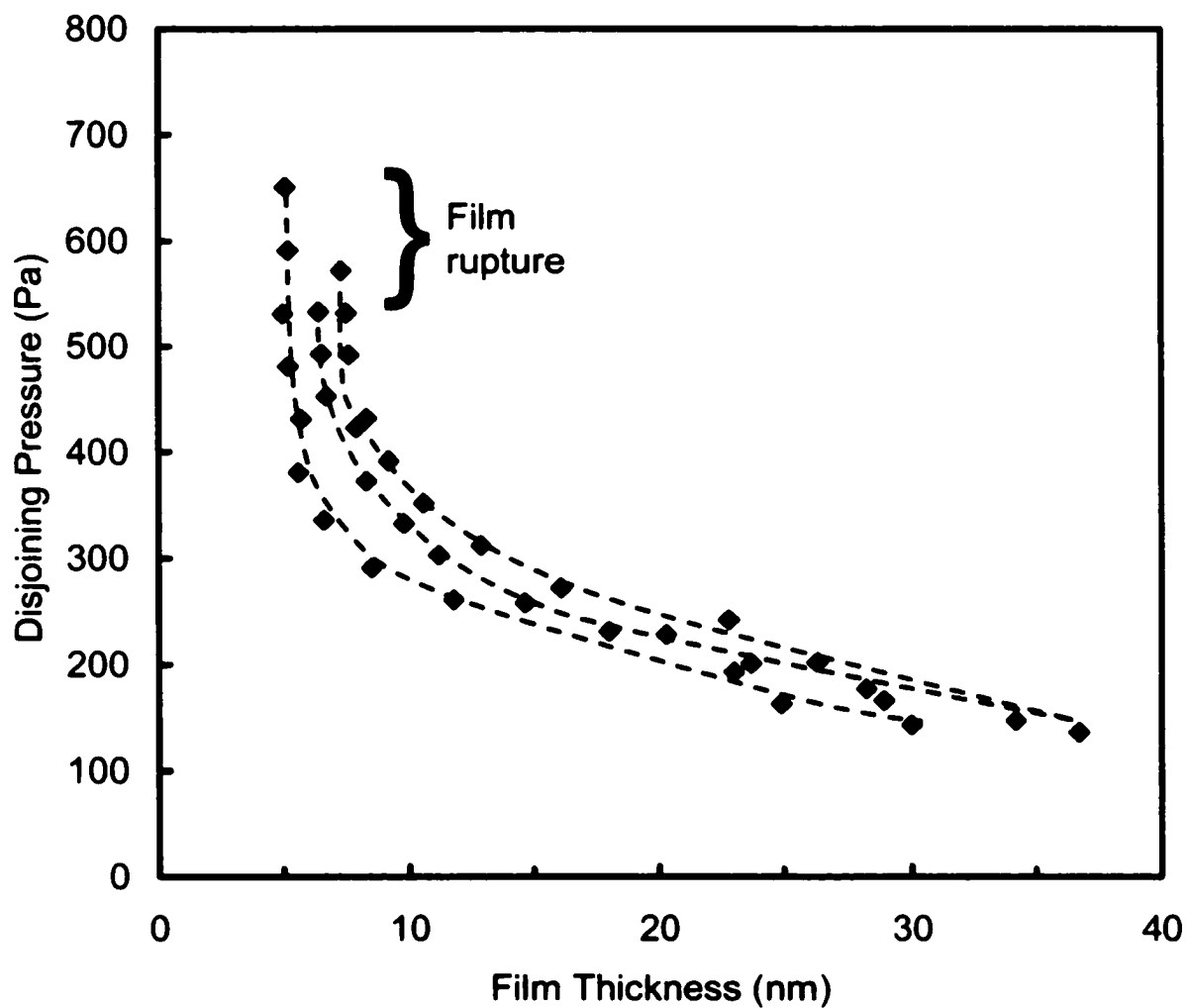
FIGURE 3.11: Disjoining pressure isotherms for a water/toluene-diluted-asphaltene-II/water film at a concentration of 60 g/L asphaltenes. Asphaltenes were produced using method-II to remove fine solids. Lines drawn to guide the eye.
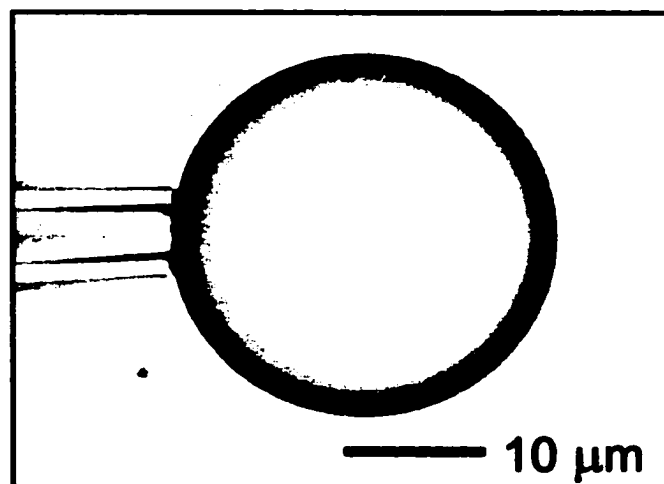
(a)
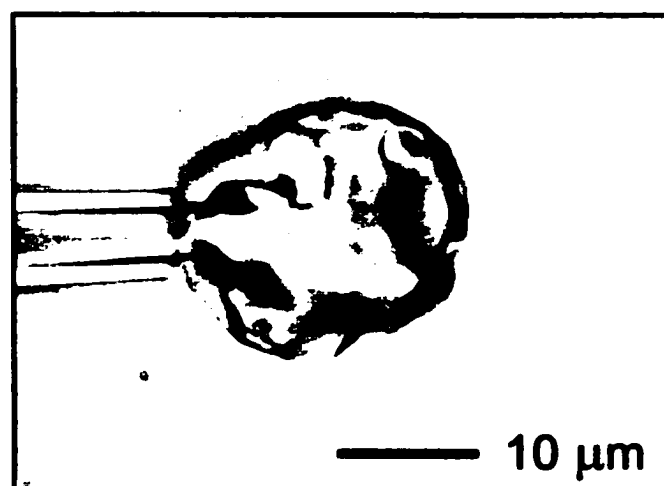
(b)

FIGURE 3.12: (a) Using a micropipette to form a water droplet in a mixture of bitumen and heptol (0.1 %wt bitumen). (b) Protective skin can be observed when attempts are made to reduce the size of the water droplet (Reproduced from Yeung et al. (1999)).
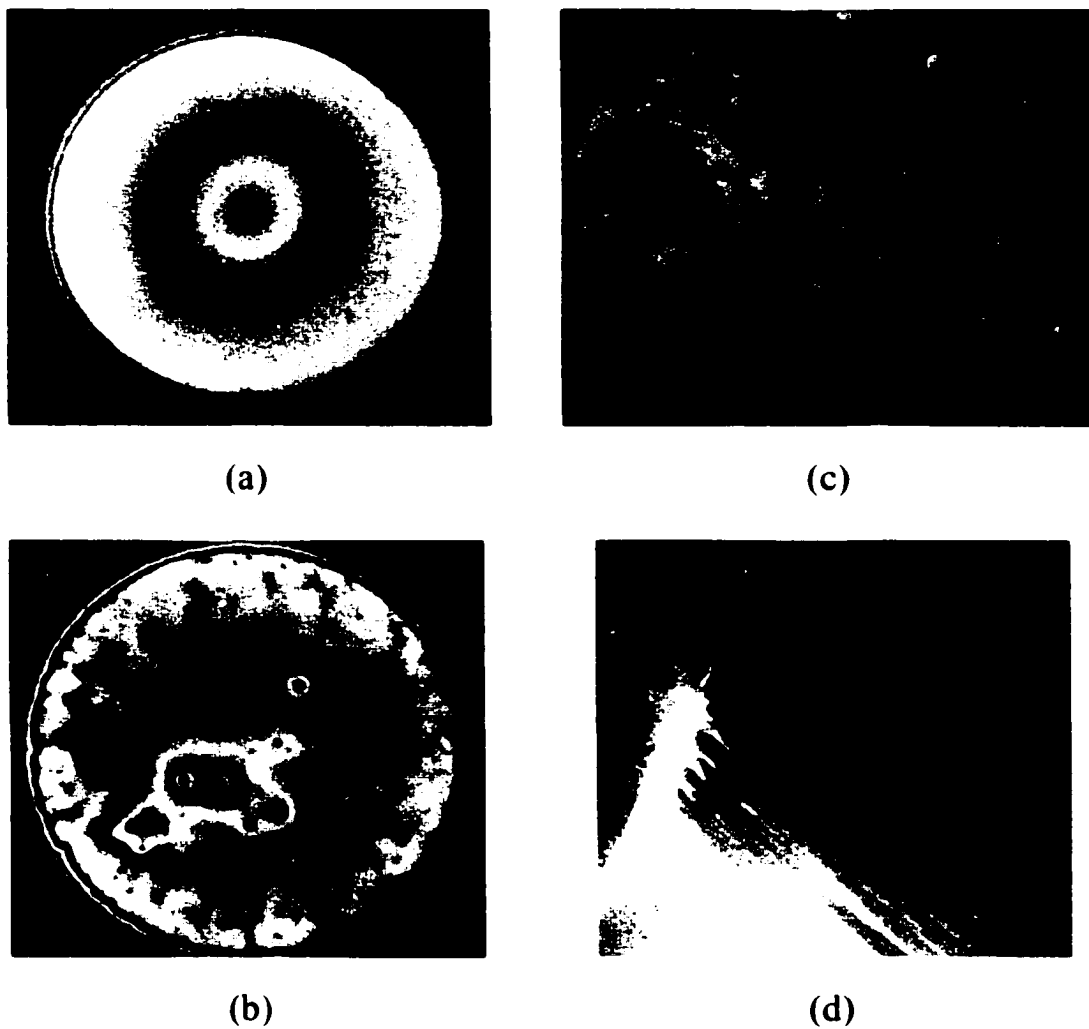
FIGURE 3.13: Effect of fluid and rigid interfaces on the behavior of water/toluene-diluted-asphaltene-cut#4/water films at a concentration of 60 g/L. (a) Fluid interfaces. (b) Rigid interfaces. (c) Protective skin formed on interfaces. (d) Protective skin remains in hole of porous plate after film rupture.

Chapter 4

Aqueous Foam Films Stabilized by Sodium Naphthenates

4.1 Introduction

In the oil sands industry, undesirable water-in-diluted-bitumen emulsions are often formed during the bitumen extraction process (Czarnecki, 2001). The stability of these emulsions depends, to some extent, on the nature of the colloidal forces between the emulsified water droplets. A preliminary study has been conducted to measure these colloidal forces using the Thin Liquid Film-Pressure Balance Technique (see Chapter 3). The net colloidal force for a water/toluene-diluted-bitumen/water film was measured in terms of a disjoining pressure-thickness isotherm. The findings suggested that the organization of the surfactant molecules within the film changed with bitumen concentration. In particular, it was speculated that a specific molecular organization existed at toluene:bitumen ratios of 3:1 or less while a different organization was present at toluene:bitumen ratios of 5:1 or higher. Other studies have shown that a particular organization of surfactant molecules within an aqueous foam film may correspond to a similar surfactant structure in the bulk liquid used to form the film (Nikolova et al., 1996). Therefore, it is possible that the molecular organizations within the water/toluene-diluted-bitumen/water films may have corresponded to similar molecular organizations or phases in the bulk toluene-bitumen solutions.

To avoid the complexities related to emulsion films, this chapter focuses on simpler aqueous foam films. The foam films are used as the model for the initial investigation into the link between the organization of surfactant molecules in a thin film and the organization of surfactant molecules in a corresponding bulk liquid. The structure of surfactant molecules within a foam film can have a significant effect on the nature of the colloidal forces. This necessarily implies that the nature of the colloidal forces will also depend on the molecular organization of the surfactant molecules in the bulk liquid. Such dependency has been observed in foam films for a system of water and

dipalmitoylphosphatidylcholine (Nikolova et al., 1996) where an increase in temperature resulted in a sharp reduction in the thickness of the bilayer film. The change in thickness indicated that the molecular organization within the bilayer film had switched from a gel to liquid crystalline state. The molecular rearrangement occurred at the same temperature as the corresponding bulk transition from a gel to liquid crystalline phase.

The presence of organized surfactant structures within a bulk liquid is also known to cause stratification within thin films. Stratification is normally attributed to a multi-layered structure within the confined volume of the thin film (Manev et al., 1984; Nikolov and Wasan, 1989). During film drainage, one or more layers of this lamellae structure are drained from the film. As these layers are removed over time, the film thickness will decrease in a series of discrete steps. This drainage process is known as stepwise thinning. A schematic of a single stepwise thinning transition in a stratified film containing multiple layers of nanospheres is shown in Figure 4.1. Nikolov and Wasan (1992) have observed stepwise thinning in an aqueous foam film containing layers of silica nanospheres. Stepwise thinning has also been observed in foam and emulsion films formed from aqueous solutions of sodium dodecylsulfate (SDS) where the SDS concentration was sufficient to form spherical micelles in the bulk solution (Manev et al., 1984; Nikolov and Wasan, 1989; Bergeron and Radke, 1992). For these films, it was concluded that the stepwise thinning was due to layers of spherical micelles within the film and the size of the step transitions was roughly equal to the effective diameter of the spherical micelle. Stepwise thinning has also been observed in thin films drawn from thermotropic liquid crystals[+] (Friberg, et al., 1974; Manev, et al., 1977). For these films, the size of a single step transition is approximately equal to the bilayer thickness or twice the length of the surfactant molecule (Manev, et al., 1977).

In order to understand the stability of water-in-diluted-bitumen emulsions, we need to determine the relation (if any) between the molecular structure within the

---

[+] Liquid crystals are crystals which have lost some or all of their positional ordering while maintaining full orientational ordering. Thermotropic (or conventional) liquid crystals are formed from a single compound (i.e. no solvent is present). In a thermotropic liquid crystal, the specific liquid crystal structure (or phase) is determined by the temperature of the material. In contrast, the formation of lyotropic liquid crystals from amphiphilic-solvent mixtures is determined by the solvent concentration.

water/toluene-diluted-bitumen/water film and the molecular organization of surface active material in the water-solvent-bitumen mixture. Bitumen itself is a complex mixture of hydrocarbons that contains some naturally occurring surface active material. Typically, asphaltenes and resins have been identified as the bitumen fractions that contain surface active material. Bitumen also contains about 2% low molecular weight natural surfactants, such as sodium naphthenates (Strausz, 1988). The molecular interactions between the resins, asphaltenes, and low molecular weight natural surfactants in water-toluene-bitumen mixtures are quite complex and are far from being fully understood. Therefore, it would be advantageous to begin with a model system in order to develop a basis for understanding the link between the organization of surfactant molecules in a thin film and the organization of surfactant molecules (i.e. the surfactant structures) in bulk liquids.

For this study, a simple aqueous foam film was chosen as the model system to begin an investigation into the link between the molecular organization (i.e. phase behavior) of surfactant molecules in a bulk mixture and the molecular organization of the surfactant molecules in a thin film. The foam film was formed from a mixture of water and sodium naphthenates. Sodium naphthenates are naturally occurring surfactants that are easily extracted from most bitumen or crude oil sources. The exact nature and concentration of these surfactants varies with the source of crude oil or bitumen. Sodium naphthenates are a mixture of cyclic carboxylic acids that may contain small aliphatic side chains (Strausz, 1988; Herman et al., 1993). The molar mass of these surfactants ranges from 166 to 450 g/mol (Schramm et al., 2001). The phase behaviour of water-sodium naphthenates mixtures has been studied previously by Horváth-Szabó et al. (2001). Organized structures that have been observed in this system include an isotropic solution, a birefringent gel, a lamellar liquid crystal, and a crystalline solid (Horváth-Szabó et al., 2001).

4.2 Experimental Description

4.2.1 Materials

The sodium naphthenates used in this study were obtained from Fisher Scientific and were used as received. Samples were prepared by combining a predetermined mass

of de-ionized ultra filtrated (DIUF) water and sodium naphthenates. A total of six samples were prepared ranging in concentration from 5 to 50 %wt sodium naphthenates. The samples were gently mixed by hand over a period of an 1 h. Gentle mixing was required to ensure that few or no air bubbles were formed. As a precaution, all samples were left overnight undisturbed to allow any air bubbles to escape from the mixture.

After standing overnight, a subsample of each mixture was taken and transferred to a glass centrifuge tube. Following the procedure of Horváth-Szabó et al. (2001), the subsamples were then centrifuged for 90 min at 26,500 g and 23.0°C. Immediately after centrifugation, the subsamples were observed in normal light to determine the number of phases in the mixture. The subsamples were then placed between two crossed polarizers in order to observe the birefringent properties of each phase. Each phase was then identified by comparing these observations with the findings of Horváth-Szabó et al. (2001).

4.2.2 Apparatus

The Thin Liquid Film-Pressure Balance Technique (TLF-PBT), originally developed by Scheludko and Exerowa and described previously in Chapters 2 and 3 (Scheludko, 1967, Exerowa and Scheludko, 1971, Exerowa and Kruglyakov, 1998), was used to study foam films formed from the sodium naphthenate-water mixtures. The microscopic, horizontal films were formed in the measuring cell shown in Figure 4.2. The measuring cell consisted of a cylindrical film holder made from a short piece of hydrophilic glass tubing. The holder was 4.0 mm in length and had an inner radius of R = 1.4 mm. The holder was suspended inside a sealed glass cell by a long glass capillary attached to a micrometer syringe. The syringe was used to draw a small amount of the sodium naphthenate-water mixture into the film holder and capillary. This allowed a biconcave drop to form in the film holder. A microscopic thin film was then formed by using the micrometer syringe to withdraw some of the liquid from the biconcave drop into the glass capillary. The diameter of the film was controlled by the amount of liquid withdrawn from the biconcave drop.

The measuring cell rested inside a thermostating device that maintained the temperature of the cell at 23.0 ± 0.1°C. The thermostating device was mounted on top of

an Axiovert 100 reflected light microscope (Carl Zeiss Canada Ltd.). An optical flat on the bottom of the cell allowed the film to be viewed from below. Images of the film were captured with a CCD camera (VK-C730, Hitachi) and recorded using a VCR (M-752C, Toshiba). A complete description of the TLF-PBT apparatus can be found in Chapter 2 or Khristov et al. (2000).

4.2.3 Film Thickness

The equivalent film thickness was obtained using the microinterferometric technique of Scheludko and Exerowa (Scheludko, 1967; Exerowa and Scheludko, 1971; Exerowa and Kruglyakov, 1998). Heat filtered light from a 100 W mercury arc lamp was directed through a monochromatic filter (λ = 546 nm). The light then passed through an iris (or pin-hole) diaphragm creating a ~10 µm diameter beam of light that was focused onto the centre of the film. Light reflected from the film was directed through a second pin-hole diaphragm to eliminate any unnecessary light scatter from the film meniscus or the film holder. Intensity of the reflected light was measured using a highly sensitive low-light, low-noise Si-photodiode (Hamamatsu Corp.). The signal from the photodiode was recorded using strip chart.

The recorded light intensity was converted into an equivalent film thickness using the equation developed by Scheludko and Platikanov (1961):

$$h = \left(\frac{\lambda}{2\pi n_f}\right)\left[k\pi \pm \arcsin\left(\frac{\Delta}{1 + [4N/(1-N)^2][1-\Delta]}\right)^{1/2}\right] \qquad [4.1]$$

where k is the interference order, $\Delta = (I - I_{min})/(I_{max} - I_{min})$ and $N = (n_f - n_s)^2/(n_f + n_s)^2$. Here, I is the recorded light intensity with I_{max} and I_{min} corresponding to last maximum and minimum interference values. The refractive index of the surrounding air, n_s, was taken to be unity and the refractive index of the film, n_f, was assumed to be equal to the refractive index of the bulk mixture from which the film was formed. The refractive indices of the sodium naphthenate-water mixtures were measured using an automatic

TABLE 4.1: Summary of refractive index data.

Sodium Naphthenate Concentration (wt %)	Refractive Index
5	1.3415
10	1.3509
20	1.3676
30	1.3859
45	1.4144
50	1.4200

refractometer (Model GPR 12-70, Index Instruments U.S., Inc.). All measurements were performed at a wavelength of 589 nm and a constant temperature of $23.0 \pm 0.1^{\circ}C$. The refractive index values are shown in Table 4.1.

4.3 Results and Discussion

4.3.1 Phase Behaviour of a Sodium Naphthenates-Water System

In order to interpret the thin film observations, it is important to first have an understanding of the bulk phase behaviour of the sodium naphthenates-water system. The phase behaviour of this system was originally studied by Horváth-Szabó et al. (2001). The phase diagram from that study has been reproduced in Figure 4.3. As Figure 4.3 indicates, only a single, isotropic solution existed at sodium naphthenate concentrations less than 41.8 %wt. The isotropic solution probably contained micelles of sodium naphthenates since a critical micelle concentration of about 0.1 %wt has been detected from surface tension measurements of sodium naphthenates extracted from Karamay AGO-II and AGO-III (Mingqing, 1997). At concentrations between 41.8 and 51.5 %wt, the isotropic solution co-existed with a turbid, birefringent gel phase and a lamellar liquid crystal phase. Figure 4.4 is an image of a 48.6 %wt mixture after centrifugation in both normal light and between two crossed polarizers. The birefringence of the lamellar liquid crystal and gel phases are clearly observed with the crossed polarizers. The critical concentration for the transition between single and multiple phase behaviour was found

to decrease with temperature. The above results describe the phase behaviour at a temperature of 25.0°C.

In the present study, a sub-sample of each sodium naphthenates-water mixture was centrifuged at 23.0°C and then observed in normal light and between cross polarizers. The findings were similar to those of Horváth-Szabó et al. (2001). A single, isotropic solution was observed for concentrations of sodium naphthenates up to and including 45.0 %wt. At a concentration of 50.0 %wt, a birefringent gel, lamellar liquid crystal, and isotropic solution could be observed. Hence, the critical concentration for the transition from single to multiple phase behaviour was between 45 and 50 %wt. This is clearly higher than the critical concentration observed by Horváth-Szabó et al. (2001). The sodium naphthenates used in the two studies were obtained from the same chemical supplier but from two different batches. The exact composition of sodium naphthenates is known to vary from batch to batch. As a result, some variation in the critical concentration at which there is a transition from single to multiple phase behaviour should be expected.

4.3.2 Foam Films Formed from an Isotropic Solution

As mentioned, only an isotropic solution was formed at sodium naphthenates concentrations of 45 %wt or lower. Figure 4.5 shows a series of images in time for a typical film drawn from this isotropic solution. During the initial formation of the film, rings of colour appeared indicating that the circular film was quite thick (i.e. few hundred nanometers) and contained a large centre dimple. The film drained quickly via asymmetric drainage until a critical thickness was obtained. At the critical thickness, one or more grey spots began to appear near the film boundary (Figure 4.5a). The uniform, light grey shade of each spot indicated that the film had a uniform thickness within the area covered by the spots. The spots would quickly grow in size until almost the entire area of the film was light grey (Figure 4.5b). Slightly darker grey spots would then begin to appear at the film boundary. Again, these spots would grow until the entire film was a uniform and slightly darker shade of grey (Figures 4.5c and 4.5d). The film would remain at this metastable thickness until new, even darker grey spots would appear in the film (Figure 4.5e). The appearance and growth of progressively darker grey spots would

continue until a final equilibrium thickness was obtained (Figure 4.5f). For the 20 %wt sodium naphthenates film shown in Figure 4.5, the time from film formation to the final equilibrium thickness was approximately 4 min. Film rupture was never observed in this system. The progressive appearance and growth of the uniformly shaded spots has been observed previously (Perez et al., 1988; Nikolov and Wasan, 1989) and it is a well-known sign of stepwise thinning.

The film thickness was measured throughout the stepwise thinning process. Measurements were obtained for films formed from mixtures containing sodium naphthenates concentrations of 5, 10, 20, 30, and 45 %wt. During the thickness measurements, the film diameter was held constant at 250 μm. Figure 4.6 is an example of a typical thickness measurement. It is a plot of the change in light intensity over time for a film containing 10 %wt sodium naphthenates. Here, the film drains quickly after film formation until the first step is formed. A total of 3 stepwise thinning transitions are observed. The film remains stable at a final thickness of 20.3 nm.

The plot of light intensity versus time may be converted into film thickness versus time using Eq. [4.1]. Figure 4.7 is a sketch of a typical film thickness versus time plot. The figure shows a monotonic decrease in the film thickness during the initial stages of film drainage. At a critical thickness, the film thickness would then begin to decrease in a series of discrete stepwise thinning transitions. A single, stepwise thinning transition appeared as a jump from one constant thickness to a lower constant thickness. Following a step transition, the film often remained at a metastable equilibrium. This appears as a short duration of constant thickness in Figure 4.7. After several minutes, the film would reach a final, equilibrium thickness where no further thinning takes place.

The number of observed step transitions depended strongly on the concentration of sodium naphthenates with the number of step transitions increasing with concentration. For example, only one or two step transitions were observed at 5 %wt whereas up to 23 step transitions were observed at 45 %wt. It was also quite common to observe the start of a second stepwise thinning transition inside the spot of the previous stepwise thinning transition. This is clearly shown in Figure 4.8. Here, a new, darker grey spot of a second step transition appeared before the mid-grey spots of the first step transition were able to cover the entire film area. Similar results have been reported in films containing layers of

silica nanospheres where there was a polydispersity in the size of the nanospheres. However, the formation of a spot within another spot was not observed for a system containing monodisperse silica nanospheres (Nikolov and Wasan, 1992). Previous findings have also suggested that the time at which the film remains at a metastable equilibrium increases with each subsequent step transition (Nikolov and Wasan, 1989). However, no such correlation was observed for the water-sodium naphthenates system.

Figure 4.9 provides a summary of the film thickness after each stepwise thinning transition and at the final equilibrium. To understand the data presented in Figure 4.9, it is important to note how this plot was produced. First, only 10 step transitions have been reported. Above 10 transitions, both the number and size of each step became variable making it nearly impossible to obtain repeatable measurements of film thickness. Next, at a sodium naphthenates concentration of 5 wt%, both the first and second stepwise thinning transitions occurred in less than one second making it extremely difficult to obtain reliable thickness measurements after each step transition. For this reason, only the final film thickness has been reported for 5 %wt. Finally, after the final equilibrium was obtained, the film diameter was increased to 500 μm in order to increase the capillary pressure applied to the film. The increase in capillary pressure induced additional step transitions at concentrations of 30 and 45 %wt. These induced step transitions are indicated by the open symbols in Figure 4.9. For concentrations of 20 %wt or less, the change in film diameter did not affect the final equilibrium thickness. These results have also been summarized in Table 4.2. For each concentration, Table 4.2 list the final film thickness, the average size of the step transitions, and the number of observed step transitions.

From previous studies, it is clear that stepwise thinning is caused by the formation of a lamellae structure within the film. It is possible that the lamellae structure may consist of a series of surfactant bilayers with a lamellar liquid crystal-like structure (Manev, et al., 1977). It is also possible that the lamellae structure may consist of several layers of spherical micelles (Nikolov and Wasan, 1989). The difficulty in the sodium naphthenates-water system involves identifying which of these two possible structures best describes the lamellae structure within the film. It is known that a particular

TABLE 4.2: Summary of experimental data.

Sodium Naphthenates Concentration (wt %)	Final Film Thickness (nm)	Average Size of Last Three Step Transitions (nm)	Number of Step Transitions
5	19.2	-	1 or 2
10	13.2	6.8	3
20	10.0	5.1	7
30	8.0	4.3	up to 15
45	7.1	4.5	up to 23
50	-	-	over 20

molecular organization at an interface can be formed at a concentration much lower than that required for the formation of the corresponding bulk phase (Pomianowski and Czarnecki, 1974; Pomianowski and Czarnecki, 1987). Hence, it may be possible for the sodium naphthenate molecules to form a lamellar liquid crystal-like structure within the film at concentrations lower than 50 %wt. Such a liquid crystal-like structure could be responsible for the observed stepwise thinning phenomena (Figure 10(a)). However, stepwise thinning was observed at a concentration as low as 5 %wt, a concentration that is nearly a full order of magnitude less than the concentration needed to form a bulk lamellar liquid crystal phase. Without supporting experimental data, it is difficult to be convinced that a lamellar liquid crystal-like structure exists in the film at such low concentrations. In contrast, previous studies have shown that spherical micelles can form layers that result in stepwise thinning within a thin film (Manev et al., 1984; Nikolov and Wasan, 1989). The surface tension measurements of Mingqing (1997) indicate that the isotropic solution used to form these films probably contained micelles. If *spherical* micelles exist in the isotropic solution, then it is possible that layers of spherical micelles may be responsible for the observed stepwise thinning (Figure 4.10(b)). However, it is not yet known if the isotropic solution contains spherical micelles. It is quite possible that the isotropic solution may contain non-spherical micelles. Again, more experimental data is needed.

Some information about the lamellae structure within the film can be obtained by realizing that the average size of the step transitions is approximately equal the thickness of a single layer within the lamellae structure. Table 4.2 indicates that the thickness of a single layer is about 6.8 nm at 10%wt and then decreases to about 4.3 nm for concentrations of 30 and 45 %wt. With a molecular weight in the range of 166 to 450 g/mol (Schramm et al., 2001), the length of a sodium naphthenates molecule is expected to be on the order of 2 nm. Therefore, a 4.3 nm layer thickness corresponds well to twice the expected length of a sodium naphthenate molecule. The question remains as to why the layer thickness decreased with increasing sodium naphthenates concentration.

In modeling of stepwise thinning in a sodium dodecylsulfate-water system, Nikolov et al. (1989) found that the size of a step transition was similar to the effective diameter of the spherical micelles where the effective diameter was equal to the micelle diameter plus two times the Debye length that is associated with the micelle. This suggests that, for the sodium naphthenates-water system, it is possible for a significant electrostatic repulsive force to exist between the spherical micelles or the liquid crystal-like layers. In the sodium naphthenates-water system, sodium ions are generated by the disassociation of the sodium naphthenates molecules. An increase in sodium naphthenates concentration will result in an increase in the sodium ion concentration. Thus, a reduction in the Debye length with increased sodium naphthenates concentration could then explain the observed decrease in the size of the layers. However, the sodium ion concentration is about 0.3 mol/L for a sodium naphthenates concentration of 10 %wt. At 0.3 mol/L, the Debye length is on the order of 0.5 nm. Since the sodium ion concentration will only increase with the sodium naphthenate concentration, the Debye length will remain less than 0.5 nm over the entire range of surfactant concentration. Therefore, a reduction in the Debye length with increased sodium naphthenate concentration can not fully explain the change in the size of the layer thickness.

Some additional information about the film structure can also be obtained from the final film thickness. Table 4.2 shows that the final film thickness decreased from 19.2 nm at 5 %wt to 7.1 nm at 45 %wt. At these large thicknesses, the film is clearly not a surfactant bilayer. A bilayer would have a thickness of twice the average length of a sodium naphthenate molecule, about 4 nm. An electrostatic repulsive force cannot be

considered the cause of the large thicknesses since the Debye length is 0.5 nm or less. However, a comparison between the average step size and the final thickness indicates that, except for 5 %wt, the final film thickness is roughly twice the size of the average step transition. Therefore, the film interfaces were probably still separated by a single layer. This means that the film may have contained a single liquid crystal-like layer or a single layer of spherical micelles between the two film interfaces. A significant increase in the capillary pressure is likely needed to force the last layer to drain from the film and obtain a film bilayer. At 5 %wt, the large thickness suggests that the final film probably contained two layers between the film interfaces, either two layers of spherical micelles or two liquid crystal-like layers.

4.3.3 Foam Films Formed from a Liquid Crystal

As mentioned, an isotropic solution, a birefringent gel and lamellar liquid crystal are formed at a sodium naphthenate concentration of 50 %wt (refer to Figure 4.3 and 4.4). The *entire* 50 %wt mixture was used to form an aqueous foam film. The drainage of this film over a period of several minutes is shown Figure 4.11. In the initial formation of the film, several rings of colour appeared indicating that the film contained a large dimple of liquid. The film began to drain via asymmetric drainage. While the film was still quite thick, small circular spots of uniform colour began to appear around the edge of the film (Figure 4.11a). Over time, several more uniformly coloured spots appeared throughout the film (Figure 4.11b). Some of spots would grow in size while other spots decreased in size until they disappeared. These spots were regions of uniform film thickness and the appearance of various non-primary colours indicated that the film thickness in that region was on the order of a wavelength or more. Eventually, new spots of varying shades of grey began to appear in the film. The grey spots indicated that the film thickness was less than 100 nm (Figure 4.11c). At equilibrium, the entire film was a uniform, light shade of grey similar to the large spot in the top left of the film shown in Figure 4.11c. Note that the small grey, moon-shaped region to the right of the film was a small air bubble trapped in the film.

Again, the appearance and growth of uniformly shaded spots indicated stepwise thinning caused by a lamellae structure within the film. Previous studies have shown that

stepwise thinning will occur in a thin film drawn from a thermotropic liquid crystal (Manev et al., 1977; Perez et al., 1988). Since a liquid crystal phase is known to exist in the bulk mixture of 50 %wt sodium naphthenates, it is quite probable that the film contained a lamellar liquid crystal-like structure. Hence, the removal of a single bilayer or several bilayers of liquid crystal would result in the observed stepwise thinning phenomena. An attempt was made to form a thin film from just the lamellar liquid crystal phase. Unfortunately, a thin film could not be formed using the current apparatus. However, air bubbles were often trapped in the extremely viscous liquid crystal phase and thin liquid films could be observed when the air bubbles were close to the liquid crystal-air interface. An example of such a film is shown in Figure 4.11d. Here, the thin liquid film formed between the air bubble and the liquid crystal-air interface shows several bands of uniform colour similar to those observed in Figures 4.11b and 4.11c. These results are certainly not conclusive, but they do suggest that the films formed from the 50 %wt mixture contained a lamellar liquid crystal structure.

4.3.4 Stepwise Thickening

In addition to stepwise thinning, it was found that the films can undergo stepwise thickening during film drainage. Stepwise thickening is a phenomena that has only recently been observed in thin liquid films (Nikolov and Wasan, 2001). As the name implies, it involves a series of discrete increases in film thickness within a localized area of the film. An example of stepwise thickening is shown in Figure 4.12.

A 400 μm diameter foam film was formed from a 45 %wt mixture of sodium naphthenates and water (i.e. the isotropic solution). As described earlier, the film undergoes a series of stepwise decreases in film thickness over time. Figure 4.12a shows the lower portion of the film during one transition in the stepwise thinning process. The large, mid-grey spots had initially appeared near the boundary of the grey film and had grown to the size shown in Figure 4.12a. Before this first stepwise thinning transition was complete, a second stepwise thinning transition began to occur. This second transition began as a small dark-grey spot (A) near the centre of the film and inside the mid-grey spot (Figure 4.12b). At the same instant, a small light-grey spot (B) appeared to the left

and in point contact with the small dark-grey spot (A). The appearance of the light-grey spot (B) was the beginning of the stepwise thickening process.

As the step thinning dark-grey spot grew in area (A), the step thickening light-grey spot (B) also began to grow in area (Figure 4.12c). Lighter-grey and white spots also began to appear within this expanding stepwise thickening spot (Figures 4.9c and 4.9d). These new, lighter-grey and white spots (C) were indications of further stepwise increases in the film thickness and, similar to the initial stepwise increase, the spots always formed in point contact with the dark-grey stepwise thinning spot. Several very small, circular stepwise thickening spots were also formed along the boundary of the first stepwise thinning spot (A) (Figure 4.13). These spots quickly grew in size and moved rapidly along the boundary towards the existing, large stepwise thickening spots. The small spots would then coalesce with the existing stepwise thickening spots. After a few minutes, the first and second stepwise thinning grey spots would grow to cover a large portion of the film area. The growth of the darker grey spots forced the stepwise thickening spots towards the film boundary (Figure 4.12e). As a result, the stepwise thickening spots began to lose their circular shape. The liquid from stepwise thickening region would then be forced to drain from the film and into the bulk liquid of the surrounding plateau border region (Figure 12f).

The occurrence of stepwise thickening, like stepwise thinning, was an indication of a lamella structure within the film. However, in the case of stepwise thickening, a new lamella is added to the existing structure resulting in an increase in the film thickness. Measurements of film thickness within the small area of stepwise thickening indicated that the average size of the step increase was about 4.3 nm. The same size of step was observed for stepwise thinning. Hence, the structure introduced during the stepwise thickening process was the same structure as the lamellae being removed during the stepwise thinning process. A cross-section of the film during the early stages of the stepwise thickening process is shown in Figure 4.14. For simplicity, the schematic was drawn with a film consisting of several layers of spherical micelles. A similar drawing could be imagined for a film consisting of multiple liquid crystal-like layers.

It is important to note that the observed stepwise thickening was only a temporary kinetic process related to the thinning of the film. This is clearly demonstrated by the fact

that the stepwise thickening spots only appeared beside a stepwise thinning spot. Also, the appearance of stepwise thickening was limited to situations where a second stepwise thinning spot appeared inside another stepwise thinning spot far from the film boundary. For any stepwise thinning spot to expand, a layer of material must be removed from the advancing edge of that spot. Normally, the stepwise thinning spots are formed and grow along the film boundary, which allows the material to easily drain into the plateau border (the exact mechanism of film drainage is not known). When a stepwise thinning spot is formed in the middle of the film, the advancing edge of the spot will move from the middle of the film towards the film boundary. This means that a layer of material must somehow drain from the middle of the film to the film boundary and into the plateau border. If one assumes that there is a 'weak point' in the film structure somewhere between the advancing edge of the stepwise thinning spot and the film boundary, then it is conceivable that it would be more energetically favorable for the layer of material to accumulate at the 'weak point'. The accumulation of the material would then result in a temporary reversal of the step thinning process meaning that layers of material are added to that region of the film. This would result in the observed stepwise thickening process.

4.4 Conclusions

The goal of this chapter was to link the bulk phase behaviour of a sodium naphthenates-water system to the behaviour of a foam film drawn from the same bulk mixtures. This link was clearly seen in films formed from the lamellar liquid crystal phase and from the 50 %wt mixture where lamellar liquid crystal is one of three known phases. These films displayed stepwise thinning behaviour indicating that the film contained a lamellae structure. The structure was probably made up of sodium naphthenate molecules in a lamellar liquid crystal-like organization. Stepwise thinning was also observed for foam films drawn from an isotropic solution. Again, the film must have been composed of a lamellae structure. Thickness measurements indicated that a single layer had a thickness ranging from 6.8 nm at 5 %wt to 4.3 nm at 45 %wt. Unfortunately, it was impossible to identify the nature of the lamellae structure without additional information. It is suspected that the structure consisted of either multiple layers of sodium naphthenate molecules organized in a liquid crystal-like structure or multiple

layers of spherical micelles. Some insight could be gained by studying the molecular organization of the sodium naphthenates in the isotropic solution. In particular, determining the size and shape of micelles that are formed in the isotropic solution.

While a definite link between the bulk phase behaviour and thin film behaviour could not be established, this study did provide some other useful insights. It was shown that a solution of mixed, naturally occurring surfactants could produce a stratified film and hence, stepwise thinning. Previous research has been limited to systems where the chemical properties of the surfactants are constant and well known. The relatively new process of stepwise thickening was also observed. The stepwise thickening process was limited to a small region within the film and it was directly related to the stepwise thinning process.

4.5 References

Bergeron, V. and Radke, C.J., *Langmuir* **8** (1992) 3020-3026.

Czarnecki, J., *in* "Encyclopedic Handbook of Emulsion Technology", edited by Sjöblom, J., p.497, Marcel Dekker, New York, 2001.

Exerowa, D. and Kruglyakov, P.M., "Foam and Foam Films" Elsevier, New York, 1998.

Exerowa, D. and Scheludko, A., *Compt. Rend. Acad. Bulg. Sci.* **24** (1971) 47.

Friberg, S., Linden, St.E. and Saito, H., *Nature* **251** (1974) 494-495.

Herman, D.C., Fedorak, P.M., MacKinnon, M.D., and Costerton, J.W., *in* "Hydrocarbon Bioremediation", edited by Hichee, R.E., Alleman, B.C., Hoeppel, R.E. and Miller, R.N., pp.274-277, Lewis Publishers, Boca Raton, 1993.

Horváth-Szabó, G., Czarnecki, J. and Masliyah, J., *J. Colloid Interface Sci.* **236** (2001) 233-241.

Khristov, K., Taylor, S.D., Czarnecki, J. and Masliyah, J., *Colloid Surf. A.* **174** (2000) 183-196.

Kralchevsky, P.A., Nikolov, A.D., Wasan, D.T., and Ivanov, I.B., *Langmuir* **6** (1990) 1180-1189.

Manev, E., Proust, J.E. and Ter-Minassian-Saraga, L., *Colloid & Polymer Sci.* **255** (1977) 1133-1135.

Manev, E.D., Sazdanova, S.V. and Wasan, D.T., *Dispersion Sci. Technol.* **5** (1984) 111-117.

Mingqing, W., Ph.D. Thesis, Research Institute of Petroleum Processing, Beiging, 1997.

Nikolov, A.D., Kralchevsky, P.A., Ivanov, I.B. and Wasan, D.T., *J. Colloid Interface Sci.* **133** (1989) 13-22.

Nikolov, A.D. and Wasan, D.T., *J. Colloid Interface Sci.* **133** (1989) 1-12.

Nikolov, A.D. and Wasan D.T., *Langmuir* **8** (1992) 2985-2994.

Nikolov, A.D. and Wasan D.T., "Role of Micellar Interactions in Foam Lamella Stability", Presented at 75th ACS Colloid and Surface Science Symposium, Carnegie Mellon, Pittsburgh, June 10-13, 2001.

Nikolova, A., Koynova, R., Tenchov, B. and Exerowa, D., *Chemistry and Physics of Lipids* **83** (1996) 111-121.

Perez, E., Proust, J.E. and Ter-Minassian-Saraga, L., *in* "Thin Liquid Films", edited by Ivanov, I.B., pp.891-925, Marcel Dekker, New York, 1988.

Pomianowski, A. and Czarnecki, J., *J. Colloid Interface Sci.* **47** (1974) 315.

Pomianowski, A. and Czarnecki, J., *Fizykochemiczne Problemy Mineralurgii* **19** (1987) 83.

Scheludko, A., *Adv. Coll. Interface Sci.* **1** (1967) 391.

Scheludko, A. and Platikanov, D., *Kolloid Z.* **175** (1961) 150.

Schramm, L.L., Stasiuk, E.N. and MacKinnon, M., *in* "Surfactants, Fundamentals and Applications in the Petroleum Industry", edited by Schramm, L.L., 2001, in press.

Strausz, O.P., *in* "44th UNITAR/UNDP International Conference on Heavy Crude and Tar Sands", Vol.2, p.607, 1988.
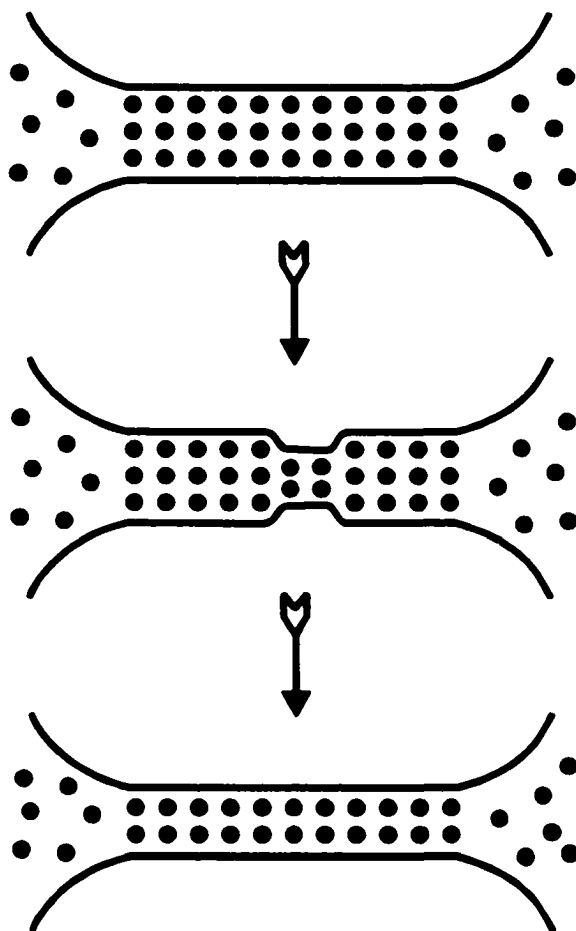
FIGURE 4.1: Schematic of a single stepwise thinning transition in a stratified film containing multiple layers of spherical micelles (Kralchevsky et al., 1990; Nikolov and Wasan, 1992).
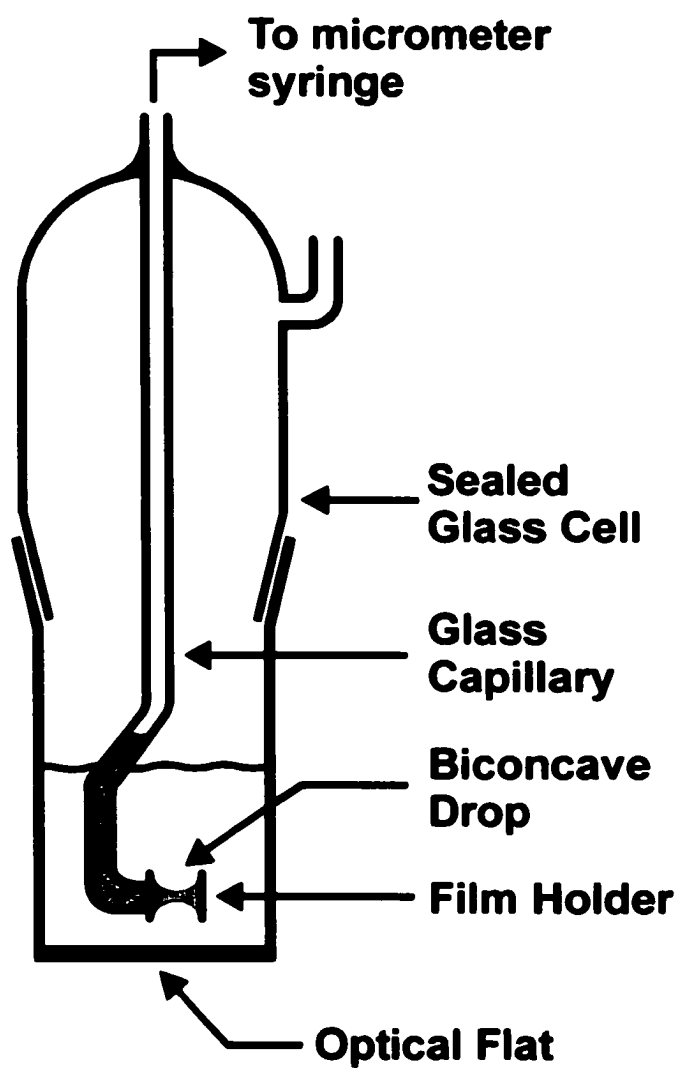
FIGURE 4.2: Schematic of measuring cell used to form aqueous foam films.
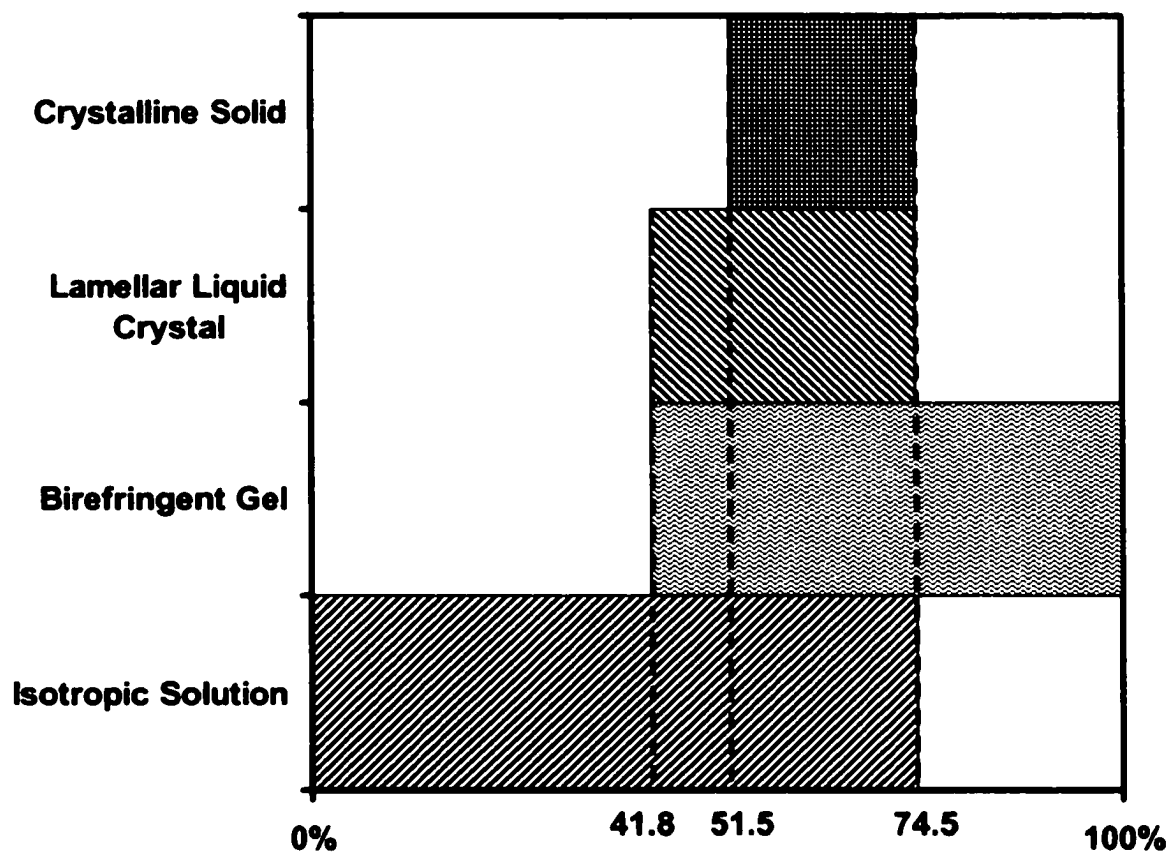
FIGURE 4.3: Binary phase diagram of a sodium naphthenates-water system (Reproduced from Horváth-Szabó et al.. 2001).
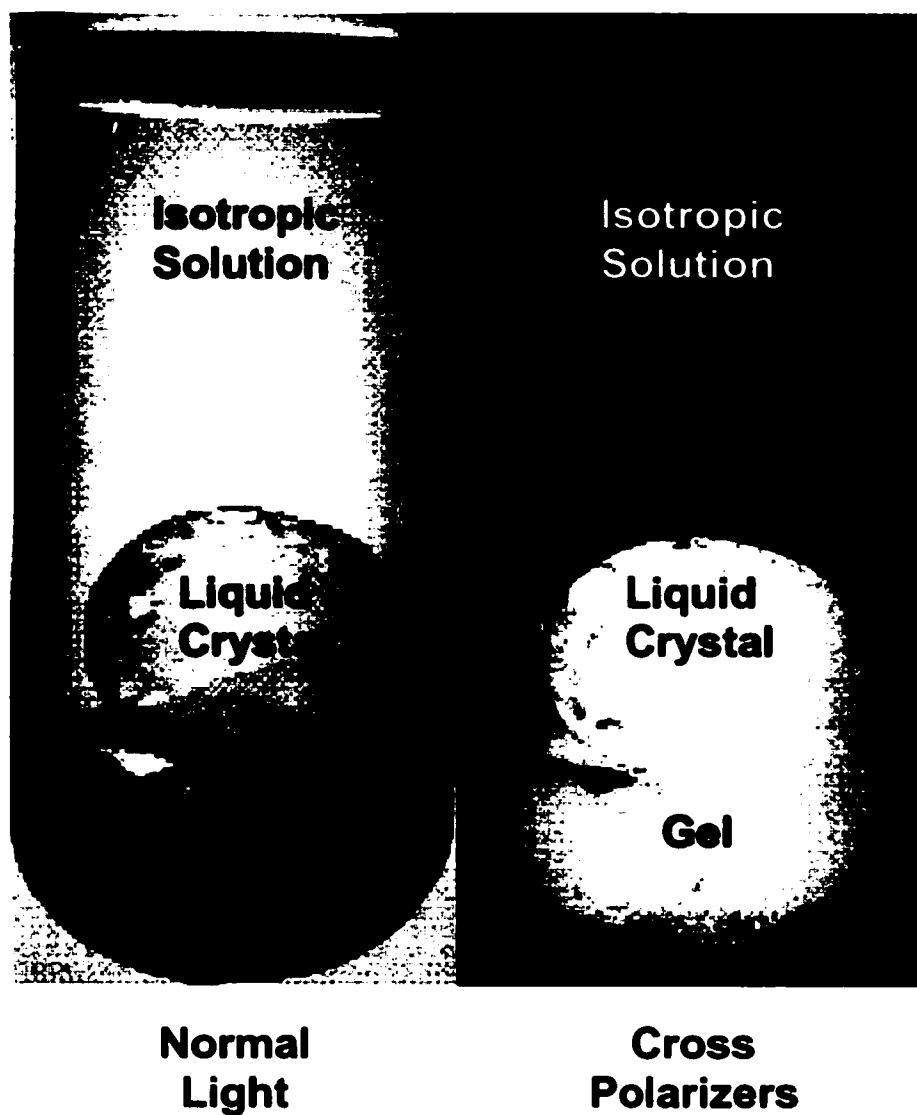
FIGURE 4.4: Multi-phase behaviour in a system of sodium naphthenates and water. Images were obtained for system with an overall concentration of 48.6 %wt sodium naphthenates (Reproduced from Horváth-Szabó et al. (2001)).
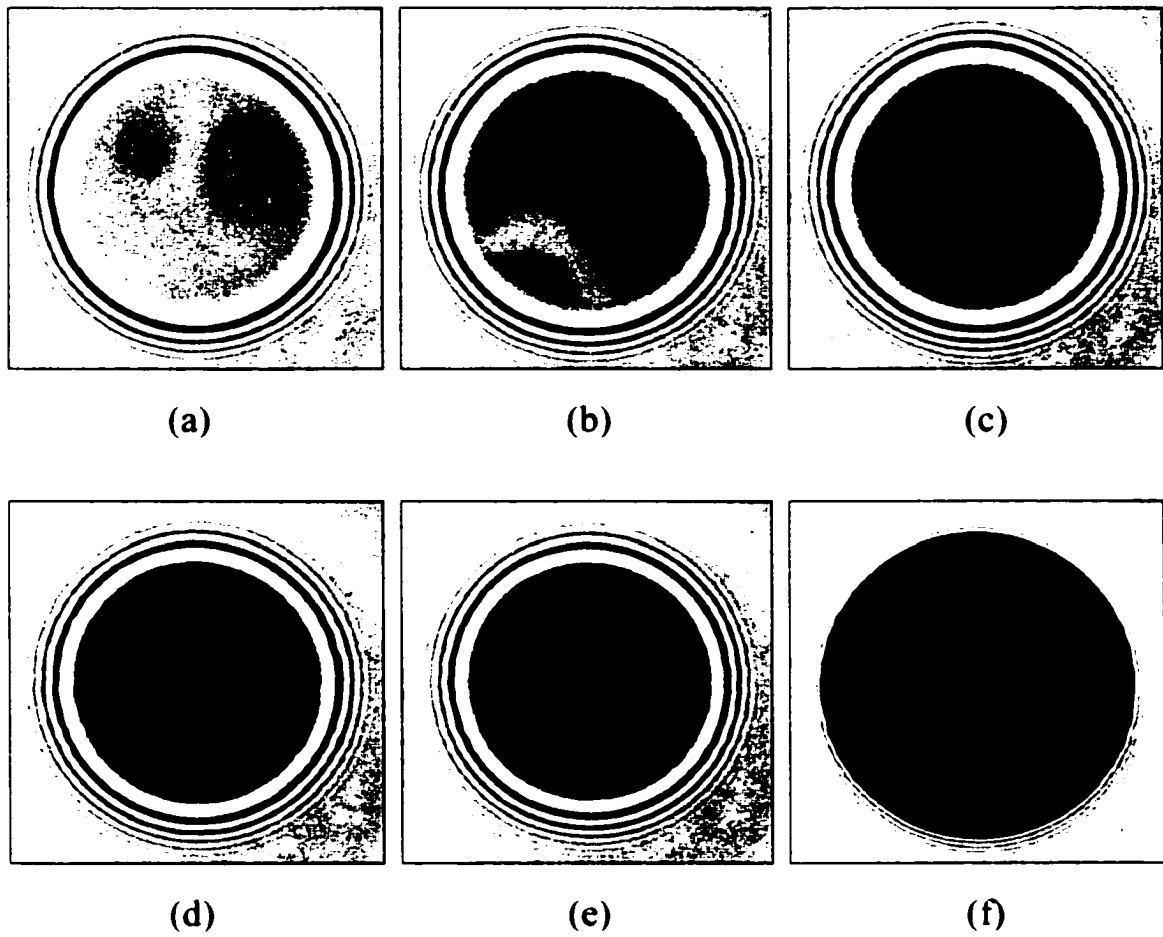
FIGURE 4.5: Images (a) through (e) are a sequence in time showing the first three stepwise thinning transitions for a 20 %wt sodium naphthenates foam film. Image (f) shows the same film once it has reached equilibrium thickness.
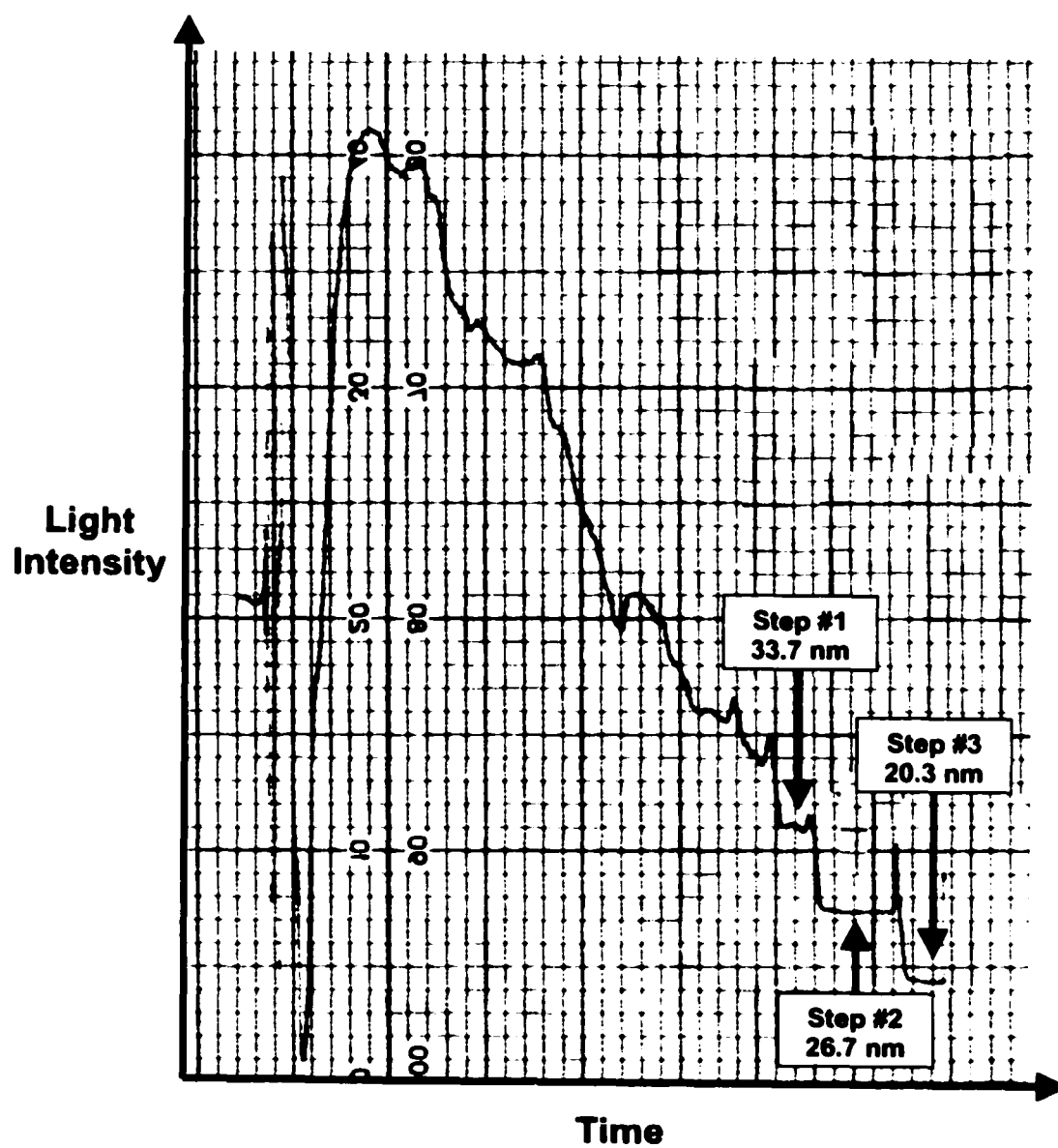
FIGURE 4.6: Typical light intensity versus time plot for a 10 %wt sodium naphthenates foam film. The plot represents a period of about 2 to 3 minutes.
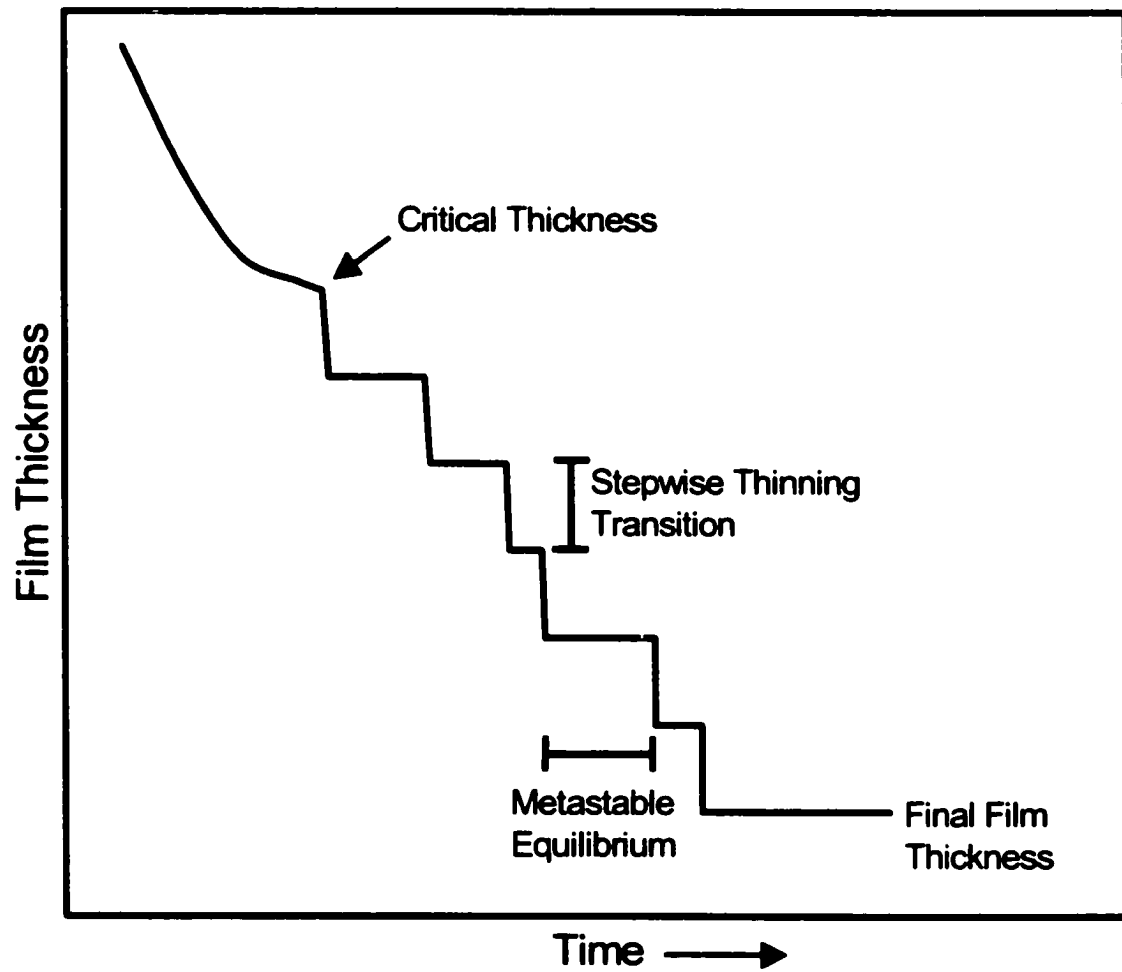
FIGURE 4.7: Sketch of the change in thickness over time for a typical stepwise thinning film.
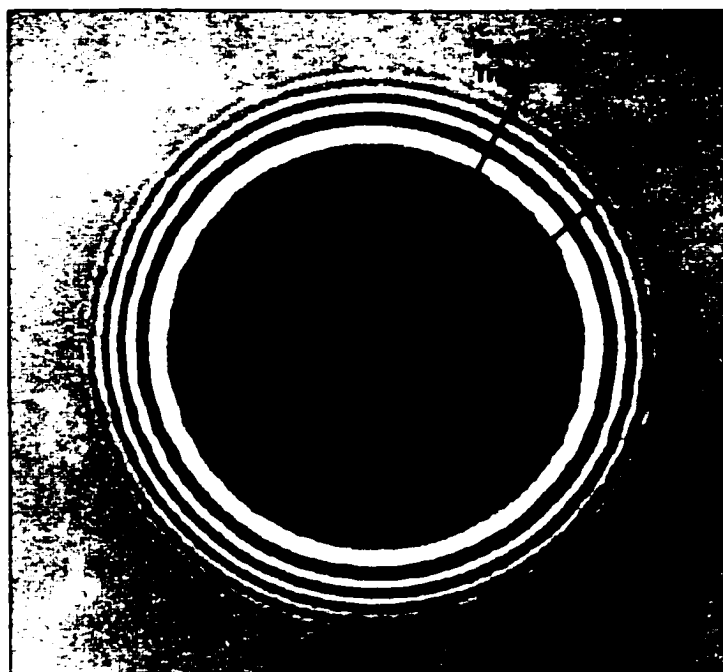
FIGURE 4.8: A second, darker stepwise thinning spot often appears inside another stepwise thinning spot. This image was obtained from a foam film of 20 %wt sodium naphthenates.
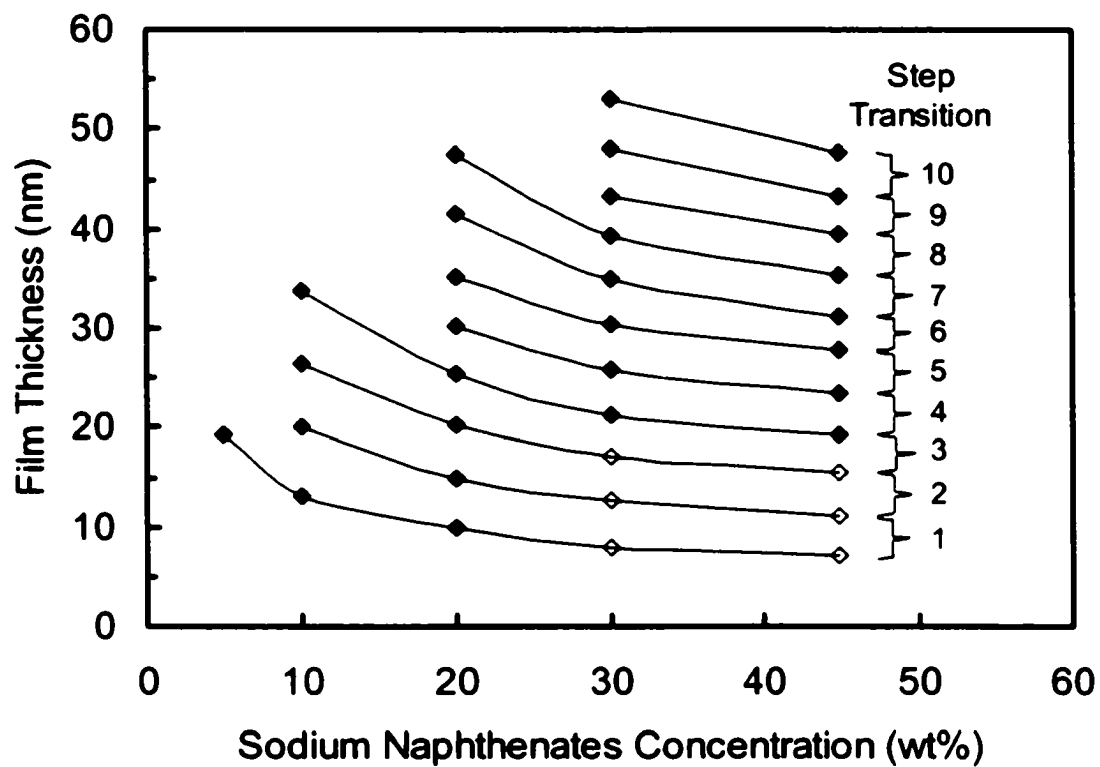
FIGURE 4.9: Thickness of stepwise thinning sodium naphthenate foam films as a function of bulk concentration. Induced step transitions indicated by open symbols.
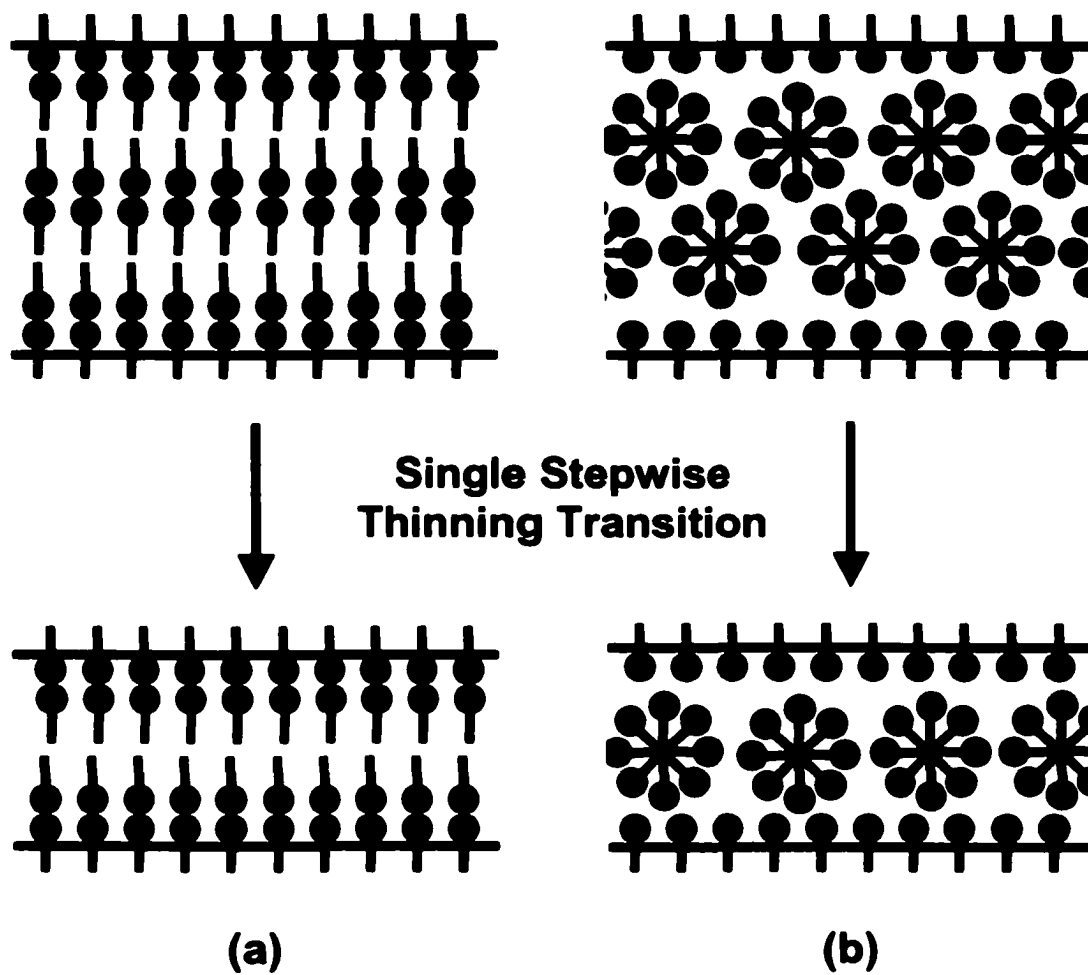
FIGURE 4:10: Stepwise thinning in the sodium naphthenate-water foam films may be due to the removal of (a) liquid crystal-like layers or (b) layers of spherical micelles.
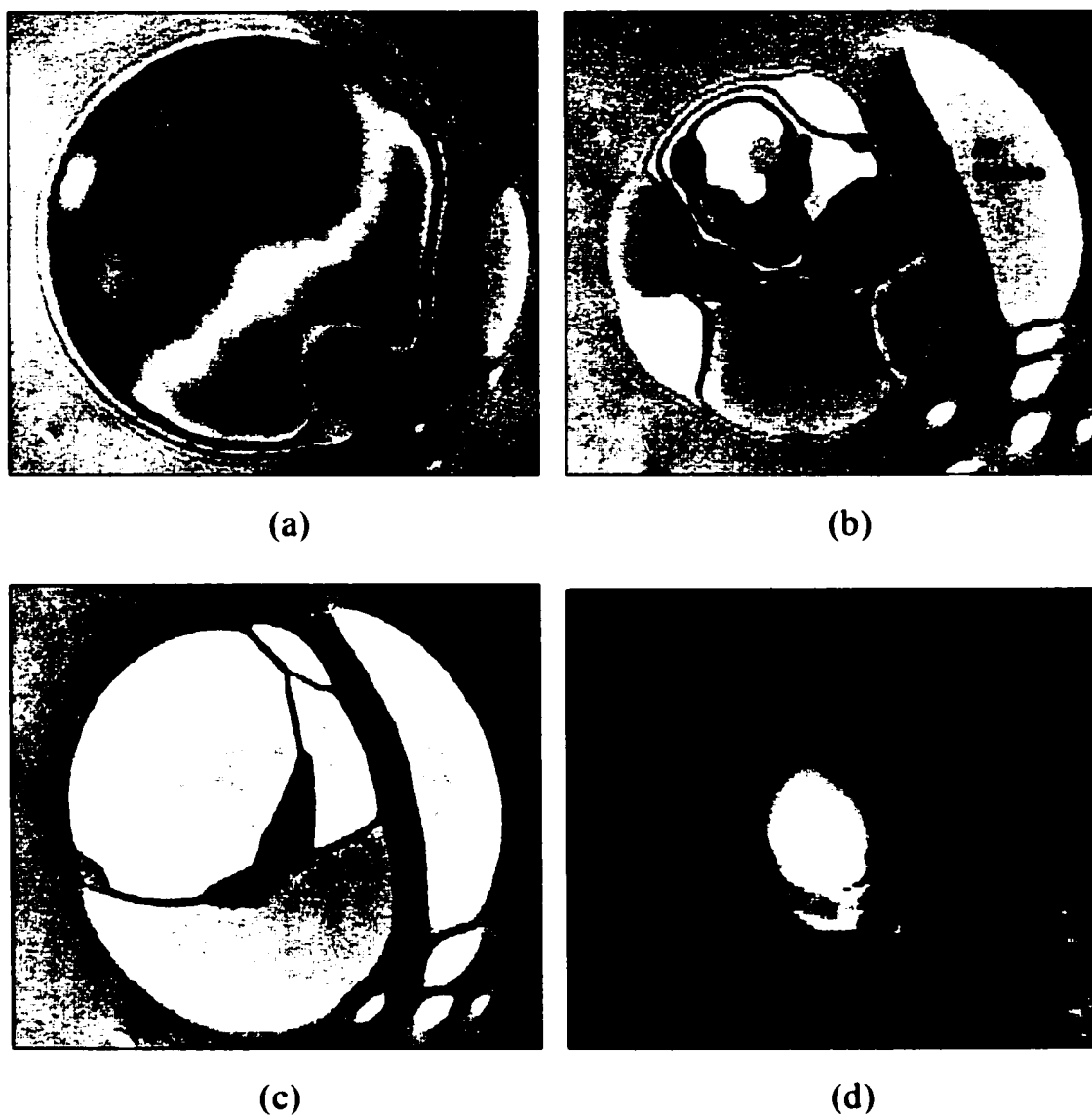
FIGURE 4.11: Images (a) through (c) show a sequence in time of the stepwise thinning process in a foam film drawn from the 50 %wt sodium napthenates mixture. Image (d) is a thin film formed between an air bubble and the liquid crystal-air interface.

(a)

B, Stepwise
Thickening

A. Second Stepwise
Thinning Transition

(b)

B   C

(c)

(d)

(e)

(f)
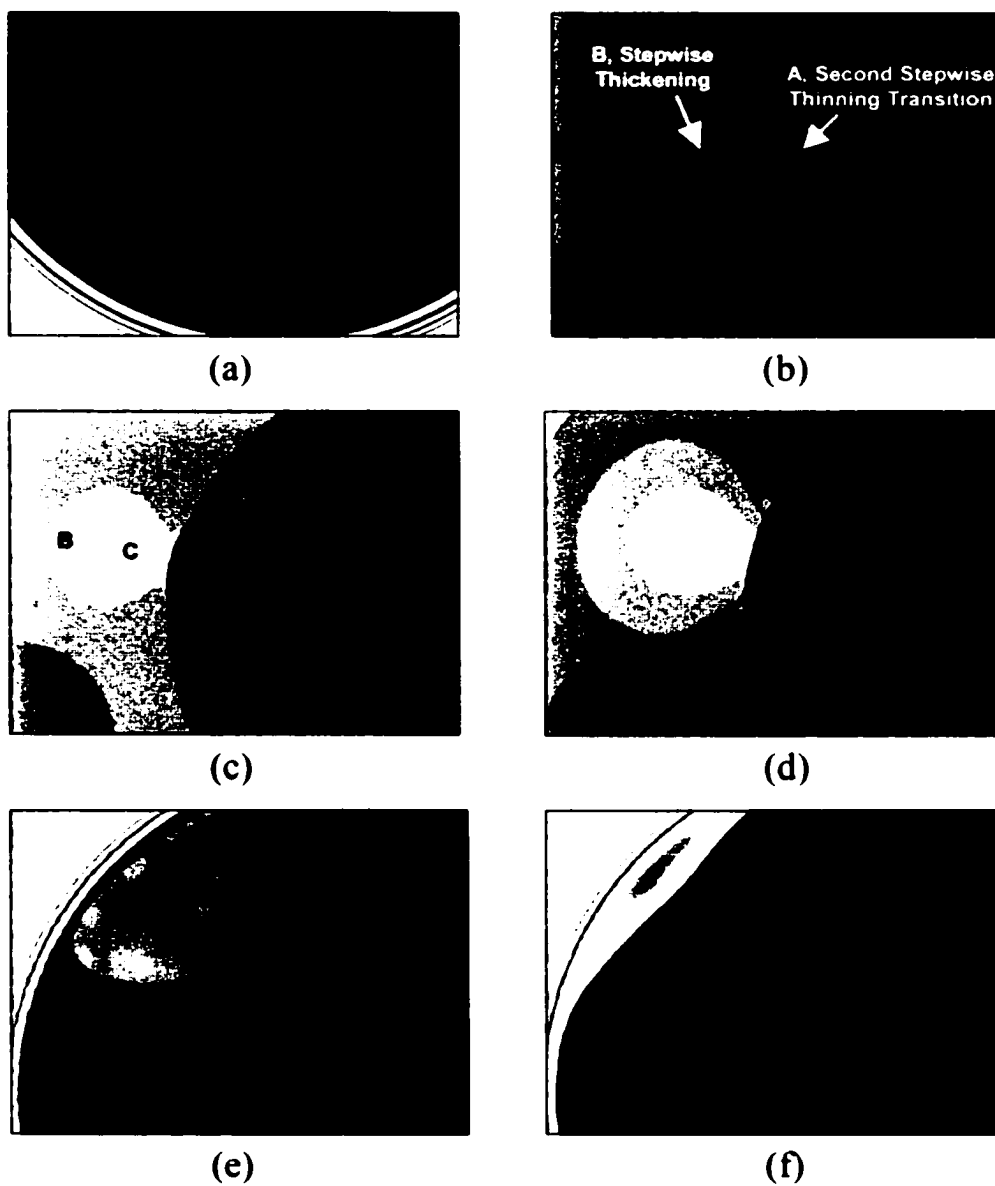
FIGURE 4.12: Images (a) through (f) show the growth and subsequent drainage of light-grey, stepwise thickening spots beside the growth of dark-grey, stepwise thinning spots. Images were obtained from a foam film containing 45 %wt sodium naphthenates.
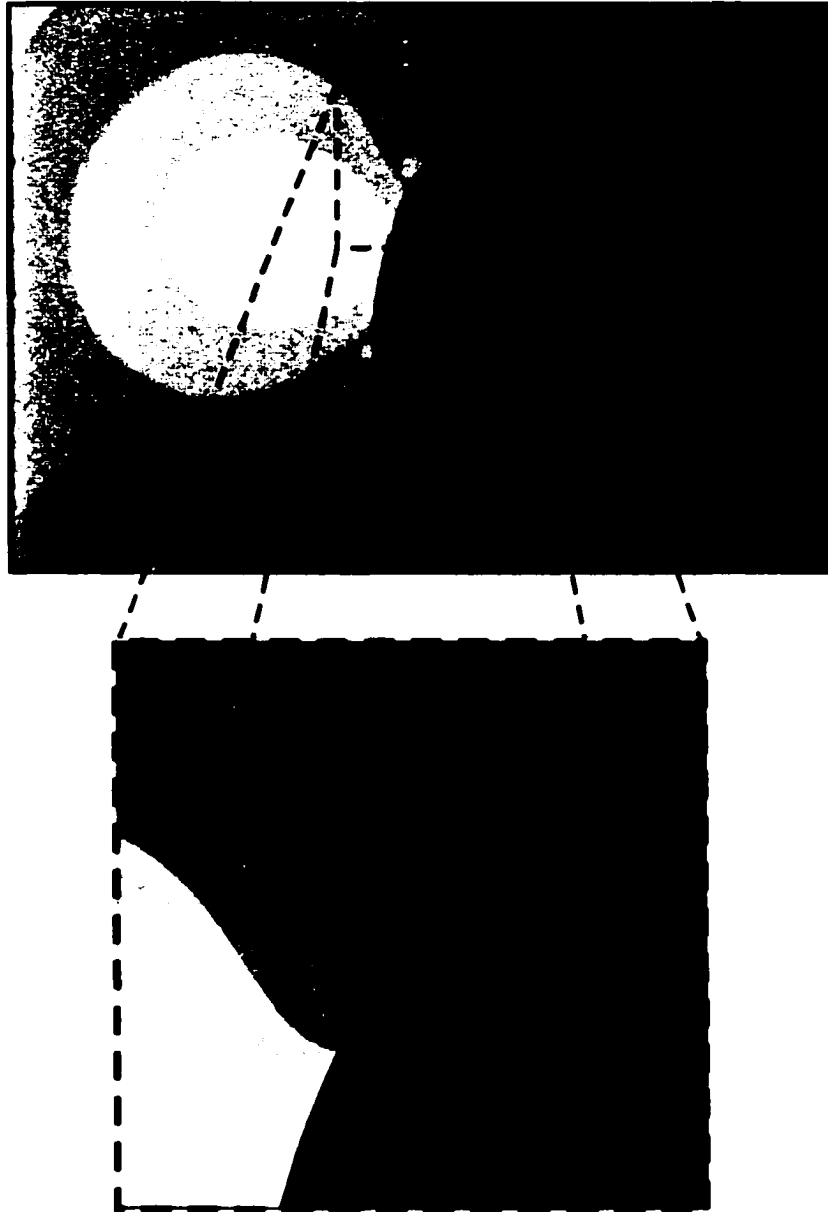
FIGURE 4.13: The schematic of Figure 4.12d highlights the small stepwise thickening spots that are formed near edge of second stepwise thinning spot. These small spots quickly migrate to the left and coalesce with the large existing stepwise thickening spots.

Before Stepwise
Thinning: 1ˢᵗ Stepwise
Thinning Spot

Appearance of 2ⁿᵈ
Stepwise Thinning
Spot & 1ˢᵗ Stepwise
Thickening Spot

Growth of 2ⁿᵈ Stepwise
Thinning Spot &
Appearance of 2ⁿᵈ
Stepwise Thickening Spot
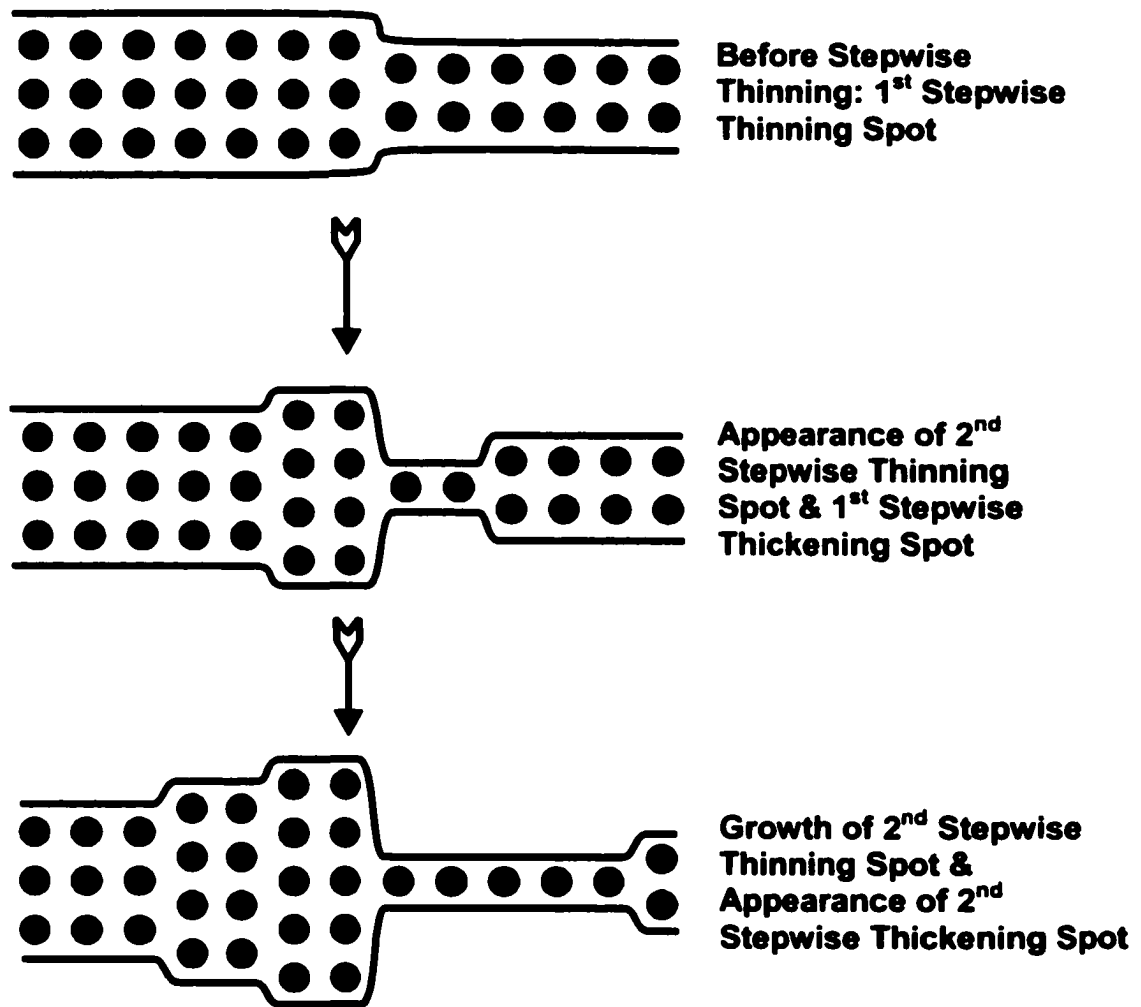
FIGURE 4.14: Schematic of the early stages of the stepwise thickening process. Black circles represent spherical micelles.

Chapter 5

Refractive Index Measurements of Diluted Bitumen Solutions[+]

The results presented in Chapters 2 and 3 included several thicknesses of water/solvent-diluted-bitumen/water films. The thickness measurements involved two basic steps: 1) recording the intensity of light reflected from the film and 2) converting the intensity measurement into an 'equivalent' thickness using a mathematical model of the film. The model for equivalent thickness is derived in Appendix A. The derivation of the equivalent thickness equation required certain assumptions about the structure and properties of the film. One important assumption required the film to be treated as a single slab of liquid of uniform refractive index. It is common practice to assume that the refractive index of the film is equal to the refractive index of the bulk liquid. The accuracy of the thickness measurements depends, to a large extent, on the validity of these assumptions.

Due to a lack of available data, the thickness results presented in Chapters 2 and 3 involved one additional assumption. The refractive index of the bulk solvent-bitumen mixtures was assumed to be equal to the refractive index of the pure diluent (e.g. toluene or heptane). Subsequent measurements have been obtained for the refractive index of solvent-bitumen mixtures at various concentrations. Instead of correcting all of the previous thickness calculations, the error associated with the assumption was calculated and found to be less than 2.5% of the film thickness. A complete discussion about the validity of this assumption is provided in Appendix A.

While performing the refractive index measurements, we found that the refractive index of 'pure' bitumen, 'pure' asphaltenes, and 'pure' maltenes could be estimated using extrapolation and a simple mixing model. The refractive index data of various oil solutions and the calculation of the 'pure' component refractive indices are presented in this chapter.

[+] Published in part: Taylor, S.D., Czarnecki, J. and Masliyah, J., *FUEL* **80** (2001) 2013-2018.

5.1 Introduction

Most of the physical properties of various crude oils can be obtained from literature (Hepler and Hsi, 1989; Hepler and Smith, 1994) or are readily measured using established laboratory methods (ASTM, 1993). For example, the refractive index of most light crude oils can be directly measured using conventional refractometers (Buckley, 1996; Buckley et al., 1998; Buckley, 1999). However, direct measurements of the refractive index of some heavy crude oils are unattainable since these liquids are often too opaque (or too black).

Bitumen is a heavy crude oil recovered from oil sands. It is a complex mixture of hydrocarbons that may be divided for convenience into several fractions. These include saturates, aromatics, resins, asphaltenes, and insolubles. Collectively, saturates, aromatics, and resins are known as maltenes or deasphalted bitumen. Except for the insolubles, all of the bitumen components can be completely dissolved by aromatic solvents like toluene. An aliphatic solvent, such as heptane, may be used to precipitate asphaltenes from the bitumen. The amount of asphaltene precipitate depends on the type and concentration of solvent (Mitchell and Speight, 1973). For example, the onset of asphaltene precipitation of Cold Lake and Athabasca bitumens in heptane occurs at a bitumen volume fraction of about 0.42 to 0.37 (Clarke and Pruden, 1998).

The asphaltene fraction consists of polyaromatic hydrocarbon molecules that vary in molecular weight. At the onset of precipitation, only the heaviest portion of the asphaltene fraction is expected to precipitate. The lighter portions of the asphaltene fraction will precipitate with further increases in heptane concentration with the lowest molecular weight asphaltenes being the last to come out of solution (Fuhr et al., 1991; Yarranton and Masliyah, 1996). Due to the range of asphaltene molecular weight, precipitation occurs over a range of concentration. Most experimental procedures use bitumen volume fractions of 0.03 or less to ensure complete asphaltene precipitation (Speight et al., 1984).

Buckley and coworkers have used refractive index (RI) to determine the solubility state of various crude oil-solvent solutions at the onset of asphaltene precipitation (Buckley et al., 1998; Buckley, 1999). It was observed that the onset of asphaltene precipitation occurred over a constant and narrow range of refractive index for given

combinations of crude oil and precipitating solvent. It has also been observed that both RI and the onset of asphaltene precipitation are affected by changes in the mixture composition, temperature, and pressure (Buckley, 1996). This suggests that the onset of asphaltene precipitation from a crude oil may be detected directly from RI measurements. It has also been shown that a mixture of a light crude oil and a non-precipitating solvent (e.g. toluene) behaves like an ideal binary mixture where the crude oil is treated as a single component (Buckley et al., 1998; Buckley, 1999). A simple mixing rule for the refractive index can then be applied to such an ideal mixture.

5.2 Refractive Index of a Mixture

The refractive index of a mixture, n, may be calculated from its specific refraction, N_s. The specific refraction of the mixture is simply the sum of the specific refraction of each component multiplied by the volume fraction (Glasstone, 1946; Synovec and Yeung, 1983):

$$N_S \equiv \frac{n^2 - 1}{n^2 + 2} \frac{1}{\rho} = \sum_i f_i \left(\frac{n_i^2 - 1}{n_i^2 + 2} \right) \frac{1}{\rho_i} \qquad [5.1]$$

where ρ is the density of the mixture. The refractive index, density, and volume fraction of component i in the mixture are given by n_i, ρ_i, and f_i, respectively. For Eq. [5.1], it is assumed that there is ideal mixing of the components and that there is no change in volume upon mixing. Further assuming that all of the densities are close to unity and that there are only two components in the mixture, Eq. [5.1] simplifies to the following relationship:

$$\frac{n^2 - 1}{n^2 + 2} = \left(\frac{n_1^2 - 1}{n_1^2 + 2} - \frac{n_2^2 - 1}{n_2^2 + 2} \right) f_1 + \left(\frac{n_2^2 - 1}{n_2^2 + 2} \right) \qquad [5.2]$$

where the subscripts 1 and 2 refer to the two components of the mixture and $f_2 = 1 - f_1$. As an example of the validity of Eq. [5.2], the refractive index measurements of an ideal mixture of heptane and toluene are shown in Figure 5.1. The straight line

prediction from Eq. [5.2] agrees with the measured RI data to within ± 0.0005. Once Eq. [5.2] is known to be applicable to a certain mixture, as is the case with the heptane and toluene, then one only needs to know n_1 and n_2 to readily evaluate the volume fractions of the components in the binary mixture.

Assuming that the complex mixture of bitumen and solvent constitutes an ideal binary mixture with the bitumen being treated as a single component, then the refractive index of the mixture can be calculated from the relation:

$$\frac{n^2-1}{n^2+2} = \left(\frac{n_B^2-1}{n_B^2+2} - \frac{n_S^2-1}{n_S^2+2}\right)f_B + \frac{n_S^2-1}{n_S^2+2} \qquad [5.3]$$

where f_B is the volume fraction of bitumen. The refractive index of the solvent, n_s, is readily obtained from direct measurement. Unfortunately, the refractive index of 'pure' bitumen, n_B, cannot be measured directly due to the opacity of the bitumen. In a commercial operation, it is difficult to readily obtain the composition of a bitumen-solvent mixture needed for process control. If Eq. [5.3] were found to be valid and n_B were known, then a refractive index measurement could be used as a tool to rapidly evaluate the volume ratio of a bitumen-solvent mixture.

It will be shown later that RI measurements can be obtained for mixtures up to a bitumen volume fraction of about 0.5. This raises the possibility of using Eq. [5.3] to extrapolate the RI data beyond the $f_B \sim 0.5$ measurement limit to obtain an estimate of n_B (i.e. n at $f_B = 1$). For the extrapolation to be considered valid, the estimate of n_B should not be affected by the choice of solvent and the solvent should not cause asphaltene precipitation. As observed in previous studies (Buckley, 1996; Buckley et al., 1998; Buckley, 1999), the onset of asphaltene precipitation from light crude oils can be detected as a deviation from the straight line prediction of Eq. [5.3].

There are two objectives to this study. The first objective is to determine whether Eq. [5.3] is valid for bitumen-solvent mixtures and, if so, to obtain estimates of the refractive indices of bitumen, maltenes (deasphalted bitumen), and asphaltenes. The second objective is to determine if the onset of asphaltene precipitation can be detected from refractive index measurements of a bitumen-heptane mixture.

5.3 Experimental Description

5.3.1 Materials[†]

The bitumen used in this study was a coker feed bitumen supplied by Syncrude Canada, Ltd. It is derived from oil sands that have been treated to remove coarse solids and water. Both asphaltenes and maltenes were also used for the RI measurements. The maltenes were obtained by diluting the bitumen with heptane to a volume ratio of 40:1 (heptane:bitumen). The mixture was stirred for 4 h and then left to allow the precipitated asphaltenes to settle overnight. The supernatant liquid was filtered to remove the asphaltene precipitate and then placed in an oven at 40°C to evaporate the solvent. The maltenes were considered 'dry' when the change in mass was less that 0.1 % over a 24 h period.

The asphaltene precipitate was dissolved into toluene at a volume ratio of 100:1 (toluene:precipitate) and then centrifuged at 9400 g for about 45 min to remove any fine mineral particles that might be associated with the asphaltenes. The supernatant was decanted and placed in an oven at 40°C to evaporate the solvent. The asphaltenes were considered 'dry' when the change in mass was less than 0.1% over a 24 h period (Yarranton and Masliyah, 1996; Khristov et al., 2000). The asphaltenes were obtained as solids and the recovery was approximately 14 %wt (or 12.4 %vol) of the original bitumen.

The mixture solvents included heptane, toluene, tetralin, anisole, naphtha, and cyclohexane. Except naphtha, all solvents were HPLC grade or better and were used as received (Fisher Scientific). Naphtha is a solvent that is produced at Syncrude Canada, Ltd. and it is used as a commercial diluent for bitumen during the extraction process. Naphtha is a hydrocarbon mixture of about 70% paraffin and 30% aromatic compounds containing some polar groups. It has a specific gravity of 0.74 at 15°C.

5.3.2 Refractive Index Measurements

Solutions of bitumen and solvent were mixed on a bench top shaker for a minimum of 2 h. The RI of the solutions were then measured using an automatic refractometer (Model GPR 12-70, Index Instruments U.S., Inc.). All measurements were

---

[†] A complete description of the procedures used for materials preparation can be found in Appendix D.

performed at a wavelength of 589 nm and a constant temperature of 23.0 ± 0.1°C. In the case of bitumen-heptane mixtures, the solution samples were left undisturbed for a minimum of 1 h after shaking to allow for the asphaltene precipitate to settle under gravity. A few samples of the bitumen-heptane mixtures were also centrifuged to ensure that all precipitate was removed. However, there was no observable difference between the measured RI of the centrifuged samples and the samples left to settle under gravity for 1 h. Based on repeat experiments, measurement error was estimated to be ±0.0005.

5.4 Results and Discussion

5.4.1 Refractive Indices of Bitumen, Maltenes, and Asphaltenes

As was pointed out earlier, it is not possible to measure the refractive index of bitumen-solvent mixtures when the bitumen volume fraction exceeds about 0.5. This is also true for maltenes-solvent and asphaltene-solvent mixtures. For this reason, it becomes advantageous to extrapolate to 'pure' bitumen (i.e. to $f_B = 1$) using Eq. [5.3]. As in any extrapolation exercise, one needs to be extremely cautious. To ensure that our extrapolation estimate of n_B was invariant to the choice of solvent, it was necessary to perform the extrapolation using data from several solvents each with a different refractive index.

The RI data for various bitumen-solvent mixtures is plotted in Figure 5.2. Eq. [5.3] has been fit to each set of data using least squares regression. The equation was capable of fitting the RI measurements for all the bitumen-solvent mixtures to within ±0.0005. The data for cyclohexane was expected to show some non-linearity since cyclohexane is known to precipitate a small amount of asphaltene (<1.0 wt%) (Mitchell and Speight, 1973). However, the data was linear up to a bitumen volume fraction of about 0.52 and no visual evidence of precipitation was observed.

From the data for each bitumen-solvent mixture, the confidence interval for the estimate of n_B was calculated using the following relation:

$$n_B \pm T_{\alpha,m-2} \sqrt{Var(n_B)} \tag{5.4}$$

TABLE 5.1: Estimates of n_B from various bitumen-solvent mixtures.

Solvent	Estimated RI of Bitumen n_B	95% Confidence Interval
Naphtha	1.5921	± 0.0020
Cyclohexane	1.5865	± 0.0012
Toluene	1.5820	± 0.0016
Tetralin	1.5801	± 0.0008
Anisole	1.5788	± 0.0012

where T refers to the value for the Student-t statistic, α is the confidence level, and m is the number of data points. The variance was calculated, as follows:

$$Var(n_B) = \left(\frac{\sum(n_j - \hat{n}_j)^2}{m - 2} \right) \left(\frac{1}{m} + \frac{(f - \bar{f})^2}{\sum(f_j - \bar{f})^2} \right)$$ [5.5]

where n_j is the refractive index at a given volume fraction of bitumen, f_j. Here, $\hat{n}_j$ is the prediction of the RI from Eq. [5.3] at the same f_j and $\bar{f}$ is the average volume fraction from all of the RI measurements. The estimates of n_B and the 95% confidence intervals obtained from each solvent-bitumen data set are given in Table 5.1. From this data, it appears that the estimates of n_B are dependent on the choice of diluent. However, at a confidence level of 0.95, the estimates of n_B were not significantly different. Therefore, we concluded that the estimates of n_B are independent on the type of solvent. From the linear trend in the data, it can be concluded that the mixture may be treated as a binary mixture solvent and bitumen and thus, Eq. [5.3] is valid. The values for n_B from each bitumen-solvent mixture have been averaged to give an overall estimate for the refractive index of bitumen of n_B = 1.5839 ± 0.0039.

TABLE 5.2: Estimates of n_M from various maltene-solvent mixtures.

Solvent	Estimated RI of Maltenes n_M	95% Confidence Interval
Heptane	1.5796	± 0.0032
Naphtha	1.5766	± 0.0021
Cyclohexane	1.5727	± 0.0013
Anisole	1.5710	± 0.0014
Toluene	1.5640	± 0.0009
Tetralin	1.5613	± 0.0003

Figure 5.3 shows that RI data for various maltene-solvent mixtures. Again, Eq. [5.3] has been fit to each set of data using least squares regression. The estimates of n_M and the 95% confidence intervals are given in Table 5.2. Similar to n_B, the estimates of n_M were not significantly different at a confidence level of 0.95. Therefore, we concluded that the estimates of n_M are independent on the type of solvent. The overall estimate for the refractive index of maltenes is $n_M = 1.5709 \pm 0.0048$.

The RI data for a mixture of asphaltenes and toluene (Figure 5.4) has been used to estimate the refractive index of asphaltenes, n_A. Eq. [5.3] has again been fit to the data using least squares regression. Extrapolation to $f_A = 1$ gives an estimate of $n_A = 1.7075 \pm 0.0055$.

Comparisons of n_B and n_M, using the toluene mixtures as an example, reveals a statistically significant drop from 1.5820 to 1.5640 when the asphaltenes are removed from the bitumen. A similar drop in refractive index has also been observed in Prudhoe Bay crude oil where the RI of the crude oil changed from 1.516 to 1.495 after asphaltene precipitation (Buckley, 1999). Bitumen, like all crude oils, consists of a large variety of hydrocarbons and each compound will contribute to the overall or average refractive index of the crude oil 'mixture'. Highly aromatic compounds, like asphaltenes, tend to have higher refractive indices compared to more paraffinic compounds contained within the bitumen. By removing the asphaltene fraction, the concentration of aromatic

compounds in the crude oil is reduced and hence. the RI of the crude oil 'mixture' is expected to be lower.

To observe how the maltenes and asphaltenes contribute to the refractive index of a crude oil 'mixture'. let us consider Eq. [5.1] again. The equation provides a relation for calculating the refractive index of a crude oil 'mixture' from the refractive indices of its various components, namely maltenes and asphaltenes. This means an alternate relation exists for estimating the refractive index of bitumen:

$$\left(\frac{n^2-1}{n^2+2}\right) = \left(\frac{n_M^2-1}{n_M^2+2}\right)f_M + \left(\frac{n_A^2-1}{n_A^2+2}\right)f_A \qquad [5.6]$$

where $n = n_B$ when $f_A = 0.124$. For toluene diluted mixtures, n_M and n_A are already known (see Table 5.2). Substituting these values into Eq. [5.6] provides an estimate of $n = 1.5809 \pm 0.0015$. This is comparable to the estimate of $n_B = 1.5820 \pm 0.0016$ obtained earlier (see Table 5.1).

This result suggests that a crude oil may be treated as an ideal mixture of its components. Hence, Eq. [5.6] may be applied to calculate the RI of a crude oil. Of course, care must be taken to account for the variation in the composition of the maltenes or asphaltenes. The exact composition will depend on the source of the crude oil and the procedures used to prepare the maltene and asphaltene fractions. This variation will affect the estimates of n_M and n_A.

5.4.2 Asphaltene Precipitation

As mentioned earlier. an 'ideal' mixture of solvent and bitumen is expected to follow a linear relation with bitumen concentration (i.e. Eq. [5.3]). However, with heptane as the solvent, the refractive index is expected to deviate from this linear relation at the onset of asphaltene precipitation (Buckley et al., 1998; Buckley, 1999).

RI data for a bitumen-heptane mixture at various concentrations is plotted in Figure 5.5(a). The straight lines shown in the plot are the Eq. [5.3] predictions for a bitumen-heptane mixture (upper dot-dash line) and a maltene-heptane mixture (lower solid line). At high bitumen concentrations, there is no visible asphaltene precipitation

and the RI data fall onto the straight line for a bitumen-heptane mixture, as expected. At very low bitumen concentrations where the asphaltene precipitation is assumed to be complete, the RI data falls on the straight line prediction for a maltene-heptane mixture. Significant asphaltene precipitation appears to occur over a range of bitumen volume fraction from about 0.15 to about 0.35. Qualitatively, this agrees with the notion that a distribution in asphaltene molecular weight would result in precipitation occurring over a range of bitumen concentration.

Between a bitumen volume fractions of 0.35 to 0.3, the RI data starts to deviate from the straight line prediction for bitumen-heptane mixture and some asphaltene precipitate is visible in the prepared samples. This clearly indicates the onset of asphaltene precipitation. A more accurate estimate of the onset of precipitation can be obtained from a plot of the difference between the refractive index data for the bitumen-heptane mixture $((n^2-1)/(n^2+2)_{Data})$ and the straight line prediction from Eq. [5.3] for a maltene-heptane mixture $((n^2-1)/(n^2+2)_{Theory})$. Such a plot is shown in Figure 5.5(b). Above a value of about 0.0030, the difference between the data and prediction is approximately constant. The onset of asphaltene precipitation appears to occur when the difference falls below the 0.0030 threshold at a bitumen volume fraction of about 0.32. This fraction is slightly lower than a previous finding, which suggested that the onset of asphaltene precipitation for an Athabasca bitumen occurs within a bitumen volume fraction of 0.42 to 0.37 (Clarke and Pruden, 1998). This discrepancy may be simply due to a variation in the composition of the bitumen sources or it may indicate that the refractive index may not be sensitive enough to detect the initial onset of asphaltene precipitation. The discrepancy may also be related the protocol utilized in this study, particularly in the amount of time allowed for asphaltene precipitation to occur. A longer time between mixing and the RI measurement may cause an additional shift in the measured onset point.

5.5 Conclusions

A well known mixing model for predicting the refractive index of an ideal mixture has been applied to various bitumen-solvent mixtures. The investigation has lead to the following conclusions:

1. There was excellent agreement between the refractive index data and the predictions made from the mixing model. This clearly showed that in a bitumen-solvent mixture, bitumen may be considered a single component. However, this result was limited to 'good' solvents that were capable of completely solubilizing the bitumen. Solvents that lead to precipitation do not fit the mixing model over the entire range of bitumen concentration.

2. Using several bitumen-solvent mixtures, estimates of 1.584, 1.571 and 1.708 were obtained for the refractive indices of bitumen, maltenes, and asphaltenes, respectively.

3. A precipitating solvent, heptane, was used to show that the onset of asphaltene precipitation could be detected from refractive index measurements. For mixtures of heptane and bitumen, the onset of asphaltene precipitation appeared to occur at a bitumen volume fraction of about 0.32.

5.6 References

Annual Book Of ASTM Standards, Philadelphia: American Society for Testing and Materials (ASTM), 1993.

Buckley, J.S., *Fuel Sci. Technol. Int.* **14** (1996) 55.

Buckley, J.S., Hirasaki, G.J., Liu, Y., Von Drasek, S., Wang J.X. and Gill, B.S., *Pet. Sci. Technol.* **16** (1998) 251.

Buckley, J.S., *Energy & Fuels* **13** (1999) 328.

Clarke, P.F. and Pruden, B.B., *Pet. Sci. Technol.* **16** (1998) 287.

Fuhr, B.J., Cathrea, C., Coates, L., Kalra, H. and Majeed, A.I., *FUEL* **70** (1991) 1293.

Glasstone, S., "Textbook of Physical Chemistry" 2nd Ed. New York: D. Van Nostrand Company, Inc, 1946.

Hepler, L.G. and His, C. (Ed.), "AOSTRA Technical Handbook on Oil Sands, Bitumens, and Heavy Oils" Edmonton: Alberta Oil Sands Technology and Research Authority (AOSTRA), 1989.

Hepler, L.G. and Smith, R.G., "The Alberta Oil Sands: Industrial Procedures for Extraction and Some Recent Fundamental Research" Edmonton: Alberta Oil Sands Technology and Research Authority (AOSTRA), 1994.

Khristov, K., Taylor, S.D., Czarnecki, J. and Masliyah, J., *Colloid Surf. A* **174** (2000) 183.

Mitchell, D.L. and Speight, J.G., *FUEL* **52** (1973) 149.

Speight, J.G., Long, R.B. and Trowbridge, T.D., *FUEL* **63** (1984) 616.

Synovec, R.E. and Yeung, E.S., *Anal. Chem.* **55** (1983) 1599.

Yarranton, H.W. and Masliyah, J.H., *AIChE J.* **42** (1996) 3533.
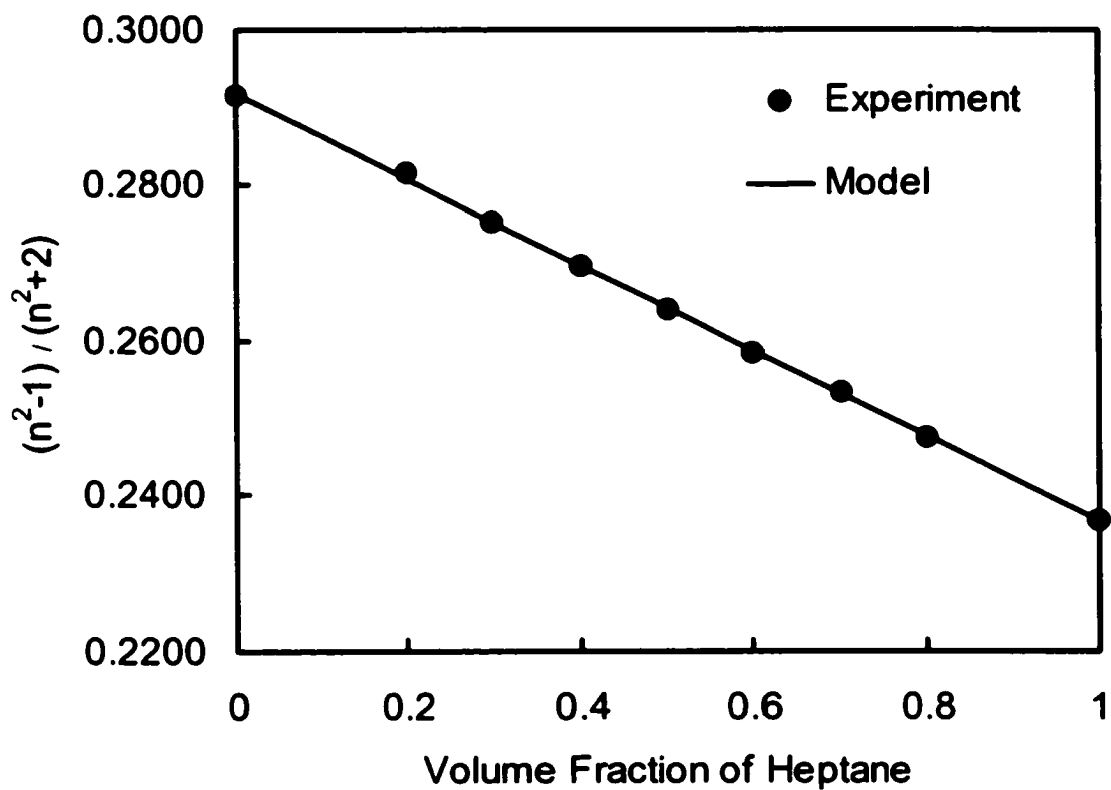
FIGURE 5.1: RI measurements of an ideal binary mixture of heptane and toluene show the validity of Eq. [5.2].
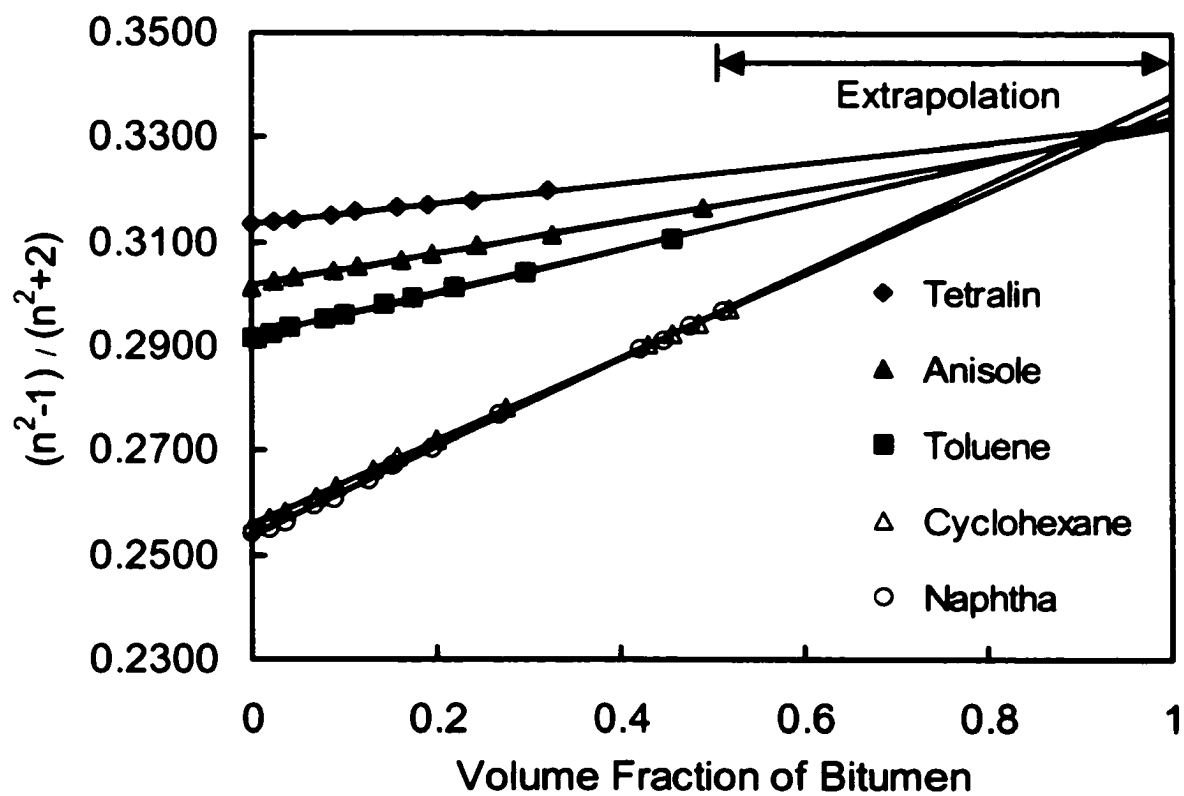
FIGURE 5.2: RI measurements of mixtures of bitumen with various solvents.
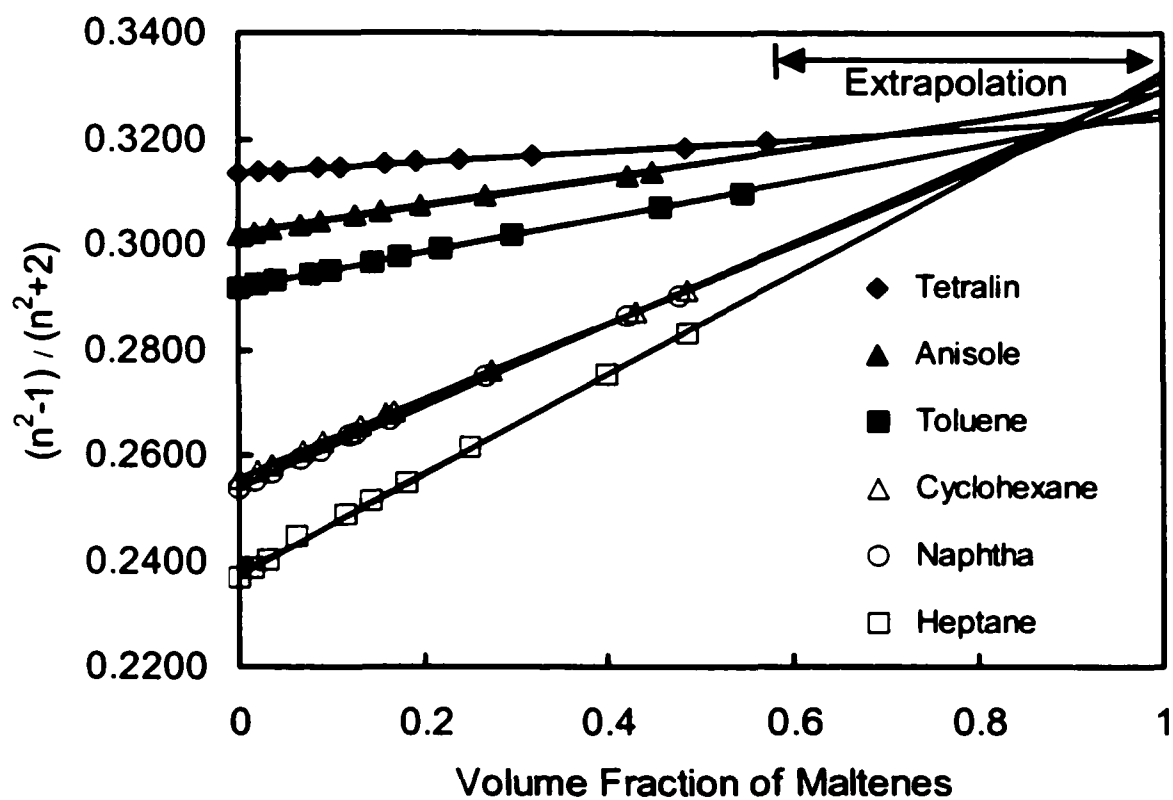
FIGURE 5.3: RI measurements of mixtures of maltenes with various solvents.
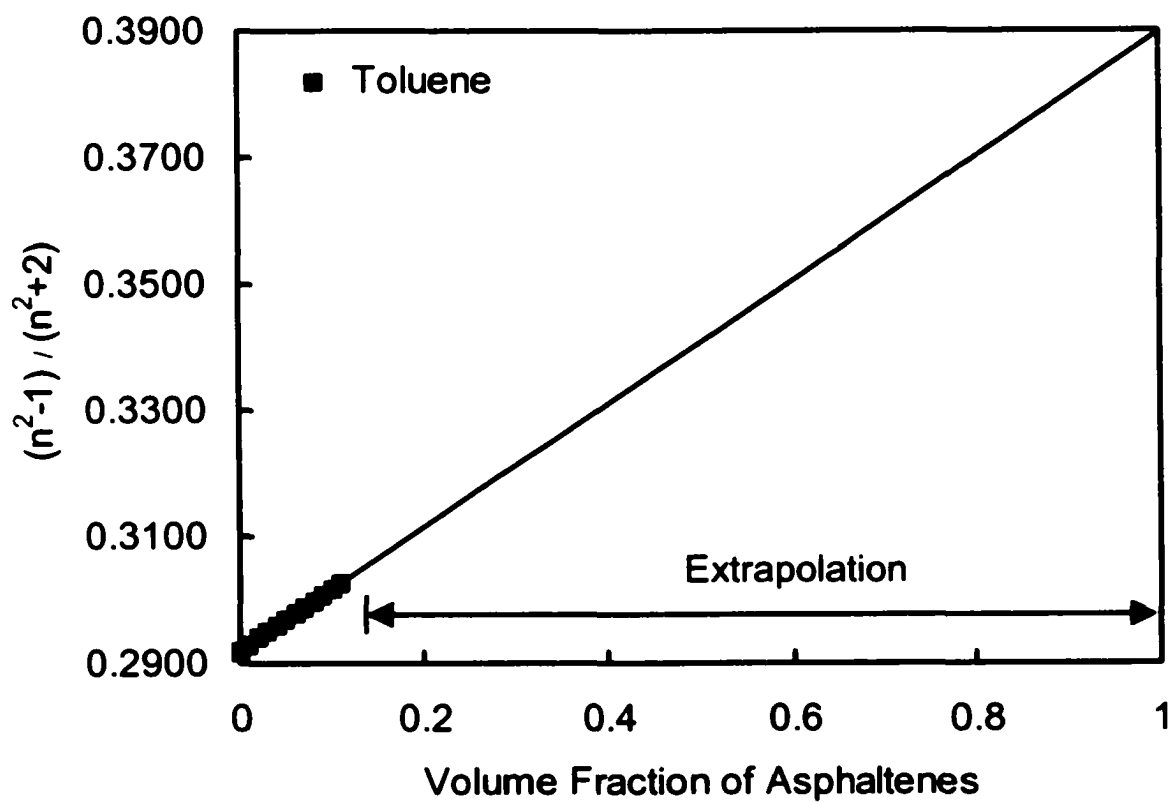
FIGURE 5.4: RI measurements of an asphaltene and toluene mixture.
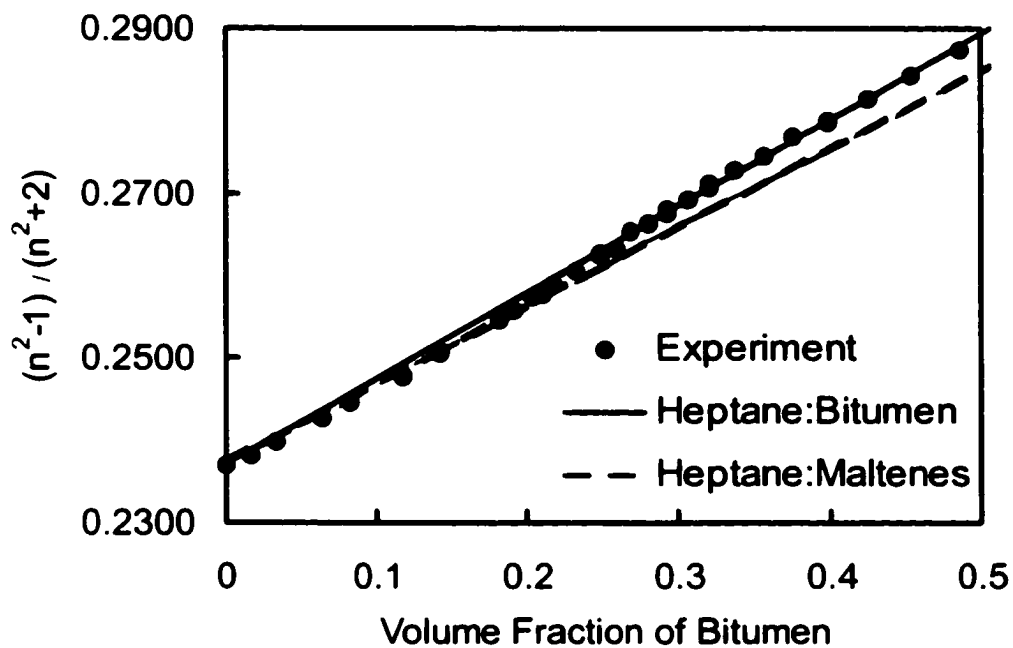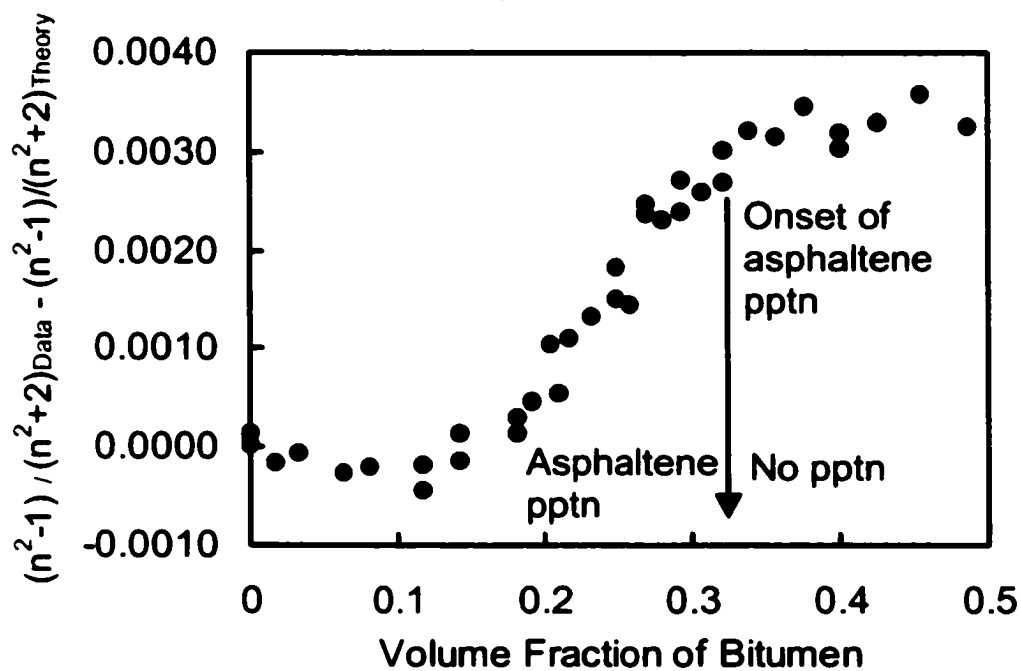
FIGURE 5.5: (a) Slight deviation in RI measurements of bitumen-heptane mixtures indicate the onset of asphaltene precipitation. (b) Difference between the RI experiment and straight line prediction for maltene-heptane clearly shows the onset of asphaltene precipitation.

Chapter 6

Conclusions and Recommendations

This chapter provides a brief discussion of the conclusions related to each of the thesis objectives outlined in Chapter 1 followed by recommendations for future research. The objectives of this thesis are, as follows:

1. Develop a new modification of the TLF-PBT that allows for the investigation of toluene-diluted-bitumen films formed in an aqueous environment.

2. Determine the basic behaviour of a water/toluene-diluted-bitumen/water film, including observations of equilibrium film thickness, drainage rates, drainage patterns, and film lifetimes.

3. Identify the type and magnitude of the surface forces in water/toluene-diluted-bitumen/water films from measurements of the disjoining pressure-thickness isotherms.

4. Determine if there is a link between the phase behaviour of a sodium naphthenates-water system and the behaviour of the foam films formed from the same sodium naphthenates-water system.

5. Measure the refractive index of various diluted bitumen solutions. Use the data to develop a mixing model for the refractive index of diluted bitumen solutions.

6.1 Development of the Thin Liquid Film Apparatus

There are several techniques that may be used to study the interactions between colloidal particles, the most popular being the Surface Force Apparatus, Atomic Force Microscopy, and the Thin Liquid Film apparatus. Most techniques are limited to studying interactions in well-defined systems, such as the interaction between two solid particles or between a droplet and a solid surface. The Thin Liquid Film-Pressure Balance Technique apparatus is limited to measurements between two fluid interfaces. This includes the interaction between gas-liquid interfaces found in foams or the interaction between liquid-liquid interfaces found in emulsions. The specific technique used in this

thesis was also limited to modeling interactions between two equally sized spherical droplets (or bubbles). Traditionally, the Thin Liquid Film apparatus has been limited to studying well-defined aqueous and non-aqueous foam films as well as aqueous emulsion films. The previous systems are well defined in the sense that the chemical and physical properties of the surfactant and continuous phase are known. In this work, the apparatus has been modified to study a poorly defined non-aqueous emulsion film. Specifically, a water/solvent-diluted-bitumen/water film for which the chemical identity and properties of the stabilizing surfactant are not clearly known.

A hydrophobic surface was required to form a water/solvent-diluted-bitumen/water film. Thus, the most important modification to the TLF-PBT was a change in the protocols used to prepare, clean and store the porous plate film holders. The protocols helped to create and maintain a hydrophobic surface on the porous plate film holder. Preparation involved treating the porous glass with a solution of toluene and bitumen to convert the glass surface from a hydrophilic to a hydrophobic nature. To maintain the hydrophobic nature of the glass surface, glass cleaners (e.g. chromic acid) could not be used during the cleaning procedure. Only organic solvents could be used to clean the film holder. Finally, storing the film holders in a dilute solution of toluene and bitumen prevented degradation of the hydrophobic surface.

6.2 Properties of Water/Solvent-Diluted-Bitumen/Water Films

A water/toluene-diluted-bitumen/water film was chosen as the base model for this study. The base model was characterized using visual observations combined with quantitative measurements of film thickness, film lifetime, and drainage rate as a function of toluene:bitumen weight ratio. All of the measurements were performed at constant film diameter (i.e. constant capillary pressure). The toluene-bitumen films drained monotonously to a uniform dark grey film that remained stable for several hours. At low weight ratios, the equilibrium thickness was about 50 nm. Between weight ratios (2:1) and (5:1), there was an abrupt decrease in the equilibrium thickness. The equilibrium thickness then remained at a constant 15 nm at weight ratios of 10:1 or larger. The abrupt change in equilibrium thickness was an early indication of a change in the film structure and surface forces acting within the film.

The effect of solvent strength was determined from a comparison between the properties of the base model and the properties of a water/heptane-diluted-bitumen/water film. At heptane:bitumen weight ratios below the precipitation point of asphaltenes (i.e. less than 1.7:1), the heptane-bitumen film drained monotonously to a dark grey film that remained stable for a long period of time. The film behaviour was nearly identical to the behaviour of toluene-bitumen films. However, the onset of asphaltene precipitation had a significant effect on the heptane-bitumen film behaviour. Black spots began to appear during film drainage indicating a dramatic change in the surfaces forces within the film. The film also became unstable, rupturing within a few minutes of film formation. From these results, it is quite clear that surface active material contained within the asphaltenes plays a dominant role in the stability of thin films.

6.3 Surfaces Forces in Water/Toluene-Diluted-Bitumen/Water Films

The same Thin Liquid Film-Pressure Balance Technique was used to measure the disjoining pressure-thickness isotherms of water/toluene-diluted-bitumen/water films. The isotherms provide a direct measure of the net surface force that exists within a thin liquid film. In this study, isotherms were obtained for several different toluene:bitumen mass ratios. Only two distinct isotherms were obtained. One isotherm was obtained at low toluene:bitumen mass ratios (1:1 and 2:1) and a second isotherm was obtained for higher mass ratios (5:1 and 10:1). The transition between the two isotherms occurred at a critical mass ratio of (3:1).

The first isotherm indicated that the films of low mass ratios were extremely stable. An 8 to 8.5 nm thick surfactant bilayer produced a strong, short range steric repulsion that stabilized the film. A similar isotherm with the same bilayer thickness was also obtained from a water/toluene-diluted-asphaltene/water film. These results have two important implications: (1) the dominant surface active material absorbed on the film interfaces must be from the asphaltene fraction of bitumen and (2) the absorbed surface active material must have a length of about 4 nm when compressed. The second isotherm indicated that the films of high mass ratio were relatively unstable. Only a weak repulsive force was present which resulted in the film rupturing at relatively low disjoining pressures.

Finally, the sharp transition between the two isotherms provided a potentially valuable insight into the structure of the film. It was suspected that the sharp transition might be due to a change in the organization of the surface active material at the film interfaces (i.e. a change in the film structure). There was some correlation between the film stability and transition between the two isotherms. It appears that the organization associated with low mass ratios provided a strong repulsive force that stabilized the film whereas the organization that was associated with high mass ratios produced only a weak repulsive force that was unable to stabilize the film.

6.4 Linking Thin Film and Bulk Phase Behaviour

Previous studies have shown that a particular organization of surfactant molecules within a film may correspond to a similar surfactant structure in the bulk liquid used to form the film. This suggests that, for water/toluene-diluted-bitumen/water films, the observed change in the film structure may have been related to a change in the organization of surfactant molecules within the bulk water-toluene-bitumen mixture. Unfortunately, it is difficult to link the bulk phase behaviour and thin film behaviour for a water-toluene-bitumen system since we do not have a good understanding of the molecular interactions between the resins, asphaltenes, and low molecular weight natural surfactants in water-toluene-bitumen mixtures. Therefore, this study used a model foam film formed from a mixture of sodium naphthenates and water to investigate the link between the organization of surfactants in a thin film and the organization of surfactants in a bulk liquid.

A possible link between the bulk and thin film behaviour was observed in foam films formed from a lamellar liquid crystal phase and from a 50 %wt mixture where lamellar liquid crystal is one of three known phases. These films displayed stepwise thinning behaviour indicating that the film contained a lamellae structure. It is suspected that the structure consisted of sodium naphthenate molecules in a lamellar liquid crystal-like organization. No clear link could be established between the stepwise thinning behaviour observed in films drawn from the single isotropic solution formed at concentrations of 45 %wt or less. Without additional information about the surfactant structure in the isotropic solution, it was impossible to determine the origins of the

lamellar structure of these films. It was speculated that the films might have consisted of a liquid crystal-like structure or multiple layers of spherical micelles.

In addition to the stepwise thinning, the foam films formed from the isotropic solution also displayed a stepwise thickening behaviour. Stepwise thickening involved discrete increases in the film thickness within a small region of the film. The phenomenon was always temporary and it was directly related to the stepwise thinning process. It is one of the first times that such a phenomena has been observed in thin films.

6.5 Refractive Index of Bitumen, Maltenes, and Asphaltenes

Part of the thin film investigation required refractive index measurements for the various solvent-bitumen solutions. Refractive index data was obtained for bitumen volume fractions ranging from 0 to about 0.5. The data showed excellent agreement with a well-known mixing model used to predict the refractive index of ideal mixtures. The model related the volume fraction to the refractive indices of the pure components. In this study, the solvent and bitumen were treated as 'pure' components in an ideal binary mixture. Since the refractive index of the bitumen could not be measured, the model was used to extrapolate the data to a bitumen volume fraction of 1.0. Using several different types of solvent, an accurate estimate of the refractive index of bitumen was obtained. Estimates of 1.584, 1.571, and 1.708 were obtained for the refractive indices of bitumen, maltenes, and asphaltenes.

The mixing model was limited to 'good' solvents that were capable of completely dissolving the bitumen. 'Poor' solvents led to the precipitation asphaltenes from the solvent-bitumen mixtures causing the refractive index data to deviate from the model predictions. However, the onset of asphaltene precipitation corresponded to point at which the data began to deviate from the predictions of the mixing model. Hence, the model could be used to detect the onset of asphaltene precipitation. For mixtures of heptane and bitumen, the onset of asphaltene precipitation appeared to occur at a bitumen volume fraction of 0.32.

6.6 Recommendations for Future Research

The phase behaviour of the bulk liquid has not been an important consideration in most of the previous thin liquid film investigations. The vast majority of thin film studies have been limited to foam films or emulsion films in which the surfactants are soluble in only one phase. In both cases, the surfactant concentrations are normally on the order of the CMC or lower, concentrations at which multiple phase behaviour does not occur. Emulsions are commonly perceived as two-phase systems, however emulsions are a multiphase system by definition and it is possible for more than two phases to exist. Water-in-bitumen emulsions appear to be capable of forming more than two phases and the natural surfactants (e.g. sodium naphthenates) found in bitumen are known to partition between the aqueous and oil phases. Therefore, bulk phase behaviour should be an important consideration when designing future thin film investigations related to water-solvent-bitumen systems. The following recommendations are based on this argument:

1. The current porous plate film holder was designed to hold fixed amounts of the water and oil phases. However, the partitioning of surfactant between these two phases depends on the relative amounts of each phase. It would be beneficial to redesign the film holder to allow for changes in the relative amounts of the water and oil phases.

2. It is clear that surface active material from the asphaltene fraction plays an important role in stabilizing the thin films. This conclusion is based on a comparison between two extreme cases: i) films formed from bitumen dissolved in a strong aromatic solvent and ii) films formed from heptane-precipitated asphaltenes dissolved in a strong aromatic solvent. However, the solubility state of asphaltenes is known to change with gradual changes in solvent strength. A future investigation of water/solvent-diluted-bitumen/water films in which the solvent strength is gradually changed from aromatic to more aliphatic will probably reveal significant changes in the film properties. Such changes may provide some valuable information about the film structure or the material that is absorbed on the film interfaces. Also, the results of such an investigation may correlate with known information on the

bulk phase behaviour of asphaltenes. Such a study may provide a link between the thin film behaviour and the phase behaviour of asphaltenes in the water-solvent-bitumen system.

3. From a fundamental perspective, the relationship between bulk phase behaviour and thin film behaviour in an emulsion system is still poorly understood. Several questions still remain. Is there a difference between the critical concentration for the bulk phase transition and the critical concentration for the corresponding transition in the film structure? Would the same effect be observed with temperature? What is the structure of the sodium naphthenates in the isotropic solution? What is the structure of the film formed from the isotropic solution? Previous studies using thermotropic liquid crystals have shown that there are significant differences between the structure of a bulk liquid crystal and the liquid crystal-like structure in a thin film. Would a similar difference exist in the liquid crystal region of the water-sodium naphthenates system? Any one of these questions may be used as a basis for a future investigations and provide valuable insights into systems of mixed surfactants.

4. Some excellent research has been completed in the area of stepwise thinning of stratified films. However, the appearance of stepwise thickening in a region immediately adjacent to a region of stepwise thinning has introduced a new dimension to this area of research. Little is known at this stage about stepwise thickening. Even the conditions under which stepwise thickening will occur have not been fully explored. It is also quite clear that the observed stepwise thickening cannot be explained using the existing models for drainage behaviour and stability of stratified films. Thus, revisions to these models are required.

As a final note, it is important to realize that the Thin Liquid Film-Pressure Balance Technique cannot account for the complexity of an emulsion. While there has been success in isolating some of the colloidal interactions in the water/solvent-diluted-bitumen/water films, one must also realize that the results are limited to a single droplet-

droplet interaction and cannot be *directly* extrapolated to describe the overall behaviour of an emulsion. The implications of the thin film results must be considered as one part of a large body of existing knowledge. Advances in our understanding of water-in-diluted-bitumen emulsion stability can be obtained by combining the thin film data with standard emulsion stability tests, chemical analysis, solubility modeling, and other valuable information.

Appendix A
Equivalent Film Thickness

Most of the data presented in this thesis has involved measuring the thickness of a water/oil/water film and determining how the thickness is affected by concentration or applied pressure. The measurement of film thickness involved two basic steps: 1) recording the intensity of light reflected from the film and 2) converting the intensity measurement into a thickness value using a mathematical model. The model requires certain assumptions about the structure and properties of the film. The common practice is to assume that the film is represented as a single layer of liquid and that this liquid layer has a constant refractive index equal to the refractive index of the bulk liquid. The accuracy of the thickness measurement depends, to a large extent, on the validity of these assumptions.

In this appendix, we discuss the model used to calculate the thickness of water/oil/water films. The first section provides a brief derivation of the single layer model. The section that follows discusses the advantages of using the single-layer model in lieu of more sophisticated models for calculating the film thickness. The third section provides a brief discussion on the validity of the chosen value for the refractive index of the film. The appendix ends with examples describing how to convert raw data into a thickness value using the single layer model.

A.1 Derivation of the Equivalent Film Thickness

When a thin film of liquid is illuminated with white light, a number of coloured fringes appear during the initial stages of film drainage. These bands of colour correspond to ranges of film thickness on the order of hundreds of nanometers. In monochromatic light, these bands appear as a series of light and dark fringes. In the later stages of thinning when the thickness is less than a quarter wavelength of light (about 100 nm), the film appears as a uniform, bright grey film that slowly shifts to a dark grey or black film at equilibrium. These patterns of light or the intensity of the monochromatic

light may be used to determine the thickness of the film at various stages of drainage and at the final equilibrium thickness.

To derive an equation for the film thickness, one may begin by assuming that the film is a flat layer of liquid having a uniform composition. The liquid layer is sandwiched by a second fluid of uniform composition. The surrounding fluid has a refractive index that is lower than the refractive index of the film. The physical illustration of such a system is shown in Figure A.1.

When a beam of incident light strikes the film at an angle of incidence, θ, two primary reflections occur; the first at the water/oil interface and the second at the oil/water interface. Secondary reflections also occur, but the intensity of these reflections is assumed to be too weak to be significant. The difference in length of the optical paths of the two reflected beams results in a phase shift between the two beams. Depending on the thickness of the film, the phase shift leads to a constructive (brighter) or a destructive (darker) interference pattern. Complete constructive and destructive interference corresponds to measurements of maximum and minimum light intensities, respectively. For normal incidence, as is the case in the current experimental set-up, complete constructive interference occurs when the film has an optical thickness of $\lambda/4$, $3\lambda/4$, $5\lambda/4$.... etc. λ is the wavelength of the monochromatic light used to illuminate the film (Jones, 1975).

The thickness of the film is derived from the ratio of the reflectance at the thickness of interest to the maximum reflectance. The reflectance, K, is the ratio of the reflected to incident light intensity (Heavens, 1955):

$$K = \frac{k_1^2 + 2k_1 k_2 \cos\delta + k_2^2}{1 + 2k_1 k_2 \cos\delta + k_1^2 k_2^2} \qquad [A.1]$$

where Fresnel coefficients are given by:

$$k_2 = -k_1 = \frac{n_f - n_s}{n_f + n_s} \qquad [A.2]$$

and

$$\delta = \frac{4\pi n_f h \cos\phi}{\lambda}$$ [A.3]

where h is the optical thickness of the film, ϕ is the angle of refraction within the film, and n_f and n_s are the refractive indices of the film and surrounding fluid, respectively. The current experimental set-up (i.e. Thin Liquid Film-Pressure Balance Technique) uses a nearly normal angle of incidence. So, $\cos\phi \cong 1$.

Expressing Eq. [B.1] in terms of k_2 and using the identity $\cos 2\theta = 1 - 2\sin^2\theta$:

$$K = \frac{k_2^2 - 2k_2^2 \cos\delta + k_2^2}{1 - 2k_2^2 \cos\delta + k_2^4}$$

$$= \frac{4k_2^2 \sin^2(\delta\,2)}{1 - 2k_2^2 + k_2^4 + 4k_2^2 \sin^2(\delta\,2)}$$ [A.4]

Maximum reflectance, K_{max}, will occur at an optical thickness of $\lambda/4$. At this thickness, $\sin^2(\delta/2)$ becomes unity and Eq. [A.4] reduces to the following expression:

$$K_{max} = \frac{4k_2^2}{1 + 2k_2^2 + k_2^4}$$ [A.5]

The ratio of measured to maximum light intensity is equal to the ratio of the film reflectance to the maximum reflectance:

$$\Delta \equiv \frac{I - I_{min}}{I_{max} - I_{min}} = \frac{K}{K_{max}}$$ [A.6]

where the measured light intensity is I. I_{min} and I_{max} are the minimum and maximum values of the measured light intensity, respectively. In the current experimental set-up, I_{min} is set to zero.

An expression for the optical thickness is then obtained by substituting Eqs. [A.4] and [A.5] into Eq. [A.6]:

$$\Delta = \frac{1 + 2k_2^2 + k_2^4}{1 - 2k_2^2 + k_2^4 + 4k_2^2 \sin^2(\delta\ 2)} \cdot \sin^2(\delta/2) \qquad [A.7]$$

Rearranging the expression in terms of δ:

$$\delta = 2\arcsin\left(\frac{\Delta}{1 + 4k_2^2(1 - \Delta)\ (1 - k_2^2)^2}\right)^{\frac{1}{2}} \qquad [A.8]$$

Substitution of Eq. [A.3] provides the final expression for the optical thickness of the thin liquid film:

$$h = \frac{\lambda}{2\pi n_f} \cdot \arcsin\left(\frac{\Delta}{1 + 4k_2^2(1 - \Delta)\ (1 - k_2^2)^2}\right)^{\frac{1}{2}} \qquad [A.9]$$

This is the form of the equation used throughout this study to calculate the optical thickness of a thin film. However, h is more commonly known in the literature as the 'equivalent film thickness'.

It is important to emphasize that the equivalent film thickness was derived with using two assumptions: the film was represented by a single layer of liquid and this liquid layer had a constant refractive index equal to the refractive index of the bulk liquid. In this work, an additional assumption was made that the refractive index for all diluted bitumen solutions was equal to the refractive index of the pure diluting solvent. Each of these assumptions introduces a possible bias or error into the measurement of the film thickness. These assumptions are addressed in the next two sections.

A.2 Triple Layer Model

For thicker films (h>30 nm), the single-layer model provides an accurate measure of the film thickness. For thinner films, the single-layer model provides only an approximate measure of the film thickness. More accurate measurements can be obtained by accounting for the molecular structure within the film (Exerowa and Krugkyakov, 1998). For example, a thinner film typically contains a small core of liquid separated by two layers of surfactant molecules where the hydrophilic heads are positioned side-by-side and the hydrophobic tails are oriented in a similar direction. The liquid core is similar in composition to the bulk liquid and may contain additional surfactant in the form of monomers or micelles. An example of a typical thin film structure is shown in Figure A.2. Such an ordered system is not likely to lead to a uniform refractive index throughout the film. Instead, the refractive index is expected to vary in a direction normal to the plane of the film.

To address this problem, the film can be modeled as a series of parallel liquid layers stacked on top of one another. Each layer is then assigned a refractive index corresponding to the composition of that layer. The triple-layer model (Duyvis, 1962, Smart and Senior, 1966) is usually adequate for estimating the thickness of thinner films, although a five-layer model (Leermakers, et. al., 1983) has been utilized.

The triple-layer model for an aqueous foam film is shown in Figure A.2. The hydrophobic tails make up the two outer layers where each layer is assumed to have a thickness, h_{out}, and a refractive index, n_{out}. The inner layer consists of the aqueous core of thickness, h_{in}, and refractive index, n_{in}. The dividing plane between the layers depends on the specific system being studied. In some situations, it is more reasonable for the hydrophilic heads to be included within the outer layers. Other situations require the dividing plane to pass through the middle of the hydrophilic heads (Exerowa and Krugkyakov, 1998).

According to the triple-layer model, the film thickness is simply:

$$h_{trip} = 2h_{out} + h_{in} \qquad [A.10]$$

Here, h_{in} may be calculated from Duyvis' formula (Duyvis. 1962):

$$h_{in} = h - 2h_{out}\left(\frac{n_{out}^2 - 1}{n_{in}^2 - 1}\right)$$

[A.11]

where h is the equivalent film thickness calculated from Eq. [A.9]. The thickness of the outer layers, h_{out}, must be estimated from theoretical calculations or from data obtained from different experimental techniques. The triple layer model typically provides a thickness estimate that is 5 to 10% lower than the equivalent film thickness (Nikolova and Exerowa, 1995; Nikolova. et al., 1996; Exerowa and Krugkyakov, 1998).

The thicknesses of the films created from diluted bitumen are typically less than 20 nm (refer to Figure 2.12). For such films. one should be able to use the triple layer model to obtain more accurate estimates of the film thickness. However, this would require some knowledge of the chemical structure of the material at the oil-water interface, as well as an idea of how the molecules are arranged at the interface. It is clear from previous research that molecules within the resin and asphaltene fractions are surface active and are the main stabilizers of water-in-oil emulsions (McLean and Kilpatrick, 1997a, 1997b). However, the chemical structure of these molecules (Strausz, et al., 1992; Groenzin and Mullins, 2000) and how the molecules are arranged at the interface is still not well understood (McLean et al., 1998). Until more information is accumulated about the diluted bitumen-water interface, there is little benefit to using the triple layer model to estimate the thickness of water-bitumen-water films.

A.3 Refractive Index of the Film

As mentioned earlier, the refractive index of the film in the single layer model is usually assumed to be equal to the refractive index of the bulk liquid. For this study, the natural assumption would then be to set n_f equal to the refractive index of the bitumen solution. However, at the beginning of the study, data on the refractive index of diluted bitumen solutions were not available in the literature and the bitumen solutions were too opaque for standard methods of measuring the refractive index of oils (ASTM D1218-92). For that reason, the refractive index of the film was assumed to be equal to the

refractive index of the diluting solvent (i.e. the refractive index of pure toluene, $n_{tol} = 1.4961$, or pure heptane, $n_{hep} = 1.3876$). After a significant portion of the thickness measurements and disjoining pressure isotherms were complete, a commercial refractometer that was capable of measuring the refractive index of a thin film of diluted bitumen became available. The refractive index data generated from that equipment appears in Chapter 5. This new refractive index data has been used to determine the error associated with the assumption of setting the refractive index of the film equal to the refractive index of the pure solvent (i.e. $n_f = n_{tol}$ or $n_f = n_{Hep}$).

The refractive indices of the bitumen solutions at dilutions of (10:1) or less (solvent:bitumen by weight) were reasonably close to the refractive indices of the pure solvent. Thus, the error related to the above assumption was negligible (< 0.1 nm). At dilutions of (5:1) to (2:1), the refractive indices of the solvent:bitumen solutions begin to differ significantly from the refractive index of the pure solvents. As a result, the measurements made using the above assumption overestimated the thickness of the films by 0.2 to 0.7 nm. This is comparable to the resolution of the Thin Liquid Film-Pressure Balance Technique for thickness measurements of water/diluted-bitumen/water films. From calibrations using foam films (see Appendix C) and from several repeats of water/diluted-bitumen/water films, the error associated with the technique itself was estimated to be ± 0.5 nm. At the highest bitumen concentration (i.e. (1:1)), assuming that the RI of the film was equal to the RI of the pure solvent resulted in the film thickness being overestimated by as much as 1.2 nm. However, this error is quite small in comparison to the thickness measurements reported in Figure 2.12 where the scatter in the data was roughly ± 10 nm at a concentration of (1:1).

Considering the large scatter in the data at high bitumen concentration and the error of the technique itself, the above assumption appears to be fairly reasonable for such an exploratory study into the stability of water/diluted-bitumen/water films. However, now that proper refractive index data is available, all future work should look to minimize any errors in the thickness measurements by assuming the refractive index of the film is equal to the refractive index of the bulk diluted bitumen solution.

A.4 Measuring Film Thickness

The technique used to obtain measurements of film thickness is commonly referred to as microinterferometry. A low light, low noise photodiode was used to measure the intensity of light reflected from the thin film. The intensity is converted to an electrical signal that is amplified and sent to a chart recorder. The result is a diagram of voltage over time, an example of which is shown in Figure A.3. The diagram clearly shows the initial formation of the film followed by a relative fast rate of drainage. During this stage of film drainage, the voltage appears as a series maxima and minima. In the case of a grey film, the rate of drainage begins to slow as the equilibrium thickness is approached. This appears as a slow exponential decline is the voltage after the last maxima. The voltage becomes a constant value when the film has obtained an equilibrium thickness. Eq. [A.9] is then used to convert the photo-current into an estimate of the equilibrium film thickness.

Most of the terms in Eq. [A.9] are obtained from experimental measurements. The refractive index of the film and surrounding fluid, n_f and n_s, are assumed to be equal to the refractive index of the bulk solutions. A bench-top refractometer may be used to obtain the refractive index of the bulk solutions. For the current set-up, the wavelength of light reflected from the film, $\lambda = 546.0$ nm. The last maxima and minima on the voltage-time diagram correspond to the maximum and minimum light intensities, I_{max} and I_{min}. The light intensity of interest, I, is the constant voltage corresponding to an equilibrium film. I_{max}, I_{min}, and I may simply be measured as the straight line distance from a line of constant reference located below I_{min}. The straight line distance is shown in Figure A.3.

Figure A.3 is an example of a voltage versus time plot for a water/toluene-diluted-bitumen/water film. The various parameter values are $n_f = 1.4961$, $n_s = 1.334$, $\lambda = 546.0$ nm, $I_{min} = 0$ mm, $I_{max} = 74.5$ mm, and $I = 33.5$ mm. From these values, one obtains a film thickness of $h = 42.5$ nm.

A.5 References

ASTM D1218-92 "Standard Test Method for Refractive Index and Refractive Dispersion of Hydrocarbon Liquids". ASTM (1992) 409.

Duyvis, M., Ph.D. Thesis, Utrecht University, Utrecht, 1962.

Exerowa, D. and Kruglyakov, P.M., "Foam and Foam Films", Elsevier, New York, 1998.

Groenzin, H. and Mullins, O.C., *Energy & Fuels* 14 (2000) 677-684.

Heavens, O.S., "Optical Properties of Thin Solid Films", Butterworth, London, 1955.

Jones, M.N., "Biological Interfaces", Elsevier Scientific Publishing Company, New York, 1975.

Leermakers, F., Schentjens, J. and Lyklema, J., *Biophysical Chemistry* 18 (1983) 353.

McLean, J.D. and Kilpatrick, P.K., *J. Colloid Interface Sci.* 189 (1997a) 242.

McLean, J.D. and Kilpatrick, P.K., *J. Colloid Interface Sci.* 196 (1997b) 23.

McLean, J.D., Spiecker, P.M., Sullivan, A.P. and Kilpatrick, P.K., *in* "Structures and Dynamics of Asphaltenes" edited by Mullins, O.C. and Sheu, E.Y., Plenum Press, New York, 1998.

Nikolova, A. and Exerowa, D., *J. Statistical Phys.* 78 (1995) 147-160.

Nikolova, A., Koynova, R., Tenchov, B., Exerowa, D., *Chemistry and Physics of Lipids*, 83 (1996) 111-121.

Smart, C. and Senior, W., *Trans. Faraday Soc.* 62 (1966) 3253.

Strausz, O.P., Mojelsky, T.W. and Lown, E.M., *FUEL* 71 (1992) 1355-1363.
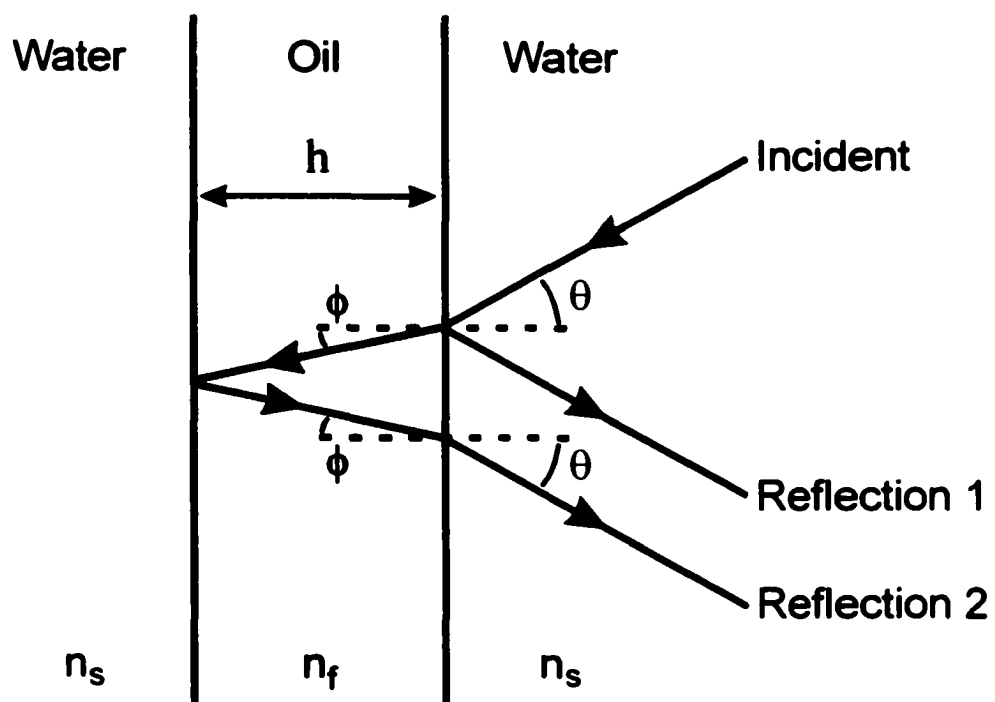
FIGURE A.1: Single layer model of a thin liquid.

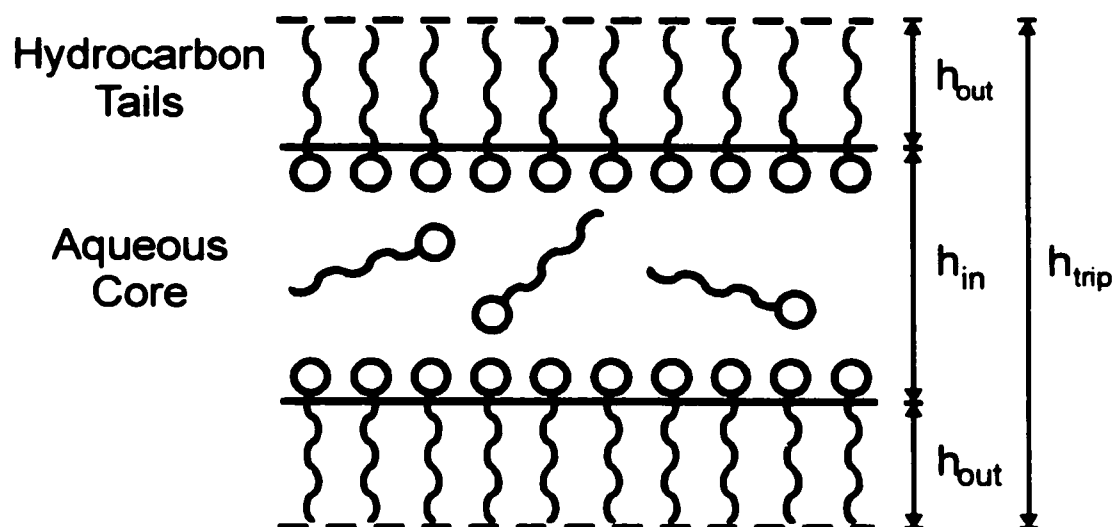FIGURE A.2: Triple layer model of a thin liquid film.

Light Intensity (Voltage)
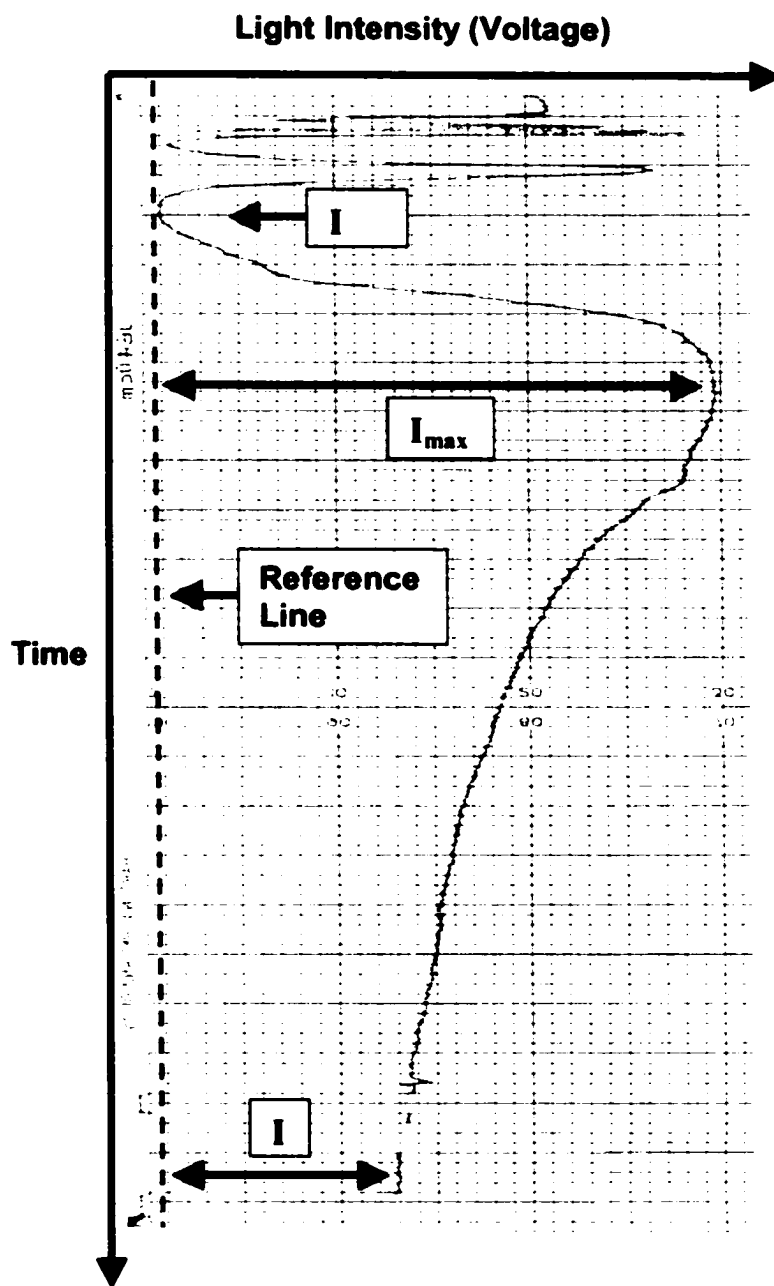
FIGURE A.3: Example of voltage versus time plot obtained from a water/toluene-diluted-bitumen/water film. Note that the plot has been modified to fit onto a single page.

Appendix B

Capillary Pressure

Figure B.1 is a cross-section of a thin film formed within the hole of a porous plate film holder. The thin film is assumed to form in the geometric center of the hole creating a radial symmetry in shape of the oil/water interfaces. The curvature of the oil/water interfaces generates a capillary pressure in the plateau border region adjacent to the thin film. Under static conditions and constant interfacial tension, the capillary pressure may be estimated from the Young-Laplace equation:

$$\frac{\Delta P}{\gamma} = \frac{1}{s}\frac{d}{ds}(s\sin\theta)$$

[B.1]

where ΔP is the pressure difference across the oil/water interface, γ is the interfacial tension, s is the radial distance from the center of the hole, and θ is the angle of the interface relative to the horizontal film.

To obtain an expression for the capillary pressure, we must integrate Eq. [B.1] from the film boundary to the point where the oil/water interface touches the hole wall. At the film boundary, the radial distance from the center of the hole is simply the radius of the film (s = r) and the angle between the film and the oil/water interface is θ (known as the film contact angle). At the hole wall, the radial distance is simply the radius of the hole (s = R) and the angle of the interface relative to the horizontal film is 90° - φ where φ is known as the wetting contact angle. Using these terms for the limits of integration, Eq. [B.1] becomes:

$$\frac{\Delta P}{\gamma}\int_{r}^{R} s\,ds = \int_{r\sin\theta}^{R\sin(90°-\varphi)} d(s\sin\theta)$$

[B.2]

Integrating, we obtain:

$$\frac{\Delta P}{2\gamma}\left(R^2 - r^2\right) = R\sin(90° - \varphi) - r\sin\theta \qquad [B.3]$$

Eq. [B.3] then simplifies to:

$$\Delta P = P_C = 2\gamma\frac{R\cos\varphi - r\sin\theta}{R^2 - r^2} \qquad [B.4]$$

where P_C is the capillary pressure. In general, both contact angles are assumed to be sufficiently small such that $\cos\varphi \approx 1$ and $\sin\theta \approx 0$. Eq. [B.4] may then be simplified as:

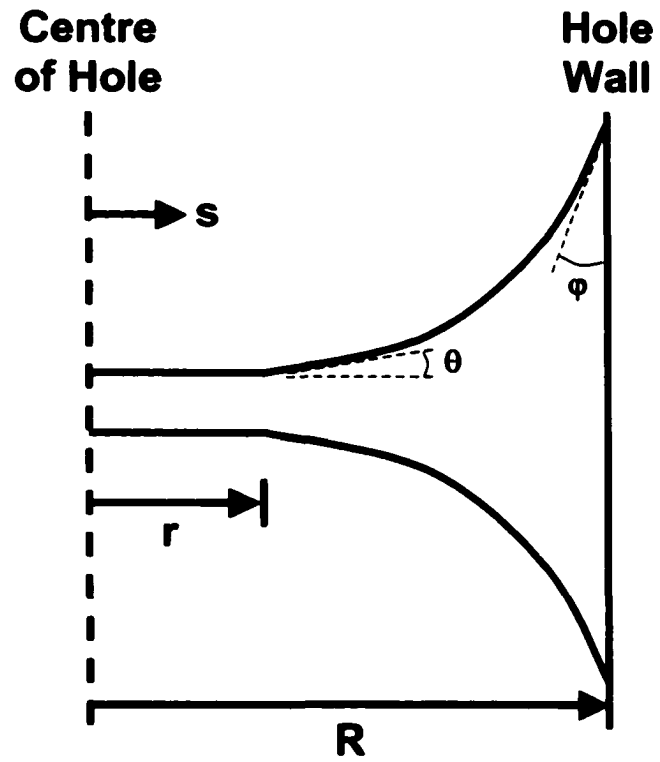$$P_C = 2\gamma\frac{R}{R^2 - r^2} \qquad [B.5]$$

FIGURE B.1: Cross-section of a thin film formed within the hole of a porous plate film holder.

Appendix C

Preparation and Calibration of Measuring Cells

C.1 Cell Preparation

New cells were provided by the Institute of Physical Chemistry at the Bulgarian Academy of Sciences (Sofia, Bulgaria). Examples of finished cells with a capillary film holder and a porous plate film holder are shown in Figure C.1. Figure C.2 provides a close-up view of these two types of film holders. Note the brown/black shading of the porous plate holder. The shading indicates that the film holder has already been treated to convert the glass from a hydrophilic to a hydrophobic surface.

Cells fitted with a porous plate film holder arrived unfinished and thus, required some modifications before being used in the Thin Liquid Film-Pressure Balance Technique (TLF-PBT) apparatus. Modifications include drilling the hole through the porous plate, smoothing of the cut edges, and treating the glass surface to be hydrophobic. The procedures for finishing and preparing the new cells for use in the Thin Liquid Film technique follows.

C.1.1 Finishing a Cell

1. The center point of the cell was located and then marked clearly on the porous plate.

2. A vice was used to gently hold the cell so that the porous plate was in a horizontal position with the bottom of the plate facing up.

3. Using a sharp drill bit, a hole was drilled through the porous plate at the marked center point. Water was used as a lubricant when drilling. The best results were obtained by starting with a small hole diameter and then slowly enlarging the hole diameter as needed. Note that this step had to be completed with great care; too large of a hole would be unable to hold the oil film and too small of a hole would cause undesirable light reflections from the hole walls.

4. The edges of the porous plate were gently smoothed and rounded with a file. The top and bottom of the plate were also filed to remove any rough edges around the hole

and to reduce the thickness of the plate to about 2.2 mm. It was especially important to keep the plate thickness between 2.5 and 2 mm. Below 2 mm, the thickness of the porous plate begins to significantly affect the film stability. In general, the plate should be made thicker for larger hole diameters.

5. The porous plate was cleaned with copious amounts of DIUF water and then placed under a microscope for viewing. The hole was checked to ensure that it was straight, cylindrical in shape, and was oriented vertically when placed in the TLF-PBT apparatus. To correct any defects that exist, the hole may be reamed out with the drill bit or slightly enlarged. Alternatively, the plate could be filed to a slightly lower thickness.

C.1.2 Preparing a Cell for Use

1. Finished cells were placed into a concentrated solution of chromic acid and left to sit overnight. The entire cell was then flushed with a large amount of DIUF and placed in an oven at 175°C (or greater) to dry for a minimum of 1 h.

2. Cells were loaded with an aqueous soap solution known to form Newton Black Films (NBF; 10^{-3} M sodium dodecyl sulfate and 5x 10^{-3} M NaCl) and placed in the TLF-PBT apparatus. A number of small observations were made to ensure the porous plate was finished with the desired dimensions and that it was working properly:

   - The diameter of the hole was measured.

   - A thin aqueous foam film was formed within the hole and then observed to ensure that the Newton Black Film (NBF) film remained stable for an indefinite period of time independent of the film or hole diameter.

   - The film was forcibly ruptured in order to observe the change in the measured light intensity. The signal should immediately return to the zero point. If not, this was an indication of undesired reflection off the bottom of the porous plate or the side walls of the hole.

   - The thickness of the foam film was measured and checked against the accepted thickness of 4.3 ± 0.2 nm for a NBF formed from the aqueous sodium dodecyl sulfate solution (Exerowa and Kruglyakov, 1998).

- The diameter of the film was increased in small increments and the light intensity signal observed. The signal should remain constant and it should match the signal from another cell currently in use. If not, there is probably undesirable reflection from the bottom of the porous plate or the side wall of the hole.

3. If significant reflection is observed, a number of options are available:

- The hole could be made larger (keeping in mind that larger surface areas would lead to less stable films).

- Recalibrate the system to account for the reflection. This is a difficult and undesired option.

- Slightly reduce the plate thickness in order to decrease the amount of reflection from the walls of the hole. While this is the best and easiest option, some care must be taken to ensure that the plate does not become too thin. Thinner plates are unable to hold an oil droplet within the hole.

- If any alterations were done to the film holder, steps 1 and 2 were repeated until acceptable cell performance was obtained.

4. After all alterations were complete, the film holder was cleaned with copious amounts of DIUF water and ethanol. The cell was placed in the oven at 175°C to dry.

5. The film holder was soaked in a concentrated solution of toluene-diluted-bitumen (about 30 to 40 %wt bitumen) in order to make the porous plate more hydrophobic. The film holder was left in the solution for a minimum of 2 days.

6. The porous plate film holder was cleaned using the standard cleaning procedure for all working cells; flush with toluene, ethanol and then toluene again before placing it in the oven at 175°C for at least 1 h.

7. After cleaning, ensure that an emulsion film could be formed using toluene-diluted bitumen and industrial water. If a film can be formed, the film holder is ready for daily use. If a film can not be formed, steps 5 and 6 must repeated.

C.1.3 Cell Storage

During everyday use, the porous plate film holder should be stored overnight in a dilute toluene-bitumen solution. This will prevent any degradation of the hydrophobic

nature of the glass surface. Once a cell has been removed from the storage solution, it must be cleaned immediately. The porous plate may become clogged if the toluene-bitumen solution is allowed to dry.

For long term storage, cells may simple be cleaned, dried, and then placed in a safe location where the cells cannot be easily broken. Before using a cell that has been in long term storage, the porous plate must retreated (Steps 5 to 7 in the above section) to ensure that the glass surface remains hydrophobic.

C.2 Maximum Operating Pressure of a Cell

The measurement of disjoining pressure is limited by the size of the pores in the porous plate. As the pressure in the cell is increased, the oil-water interface begins to extend into the pores of plate. Eventually, the shape of the interface within the individual pores will reach a nearly perfect hemisphere (assuming perfect wetting of the oil-phase on the treated glass surface). This represents the limiting operating pressure of the cell. Any further increases in the cell pressure will cause the water-phase to invade the pores of the plate leading to a loss of control over the pressure applied to the film (i.e. the capillary pressure). For this reason, the size of the largest pores in the plate must be determined before performing any thin film measurements. The following is the procedure to determine the largest pore size of a porous plate.

1. Ensure that the cell is clean. Connect the cell capillary to the pressure control and manometer of the TLF-PBT apparatus.

2. Fill the bottom portion of the cell with solvent of known surface tension. HPLC grade toluene was normally used for this procedure.

3. Connect the upper and lower portions of the cell so that the porous plate is immersed in the solvent.

4. Set the cell in a vice or some other holder device so that the porous plate may be viewed from the side using a magnifying lens.

5. Slowly increase the air pressure in the capillary/porous plate using the pressure control. At some point, a small bubble of air will be released from the porous plate and rise to the surface. Note the pressure at which this occurs. This is the maximum operating pressure, P_{max}, of the cell for the given surface (or interfacial) tension.

6. Using the noted pressure and the known surface tension for the solvent, calculate the radius of the largest pore, R_{max}:

$$R_{max} = \frac{2\gamma}{P_{max}}$$

[C.1]

This radius can then be used to determine the maximum operating pressure of each cell for a given oil-water system. To account for error in this measurement and to ensure accurate and repeatable disjoining pressure isotherms, the pressure was only increased to about 90% of the maximum operating pressure of the cell. No disjoining pressure measurements were made beyond the 90% limit.

C.3 Thickness Measurement Calibrations

Before any thickness measurements were conducted on water/bitumen/water films, the TLF-PBT apparatus needed to be calibrated to ensure that all lighting and optics were aligned with the low-light, low-noise photo-diode. Calibration was performed using a capillary cell and an aqueous foam film stabilized by sodium dodecyl sulfate at a concentration of 10^{-3} M. Calibrations could be performed using one of three possible solutions. The solutions varied only in salt (NaCl) concentration with the salt concentration determining the type of film and equilibrium thickness (see Table C.1).

Newton Black Films (NBF) were almost always used for calibration since the equilibrium thickness of NBF is nearly independent of capillary pressure. For the present set-up, the calibration consistently yielded a thickness of 4.4 ± 0.1 nm for NBF, well within the range quoted in literature (Table C.1). Any measurements greater than this value indicated that an undesirable reflection was present, probably due to a very high incident light intensity. This problem was usually corrected by reducing the diameter of the iris diaphragm until the calibration measurements matched the literature values. Calibrations were repeated every few months to ensure that there was no degradation in the performance of the apparatus.

TABLE C.1: Literature values for the variation in film thickness and behaviour based on NaCl concentration.

SDS Concentration (M)	NaCl Concentration (M)	Film Type	Equilibrium Thickness (nm)
10^{-3}	10^{-3}	Grey Film	60 to 50*
10^{-3}	10^{-1}	Common Black Film (CBF)	11.8 ± 0.7
10^{-3}	5×10^{-1}	Newton Black Film (NBF)	4.3 ± 0.2

*Equilibrium thickness of a grey film depends strongly on the applied capillary pressure.

C.4 References

Exerowa, D. and Kruglyakov, P.M., "Foam and Foam Films", Elsevier, New York, 1998.
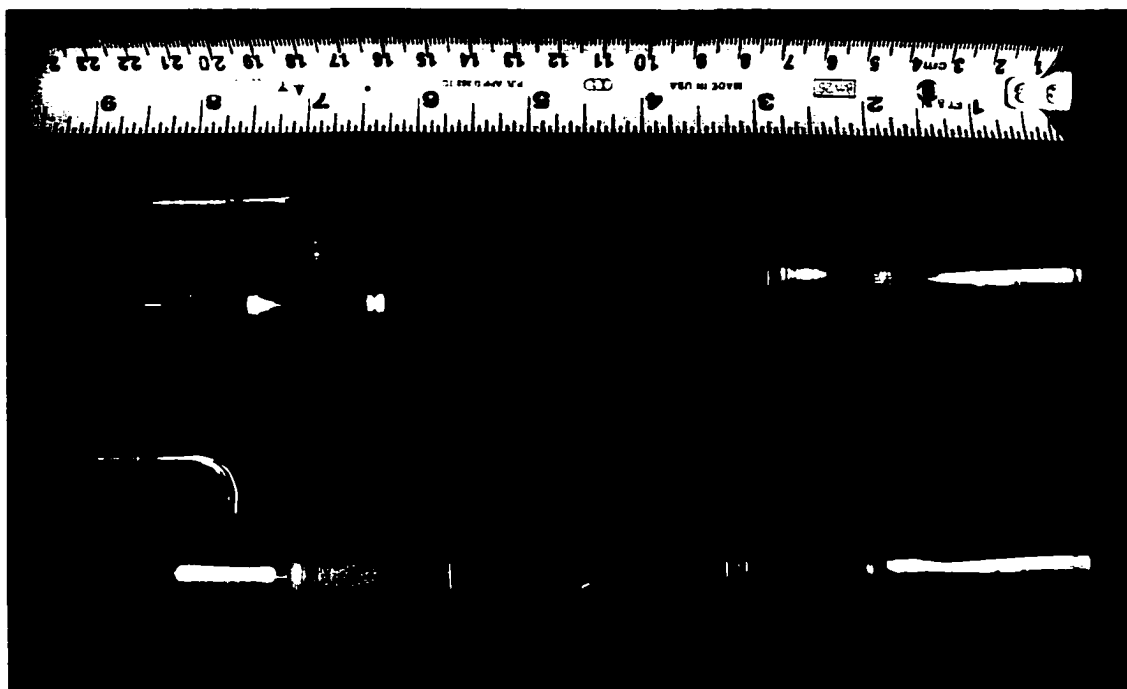
FIGURE C.1: Image of the cells used in the Thin Liquid Film-Pressure Balance Technique. Two types of film holders were utilized: a porous plate film holder (top) and a capillary film holder (bottom).

FIGURE C.2: Close-up view of the capillary film holder (left) and the porous plate film holder (right). The capillary film holder has an inside diameter of about 4 mm and the diameter of the hole in the porous plate holder is about 0.8 mm.

Appendix D

Protocols for Sample Preparation

This appendix provides a detailed account of all the procedures used to prepare the bitumen samples in their various forms including solids-free asphaltenes, deasphalted bitumen, solids-free-bitumen, and asphaltene fractions. Only one standard procedure was used to obtain each form of bitumen except for the solids-free-asphaltenes where two different procedures were used. One procedure was based on asphaltene/solid solubility in toluene while the other procedure made use of asphaltene/solid solubility in heptol (a blend of heptane and toluene). In method-I, toluene was expected to dissolve all of the asphaltenes. Centrifugation and filtering were then expected to remove all of the mineral particles greater than 0.1 μm. In method-II, the heptol was expected to cause a small fraction of the high molecular weight asphaltenes to be separated out with all of the fine mineral solids. Both solid-free-asphaltene samples were required to determine the affect of fine mineral solids on the film stability.

D.1 Separation of Bitumen into Deasphalted Bitumen and Asphaltene/Solid Fractions

1. Approximately 75 g of crude bitumen was mixed with 3200 ml of heptane; a heptane:bitumen volume ratio of 40:1.

2. The mixture was stirred at low speed for about 4 h and then left overnight to allow the solids and asphaltenes to settle to the bottom of the beaker.

3. The entire solution was centrifuged at 9400g for about 45 min. Following centrifugation, the supernatant was vacuum filtered through a 0.8 μm filter (Millipore Corporation, Cat No. H9CK87112 F).

4. The deasphalted bitumen was recovered using a hot water, rotary evaporator to drive off the heptane from the supernatant. A 2000 ml round flask was filled with about 600 ml (~1/3 capacity) of supernatant. More supernatant was added to the flask each time the liquid level grew low until all the supernatant had been added. A small amount of

viscous liquid (~100 ml) remained after the evaporation was complete. This viscous liquid was poured into a sample jar and placed inside a convection oven at 40°C to drive off the remaining heptane. The deasphalted bitumen was considered 'dry' when the change in mass was less than 0.1% over a 24 h period.

5. The asphaltene-solid precipitate recovered from filtration was left to dry in an oven at 40°C. The asphaltene-solid fraction was considered 'dry' when the change in mass was less than 0.1% over a 24 h period. The expected recovery was between 14.5 and 16 wt%.

Note that the centrifugation step (step 3) could have been skipped and the entire mixture could have been vacuum filtered. The same percentage of asphaltenes is recovered, although centrifugation requires less time and results in a smaller amount of material loss.

D.2 Preparation of Solids Free Asphaltenes

D.2.1 Method-I

1. The asphaltene-solid precipitate generated using procedure D.1 was dissolved in toluene at a volume ratio of 100:1 toluene:asphaltene-solid. The mixture was shaken for a minimum of 1 h to ensure that all the asphaltenes were dissolved.

2. The mixture was centrifuged at 9400g for 45 min followed by vacuum filtration through a 0.22 μm filter (Millipore Corporation, Cat No. GSWP04700).

3. The filtrate was placed in a clean sample jar and left in an oven at 40°C until only 'dry' asphaltenes remained.

The asphaltene-I and solid fractions accounted for about 15.5%wt and 0.9%wt of the original bitumen, respectively.

D.2.2 Method-II

1. The asphaltene-solid precipitate generated using procedure D.1 was dissolved in toluene at a concentration of 225 mL of toluene for every 5 g of precipitate. The mixture was then stirred for 1 h to ensure the asphaltenes were completely dissolved.

2. While the mixture was still being stirred, heptane was slowly add at a concentration of 275 mL of heptane for every 5 g of precipitate. The final mixture had a heptane:toluene volume ratio of 55:45 and asphaltene-solids concentration of about 10 g/L. The mixture was stirred for an additional hour and left overnight.

3. The mixture was then centrifuged at 9400g for about 45 min followed by vacuum filtration through a 0.22 μm filter.

4. The filtrate was placed in a clean sample jar and left in an oven at 40°C until only ·dry· asphaltenes remained.

The asphaltene-II and solid fractions accounted for about 14.9%wt and 1.5%wt of the original bitumen, respectively.

D.3 Preparation of Asphaltene Fractions

1. A 14 g sample of asphaltene-I was dissolved in 412 mL of toluene. The mixture was stirred for 1 h to ensure that all of the asphaltenes were dissolved.

2. While still stirring, 412 mL of heptane was slowly added to the mixture. The mixture was stirred for 1 h and then left to stand for 1 h. The mixture had a heptane:toluene volume ratio of 1:1 and an asphaltene concentration of 14 g/L.

3. After standing, the mixture was centrifuged at 9400g for 30 min and vacuum filtered through a 0.22 μm filter. The precipitate was collected and placed in a 40°C oven until the precipitate was ·dry·. The dry precipitate was designated asphaltene-cut#1.

4. The volume of the supernatant was 790 mL. It was assumed that the heptane:toluene volume ratio had not changed. Thus, the mixture contained approximately 395 mL each of toluene and heptane. To change the heptane:toluene volume ratio to 1.5:1, an additional 197.5 mL of heptane was added to the mixture. The mixture was stirred for 1 h and then left to stand for 1 h. After standing, the mixture was centrifuged at 9400g for 30 min and vacuum filtered through a 0.22 μm filter. The precipitate was collected and placed in a 40°C oven until the precipitate was ·dry·. The dry precipitate was designated asphaltene-cut#2.

5. The volume of the supernatant was 915 mL. Assuming that the heptane:toluene volume ratio had not changed, it was estimated that the mixture contained approximately 549 mL of heptane and 366 mL of toluene. To change the

heptane:toluene volume ratio to 2:1, an additional 183 mL of heptane was added to the mixture. The mixture was stirred for 1 h and then left to stand for 1 h. After standing, the mixture was centrifuged at 9400g for 30 min and vacuum filtered through a 0.22 µm filter. The precipitate was collected and placed in a 40°C oven until the precipitate was 'dry'. The dry precipitate was designated asphaltene-cut#3.

6. The volume of the supernatant was 910 mL. Assuming that the heptane:toluene volume ratio had not changed, it was estimated that the mixture contained approximately 607 mL of heptane and 303 mL of toluene. To change the heptane:toluene volume ratio to 3:1, an additional 303 mL of heptane was added to the mixture. The mixture was stirred for 1 h and then left to stand for 1 h. After standing, the mixture was centrifuged at 9400g for 30 min and vacuum filtered through a 0.22 µm filter. The precipitate was collected and placed in a 40°C oven until the precipitate was 'dry'. The dry precipitate was designated asphaltene-cut#4.

7. The volume of the supernatant was 1090 mL. Assuming that the heptane:toluene volume ratio had not changed, it was estimated that the mixture contained approximately 817.5 mL of heptane and 272.5 mL of toluene. To change the heptane:toluene volume ratio to 4:1, an additional 272.5 mL of heptane was added to the mixture. The mixture was stirred for 1 h and then left to stand for 1 h. After standing, the mixture was centrifuged at 9400g for 30 min and vacuum filtered through a 0.22 µm filter. The precipitate was collected and placed in a 40°C oven until the precipitate was 'dry'. The dry precipitate was designated asphaltene-cut#5.

8. The volume of the supernatant was 1265 mL. Assuming that the heptane:toluene volume ratio had not changed, it was estimated that the mixture contained approximately 1012 mL of heptane and 253 mL of toluene. To change the heptane:toluene volume ratio to 5:1, an additional 253 mL of heptane was added to the mixture. The mixture was stirred for 1 h and then left to stand for 1 h. After standing, the mixture was centrifuged at 9400g for 30 min and vacuum filtered through a 0.22 µm filter. The precipitate was collected and placed in a 40°C oven until the precipitate was 'dry'. The dry precipitate was designated asphaltene-cut#6.

9. The remaining supernatant contained all the asphaltenes that were soluble in the 5:1 heptane:toluene solution. The supernatant was placed in a 40°C oven until a dry powder remained. The dry powder was designated asphaltene-cut#7.

Appendix E

Derivation of the Stefan-Reynolds Equation

The Stefan-Reynolds equation may be used to describe the rate of drainage for a thin film where the liquid drains from within the film to the surrounding plateau border region. However, the equation is strictly valid for situations where the oil/water interfaces are plane parallel, the interfaces are tangentially immobile, and the viscosity remains constant throughout the entire drainage process. The equation may be derived from material balances and the convection-diffusion equation (Krotov and Rusanov, 1999) or from the continuity equation and the Navier-Stokes equations (Landau and Lifshitz, 1982). Only the latter derivation will be presented.

E.1 Defining the Flow Field

The thin film is assumed to consist of two solid discs separated by a single continuous liquid, as shown in Figure E.1. The disks are parallel and have a fixed radius, R. The bottom disc is assumed to be stationary with the top disc approaching at a velocity, u. The origin is located at the centre of the lower disc with z-axis directed upwards. Finally, we assume that the inertia forces within this system are negligible.

The first of the general equations needed to describe the flow field is obtained from the continuity equation:

$$\frac{\partial \rho}{\partial t} + \frac{1}{r}\frac{\partial}{\partial r}(\rho r V_r) + \frac{1}{r}\frac{\partial}{\partial \theta}(\rho V_\theta) + \frac{\partial}{\partial z}(\rho V_z) = 0 \qquad [\text{E.1}]$$

where t is time and V_r, V_θ, and V_z are the velocities in the r, θ, and z directions. Assuming that the density, ρ, is constant and setting V_θ to zero, the continuity equation is reduced to:

$$\frac{1}{r}\frac{\partial}{\partial r}(rV_r) + \frac{\partial V_z}{\partial z} = 0 \qquad\qquad\qquad \text{[E.2]}$$

The relevant momentum equations are given by the Navier-Stokes equations:

$$-\frac{\partial P}{\partial r} + \eta\left[\frac{\partial}{\partial r}\left(\frac{1}{r}\frac{\partial}{\partial r}(rV_r)\right) + \frac{1}{r^2}\frac{\partial^2 V_r}{\partial\theta^2} - \frac{2}{r^2}\frac{\partial V_\theta}{\partial\theta} + \frac{\partial^2 V_r}{\partial z^2}\right] = 0 \qquad \text{[E.3a]}$$

$$\frac{\partial P}{\partial\theta} = 0 \qquad\qquad\qquad \text{[E.3b]}$$

$$\frac{\partial P}{\partial z} = 0 \qquad\qquad\qquad \text{[E.3c]}$$

where η is the bulk viscosity and P is the pressure. Making use of the lubrication approximation where $\dfrac{\partial V_r}{\partial r} << \dfrac{\partial V_r}{\partial z}$ and $\dfrac{\partial V_r}{\partial\theta} = 0$, Eqs. [E.3] reduce to:

$$-\frac{dP}{dr} + \eta\frac{\partial^2 V_r}{\partial z^2} = 0 \qquad\qquad\qquad \text{[E.4]}$$

Thus, the flow field within the thin film is described by Eqs. [E.2] and [E.4].

The boundary conditions are obtained from the no-slip condition and assuming a reference pressure at the edge of the disks:

$$V_r = 0 \quad \text{at} \quad z = 0 \qquad\qquad\qquad \text{[E.5a]}$$

$$V_z = 0 \quad \text{at} \quad z = 0 \qquad\qquad\qquad \text{[E.5b]}$$

$$V_r = 0 \quad \text{at} \quad z = h \qquad\qquad\qquad \text{[E.5c]}$$

$$V_z = -u \quad \text{at} \quad z = h \qquad\qquad\qquad \text{[E.5d]}$$

$$P = 0 \quad \text{at} \quad r = R \qquad\qquad\qquad \text{[E.5e]}$$

E.2 Solving for Drainage Rate

The velocity profile is obtained by integrating Eq. [E.4a]:

$$V_r = \frac{1}{2\eta}\frac{\partial P}{\partial r}z^2 + C_1 z + C_2$$

[E.6]

The integration constants, C_1 and C_2, are obtained from the boundary conditions Eqs. [E.5a] and [E.5c]:

$$C_1 = 0$$

[E.7a]

$$C_2 = -\frac{1}{2\eta}\frac{dP}{dr}h$$

[E.7b]

Thus, the equation for the velocity profile within the thin film is, as follows:

$$V_r = \frac{1}{2\eta}\frac{dP}{dr}z(z-h)$$

[E.8]

To obtain the pressure profile within the thin film, we begin by integrating the continuity equation with respect to z. Using the boundary conditions Eqs. [E.5b] and [E.5d], we obtain the following equation:

$$u = \frac{1}{r}\frac{\partial}{\partial r}\left(\frac{-r}{12\eta}\frac{dP}{dr}h^3\right)$$

[E.9]

Further integrating with respect to r and making use of the final boundary condition, we obtain an expression for the pressure profile within the thin film:

$$P = \frac{3\eta u}{h^3}\left(R^2 - r^2\right)$$

[E.10]

Integrating the pressure profile over the entire area of the film, we obtain the total force, F, required to move the upper disk:

$$F = \int_0^{2\pi} \int_0^R Pr\,dr\,d\theta$$

$$= \frac{3\pi\eta u}{2h^3} R^4 \qquad\qquad [E.11]$$

The above equation is known as the Stefan Equation. The average pressure difference between the film and its surroundings is obtained by dividing the Stefan Equation by the area of the film:

$$\Delta P = \frac{F}{\pi R^2} = \frac{3\eta u R^2}{2h^3} \qquad\qquad [E.12]$$

Expressing the velocity of the upper disk in terms of a rate of change in the film thickness with time, we obtain the final expression:

$$-\frac{dh}{dt} = \frac{2\Delta P h^3}{3\eta R^2} \qquad\qquad [E.13]$$

The above expression is the Stefan-Reynolds Equation for the rate of drainage from a thin film of liquid. The pressure difference, ΔP, is normally expressed as a difference between the capillary pressure, P_C, and the disjoining pressure, Π:

$$\Delta P = P_C - \Pi \qquad\qquad [E.14]$$

E.3 References

Krotov. V.V. and Rusanov. A.I.. "Physicochemical Hydrodynamics of Capillary Systems". Imperial College Press, London, 1999.
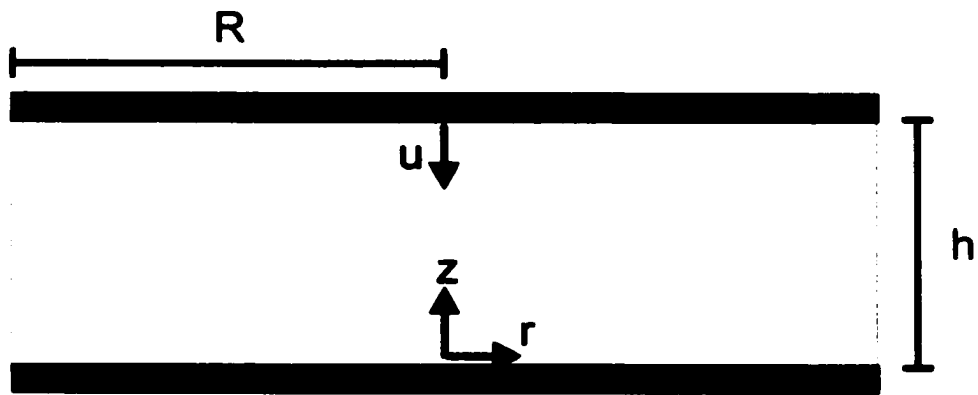
Landau. L.D. and Lifshitz. E.M.. "Fluid Mechanics". Pergamon Press. Toronto. 1982.

FIGURE E.1: Model of a draining thin liquid film.